

**Design, Synthesis and Biological Evaluation of DNA
Gyrase and Topoisomerase IV Inhibitors as Novel
Antibacterials**

Sarah Katherine Narramore

Submitted in accordance with the requirements for the degree of
Doctor of Philosophy

The University of Leeds

School of Chemistry

April 2016

The candidate confirms that the work submitted is her own, except where work which has formed part of jointly authored publications has been included. The contribution of the candidate and the other authors to this work has been explicitly indicated below. The candidate confirms that appropriate credit has been given within the thesis where reference has been made to the work of others.

Some of the work in Chapter 2 of the thesis has appeared in publication as follows:

Pyridine-3-carboxamide-6-yl-ureas as novel inhibitors of bacterial DNA gyrase: Structure based design, synthesis, SAR and antimicrobial activity, 2014, Ian A. Yule, Lloyd G. Czaplewski, Stephanie Pommier, David T. Davies, Sarah K. Narramore and Colin W.G. Fishwick

I was responsible for the synthesis of the compounds described in Chapter 2. Ian Yule was responsible for synthesis of all compounds described in the paper that are not discussed in Chapter 2. Stephanie Pommier and David T. Davies were responsible for the biological assessment of the compounds. Lloyd G. Czaplewski and Colin W.G. Fishwick provided supervisory support and guidance to the work described.

This copy has been supplied on the understanding that it is copyright material and that no quotation from the thesis may be published without proper acknowledgement.

© 2016 The University of Leeds and Sarah Katherine Narramore.

The right of Sarah Katherine Narramore to be identified as Author of this work has been asserted by her in accordance with the Copyright, Designs and Patents Act 1988.

Acknowledgements

There are many people I would like to thank for their invaluable help and guidance during my PhD. I would not have completed it without their support.

Firstly, at the University of Leeds, I would like to thank Colin Fishwick for his support and guidance throughout the project. I would like to thank the following current and past members of the Fishwick group for making the lab a relaxed and supporting environment: Katie Simmons, Martin McPhillie, Ian Yule, Fraser Cunningham, Ricky Cain, Ryan Gonciarz, Lewis Turner, James Gordon and Aaron Wilkinson. I would like to thank the technical support staff for always been willing to help me with any problems: Martin Huscroft, Tanya Marinko-Covell, Simon Barrett and Chris Empson. And also to Stuart Warriner for his efforts to keep the open access mass spec up and running. For helping me make the protein I needed and letting me use up space in their lab, I'd like to thank Gemma Wildsmith, Bruce Turnbull and Mike Webb. I would also like to thank members of Alex O'Neill's group who have assisted me with microbiological assays: Anna Lipell and Victoria Lee.

Secondly I would like to thank my industrial collaborators at Biota Ltd: David Haydon, Craig Morton and James Bennett.

Thirdly I am very grateful for the support given to me by members of the Maxwell group and others at the John Innes Centre who have collaborated with me to biologically assess my inhibitors and carryout crystallographic experiments: Tony Maxwell, Steven Hearnshaw, Lesley Mitchenall, Clare Stevenson, Maria Kunert and David Lawson.

And finally to my family and friends who have kept me going when I was struggling most: James Fleming, Jenny, Ruth, Alice and Peter Narramore and Lynley Aldridge. I couldn't have done it without you.

Abstract

The spread of antibiotic resistance is a great threat to medicine. We are in desperate need of new antibiotics to replace those for which resistance is widespread. The bacterial type two topoisomerases, DNA gyrase and topoisomerase IV, are well validated antimicrobial targets. The fluoroquinolone antibiotics target the DNA binding site of these enzymes, but no currently available antibiotics target the ATP binding site. It is hoped that simultaneously targeting the ATP binding sites of these two bacterial enzymes will slow the emergence of resistance.

This thesis describes the investigation of a series of pyridine 3-carboxamide DNA gyrase inhibitors, extending knowledge of the structure activity relationships of these compounds and making assessment of their inhibition of the topoisomerase IV enzyme in addition to their inhibition of DNA gyrase. Many of the inhibitors proved to be highly potent inhibitors of both DNA gyrase and topoisomerase IV with the most potent compound having IC_{50} s of 24 nM and 87 nM against the DNA gyrase and topoisomerase IV enzymes respectively. These compounds also showed promising antibacterial activity with MICs as low as 1 μ g/ml against *S. aureus*. Additionally, *in vitro* ADME profiling of key compounds from this series was carried out.

A subunit of the DNA gyrase protein was produced for use in crystallisation studies. Co-crystallisation of the protein with four inhibitor molecules was carried out and four crystal structures were solved revealing the binding poses of the pyridine 3-carboxamide compounds bound in the ATP site of GyrB.

Efforts were also made to identify a new series of DNA gyrase inhibitors. *De novo* design and virtual high throughput screening were utilised and a number of compounds were purchased and assessed for their ability to inhibit DNA gyrase. Two of the compounds showed activity in the enzyme assay. A scaffold hopping approach was also used to rationally design new series of potential inhibitors. Three compound series were designed and synthesis was carried out towards them. A series of quinazolinones proved to be the most synthetically tractable and a small library was produced and assessed for their biological activity. Several of the compounds were active against the DNA gyrase enzyme with IC_{50} s as low as 1.1 μ M.

Table of Contents

Acknowledgements	ii
Abstract	iii
Table of Contents	iv
Abbreviations and Symbols	viii
Amino acid notation	x
Chapter 1 Introduction	1
1.1 Antibacterial resistance and the need for new antibacterial agents	1
1.2 Bacteria as drug targets	2
1.2.1 Gram positive and Gram negative bacteria.....	3
1.3 Mechanisms of resistance.....	5
1.3.1 Modifications to the membrane to control penetration and efflux .	6
1.3.1.1 Porins.....	7
1.3.1.2 Efflux pumps.....	8
1.3.2 Resistance <i>via</i> target site modification	10
1.3.3 Inactivation of antibiotic molecules	11
1.4 Methods for antibacterial drug discovery	11
1.5 DNA topoisomerases	13
1.5.1 Structure of type II topoisomerases	15
1.5.1.1 Sequence similarity between DNA Gyrase and topoisomerase IV	16
1.5.2 Mechanism of type II topoisomerases	20
1.5.2.1 Conformational changes in GyrB/ ParE.....	21
1.5.2.2 Mechanism of DNA cleavage	24
1.6 Type II topoisomerases as antibacterial drug targets.....	25
1.6.1 Inhibition of the DNA binding site – the quinolones.....	25
1.6.2 Inhibition of the ATP binding site – a brief history.....	26
1.6.2.1 Coumarins and cyclothialidines: natural product based inhibitors	26
1.6.2.2 Dual-targeting, crystallography and the rise of non-natural product inhibitors	28
1.6.3 Summary.....	36
1.7 Project aims and objectives	37
1.7.1 To develop a series of pyridine-3 carboxamides.....	37

1.7.2	The discovery of novel inhibitor series'	37
Chapter 2 Investigation into pyridine-3-carboxamide inhibitors		38
2.1	Background to pyridine-3-carboxamide inhibitors	38
2.2	Choice of avenues of investigation	39
2.3	C-4 aminoaryl derivatives of the pyridine 3-carboxamide series	43
2.4	Biological assessment of inhibitors	49
2.4.1	Biological activity of C-4 aminoaryl pyridines	51
2.5	C-4 heterocyclic derivatives of the pyridine 4-carboxamide series	55
2.5.1	Biological activity of C4-amino heterocyclic pyridines	57
2.6	Pyrrolidine substituents	59
2.7	Investigation of ADME	61
2.8	Summary	65
2.9	Future work	66
Chapter 3 Crystallisation of inhibitor enzyme complexes		67
3.1	Introduction	67
3.2	Production of the 24 kDa subunit of GyrB	67
3.2.1	Cloning of the GyrB24 gene into a vector with a hexahistidine-tag	67
3.2.1.1	Production and purification of GyrB24 protein	69
3.3	Crystallography	71
3.4	Structure solution	72
3.5	Analysis of crystal structures	74
3.6	Summary	78
3.7	Future work	79
Chapter 4 Use of computational methods for hit identification		80
4.1	Introduction	80
4.2	<i>De novo</i> design	81
4.3	vHTS	85
4.3.1	Structure based vHTS	85
4.3.2	Ligand-based vHTS	90
4.4	Choice of ligands for purchase	97
4.5	Biological results	99
4.6	Conclusions and future work	100

Chapter 5 Rational design of a new inhibitor series using a scaffold-hopping approach	101
5.1 Introduction	101
5.2 Pyrimidines.....	101
5.2.1 Background.....	101
5.2.2 Compound design.....	102
5.2.3 Synthesis.....	105
5.3 Triazolopyrimidines.....	109
5.3.1 Background.....	109
5.3.2 Compound design.....	111
5.3.3 Synthesis.....	113
5.4 Quinazolinones	115
5.4.1 Background.....	115
5.4.2 Compound design.....	116
5.4.3 Synthesis.....	119
5.4.4 Biological evaluation of initial compound library.....	122
5.4.5 Efforts towards the synthesis of quinazolinone derivatives with improved solubility.....	123
5.5 Conclusions and future work	125
Chapter 6 Conclusions and Future Work.....	127
6.1 Development of Pyridine-3-carboxamides as inhibitors of DNA gyrase and topoisomerase IV.....	127
6.1.1 Summary.....	127
6.1.2 Future work	129
6.2 Design of novel chemical series as inhibitors of DNA Gyrase and Topoisomerase IV.....	130
6.2.1 Summary.....	130
6.2.2 Future work	131
Chapter 7 Experimental	133
7.1 Chemical methods	133
7.1.1 Instrumentation and General Methods	133
7.1.2 General Methods.....	134
7.1.3 Preparative procedures	135
7.2 Biological Methods.....	172
7.2.1 Instrumentation.....	172

7.2.2	Materials.....	172
7.2.3	Methods.....	174
7.2.4	Malachite green assay	174
7.2.5	Coupled assay	175
7.2.6	MIC determination	179
7.2.7	Cloning of DNA gyrase genes into pNIC.....	179
7.2.7.1	Linearisation of vector by digestion with BsaI	179
7.2.7.2	T4 DNA polymerase treatment of the vector	179
7.2.7.3	PCR amplification of the Insert	180
7.2.7.4	T4 polymerase treatment of the insert.....	180
7.2.7.5	Annealing of the vector and insert	181
7.2.7.6	Transformation of the annealing product into ultracompetent <i>E. coli</i>	181
7.2.7.7	DNA purification and sequence determination.....	181
7.2.7.8	Preparation of <i>E. coli</i> glycerol stocks	182
7.2.8	Production and purification of GyrB24, GyrB and GyrA proteins .	182
7.2.9	SDS-PAGE analysis	184
7.2.10	Crystallography.....	185
	References	189

Abbreviations and Symbols

<i>A. baumannii</i>	<i>Acinetobacter baumannii</i>
ABC	ATP-binding cassette superfamily
ADME	Absorption, distribution, metabolism and excretion
ADPNP	5'-adenylyl- β,γ -imidodiphosphate
ALLIGATOR	Algorithms for LIgand Testing and Ordering of Results
ATCC	American type culture collection
ATP	Adenosine triphosphate
ADP	Adenosine diphosphate
APS	Ammonium persulfate
ASU	Asymmetric unit
<i>B. burgdorferi</i>	<i>Borrelia burgdorferi</i>
Boc	<i>tert</i> -butyloxycarbonyl
BSA	Bovine serum albumin
CANGAROO	Cleft Analysis by Geometry Algorithm Regardless of Orientation
CDI	Carbonyl diimidazole
CLSI	Clinical & Laboratory Standards Institute
CTD	C-terminal domain
CV	Column volumes
CYP	cytochrome P450
DCM	Dichloromethane
dCTP	Deoxycytosinetriphosphate
dGTP	Deoxyguanidinetriphosphate
δ	Chemical shift
DMF	Dimethyl formamide
DNA	Deoxyribonucleic acid
dNTP	Deoxynucleotidetriphosphate
DTT	Dithiothreitol
<i>E. aerogenes</i>	<i>Enterobacter aerogenes</i>
<i>E. cloacae</i>	<i>Enterobacter cloacae</i>
<i>E. coli</i>	<i>Escherichia coli</i>
<i>E. faecalis</i>	<i>Enterococcus faecalis</i>
ECDC	European Centre for Disease Prevention and Control
EDC	1-Ethyl-3-(3-dimethylaminopropyl)carbodiimide
EDTA	Ethylenediaminetetraacetic acid
ELEFANT	ELEction of Functional groups and ANchoring to Target sites
EI	Electron impact
ESI	Electrospray ionisation
EMA	European Medicines Agency
<i>F. tularensis</i>	<i>Francisella tularensis</i>

FT	Fourier transform
HEPES	4-(2-hydroxyethyl)-1-piperazineethanesulfonic acid
HMBC	Heteronuclear multiple bond correlation
HIPPO	Hydrogen bonding Interaction Prediction Positions Orientations
HMQC	Heteronuclear multiple-quantum coherence
HPLC	High pressure liquid chromatography
HOBt	Hydroxybenzotriazole
HRMS	High resolution mass spectrometry
HTS	High throughput screening
ICAAC	Interscience conference on antimicrobial agents and chemotherapy
IPTG	Isopropyl β -D-1-thiogalactopyranoside
IR	infrared
<i>K. pneumoniae</i>	<i>Klebsiella pneumoniae</i>
LB	Lysogeny broth
LC-MS	liquid chromatography – mass spectrometry
LDH	Lactate dehydrogenase
LIC	Ligation independent cloning
LPS	lipopolysaccharide
<i>M. smegmatis</i>	<i>Mycobacterium smegmatis</i>
MH	Müller-Hinton
MIC	Minimum inhibitory concentration
MRSA	Methicillin resistant <i>Staphylococcus aureus</i>
M_w	Molecular weight
<i>N. gonorrhoea</i>	<i>Neisseria gonorrhoea</i>
NAD ⁺	Nicotinamide adenine dinucleotide
NADH	Nicotinamide adenine dinucleotide reduced
NDM-1	New Delhi metallo β -lactamase 1
NEB	New England Biolabs
NMR	Nuclear magnetic resonance
NTA	Nitrilotriacetic acid
NTD	N-terminal domain
PEG	polyethylene glycol
Pet	Petroleum ether
PDB	protein databank
P_i	inorganic phosphate
PPB	Plasma protein binding
PCR	Polymerase chain reaction
PEP	Phosphoenolpyruvate
Pet	Petroleum ether (40-60 °C)
PK	Pyruvate kinase

V_{\max}	Infrared absorption maximum
R_f	retardation factor
RNAP	RNA polymerase
RND	resistance-nodulation-cell division superfamily
ROCS	Rapid overlay of chemical structures
RPM	revolutions per minute
RT	retention time
<i>S. aureus</i>	<i>Staphylococcus aureus</i>
<i>S. pneumoniae</i>	<i>Streptococcus pneumoniae</i>
SAR	Structure activity relationship
SDS-PAGE	Sodium dodecyl sulfate- polyacrylamide gel electrophoresis
S_NAr	Nucleophilic aromatic substitution
SPIDER	Structure Production with Interactive DEsign of Results
T3P	Propane phosphonic acid anhydride
TEMED	Tetramethylethylenediamine
TEV	Tobacco etch virus
TFA	trifluoroacetic acid
TGED	Tris, glycerol, EDTA and DTT
THF	Tetrahydrofuran
TLC	Thin layer chromatography
TLS	translation libration screwmotion
TOPRIM	topoisomerase primase
TMS	Trimethylsilyl
Tris	Tris(hydroxymethyl)aminomethane
UV	ultraviolet
λ_{\max}	Wavelength of maximum UV absorption
ZINC	ZINC is not commercial

Amino acid notation

Alanine	Ala	A	Methionine	Met	M
Cysteine	Cys	C	Asparagine	Asn	N
Aspartate	Asp	D	Proline	Pro	P
Glutamate	Glu	E	Glutamine	Gln	Q
Phenylalanine	Phe	F	Arginine	Arg	R
Glycine	Gly	G	Serine	Ser	S
Histidine	His	H	Threonine	Thr	T
Isoleucine	Ile	I	Valine	Val	V
Lysine	Lys	K	Tryptophan	Trp	W
Leucine	Leu	L	Tyrosine	Tyr	Y

Chapter 1 Introduction

1.1 Antibacterial resistance and the need for new antibacterial agents

Antibacterial agents have changed the world, not only transforming medicine and healthcare, but also dramatically altering the strains of bacteria that live alongside us. First discovered almost a century ago, antibacterial compounds have allowed developments in medicine that would have been unthinkable without them. Infections that once were seriously debilitating or even fatal can now be cured with a short course of an antibacterial compound and being able to administer antibiotics prophylactically has allowed many surgical interventions to become routine. However, as use of antibacterial compounds has increased, so too has the spread of bacterial strains which can resist their effect. The selection pressure that widespread antibacterial use has generated has encouraged the emergence and spread of strains resistant to all of our commonly used antibacterial agents. If new antibacterial drugs are not developed in time to replace ones which are no longer effective, we may face a serious healthcare disaster.

In 2014 the World Health Organisation (WHO) reported that: “A post-antibiotic era—in which common infections and minor injuries can kill—far from being an apocalyptic fantasy, is instead a very real possibility for the 21st century” in a 256 page report detailing the spread of antimicrobial resistance worldwide.¹ A report commissioned by the UK government has recently issued a similarly stern warning based on models of the impact of antimicrobial resistance: if nothing is done to stop the spread of resistance, 300 million people will die prematurely due to antibiotic resistance between now and 2050.²

Bacterial resistance is already causing serious difficulties for the treatment of common infections. High resistance rates to some of our most important antibacterial drugs, the 3rd generation cephalosporins and the fluoroquinolones, have been observed in *Escherichia coli* and *Klebsiella pneumoniae* in all regions which report data to the WHO. These bacteria are responsible for common infections such as urinary tract infections

and pneumonia and due to the spread of resistance often have to be treated with carbapenems which are one of our last lines of defence. Even more worryingly, carbapenem resistant *K. pneumoniae* has been reported at levels up to 54%. Another serious concern is the spread of methicillin resistant *Staphylococcus aureus* (MRSA), which has become so widespread that second line antibacterials are now relied on to treat skin and wound infections.¹

Carbapenem resistance is conferred by the presence of carbapenemase enzymes such as *K. pneumoniae* carbapenemase-2 (KPC-2) and New Delhi metallo- β -lactamase-1 (NDM-1) which have spread very rapidly across the globe and been transmitted between bacterial species *via* plasmids. Treatment options for carbapenem resistant infections are limited to just tigecyclin and colistin. Until recently, the only known mechanisms of resistance to colistin and other polymyxins were chromosomally mediated, but in late 2015 a plasmid mediated colistin resistance mechanism (MCR-1) was found in livestock and some human patients in China.³ In the months following this report the MCR-1 gene has been detected in *E. coli* isolates from the Netherlands⁴, Laos, Thailand, France and Nigeria⁵ and *Salmonella* isolates from France⁶ and Portugal⁷.

Antibiotic resistance places a huge burden on healthcare systems worldwide, as resistant infections are harder to treat and lead to worse outcomes for patients. New antibacterial compounds are desperately needed to fill the void left by losing the utility of our current drugs.

1.2 Bacteria as drug targets

Antibacterial compounds target a range of features and processes which are present in bacteria, but not in mammalian cells. These include features of the bacterial membrane such as the proteins which cross link the peptidoglycan cell wall, and processes which are carried out somewhat differently in bacterial cells such as protein synthesis and DNA replication. A summary of the key bacterial targets is given in Table 1.1.

Table 1.1 Targets of common classes of antibacterials.

Bacterial process targeted	Molecular Target	Antibacterial Class
Cell wall synthesis	peptidoglycan cross-linking	β -lactams
	peptidoglycan synthesis	glycopeptides
	isoprenyl phosphatase	bacitracin
	enolpyruvyl transferase	fosfomycin
Protein synthesis	30S ribosomal subunit	aminoglycosides and tetracyclines
	50S ribosomal subunit	chloramphenicol, macrolides, lincosamides and oxazolidinones
	elongation factor G	fusidic acid
Nucleic acid synthesis	Dihydropterate synthetase	Sulfonamides
	Dihydrofolate reductase	trimethoprim
DNA replication and Transcription	Type II topoisomerases	Fluoroquinolones
	RNAP	rifamycins
Bacterial membrane	membrane damage	polymixins and daptomycin

1.2.1 Gram positive and Gram negative bacteria

Bacteria can be grouped into two classes, Gram negative and Gram positive, according to whether or not they retain crystal violet dye. Gram positive bacteria have a single phospholipid membrane surrounded by a thick peptidoglycan layer whereas Gram negative bacteria have a thinner peptidoglycan layer which is surrounded by a second phospholipid membrane (Figure 1.1). Crystal violet dye binds to the peptidoglycan layer of Gram positive bacteria, but cannot pass through the outer membrane of Gram negative bacteria, so they remain unstained. The difference in the structures of the cell wall between Gram negative and Gram positive bacteria mean that they often respond differently to antibiotics.

The dual membrane structure of Gram negative species can reduce the permeability of the cell wall to antibiotics.⁸ Many antibiotics with good antimicrobial activity against Gram positive species are not active against Gram negative organisms. This includes many of the β -lactam antibiotics, which act by inhibiting the synthesis of the peptidoglycan cell wall. Gram negative bacteria also possess efflux pumps within the cell wall, which are able to expel foreign substances from the cell or prevent them from passing through the bacterial membrane. Drugs which are unable to diffuse through the peptidoglycan cell membranes or are susceptible to efflux will be unable

to accumulate within Gram negative cells at a sufficient concentration to have an antibiotic effect.⁹

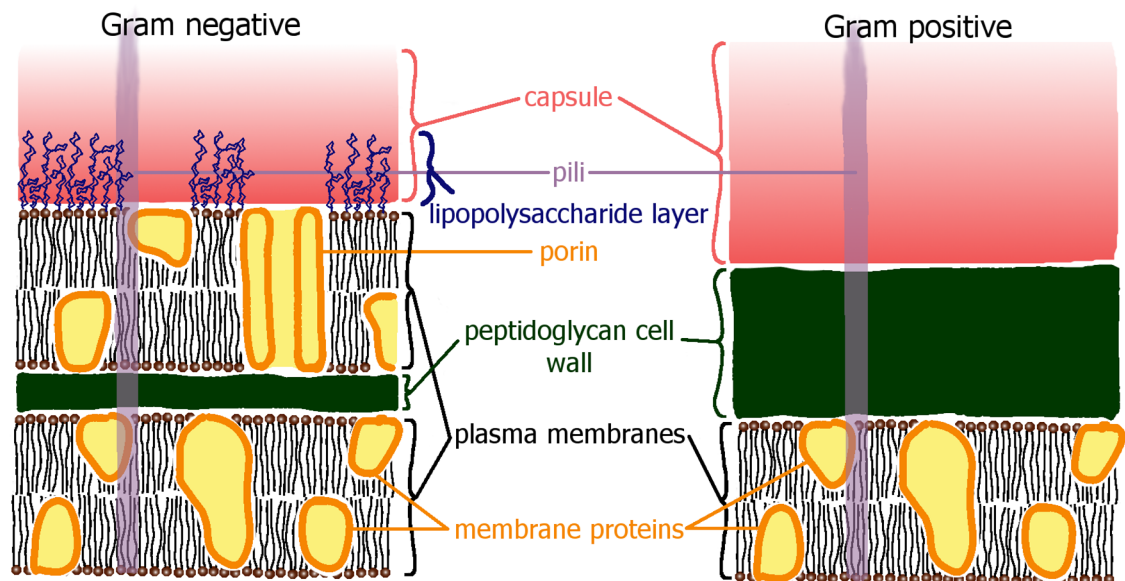


Figure 1.1 Structures of the cell wall in Gram negative and Gram positive bacteria.

The outer membrane of Gram negative bacteria contains a large proportion of lipopolysaccharide (LPS) molecules which make up the outer part of the cell membrane. Lipopolysaccharides are comprised of a lipid section and a polysaccharide section (Figure 1.2). The lipid section is called Lipid A and is comprised of a series of fatty acids attached to a pair of glucosamine residues. Lipid A is highly conserved among Gram negative species.¹⁰ Each glucosamine residue is attached to a phosphate group. The oligosaccharide portion of the LPS is comprised of a core oligosaccharide, which is bound to lipid A, and an O antigen.⁸ The composition of this region is highly variable between strains of bacteria. The O antigen region is highly endotoxic and produces a strong immune response in animals.¹¹ The lipopolysaccharide layer hampers the movement of lipophilic small molecules through the membrane as they cannot pass the highly charged region near to the surface.⁸

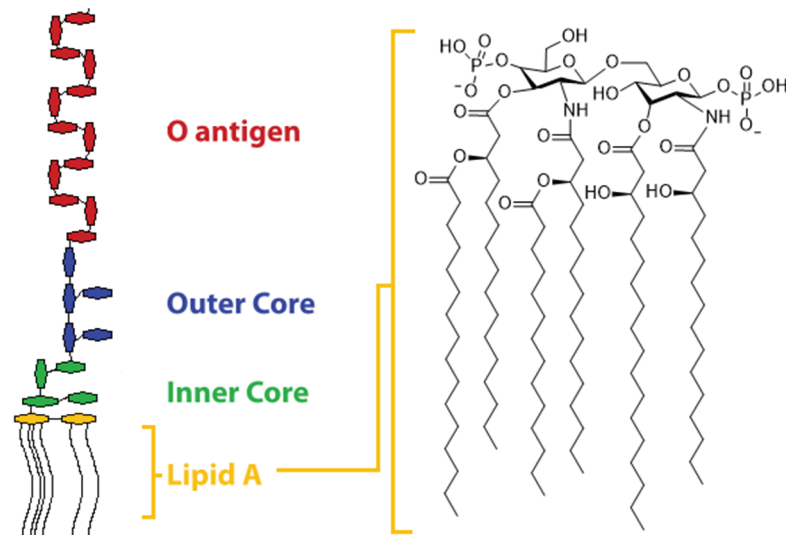


Figure 1.2 Lipopolysaccharide composition and chemical structure of lipid A.

The membranes of bacterial cells provide the most daunting challenge to the design of effective antibacterial compounds. The membranes are designed to protect bacterial cells from environmental threats including toxic chemicals. The degree to which bacterial cells are susceptible to an antibacterial compound often depends on whether it is able to penetrate the bacterial membrane.

1.3 Mechanisms of resistance

The mechanisms by which bacteria resist the effects of antibiotics are numerous and varied with some general mechanisms by which bacteria can inure themselves to the effects of a broad range of chemical species and some specific mechanisms which provide resistance to one specific antibacterial or class of antibacterials. Resistance can be innate, acquired or adaptive. An example of innate resistance is the resistance of Gram negative bacteria to glycopeptide antibiotics such as vancomycin due to poor penetration of their membranes.¹² Acquired resistance occurs through acquisition or modification of bacterial genes that provide a survival advantage to the bacteria when in the presence of an antibacterial, for example the acquisition of a gene coding for a β -lactamase which provides resistance to β -lactam antibiotics such as penicillin¹³. Adaptive resistance is a modification of the bacteria's phenotype that provides a survival advantage but is not due to a genetic mutation, for example, an increase in the transcription of efflux pump genes¹⁴.

Resistance arises due to the selection pressure placed on bacteria in the presence of an antibacterial compound. A variation present in only a small part of a population which provides a protective effect in the presence of an antibiotic will provide an advantage to those bacteria that possess it and so their population will increase relative to other bacteria that do not possess the beneficial mutation. Bacteria do not only pass on genetic information when they replicate, they can also pass genes to other bacteria in a process called horizontal gene transfer. Genes are packaged into small DNA loops called plasmids and passed on to other bacteria in the vicinity.¹⁵

There are many ways in which bacteria can increase their resistance to an antibiotic. Some mechanisms are general and provide resistance to a range of antibiotics, for example increased production of efflux pumps or decreased production of porins. Others are specific to a class of antibiotics, including methods of inactivating the antibiotic, modification of the antibiotic's target site, metabolic bypass so that the target of the antibiotic is no longer essential for cell survival and increased production of the target protein so that there is enough uninhibited protein for the cell to survive.¹⁶ Many of these resistance mechanisms have a survival cost in the absence of the antibacterial, but they will persist at low levels in a population of bacteria and if the antibacterial is reintroduced the resistant strain will rapidly regain prominence. Three of the most important types of resistance are described below.

1.3.1 Modifications to the membrane to control penetration and efflux

Compounds whose target is within the cytoplasm must be able to penetrate the bacterial membrane in order to exert their antibacterial effects. Many species of bacteria are intrinsically resistant to certain antibacterial compounds due to the barrier that their membrane provides.¹² Bacteria can also acquire increased resistance *via* genes encoding modified membrane proteins or develop adaptive resistance by producing more or less of certain membrane proteins.⁹

1.3.1.1 Porins

Polar small molecules are more easily taken up by the cell than very large or hydrophobic molecules due to the presence of porins in the membrane. Porins are β -barrel proteins that cross the outer membrane of the cell allowing transport of small polar molecules into the cell.¹⁷ Most porins possess a loop called L3 which bends into the channel of the porin creating a constriction zone which limits the size of molecules which can pass through the porin and controls the polarity of the pore. Some porins are general, allowing transport of a wide range of molecules of the appropriate size and hydrophobicity, whilst others are specific to a single molecule or class of molecules.⁹ Porins tend to have size exclusion limits which are close to the average size of a number of antibiotics, and so limit the rate at which these antibiotics can diffuse into bacterial cells. One of the best studied porins is the OmpF porin from *E. coli*. It has been identified as the main route of entry for the fluoroquinolones and beta-lactam antibacterials. The OmpF porin forms trimers in the membrane as shown in Figure 1.3.¹⁸

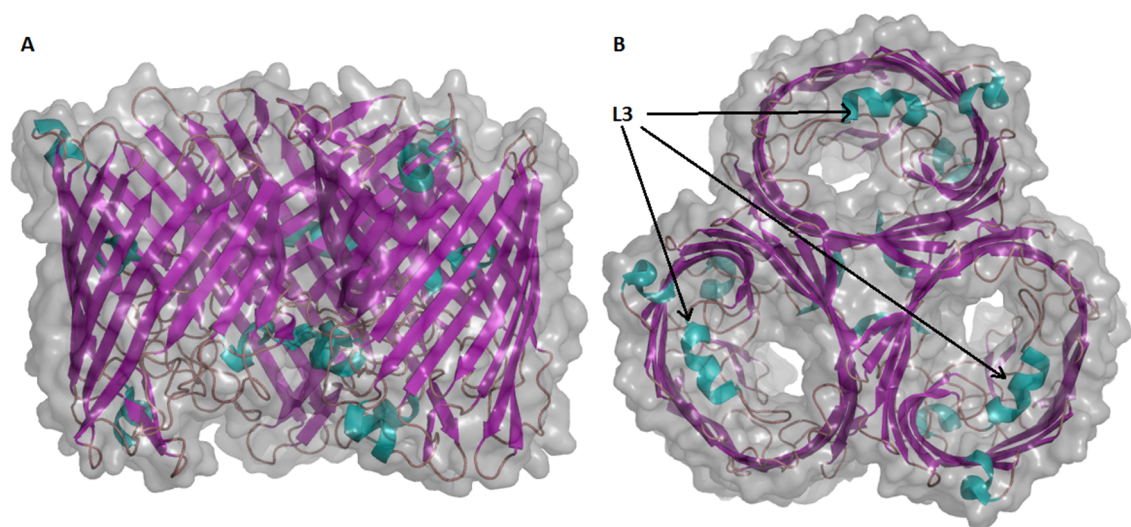


Figure 1.3 Trimer of OmpF porins from *E. coli* (PDB 3K19)¹⁹. A. View from in the plane of the membrane. B. Looking through the membrane with the L3 loops indicated.

Mutations that reduce or prevent the expression of porins or narrow the pore of a porin so that antibiotics cannot enter a cell can confer increased resistance to antibiotics. Point mutations which prevent the gene for the porin OprD from being transcribed in *P. aeruginosa* have been identified in carbapenem-resistant isolates²⁰.

Mutations in the loop 3 of porins are frequently found to confer antibiotic resistance. For instance, a glycine to aspartate mutation in loop 3 of the OmpF/OmpC-like protein of *E. aerogenes* leads to decreased susceptibility to β -lactams²¹. Mutations effecting porins have been linked to resistance to β -lactams, fluoroquinolones, tetracyclines and chloramphenicol.⁹

1.3.1.2 Efflux pumps

Active efflux is a general mechanism of resistance which is of vital importance to understanding the actions of antibacterial compounds. Foreign substances, including bile salts, dyes and drug molecules, are pumped out of bacterial cells *via* efflux pumps, preventing them from accumulating in the bacterial cell at a high enough concentration for them to exert a toxic effect. There are a variety of classes of efflux pump which are present in different species and have different mechanisms and energy sources.²² Some families of efflux pump, including the ATP-binding cassette superfamily (ABC), have members in a wide range of cell types including eukaryotic cells as well as Gram negative and Gram positive bacteria, others such as the resistance-nodulation-cell division superfamily (RND) are predominantly found in Gram negative bacteria with only a small number of examples found in other cell types.²³

The AcrAB-TolC efflux pump is a well-studied efflux pump system from the RND superfamily.²⁴ It is found in several Gram negative species including *E. coli*, *E. aerogenes* and *E. cloacae*.²⁵⁻²⁷ It has an intramembrane domain, AcrB, which is able to bind to a wide range of compounds including dyes, detergents and many antibiotics.^{28,29} Binding of a small molecule induces a structural change which transports the compounds into a transmembrane domain AcrA which can associate to the tolC channel in the outer membrane and so expel the compounds from the bacterial cell. The process is coupled to a H^+ gradient (Figure 1.4).³⁰

It was recently discovered that a small protein AcrZ can bind to AcrB and modify the activity of the pumps, *E. coli* mutants lacking AcrZ are sensitive to some antibiotics which are normally exported by AcrAB-TolC³¹. Cryo-electron microscopy combined with crystal structures of the individual components of the pump has been used to determine the structure of the whole pump assembly³². To stabilise the assembly, two

constructs were prepared, one in which the AcrA and AcrZ components were fused and one in which the AcrB and AcrA components were fused. Both constructs were designed with flexible linkers which would not interfere with interactions between the proteins. The AcrAB-TolC pump is composed in a 3:6:3 ratio of AcrB:AcrA:TolC. An expression strain was used to co-produce the fusion proteins AcrA-AcrZ and AcrA-AcrB along with TolC enabling the isolation of the assembled pump with all components remaining associated after purification thus allowing the complex to be visualised using cryo-electron microscopy.

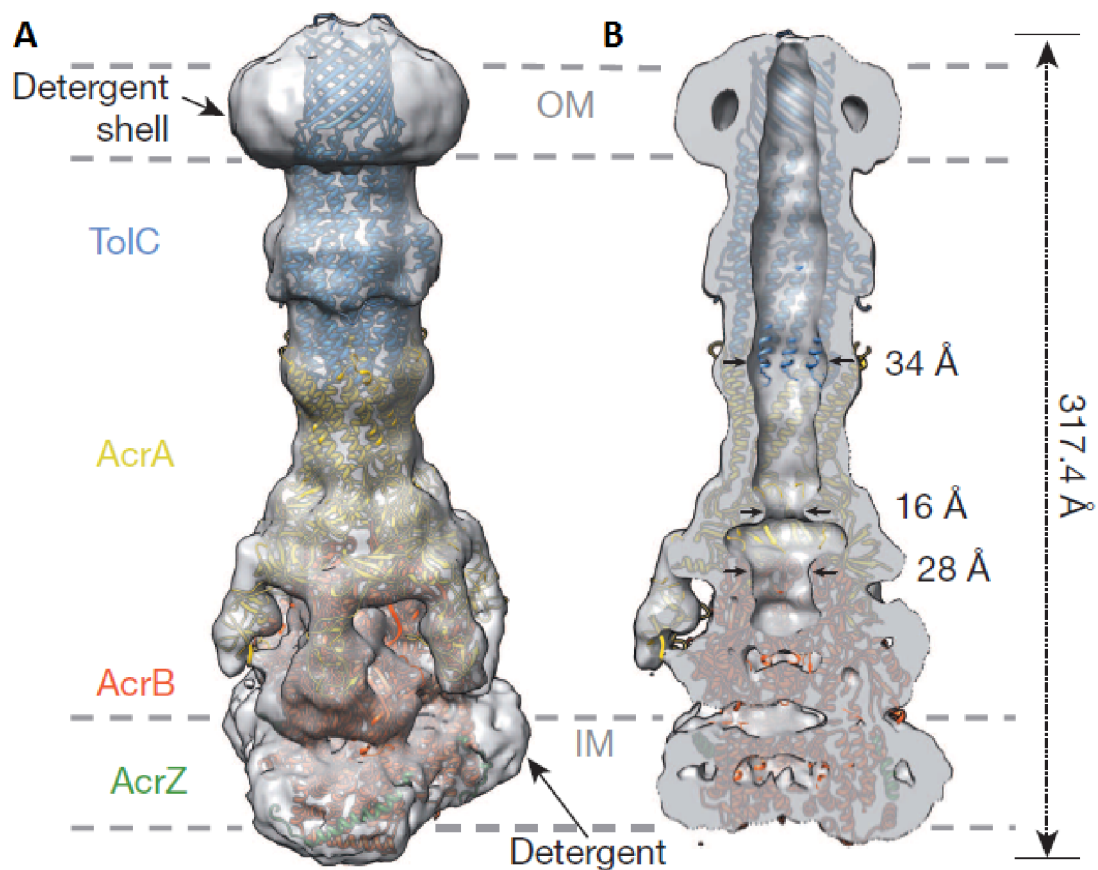


Figure 1.4 Pseudo-atomic model of the AcrABZ-TolC efflux pump. A, reconstructed map from cryo-EM and crystal structures, TolC and AcrBZ are homotrimers which interact with 6 AcrA protomers. B, A slice through the model shows a continuous conduit from the intermembrane space to the outer membrane. Adapted from Du *et. al.* used with permission.³²

Many compounds which show activity in Gram positive bacteria but not in wild type Gram negative bacteria do show activity in Gram negative bacteria which have been genetically modified to lack the tolC channel. This suggests that the resistance is due in great part to the action of the efflux pump.^{26,33}

Resistance *via* efflux can be very hard to design around when developing new antibacterials. As efflux pumps act in a general fashion, it is hard to rationally design compounds which are able to evade efflux. We do not currently know enough about the way in which drug molecules are bound to efflux pumps and the structures of the binding sites, nor what properties of a molecule will make it susceptible to the action of a particular efflux pump, and so designing compounds which can resist efflux is generally a matter of empirical “make and test” optimisation. Several studies have pointed out a correlation between polarity and efflux, but the correlation is not strong enough to enable design of efflux resistant drugs based on physicochemical properties alone.^{34,35}

1.3.2 Resistance *via* target site modification

Mutations that confer resistance often involve residues in the active site of the protein target of an antibacterial compound. They can provide an advantage by disfavouring the binding of the drug whilst still allowing the protein to carry out its normal function. These mutations may not provide full resistance on their own, but if the selection pressure caused by the presence of the antibiotic persists over extended periods of time then several beneficial mutations may arise in sequence eventually giving full resistance.¹² A mutation that grants resistance may confer a fitness cost, as the mutated protein may be less able to carry out its normal function, however this fitness cost may be counteracted by a compensatory mutation if the selection pressure persists.³⁶

Selection for resistant mutants by antibiotics can be reduced by using dual-target antibiotics or combination therapy, as single mutations are less likely to provide a sufficient advantage to the bacteria for the selection pressure to act upon them. Dual-targeting is not a perfect solution however; bacteria have been able to develop resistance to the fluoroquinolones, which target both DNA gyrase and topoisomerase IV. Mutations in the primary enzyme target (which varies between different fluoroquinolones and bacterial species) have often been shown to confer a small selective advantage and so are selected for, mutations in the secondary enzyme target can then be picked up, conferring total resistance to the drug.³⁷

1.3.3 Inactivation of antibiotic molecules

Enzymes which are capable of altering the chemical structure of an antibiotic so that it is no longer able to bind to its target provide a very effective means of resistance. This type of resistance mechanism is most clearly demonstrated in bacteria resistant to β -lactam antibiotics such as penicillin which produce β -lactamase enzymes. β -lactamase enzymes hydrolyse the key lactam ring in the antibiotics thus inactivating them. There are multiple classes of β -lactamases and they have spread rapidly since β -lactam antibiotics first started being used clinically in the 40s. These enzymes may have existed in some strains of bacteria for millennia as a defence against penicillin producing moulds. In recent years, these enzymes have spread into populations of pathogenic bacteria in a response to the selective evolutionary pressure caused by antibiotic usage.³⁸

This type of resistance could be evaded by co-administering a β -lactamase inhibitor with a β -lactam drug, thus restoring some of the activity of the β -lactam. Several combinations are currently in clinical use, but the β -lactamase inhibitors currently available are not active against all β -lactamase enzymes.³⁹

1.4 Methods for antibacterial drug discovery

The first antibacterial compounds to be used clinically, Salvarsan and the sulfa drugs, were discovered by screening collections of small molecules to look for selective antibacterial activity. However, after penicillin became a commercial success in the 40s, drug companies turned their focus instead to empirical screening of extracts from microorganisms. Many drug companies focussed their research efforts on culturing bacteria from the soil and screening it against strains of pathogenic bacteria to look for any cultures that appeared to kill the bacteria. The antibacterial compounds could then be extracted, purified and undergo further testing. This period in the 50s and 60s is often referred to as the “golden era” of antibacterial research and many of our currently used antibacterial classes originated from the natural product screens of this time, including the aminoglycosides, polymixins, tetracyclines, cephalosporins, macrolides and glycopeptides.⁴⁰

Once this initial rush of discovery was over, finding novel classes of antibiotics became more challenging. Extracts which showed antibacterial activity almost always contained antibiotics that had already been discovered rather than anything new. In order to save time and effort, techniques were developed to quickly identify whether the effects of a new culture were due to an already known antibacterial compound. These dereplication efforts led to a much greater understanding of the targets and mechanisms of action of common antibacterial compounds and companies were soon able to screen for effects on specific bacterial processes. These directed screens led to the discovery of several more antibacterial classes: monobactams, carbapenems and fosfomicin.⁴⁰

By the late 70s, discovery of new antibacterials had slowed dramatically and efforts began to shift from phenotypic screening to target focussed screening. The understanding of bacterial processes had increased dramatically and it was becoming possible to make and purify protein targets to screen compounds against. At first, natural products were the main chemical material being screened, but this was soon overtaken by the rise in popularity of screening large libraries of synthesised small molecules, particularly libraries generated during the combinatorial chemistry boom of the 90s.

In the last 20 years scientific advances have provided us with a number of new technologies which can aid drug discovery efforts including genomic analysis, structural biology, bioinformatics, high throughput screening (HTS) and computational design. However, despite the application of all these techniques to antibacterial drug discovery, very few new antibacterial classes have been discovered since the 80s.^{41,42}

In parallel to the discovery of new classes of antibacterial agents, improvements to existing classes were being developed. These are often “semi-synthetic” in nature: natural products are extracted from a microbial source and then modified chemically to give a derivative with slightly different properties. Second generation antibacterial compounds have been designed not only to evade mechanisms of resistance but also to have improved pharmacological properties. Derivatives often have improved safety profiles or an increased spectrum of activity. However, they are often susceptible to

the rapid emergence of resistance as existing mechanisms of resistance to other members of the class are adapted.⁴⁰

1.5 DNA topoisomerases

DNA molecules are huge: the genetic material of even the simplest organism requires a DNA molecule which would be many times longer than the organism if arranged as a linear strand. In order for an organism's DNA to fit inside its cells, DNA must be compacted. This is achieved by strict control of its topology. Topology is the study of the geometrical arrangement of parts of an object relative to each other. In terms of DNA, topology describes the ways in which a DNA double helix twists and coils around itself when compacted within a cell. In eukaryotic cells, DNA is compacted by supercoiling and wrapping of the DNA around histones to form chromatin. In prokaryotic cells, DNA is kept in circular rather than linear chromosomes and is highly supercoiled.⁴³ Because the ends are attached to each other in a circular chromosome, knots and supercoils cannot spontaneously relax without breaking one or both strands of the DNA double helix. During replication, daughter chromosomes become entangled forming catenanes (Figure 1.5).

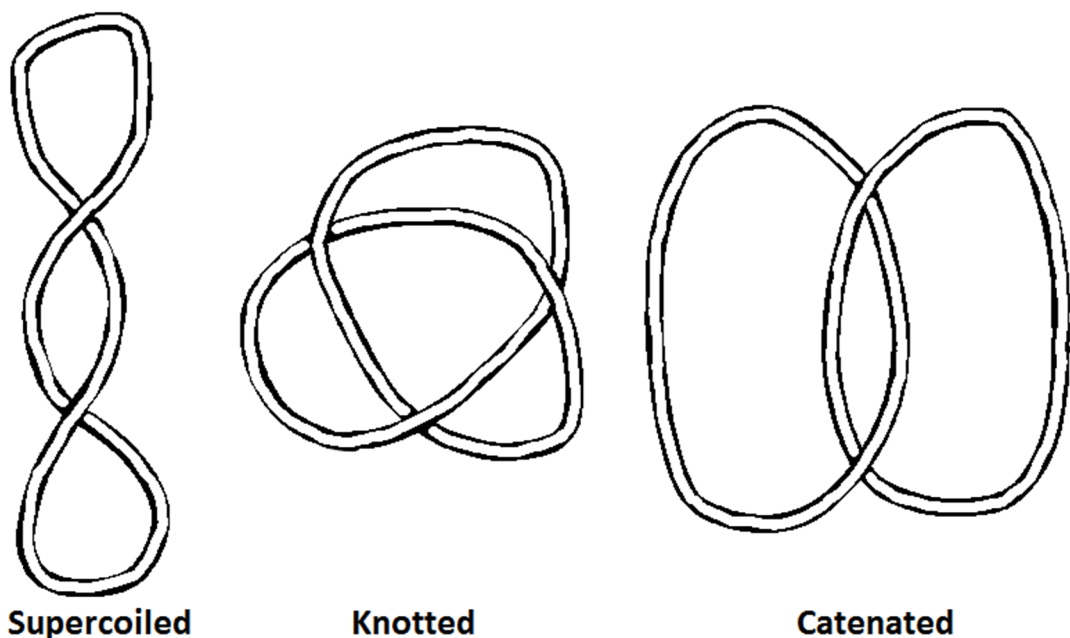


Figure 1.5 Circular pieces of DNA can exist in supercoiled and knotted topologies. Separate circular chromosomes can become entangled in catenanes.

Topoisomerase enzymes are responsible for managing the topology of DNA.⁴⁴ DNA must be locally relaxed allow transcription and replication to occur and chromosomes must be separated prior to cell division.⁴⁴ The type I topoisomerases relax supercoils by making single strand breaks so that tension can be relieved by free rotation of the helix around the unbroken strand. This process reduces the energy of the system and so is ATP independent. The type II topoisomerase increase the level of supercoiling by making double strand breaks and intertwining two strands before resealing the break; this is an ATP dependent process. The same process is used by type II topoisomerases which separate catenated chromosomes following replication (Figure 1.6).

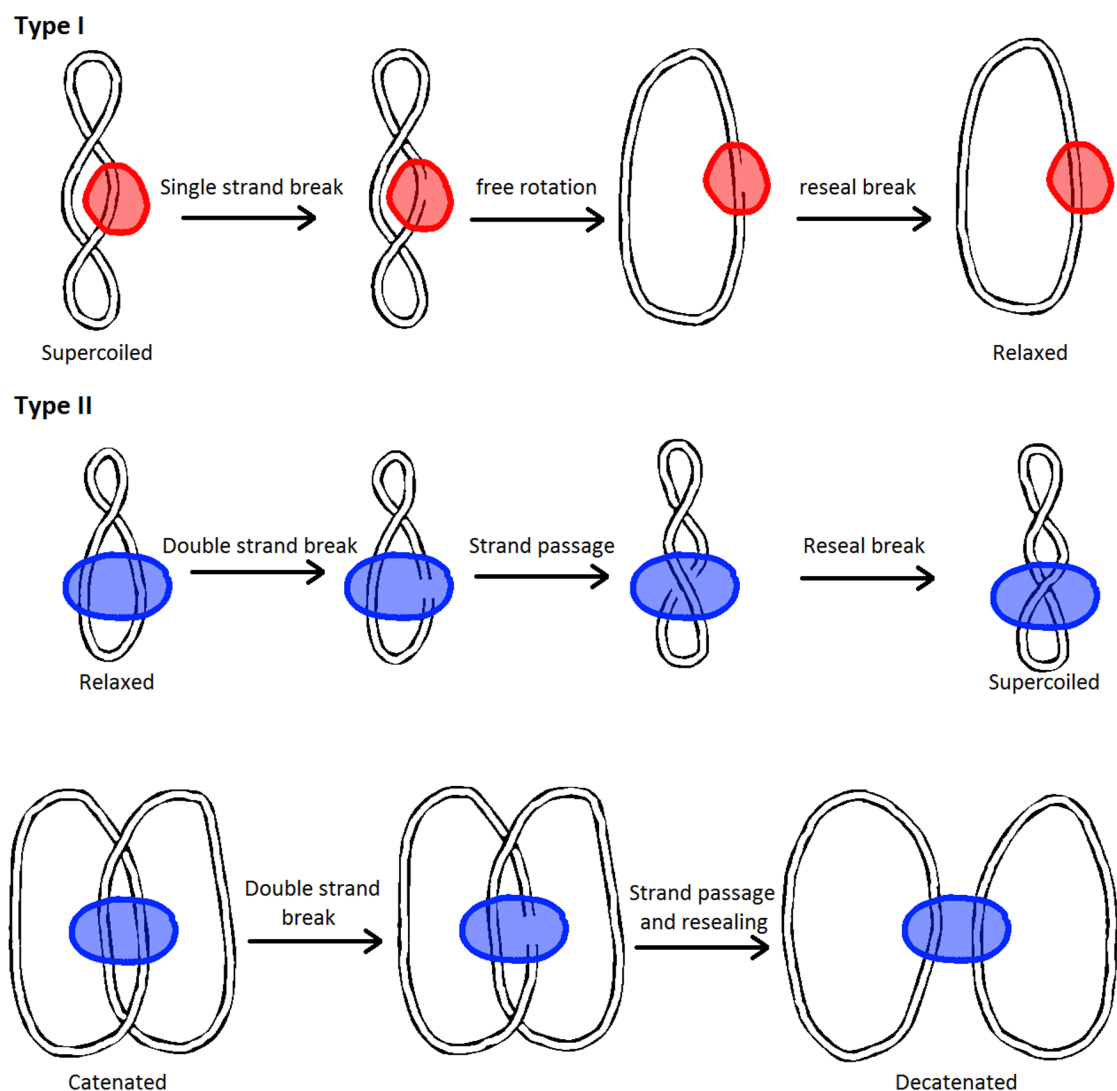


Figure 1.6 General mechanisms of topoisomerase enzymes. Type I topoisomerases (red) make single strand breaks and allow supercoils to relax by free rotation around the intact DNA strand. Type II topoisomerases (blue) make a double strand break and pass another piece of DNA through the break before resealing it. This process can induce supercoils or decatenate chromosomes.

The topoisomerases are a large class of enzymes with examples characterised from a wide range of species. These enzymes have been well studied in the search for drugs and there are several topoisomerase inhibitors on the market. Cancer drugs that target human topoisomerases include topotecan, a topo I inhibitor and etoposide, mitoxantrone and doxorubicin which are topo II inhibitors. The flouroquinolones are antibiotics which target the bacterial topoisomerases DNA gyrase and topoisomerase IV.⁴⁵

1.5.1 Structure of type II topoisomerases

DNA Gyrase and topoisomerase IV are the two type II topoisomerase enzymes found in bacteria. DNA Gyrase is predominantly responsible for generating negative supercoils and Topoisomerase IV is predominantly responsible for separating entangled DNA strands following replication. DNA gyrase is also able to decatenate chromosomes, but is less efficient than topoisomerase IV.⁴⁶ The two enzymes have a high degree of structural and sequence similarity. Both are A₂B₂ heterotetramers. In DNA Gyrase the two subunits are called GyrA and GyrB and in topoisomerase IV the two subunits are ParC and ParE. ATP hydrolysis occurs in the GyrB and ParE domains and DNA binding occurs in the GyrA and ParC domains. The segment of DNA which is cleaved and resealed by the enzyme is called the gate-segment (or g-segment) and the segment of DNA which is passed through the g-segment is called the transfer segment or t-segment.⁴⁷

The general organisational structure of the DNA gyrase and topoisomerase IV holoenzyme is shown in Figure 1.7. The N-terminal domain of GyrB/ParE (purple) is responsible for ATP hydrolysis. The C-terminal domain of GyrB/ParE (turquoise) interacts with the GyrA/ParC and with the g-segment of DNA. This domain, also called the TOPRIM domain is conserved between several other classes of DNA-associated proteins including type IA topoisomerases and DnaG-type primases.⁴⁸ The N-terminal domain of GyrA/ParC (yellow) interacts with the g-segment DNA and initiates cleavage of the DNA and religation of the DNA following strand passage of the t-segment. The C-

terminal domain of GyrA/ParC (green) is responsible for wrapping of the DNA around the enzyme and controlling passage of the t-segment.⁴⁹

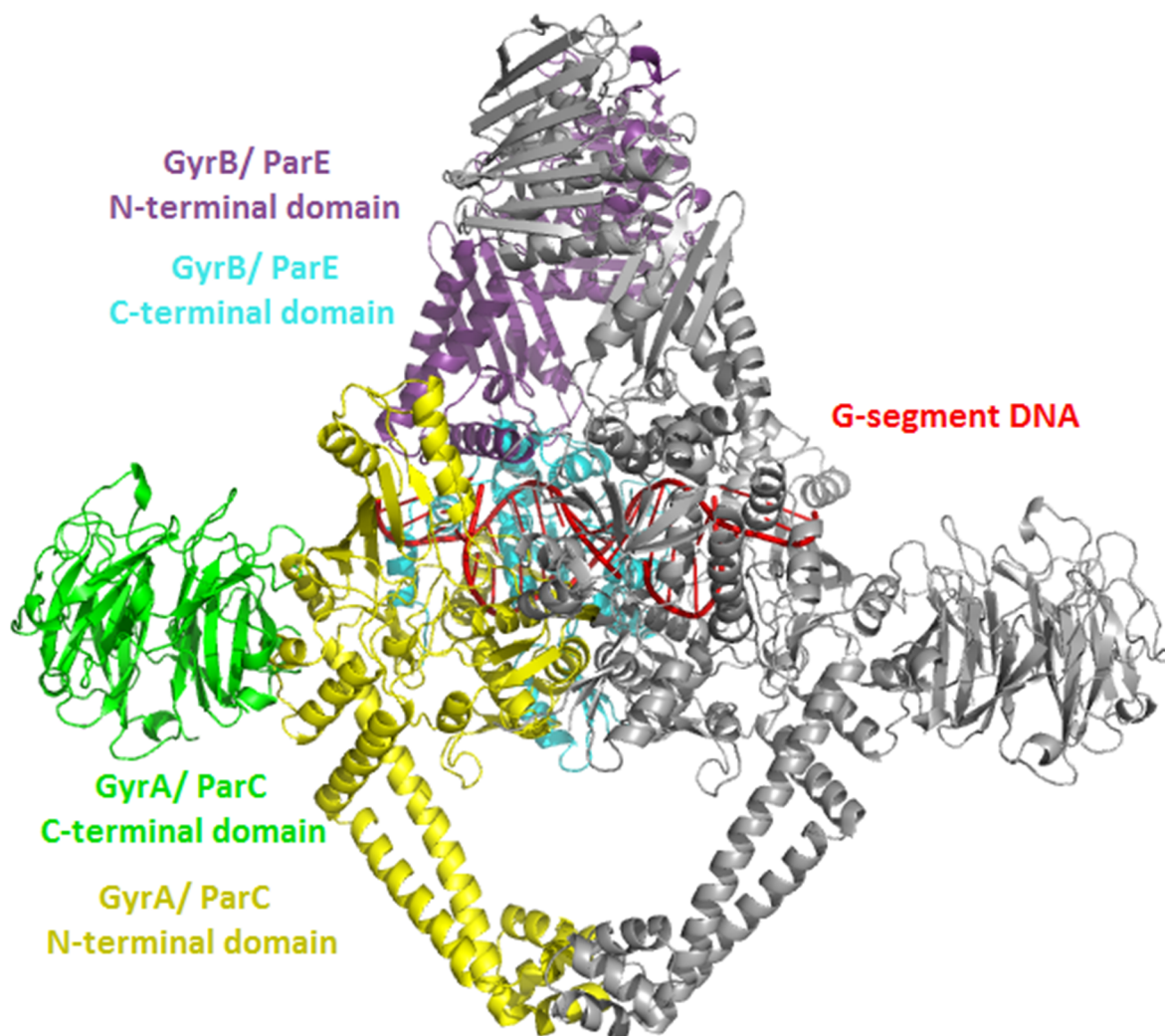


Figure 1.7 Subunit arrangement of the DNA Gyrase and topoisomerase IV holoenzymes. Image comprised of ParE N-terminal domain (purple) from *E. coli* topo IV (1S16)⁵⁰, ParE C-terminal domain (cyan) and ParC N-terminal domain (yellow) from *S. pneumonia* topo IV (3KSA)⁵¹ and GyrA C-terminal domain (green) from *B. burgdorferi* DNA Gyrase (1SUU)⁵².

1.5.1.1 Sequence similarity between DNA Gyrase and topoisomerase IV

DNA Gyrase and topoisomerase IV have a high degree of sequence similarity particularly in the ATP and DNA binding regions, meaning that they are possible to target simultaneously. The sequence similarity with human topoisomerase II is only 12%, which is sufficiently different for the design of compounds selective for DNA gyrase and topo IV over human topo II.⁵⁰ An alignment of the GyrB and ParE sequences

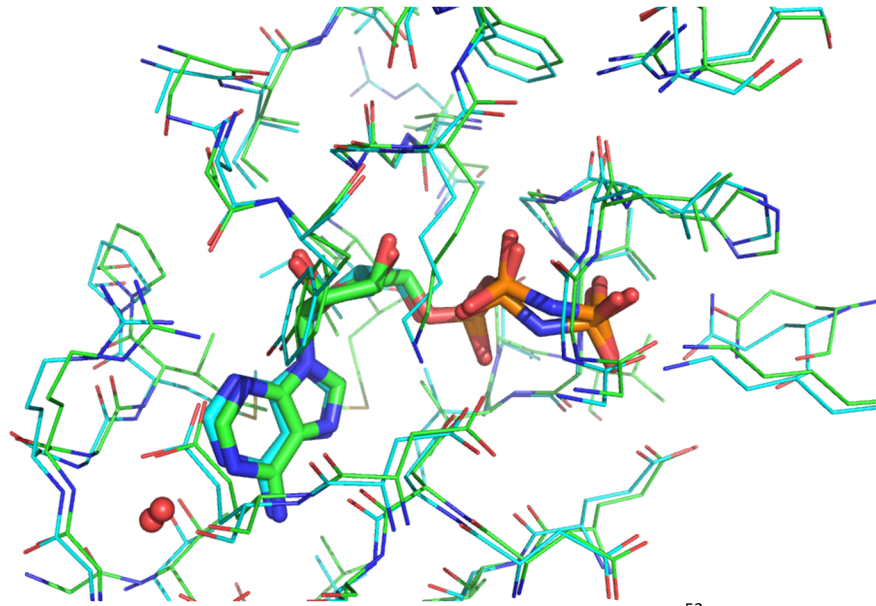


Figure 1.9 Overlap of the ATP binding regions of GyrB in green (1E11⁵³) and ParE in turquoise (1S16⁵⁰) from *E. coli* showing residues within 6 Å of the bound ADPNP (a non-hydrolysable analogue of ATP).

<i>GyrA</i> /1-875	1	MSDLAREITPVNIEELKSSYLDYAMSVIVGRALFDVRDGLKPVHRRVLYAMNVLGNDWNKAYKK	65
<i>ParC</i> /1-752	1	MSDMAERLA...LHEFTENAYLNYSMYVIMDRALFFIGDGLKPVQRRIIVYAMSELGLNASAKFKK	62
<i>GyrA</i> /1-875	66	SARVVGDVIGKYHPHGDSAVYDTIVRMAQPPSLRYMLVDGQGNFGSIDGDSAAAMRYTEIRLAK	129
<i>ParC</i> /1-752	63	SARTVGDVIGKYHPHGDSACYEAMMLMAQPPSYRYPLVDGQGNWFGAPDDPKSFAAMRYTESRLSK	127
<i>GyrA</i> /1-875	130	IAHELMADLEKETVDFVDNYDQTEKIPDVMPTKIPNLLVNGSSGIAVGMATNIPPHNLTEVINGC	194
<i>ParC</i> /1-752	128	YSELLSELGQGTADWVVPNFDGTLQEPKMLPARLPNILLNGTTGIAVGMATDIPPHNLREVAQAA	192
<i>GyrA</i> /1-875	195	LAYIDDEDISIEGLMEHIPGPDFPTAAAINGRGIEEAYRTGRGKVYIRARAEVEVDAKTGRET	258
<i>ParC</i> /1-752	193	IALIDQPKTTLDQLDIVQGPDPYTEAEIITSRAEIRKIYENGRGSRMRRAVWKKEDGA.....	251
<i>GyrA</i> /1-875	259	IIVHEIPYQVNKARLIEKIAELVKEKRVVEGISALRDESDKDGMRIVIEVKRDAVG-EVVLNNLY	321
<i>ParC</i> /1-752	252	VVISALPHQVSGARVLEQIAAQRNKKLPMVDDL RDESDHENPTRLVIVPRSNRVDMDDQMMHLF	316
<i>GyrA</i> /1-875	322	SQTQLQVSFGI--NMVALHHGQPKIMNLKDIIAAFVRRRREVVTRRTIFELRKARDRAHILEALA	384
<i>ParC</i> /1-752	317	ATTDLEKSYRINLNMIGL-DGRRAVKNLLEILSEWLVFRDTRRRRLNRYLEKVLKRLHILEGLL	380
<i>GyrA</i> /1-875	385	VALANIDPIELIRHAPTAEAKTALVANPWQLGNVAAMLERAGDDAARPEWLEPEFGVRDGLYY	449
<i>ParC</i> /1-752	381	VALFNIDEVIEIIRNEDEPK.....PALMSRFG.....	408
<i>GyrA</i> /1-875	450	LTEQQAQAILDRLRQLKLTGLEHEKLLDEYKELLDQIAELLRILGSAADRLMEVIREELVREQFG	514
<i>ParC</i> /1-752	409	LTEQQAQAILEKLRHLAKLEEMKIRGEQSELEKERDQLQGLASERKMNNLLKKELQADAQAYG	473
<i>GyrA</i> /1-875	515	DKRRTEIT--ANSADINLEDLITQEDVVVVTLSHQGYVVKYQPLSEYEAQRRGGKGSAAARIKEEDF	577
<i>ParC</i> /1-752	474	DDRRSPLQEREEAKAMSEHDMLPSEPVTIVLSQMGWVRSAGKHDIDA.....PGLNYKAGDS	530
<i>GyrA</i> /1-875	578	IDRLLVANTHDHLICFSSRGRVYSMKVYQLPEATRGRGRPIVNLLPLEQDERITAILPVTFEFE	642
<i>ParC</i> /1-752	531	FKAADVKGKSNQPVVFDSTGRSYAIDPITLPSA-RG-QQEPLTGKLTLPFGATVDHMLMES...D	590
<i>GyrA</i> /1-875	643	GVKVFMATANGTVKKTVLTEFNRLRTAGKVAIKLVLDGDELI-GVDLTSGEDEVMLFSAEGKVRF	706
<i>ParC</i> /1-752	591	DQKLLMASDAGYGFVCTFNDLVARNRAGKALITLPENAHVMPVVIEDASDMLLAITQAGRMLMF	655
<i>GyrA</i> /1-875	707	KESVVRAMGCNTTGVVIRLGEEDKVVVSLVPRGDGAILTATQNGYGKRTAVAEYPTKSRATKGV	771
<i>ParC</i> /1-752	656	PVSDLPQLS.....KQKQNKIIN--IPSAEAA--RGEDGLAQLYVL.....PPQST	697
<i>GyrA</i> /1-875	772	ISIKVTERNGLVVGAVQVDDDCQIMMITDAGTLVVRTVSEIS-IVGRNTQGVILIRTAEDENVVG	835
<i>ParC</i> /1-752	698	LTIHVQKPK.....IKLRPEELQKVTGERGRRGTLMR.....G	730
<i>GyrA</i> /1-875	836	LQRVAEPVDEEDLDTIDGSAAESDDEIAPEVDVDDPEEEE	875
<i>ParC</i> /1-752	731	LQR...IDRVEIDS-PRRASSGDS.....EE	752

Figure 1.10 Alignment of the GyrA and ParC protein sequences from *E. coli* (UniProt codes P0AES4 and P0AFI2 respectively). Conserved residues are shown in blue.

There is a significant difference in sequence between the C-terminal domains (CTD) of ParC and GyrA. This reflects the different roles of the enzymes. In DNA gyrase the C-terminal domain of GyrA is responsible for wrapping the DNA from the g-segment around the enzyme in order to present the t-segment to GyrB. The conformation of the CTD domain changes upon binding of the g-segment and 120-140bp of DNA is wrapped by the enzyme.⁵⁴ In topoisomerase IV the t-segment is from a different strand of DNA to the g-segment, so DNA does not need to be wrapped around the enzyme to present the t-segment.⁵⁵ The CTD of ParC is able to wrap DNA, but not as effectively as GyrA, this partial binding may facilitate orientation of two separate DNA strands to allow decatenation. The CTD of DNA gyrase adopts a β -pinwheel conformation, whereas topoisomerase IVs CTD adopts a conformation that has been described as a broken β -propeller (Figure 1.11).^{52,56}

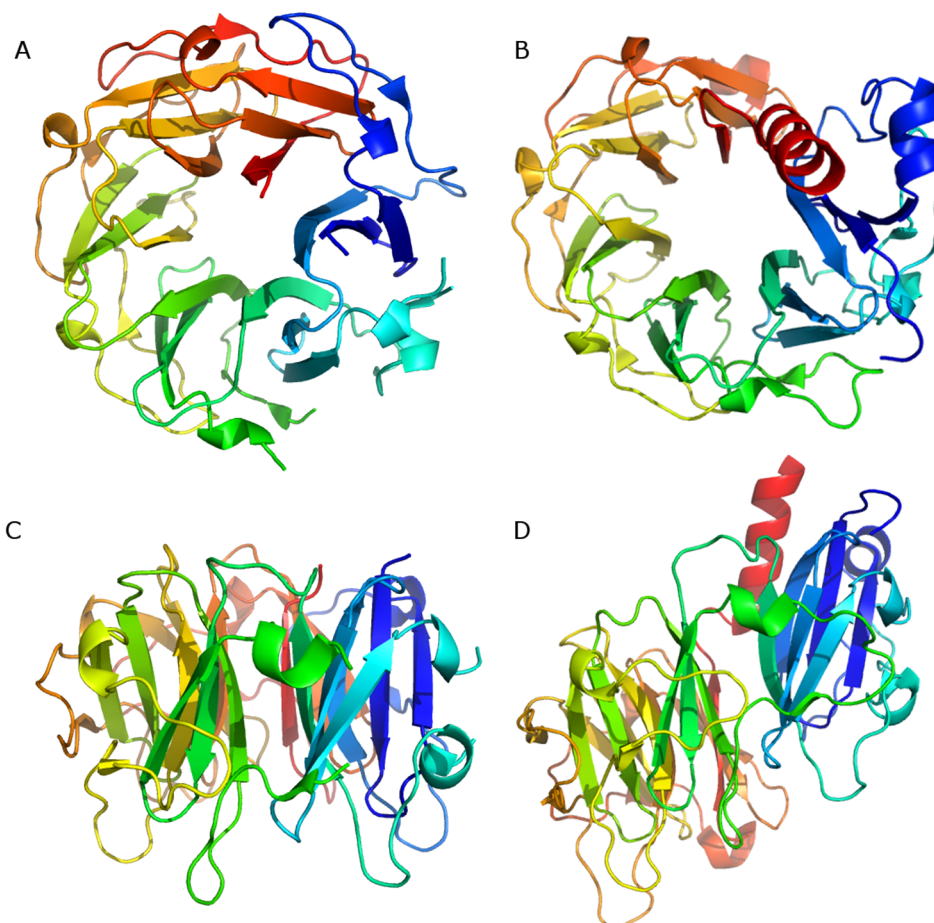


Figure 1.11 C-terminal domains of DNA gyrase (1SUU)⁵² and topoisomerase IV (1WP5)⁵⁶. A. front view of GyrA C-terminal domain showing β -pinwheel fold structure. B. front view of ParE C-terminal domain showing broken β -propeller structure. C. Side view of GyrA CTD. D. Side view of ParE CTD.

1.5.2 Mechanism of type II topoisomerases

The key steps in the mechanism of the type II topoisomerases are shown in Figure 1.12. First, the g-segment of DNA is clamped within a saddle-like groove between the GyrB/ParE subunits and the GyrA/ParC subunits. The t-segment of DNA then enters the gap between the GyrB/ParE subunits (Figure 1.12, conformation A). The presence of the t-segment of DNA and the binding of a molecule of ATP to each of the two GyrB/ParE units induces a conformational change, which closes the GyrB/ParE clamp thus trapping the t-segment (Figure 1.12, conformation B).⁵³ A further conformational change induces cleavage of the g-segment and pulls the cleaved ends apart to create a gap through which the t-segment passes (Figure 1.12, conformation C). The GyrA/ParC N-terminal gate then opens to allow release of the t-segment (Figure 1.12, conformation D) and the enzyme then resets to its initial conformation.⁴⁷

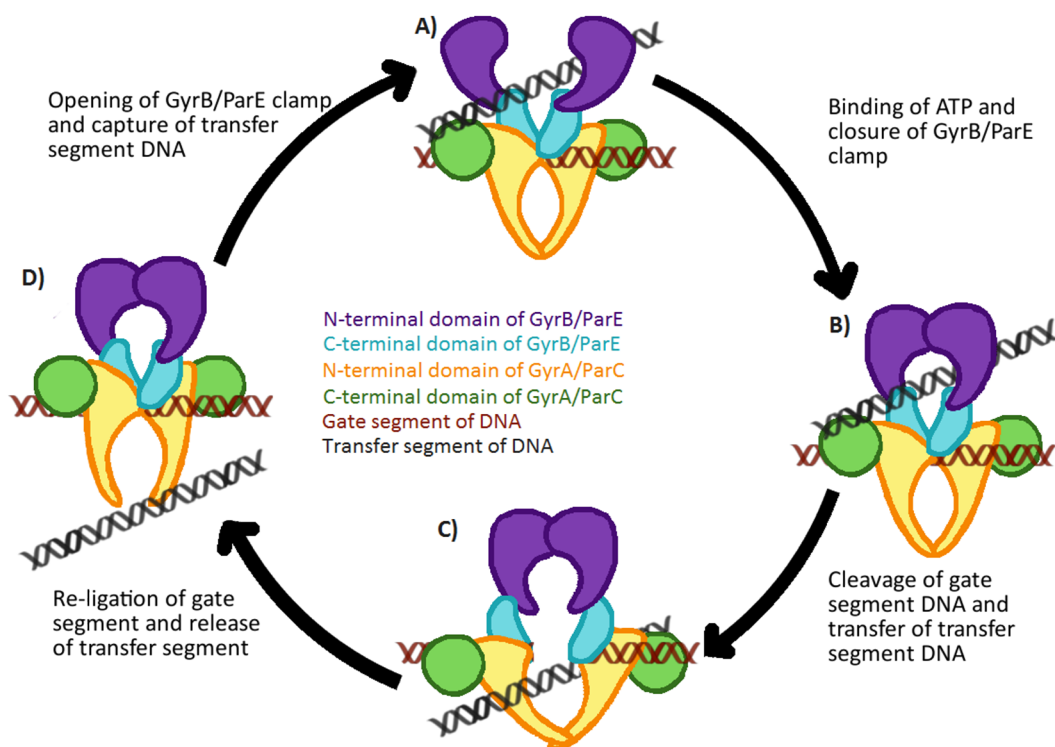


Figure 1.12 Conformational changes in type II topoisomerases. A) the GyrB/ParE domains are in an open clamp position and the t-segment has entered between the GyrB/ParE domains. B) The GyrB/ParE clamp has closed around the t-segment. C) A double strand break has been made in the g-segment and a conformational change has pulled the cleaved ends of the DNA apart and moved the t-segment through the gap. D) The g-segment has been re-ligated and the GyrA/ParC clamp has opened to allow the t-segment to leave. In the case of DNA gyrase, the g- and t-segments are part of the same DNA molecule with 120-140 base pairs separating them. In the case of topoisomerase IV, the g- and t-segments are from separate chromosomes.

The following sections will give a more detailed account of the molecular processes involved in the each of the steps involved in the mechanism of these enzymes.

1.5.2.1 Conformational changes in GyrB/ ParE

Figure 1.13 shows *S. pneumoniae* topoisomerase IV with the ParE N-terminal domains in the open clamp position. The ATP binding domain (in the N-terminal portion of ParE, purple) and the DNA binding domain of ParE (in the C-terminal portion of the protein, cyan) are connected by a flexible hinge which allows the protein to undergo a significant conformational change upon binding of the t-segment of DNA and two molecules of ATP.

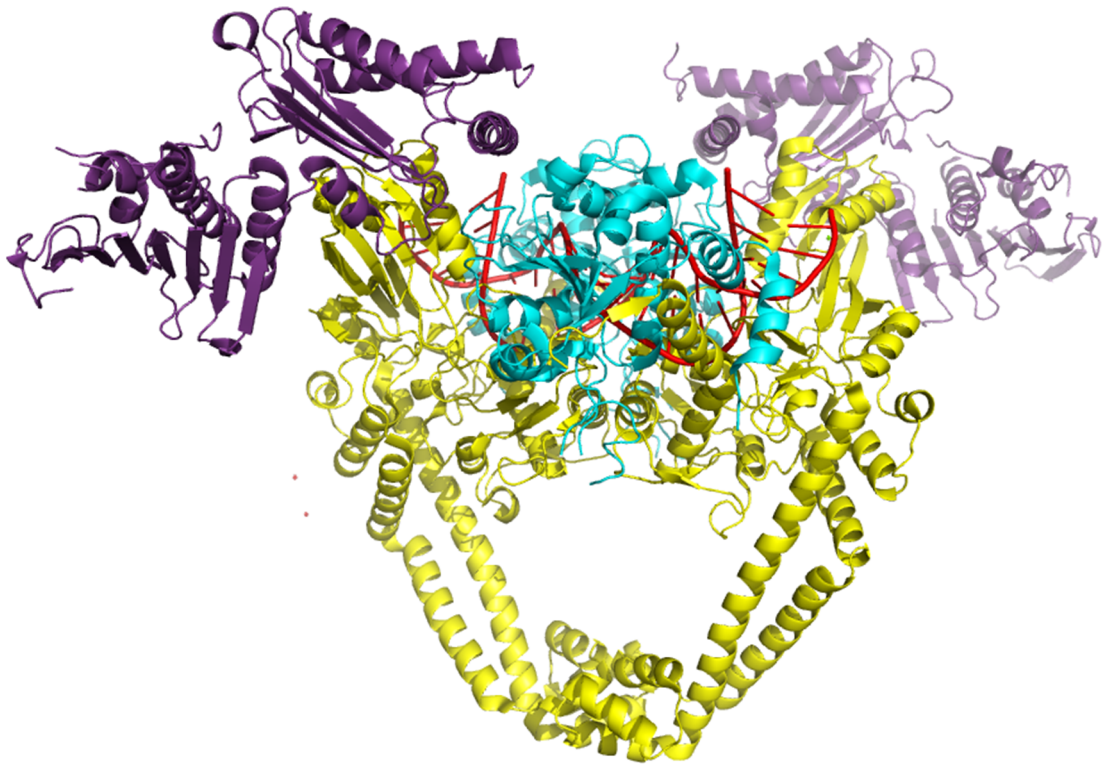


Figure 1.13 Crystal structure of *S. pneumoniae* topoisomerase IV with the ParE clamp in the open position (4I3H)⁴⁹. ParE N-terminal domain in purple, ParE C-terminal domain in cyan, ParC N-terminal domain in yellow and g-segment DNA in red. The ParC C-terminal domain is omitted.

In the crystal structure of topoisomerase IV in the open clamp configuration, several loops near the ATP binding pocket are disordered (Figure 1.14, A). This indicates a high degree of conformational flexibility in these chains in the absence of ATP. An α -helix at the entrance to the ATP binding domain moves significantly upon dimerization of the

subunits and the N-terminal tail from the opposing subunit takes its place (Figure 1.12).

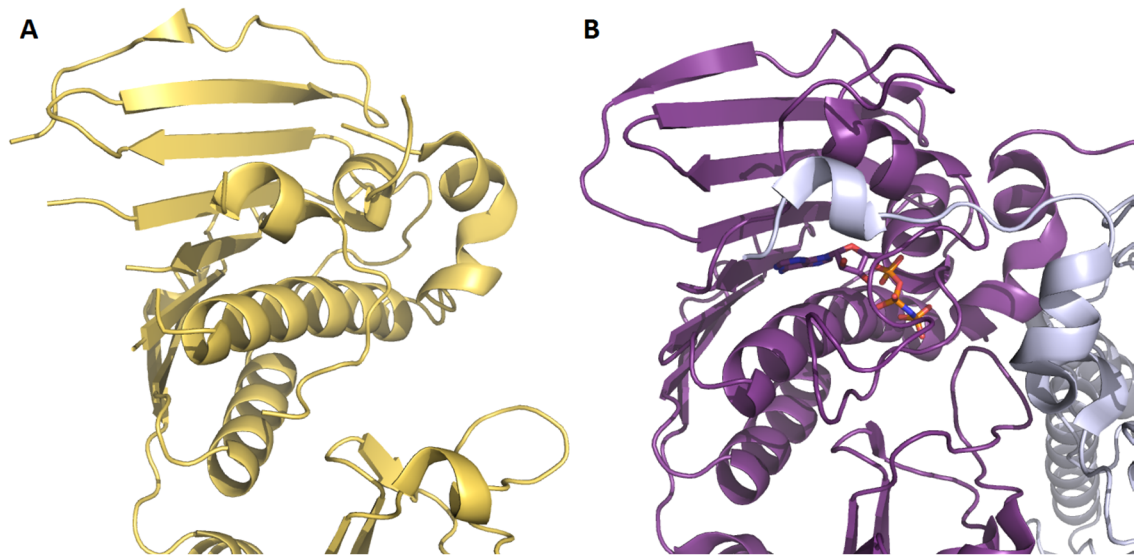


Figure 1.14 Conformational changes in the ParE ATP binding domain upon binding of ATP. A) ParE N-terminal domain in open clamp conformation (4I3H). B) GyrB dimer with ADPNP (a non-hydrolysable analogue of ATP) bound. Several loops have adopted different conformations.

Dimerisation of the N-terminal domains of GyrB/ ParE is favoured in the presence of ATP by hydrogen bonds which can form between a tyrosine residue near the N-terminus of one monomer and an ATP molecule bound in the ATPase pocket of the other monomer (Figure 1.15). This creates a very tight binding pocket for ATP and prevents diffusion of other small molecules into or out of the binding pocket. The triphosphate chain binds in a highly polar channel within the ATP binding site forming a large number of hydrogen bonds to residues and water molecules. A magnesium ion coordinates to oxygen atoms in the phosphate chain aiding the attack of a water molecule to the γ -phosphate and thus generating ADP and Pi.⁵³

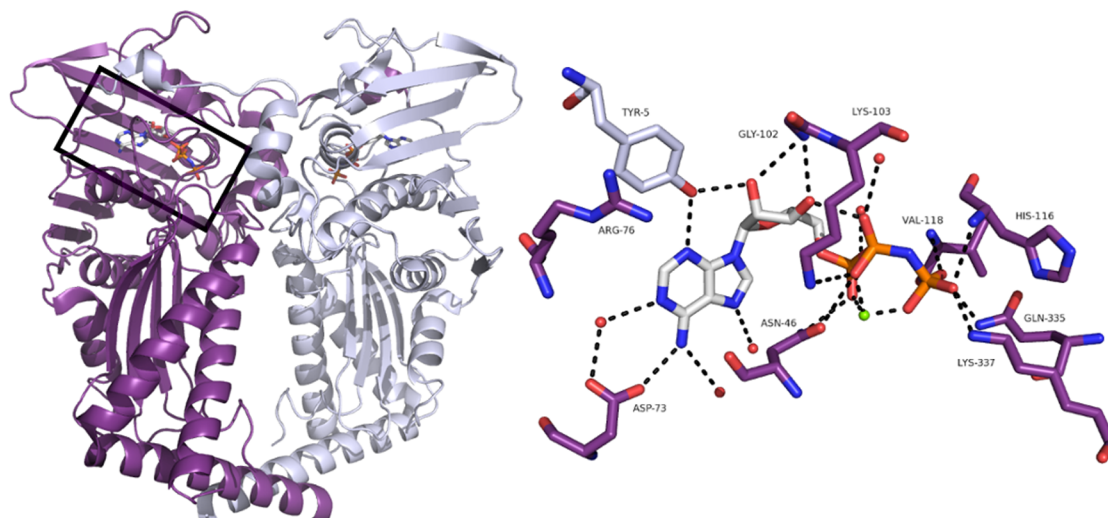


Figure 1.15 A. GyrB dimer from *E. coli* (4WUD)⁵⁷ ADPNP is present in the active site. B. The key residues involved in binding to ATP including coordination of a Magnesium ion (green) by the phosphate oxygens of ADPNP.

Recent crystallographic studies by Stanger *et al* have suggested that hydrolysis of ATP to ADP and Pi induces a conformational change in GyrB/ ParE, widening the gap between monomers close to the DNA binding domain (Figure 1.16). This conformational change is likely to be coupled to the opening of the gate-segment and passage of the transfer-segment. In the open configuration (Figure 1.16, B) the phosphate channel appears less open suggesting that the phosphate ion is unable to leave the ATP binding site in this conformation and that the conformation must reset before the phosphate can leave through the phosphate channel. The GyrB/ParE monomers would then separate to allow a new t-segment to bind.⁵⁸

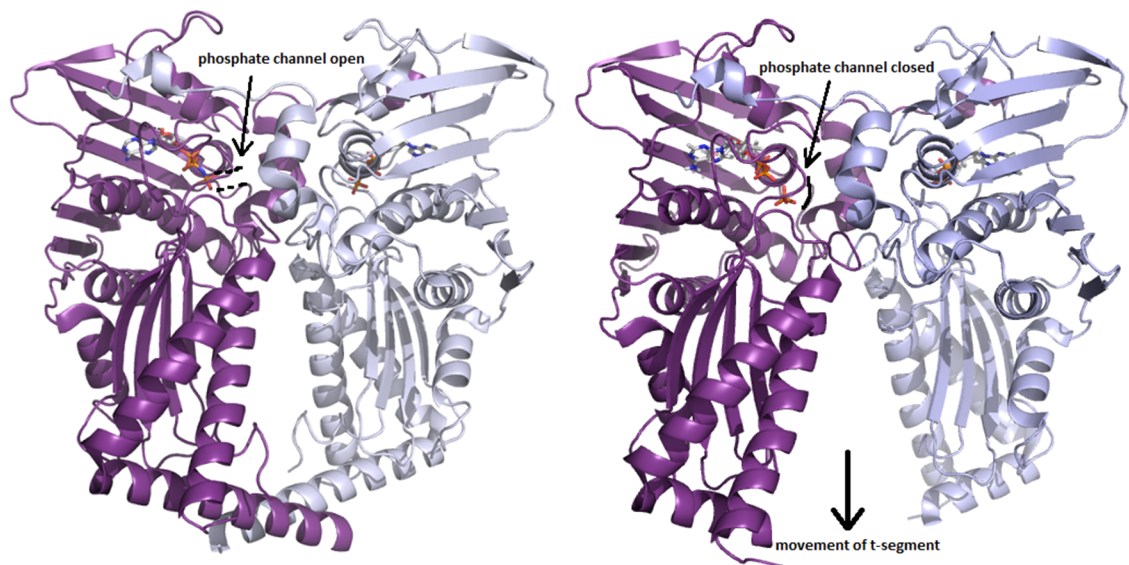
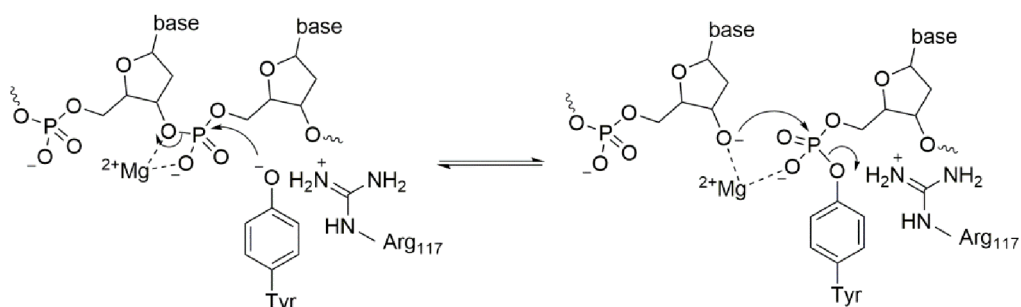


Figure 1.16 Hydrolysis of ATP causes a conformational change in GyrB. A. Non-hydrolysable ATP mimic ADPNP bound in the active site of *E. coli* GyrB (4WUD)⁵⁷. B. ADP and Pi bound in the active site of GyrB (4PRX)⁵⁸.

1.5.2.2 Mechanism of DNA cleavage

The gate segment of DNA is bound across the interface between GyrB/ParE and GyrA/ParC in a U-shape. A tyrosine residue from each GyrA/ParC monomer (Tyr-117 in *E. coli* ParE and Tyr-122 in *E. coli* GyrB) attacks the phosphate oxygen bond in the DNA backbone and forms a covalent bond to the phosphate at the 5' end of the cleaved DNA strand (Scheme 1.1).



Scheme 1.1 Mechanism of strand cleavage and re-ligation, a phosphodiester bond forms between the DNA and a tyrosine residue in the active site leaving the 3' hydroxyl end of the DNA free.

The breaks in the DNA strands are staggered by four base pairs. A magnesium ion coordinated by the three residues in the TOPRIM domain of ParE/GyrB aids in the

reaction by stabilising the $-OH$ 3' leaving group and the tyrosyl phosphate group (Figure 1.17).⁵¹

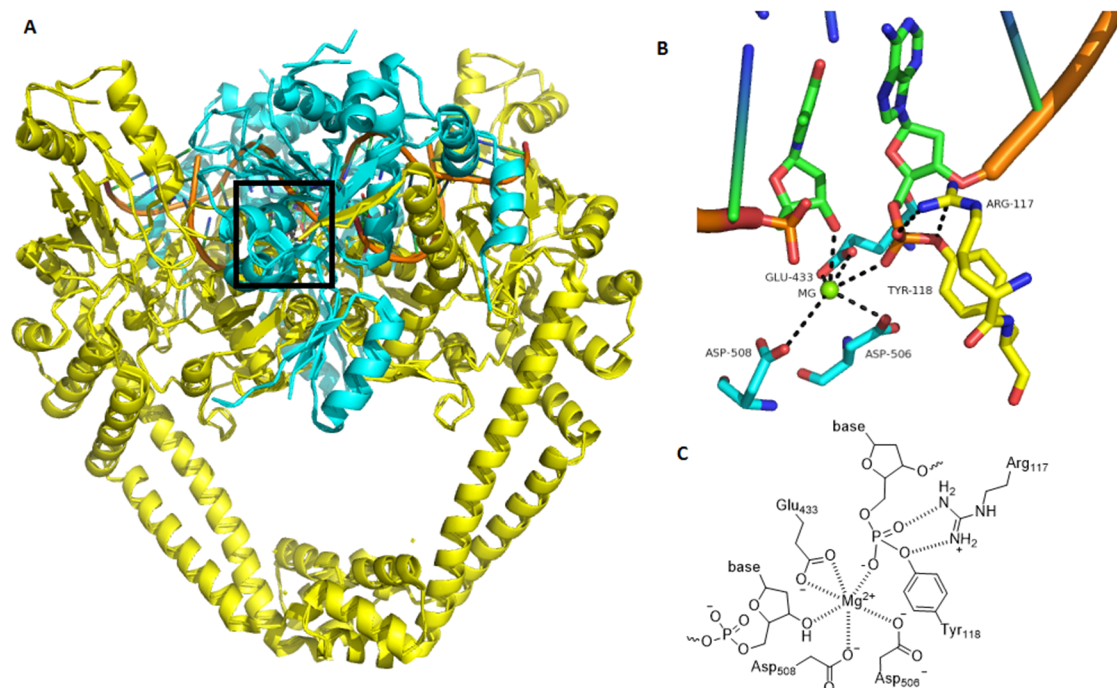


Figure 1.17 Cleavage of DNA by type II topoisomerases. A. *S. pneumoniae* topoisomerase IV crystal structure (3KSA)⁵¹, showing the binding of DNA (orange) to the C-terminal TOPRIM domain of ParE (turquoise) and the N-terminal domain of ParC (yellow). B. Close up of the cleaved DNA strand showing the residues involved in DNA cleavage and re-ligation. C. The key hydrogen bonding interactions involved in DNA cleavage and re-ligation.

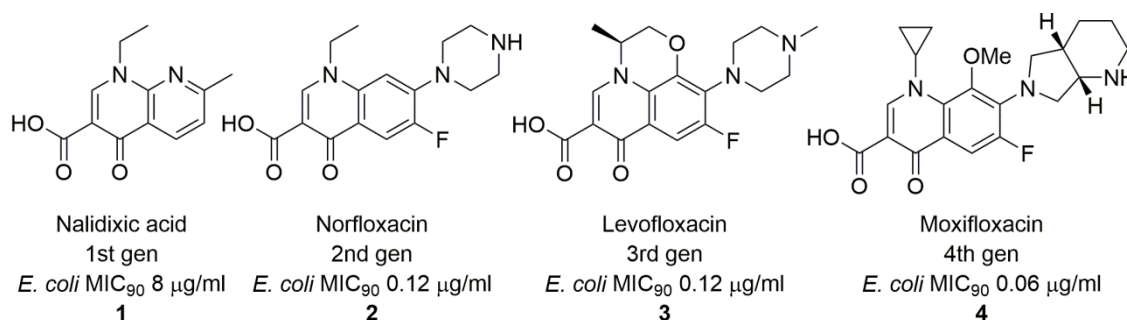
The mechanisms by which the GyrA/ ParC terminal gate opens to allow the t-segment to leave are less well understood and no crystal structures have been solved with this gate in the open configuration.

1.6 Type II topoisomerases as antibacterial drug targets

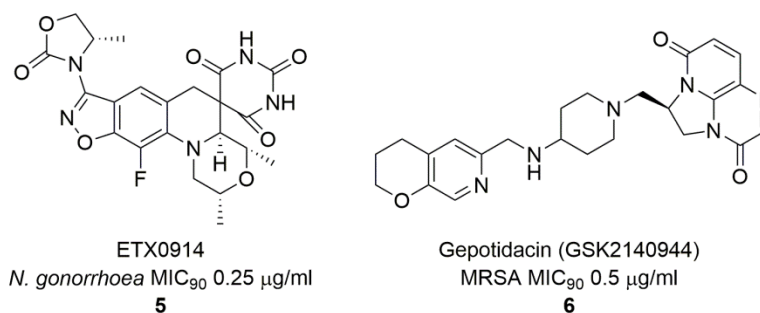
1.6.1 Inhibition of the DNA binding site – the quinolones

In 1962, Sterling Drug Inc. reported nalidixic acid **1** as an antibacterial compound derived from an impurity generated in the synthesis of chloroquin. This compound was the first of the quinolone antibiotics⁵⁹. Nalidixic acid is still in use today, but has a fairly narrow spectrum of activity, it is active against *E. coli* and many Gram negative species, but shows little activity against the majority of Gram positive species.⁶⁰ In the following years several related compounds were developed, all with broadly similar activities,

but these first generation quinolones were mostly superseded in the late 70s by the discovery that introducing a fluorine atom to the central ring and adding a basic amine containing heterocycle greatly improved the antimicrobial potency and spectrum of activity of these compounds. Norfloxacin **2** was the first of these second generation quinolones.⁶¹ Over the years, successive generations of these fluoroquinolones have been developed with improved pharmacokinetics, safety, potency and spectrum of activity over previous generations. More recently developed compounds, including levofloxacin **3** and moxifloxacin **4**, are active against some Gram positive bacteria as well as Gram negative bacteria.⁶²



New compound series which target the DNA binding region are in development. Both GSK and Entasis have DNA gyrase inhibitors in clinical trials for the treatment of gonorrhoea. Entasis's ETX0914 **5**⁶³ (formerly AstraZeneca's AZD0914)⁶⁴ is in phase 1 clinical trials and GSK's Gepotidacin (GSK2140944) **6** is in phase 2 clinical trials⁶⁵.

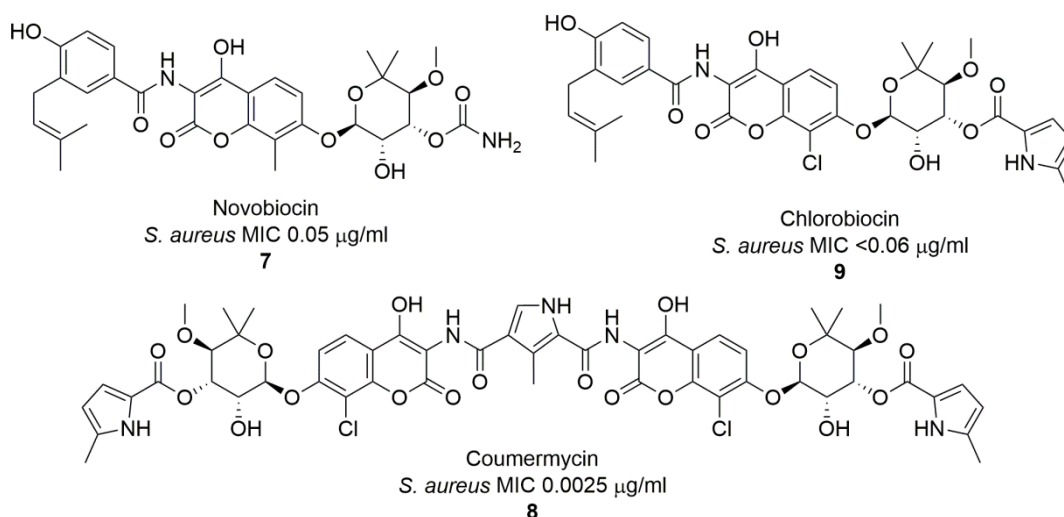


1.6.2 Inhibition of the ATP binding site – a brief history

1.6.2.1 Coumarins and cyclothialidines: natural product based inhibitors

During the Golden era of antibiotic drug discovery, most major pharmaceutical companies were working on antibacterial drug discovery and between 1955 and 1956 Upjohn, Pfizer, Lepetit and Merck all discovered the same antibacterial natural

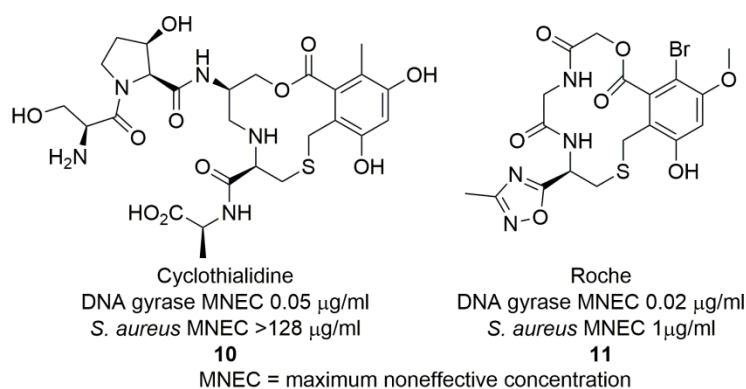
product: Novobiocin **7**. Novobiocin was marketed by Upjohn in the 60s as Albamycin for treatment of penicillin resistant *S. aureus*. Novobiocin was active against Gram positive bacteria and a few species of Gram negative bacteria and could be administered orally or in solution for IV dosing. However, resistance emerged quickly and side-effects including rash were seen fairly frequently. As second generation penicillins, such as methicillin, and the first cephalosporins became available during the late 60s, novobiocin fell out of favour. At this time, several drug companies were investigating structurally similar antibiotics. In 1965, both Roche and Bristol-Myers reported coumermycin **8** and in 1969 Rhone-Poulenc reported chlorobiocin **9**. Following disappointing clinical results, all three companies abandoned their efforts at developing novobiocin like antibiotics during the 70s.



Just as investigation of this class of agents as antibiotics was being abandoned, research into the target of these drugs started taking off. In 1976 the DNA gyrase enzyme from *E coli* was first identified and its inhibition by novobiocin and the other coumarin drugs was reported.^{66,67} The following year it was discovered that nalidixic acid also inhibited its activity.^{68,69} It was quickly understood that the enzyme was comprised of two subunits, one of which was inhibited by the coumarins and the other of which was inhibited by the quinolones, and that it was able to supercoil DNA in an ATP dependent manner *via* a strand passage mechanism.^{66,70} Research into improved quinolone antibacterials was still being carried out at this time and results of assays against DNA gyrase began being reported along with MICs against various bacterial

species in reports on the activities of the newly discovered second generation quinolones.⁷¹

In the early 90s, Roche reported the discovery of cyclothialidine **10** from a screen of 20,000 culture broths using a DNA gyrase based supercoiling assay. This was the first example of a non-coumarin inhibitor of the ATPase site of DNA gyrase. Cyclothialidine displayed only weak antimicrobial activity despite being a more potent inhibitor of DNA gyrase than novobiocin.^{72,73} Medicinal chemistry efforts to improve the antimicrobial activity of this class of inhibitors continued for several years with both Roche and Bayer pursuing analogues of the initial natural product.^{74,75} Roche has continued to work on this series through the 2000s and in 2011 reported on derivatives, such as **11**, with good MICs and improved physicochemical properties, many of which showed promise in an animal model of infection.⁷⁶



1.6.2.2 Dual-targeting, crystallography and the rise of non-natural product inhibitors

Topoisomerase IV was first identified in 1990 following sequencing of parts of the *E. coli* genome⁷⁷ and its role in the decatenation of bacterial chromosomes was soon fully elucidated⁷⁸⁻⁸⁰. The inhibitory effects of known quinolone drugs on topoisomerase IV were soon investigated and compared to their activities against DNA gyrase^{81,82}. Over the following years it became apparent that the extent of inhibition of each enzyme by quinolone antibiotics varied between bacterial species. In Gram negative species, DNA gyrase tended to be the main target and in Gram positive species topoisomerase was usually the primary target.⁸³ Studies of fluoroquinolone resistant bacterial strains suggested that a mutation in the primary target for that species conferred a significant increase in resistance with an additional mutation in the

secondary target conferring complete resistance. It was suggested that compounds which were equally potent inhibitors of both proteins might prove to be harder to develop resistance to, as simultaneous mutations in both enzymes would be needed to confer enough resistance to encourage a selective pressure.³⁷

It was also at around this time that the first crystal structure of the ATPase domain of DNA gyrase was published. In 1991, a 43 kDa fragment of the N-terminal portion of GyrB was crystallised in the presence of ADPNP and showed the arrangements of the two subunits in a dimer.⁸⁴ Crystal structures of a 24 kDa fragment of GyrB bound to novobiocin, GR1222X (a cyclothialidine analogue discovered independently by Glaxo) and chlorobiocin, were all published a few years later.^{85,86} Crystal structures of the 43 kDa subunit have been used to gain insight into the ATP hydrolysis mechanism⁵³, whereas the 24 kDa subunit has much more frequently been used to assess binding of inhibitors to the ATP binding site, as the binding site is more accessible in this subunit.

Figure 1.18 shows the differences between the 43 kDa subunit and the 24 kDa subunit. Panel A shows an overlay of the 24 kDa crystal structure with one protein molecule from the 43 kDa subunit and panels B and C show the subunits separately. As can be seen from panel C, in the 43 kDa crystal structure the N-terminal arm of the other protein molecule in the dimer closes around the ATP binding site.

The crystal structure of the GyrB 24 kDa subunit used to produce Figure 1.18 (3G7E)⁸⁷ is the only crystal structure of the 24 kDa subunit of GyrB or ParE, out of 52 which had been deposited in the PDB as of the 10th April 2016, in which all the loops surrounding the ATP binding site are fully resolved. Usually a loop adjacent to the ATP binding site is either unresolved or has been removed by mutagenesis. Loop deleted mutants of *E. coli* ParE⁵⁰ and *S. aureus* GyrB⁸⁸ have been reported and the *S. aureus* GyrB mutant has been frequently employed in the place of the native *S. aureus* GyrB unit which does not crystallise as readily⁸⁹⁻⁹¹.

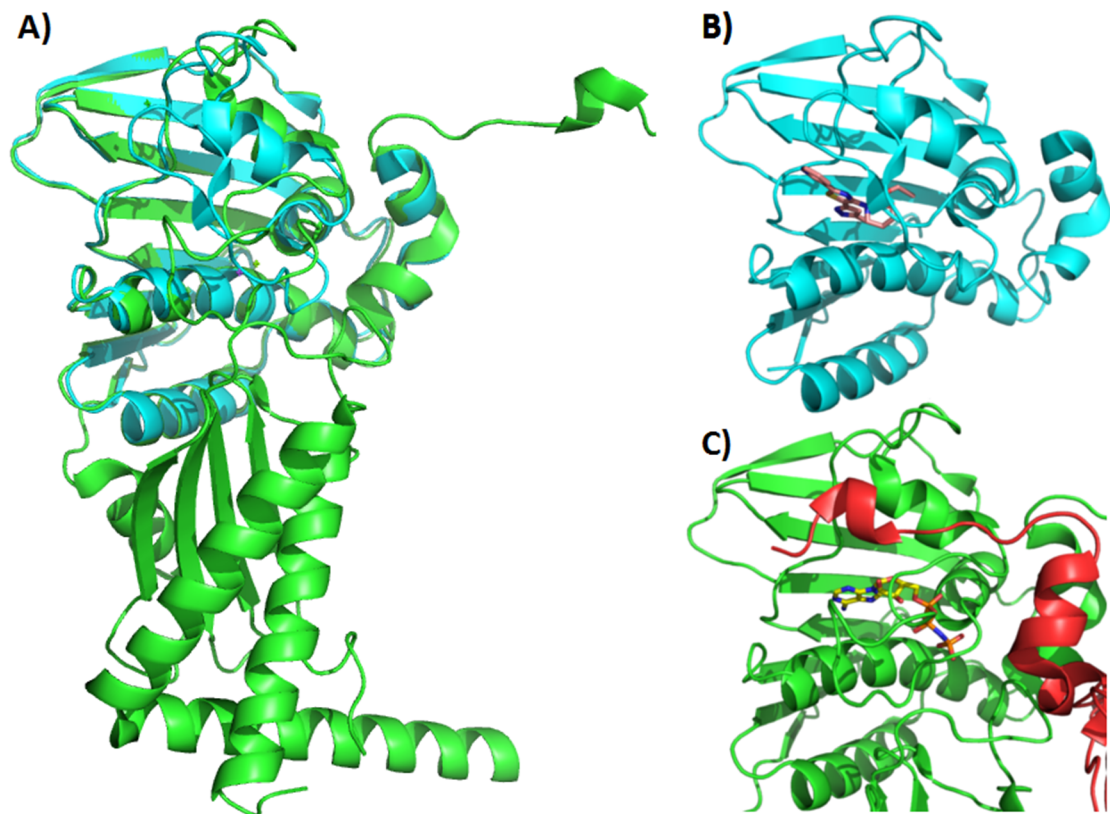


Figure 1.18 Comparison of 24 kDa and 43 kDa subunits of GyrB. A) Overlay of a crystal structure of the 24kDa subunit (3G7E⁹², cyan) and one monomer from a crystal structure of the 43 kDa subunit (4WUD⁵⁷, green) of DNA gyrase. B) An inhibitor (pink) bound in the ATP binding site of the 24 kDa subunit. C) ADPNP (yellow) bound in the ATP binding site of the 43 kDa subunit with dimer partner in red.

The crystal structures revealed the presence of a few key residues within the ATP binding site which are now known to form interactions with most published inhibitors. There is a conserved water molecule in the active site which forms a hydrogen bond network between an aspartate residue in the active site (Asp-73 in *E. coli* GyrB, Figure 10; Asp-78 in *S. pneumoniae* ParE) and the amine and a nitrogen atom from the adenosine ring of ATP. These interactions were described earlier (Figure 1.15). All inhibitors of the ATP binding site of DNA gyrase and topoisomerase IV which have been reported in the literature possess a similar hydrogen bond donor/ acceptor motif which is able to mimic the interaction between ATP and the conserved water molecule and the Asp residue (Figure 1.19). This hydrogen bonding network is so important for binding ATP that no resistant mutants have been found in which this Asp residue has been modified.⁹³

Another common feature in many published inhibitors is an aromatic ring positioned so as to form a π -stacking interaction to an arginine residue adjacent to the active site. This arginine residue forms a π -stacking interaction with the N-terminal tyrosine residue of the other protein unit in the ATP bound conformation of the protein (Figure 1.15). Many topoisomerase inhibitors also exhibit a group able to form a hydrogen bond to Arg-140. A crystal structure published recently by AstraZeneca showing one of their pyridylurea inhibitors **12** is shown in Figure 1.19 indicating these key interactions.

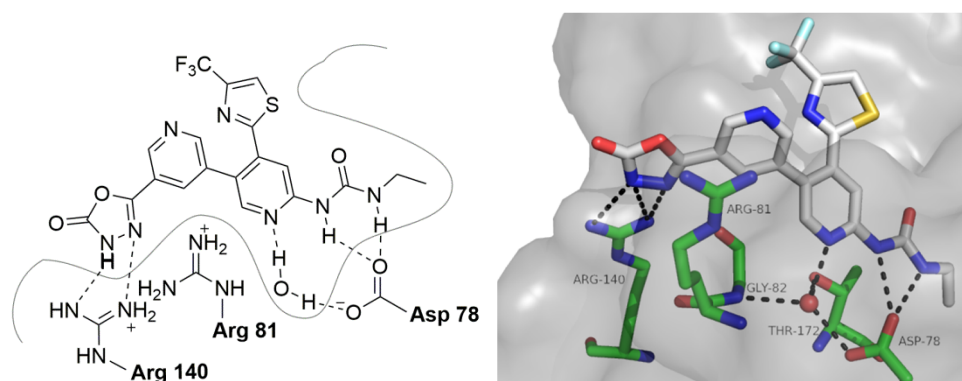
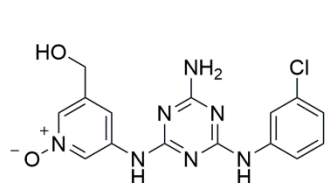


Figure 1.19 Interactions between a pyridylurea inhibitor **12** and some key residues in the binding site of *S. pneumoniae* ParE. (a) schematic showing important interactions and (b) crystal structure showing key interactions between the inhibitor and residues within the binding pocket (4LPB).⁹⁴

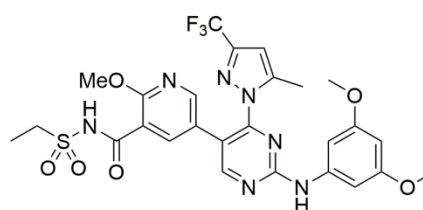
The combination of new structural information and the presumed advantages of dual-target inhibitors combined to generate a surge in interest in the development of ATPase inhibitors in the mid-90s which has continued to the present day. 52 crystal structures of the GyrB or ParE subunit with a small molecule inhibitor bound in the ATP binding site were available in the PDB as of the 10th of April 2016 (35 of GyrB and 17 of ParE). Crystal structures have been solved of the 24 kDa subunit of GyrB and ParE from a number of bacterial species: GyrB and ParE from *E. coli*, *S. aureus* and *E. faecalis*; GyrB from *M. smegmatis*, and ParE from *S. pneumoniae* and *F. tularensis*. A wide variety of inhibitor structures have been investigated in the last 25 years. A brief summary of some of the key scaffolds is given below. For a more comprehensive review of ATPase inhibitors see Bisacchi and Manchester 2015.⁹³

Triazines and pyrimidines

Zeneca was the first pharmaceutical company to report a medicinal chemistry project investigating GyrB/ParE inhibitors which weren't based on natural products. Their triazine series was developed from a hit from a high throughput screen of the Zeneca corporate compound collection against DNA gyrase. These compounds, including **13**, displayed moderate enzyme inhibition and MICs and were not pursued further.⁹⁵ AstraZeneca later reported a series of somewhat similar amino aryl pyrimidines identified by HTS and optimised to give **14** which had good enzyme activity and antibacterial potency. Both the Zeneca triazines and the AstraZeneca pyrimidines suffered from poor physicochemical properties.⁹⁶



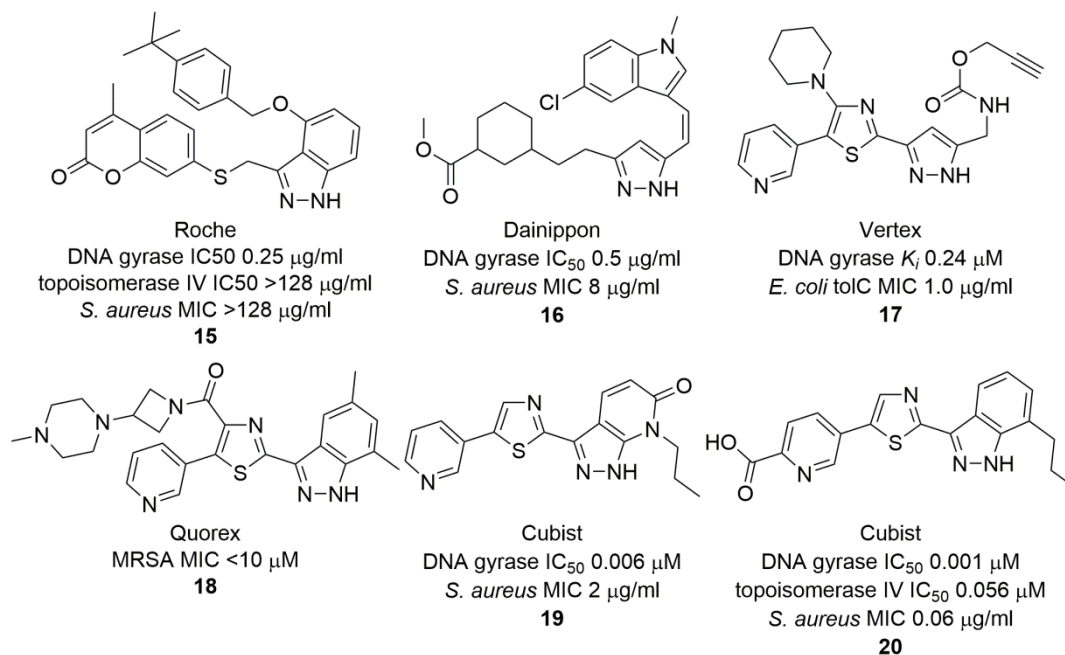
Zeneca
DNA gyrase IC₅₀ 0.55 μg/ml
13



AstraZeneca
DNA gyrase IC₅₀ <0.01 μM
topoisomerase IV IC₅₀ <0.02 μM
MRSA MIC₉₀ 0.5 μg/ml
14

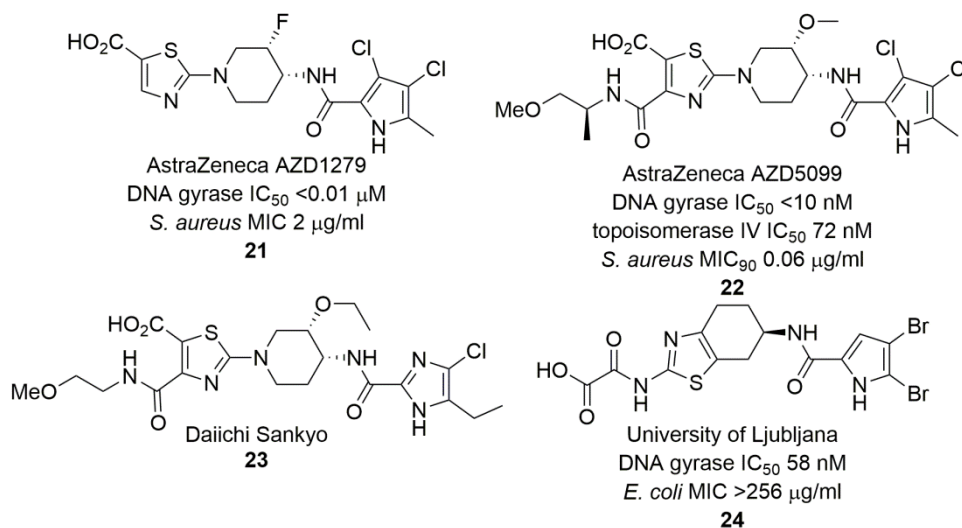
Indazoles and pyrazoles

Several companies have reported inhibitors containing an indazole or pyrazole motif. The first of these emerged from a “needle” screening effort by Roche which afforded **15** as their lead from that series.⁹⁷ At about the same time, Dainippon struck upon a pyrazole hit in a screening campaign and investigated a range of pyrazole derivatives combining features from their hit and Roche's to give **16**.⁹⁸ In the following years, Vertex, Quorex and Cubist also investigated similar pyrazole **17**, indazole **18** and pyrazolopyridone **19** inhibitors respectively.^{87,90,99,100} Last year Cubist reported a series of indazole inhibitors **20**⁹¹.



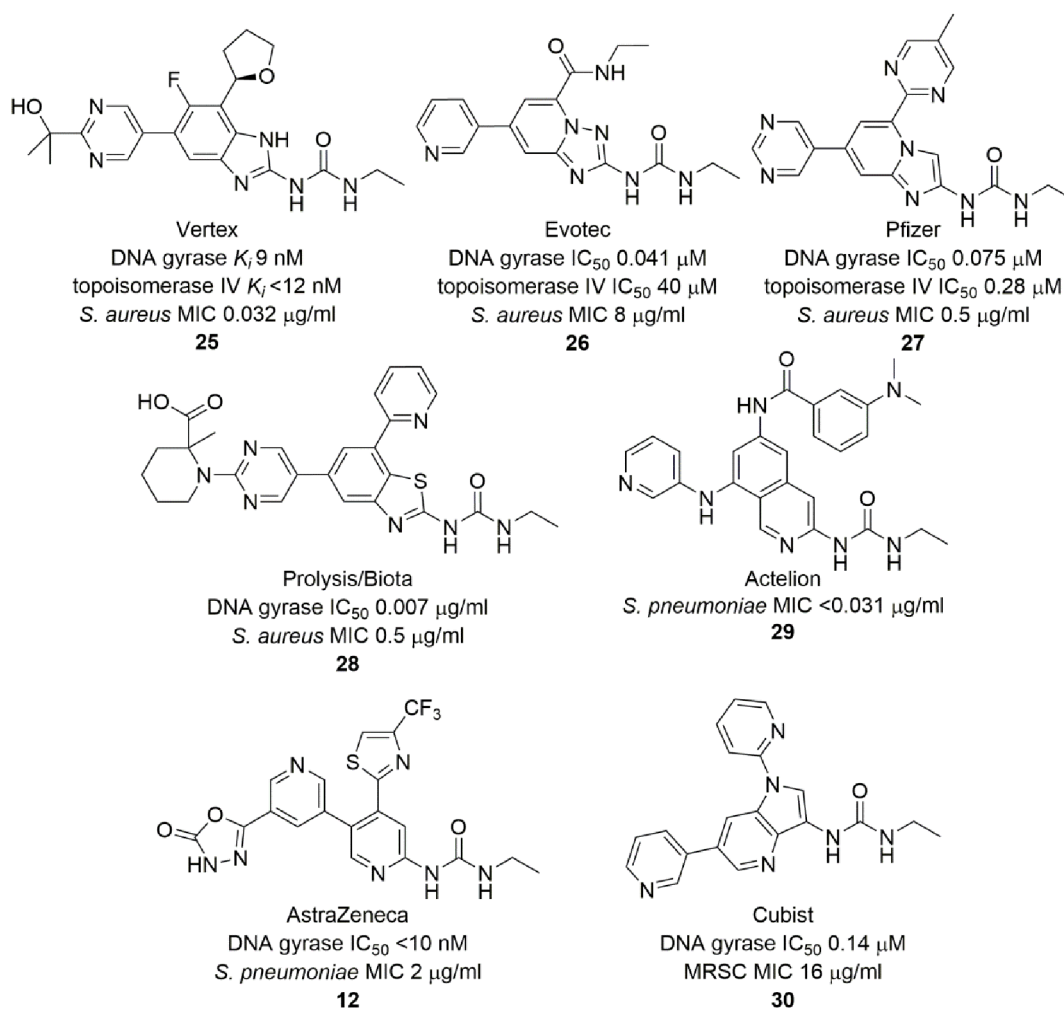
Pyrrrolamides and imidazolamides

A pyrrolamide series developed by AstraZeneca is one of the only series of ATPase inhibitors to have produced compounds which progressed as far as phase I clinical trials. Beginning with a pyrrolamide fragment from an NMR-based fragment screen, AstraZeneca developed two candidate molecules that went into phase I trials. AZD1279 **21** was the first into the clinic, but was not taken forward due to high clearance.¹⁰¹ A later derivative AZD5099 **22** was also taken into phase I, but was similarly unsuccessful.¹⁰² Daiichi Sankyo have patented imidazole variants of this series **23**¹⁰³ and a group at the University of Ljubljana have also reported a series of pyrrolamides **24**¹⁰⁴⁻¹⁰⁶.



Ethyl ureas

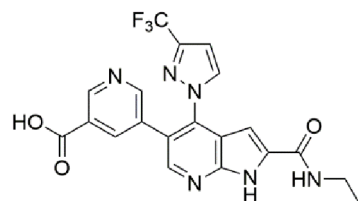
Ethyl urea based inhibitors have been very fashionable in the last 15 years. The first report of an aromatic ethyl urea series came from Vertex. Compound **25** is an example of their second generation of benzimidazole inhibitors. They have continued to develop this series through several generations with several candidate inhibitors almost making it into the clinic.^{89,107-109} Scaffold hops to closely related benzothiazoles **26**, imidazopyridines **27**, and triazolopyridines **28** have been reported by Prolysis (and developed further by Biota),¹¹⁰⁻¹¹² Pfizer¹¹³ and Evotec respectively.¹¹⁴ Different ring structures have also been investigated with isoquinolones **29** reported by Actelion¹¹⁵, pyridines **12** reported by AstraZeneca⁹⁴ and azaindoles reported by Cubist **30**¹¹⁶.



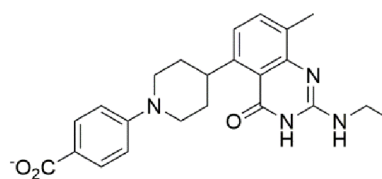
Ethyl urea mimics

A few recent disclosures at conferences have featured compounds with a similar arrangement of hydrogen bond acceptor and donors as seen in the ethyl-urea

compounds. These include a series of amidoazaindoles **31** reported by AstraZeneca¹¹⁷ and a quinazolinone series **32** reported by Cubist.^{93,100}



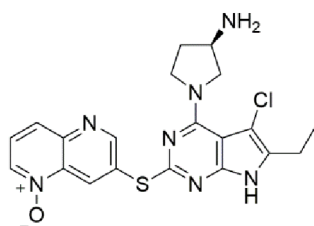
AstraZeneca
DNA gyrase IC₅₀ 0.005 μM
topoisomerase IV IC₅₀ 0.005 μM
S. pneumoniae MIC 6.25 μg/ml
31



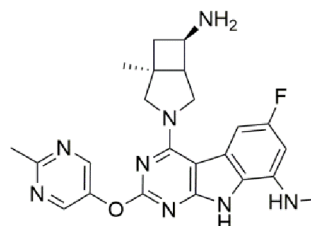
Cubist
DNA gyrase IC₅₀ <8 nM
topoisomerase IC₅₀ 47 nM
S. aureus MIC 0.13 μg/ml
32

Pyrrolopyrimidines and tricyclic variants

Trius has reported two series of inhibitors, pyrrolopyrimidines **33** and tricyclic pyrrolopyrimidine derivatives **34**. These compounds evolved from a hit from a crystallographic fragment screen and have been developed into highly potent dual-targeted inhibitors with potent MICs against a wide range of both Gram negative and Gram positive bacteria.^{92,118,119}



Trius
DNA gyrase IC₅₀ <0.3 nM
topoisomerase IV IC₅₀ 4.6 nM
S. aureus MIC 0.13 μg/ml
E. coli MIC 4 μg/ml
33

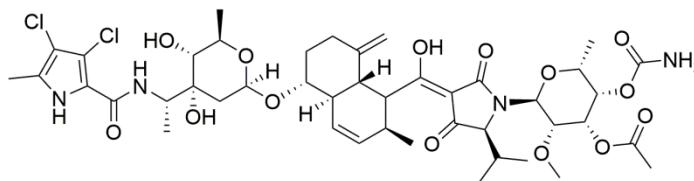


Trius
DNA gyrase IC₅₀ 0.3 nM
topoisomerase IV IC₅₀ 0.9 nM
S. aureus MIC 0.008 μg/ml
E. coli MIC 0.5 μg/ml
34

Coumarins and other natural products

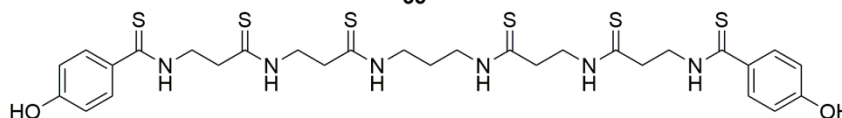
There has also been a resurgence of interest in natural product antibiotics. A natural product with a similar structure to the coumarin antibiotics such as Novobiocin was discovered separately by two research groups and named amycolamicin¹²⁰ and kibdelomycin¹²¹ **35**. Neither group have developed the compound beyond elucidating its structure and target of action. Another recently discovered natural product inhibitor of DNA gyrase is closthioamide **36**, which was isolated from the anaerobic

bacteria *Clostridium cellulolyticum* and identified as acting by inhibition of DNA gyrase via the GyrB subunit.¹²²



Amycolamicin/ Kibdelomycin
DNA gyrase IC₅₀ 0.024 μg/ml
topoisomerase IV IC₅₀ 62.5 μg/ml
S. aureus MIC 0.25 μg/ml

35



Closthioamide
DNA gyrase IC₅₀ 1.38 μM
MRSA MIC 0.14 μg/ml

36

1.6.3 Summary

Despite the wide ranging efforts by many drug companies to discover useful antibacterial drugs that target the ATPase sites of GyrB and ParE, no inhibitors have yet progressed beyond phase I clinical trials. Reasons given for discontinuing research into these compound series have been varied and include poor solubility, high plasma protein binding, rapid *in vitro* clearance, formation of reactive metabolites and hERG liability. From this wide range of reported reasons for projects being suspended, it would seem that inhibitors of the ATPase site aren't failing due to a common problem which might indicate an underlying difficulty with inhibiting this target. It should be possible to discover an inhibitor of DNA gyrase and topoisomerase IV that doesn't succumb to the same difficulties as previous inhibitors and can be successful in the clinic.

1.7 Project aims and objectives

The project was broadly divided into two parts. In the first, efforts were made to further explore a series of pyridine 3-carboxamide inhibitors previously developed at the University of Leeds. The second part of the project focused on the identification of inhibitor series with novel structures.

1.7.1 To develop a series of pyridine-3 carboxamides

A series of pyridine-3-carboxamides was previously developed at Leeds.^{123,124} These compounds showed potential as inhibitors of DNA gyrase, but their topoisomerase IV activity was never assayed. Further development of this series was undertaken as follows:

- Synthesis of additional members of the series
- Assessment of activity against both DNA gyrase and topoisomerase IV
- Assessment of the *in vitro* ADME profile of representative inhibitors
- Co-crystallisation of inhibitors in the GyrB protein

1.7.2 The discovery of novel inhibitor series'

Several approaches were used to discover novel inhibitor series:

- *De novo* design using SPROUT
- vHTS using Glide and ROCS
- Scaffold hopping to rationally design novel inhibitor structures
- Synthesis of designed compounds was carried out

Chapter 2 Investigation into pyridine-3-carboxamide inhibitors

2.1 Background to pyridine-3-carboxamide inhibitors

As discussed earlier (Chapter 1), a common motif seen in ATPase inhibitors of DNA gyrase and topoisomerase IV is a heteroaromatic ring with an ethyl urea substituent adjacent to a nitrogen atom in the ring with two other substituents branching from the ring. These common structural features are shown in Figure 2.1. Previous work at the University of Leeds identified a promising compound class which shares these structural features.^{123,124}

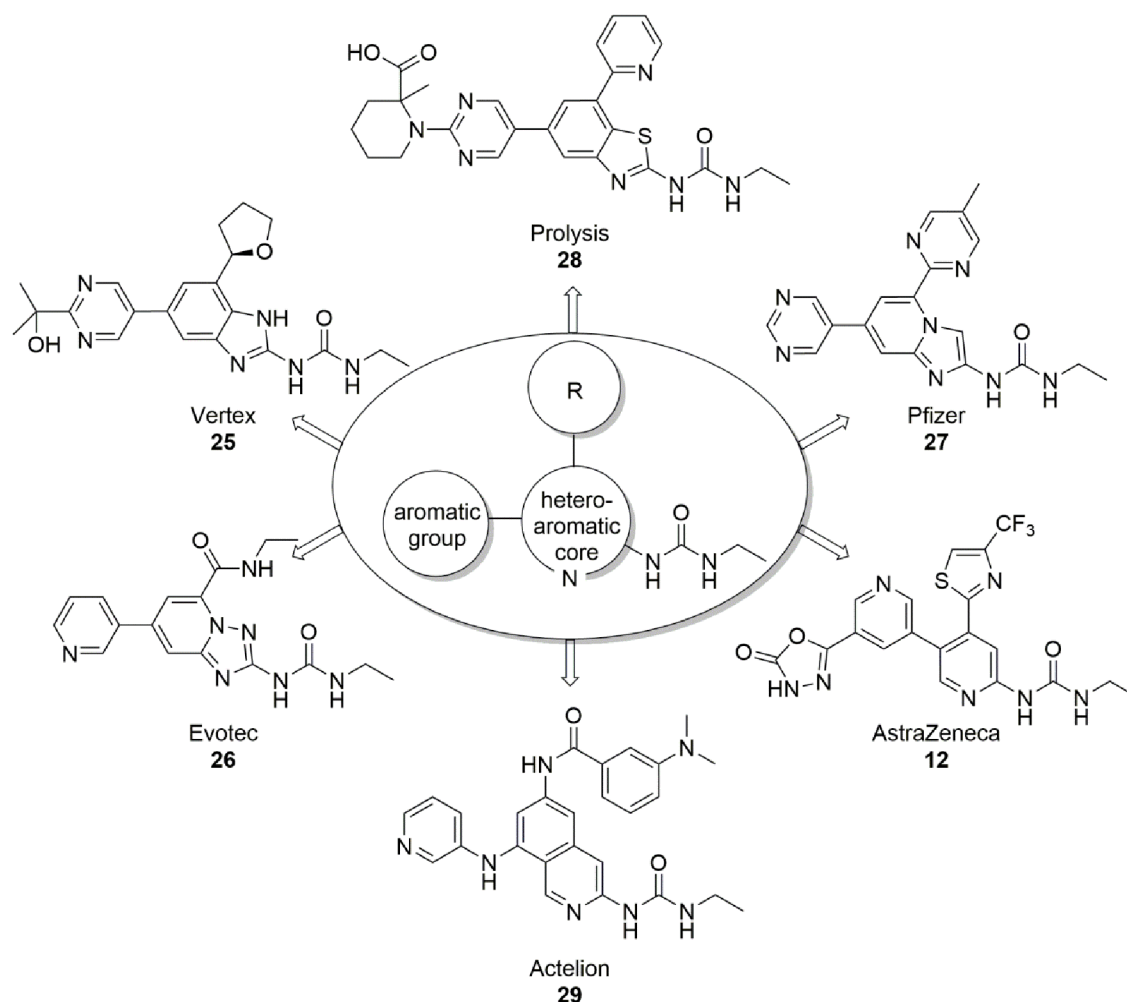


Figure 2.1 Inhibitors containing an ethyl urea motif have been published by Vertex¹⁰⁷, Prolysis¹¹¹, Pfizer¹¹³, AstraZeneca⁹⁴, Actelion¹¹⁵ and Evotec¹¹⁴. These inhibitors all have a number of structural features in common including a heteroaromatic ring system

with a ring nitrogen adjacent to the urea substituent and two other substituents on the ring.

Computational design using SPROUT¹²⁵ identified a series of compounds of the form **37** based upon a pyridine ring as the central heteroaromatic group with a carboxamide linkage to an additional aromatic group at the 3-position of the central pyridine ring and with further substitution branching from the 4-position (Figure 2.2).

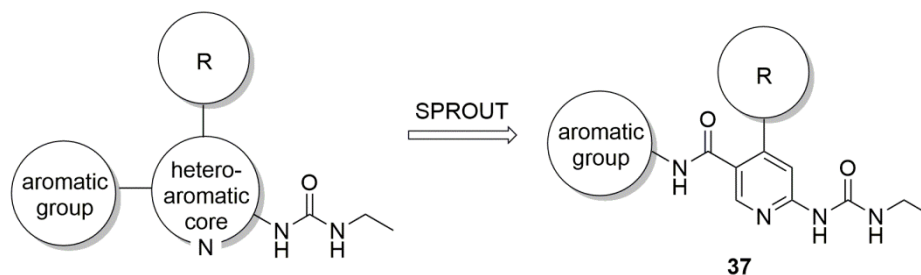


Figure 2.2 A series of pyridine-3-carboxamides with features in common to known inhibitors was designed using SPROUT.

Although initial investigation of the SAR around these compounds was performed, the full scope of substituents at the 4- position was not fully ascertained. Therefore, it was decided to further explore the effects of altering the substituent in the 4- position of the pyridine core. In the previous study, compounds were not assessed for their inhibition of the topoisomerase IV enzyme, and no *in vitro* ADME profiling was carried out, so it was decided to carry out assays against topoisomerase IV and *in vitro* ADME profiling for selected compounds.

2.2 Choice of avenues of investigation

As was mentioned in Chapter 1, a 24 kDa subunit of the GyrB or ParE protein has usually been used to obtain crystal structures of inhibitors bound in the ATP binding site. A short loop of the protein adjacent to the ATP binding site is almost always disordered in the crystal structures with the exception of one crystal structure, 3G7E (Figure 2.3, C). Mutagenesis has been used to generate a 24 kDa construct of GyrB with this flexible loop deleted as they crystallise more readily. Figure 2.3 shows three crystal structures: one with the full flexible loop resolved (A), one with part of the loop resolved and part of the loop disordered (B) and one with the flexible loop removed using mutagenesis (C). This flexible loop poses a challenge to the rational design of

inhibitors which bind to this site, as docking experiments will not be able to accurately predict interactions between a designed inhibitor and the highly flexible loop. Interactions between the inhibitor and protein residues in the rest of the protein structure can be more reliably predicted using docking experiments.

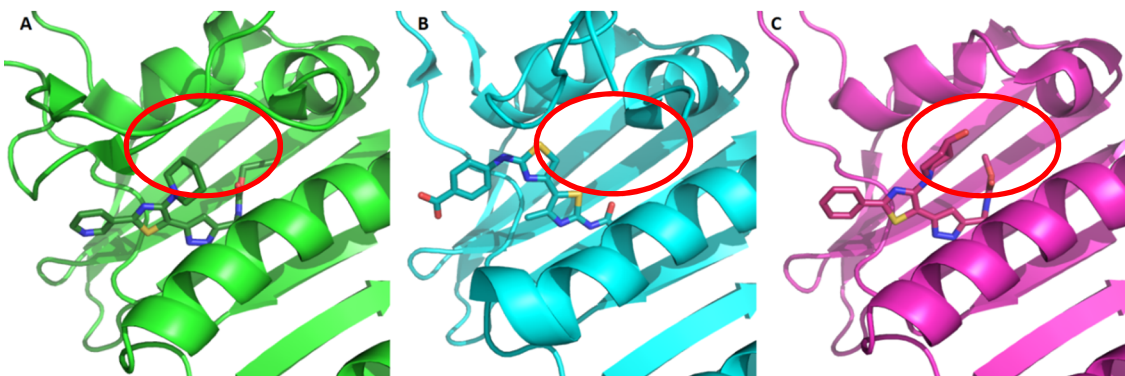


Figure 2.3 Comparison of flexible loop positions in different crystal structures. A) 24 kDa subunit of *E. coli* GyrB with all loops surrounding the ATP binding site are fully resolved (3G7E)⁸⁷. B) 24 kDa subunit of *E. coli* with a disordered loop unresolved (4DUH)¹⁰⁶. C) 24 kDa subunit of *S. aureus* GyrB with flexible loop deleted using mutagenesis (3G7B)⁸⁷. The red circles indicate the region of the binding site in which interactions between an inhibitor and the protein cannot be accurately predicted using docking.

The most potent DNA gyrase inhibitor synthesised as part of the previous work at Leeds was the bis-pyridyl compound **38**. It was noted that inhibitors such as compound **38** (Figure 2.4), which possess an amino aryl substituent at the C4- position of the pyridine ring, tended to be more potent DNA gyrase inhibitors than compounds with a directly-linked heterocycle at this position, such as compound **39**.

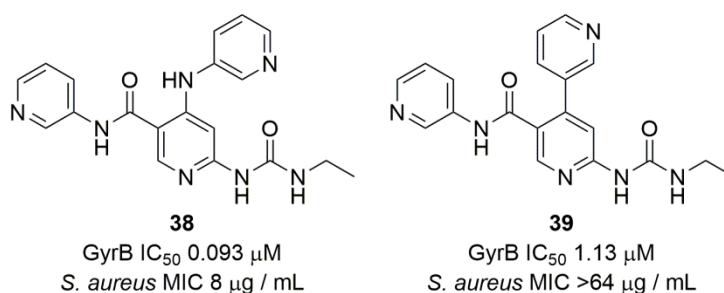


Figure 2.4 Biological activities of two previously synthesised pyridylurea inhibitors. The variant with an aminopyridine substituent in the C4 position **41** has better biological activity than the variant without the amine linker to the pyridine substituent at the C4 position **42**.

Compounds **38** and **39** were docked into the GyrB binding site from *E. coli* (4HYP), with **38** scoring -8.6 and **39** scoring -8.4. The poses generated by AutoDock¹²⁶ are shown in Figure 2.5. The difference in the structures of compounds **38** and **39** is the substituent

at the C-4 position of the central pyridine ring which is positioned in the region of the crystal structure in which the protein is disordered. This makes it hard to rationalise the greater inhibitory activity of compound **38** compared to compound **39**. Docking predicts that both compounds are able to form hydrogen bonds to Asp-73, Arg-140 and the conserved water molecule in the binding site which is consistent with crystal structures of other known inhibitors which have been reported in the literature.

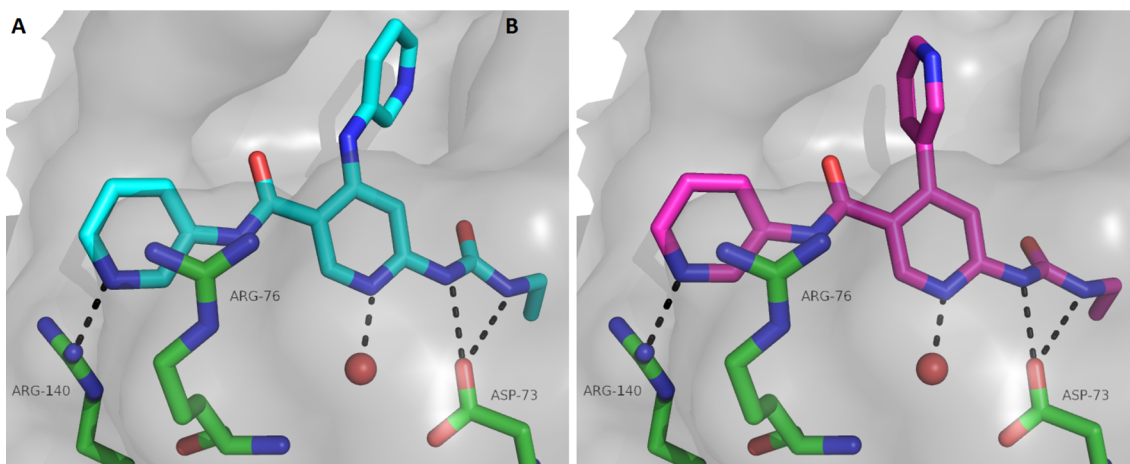


Figure 2.5 Predicted binding poses of compound **38** (A) and compound **39** (B) to *E. coli* GyrB (4HYP) generated using AutoDock.

Another pair of inhibitors exhibited activities which contrasted in an interesting way. The pyrazole-containing compound **40** had greater antibacterial activity against *S. aureus* than the imidazole-containing compound **41**, despite compound **40** exhibiting greater inhibitory activity against the DNA gyrase enzyme (GyrB) (Figure 2.6).

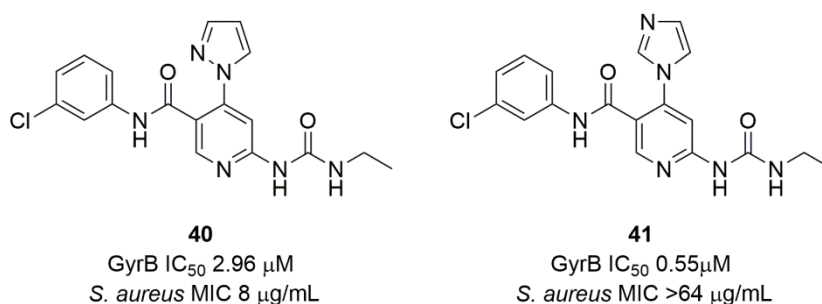


Figure 2.6 Two inhibitors which are geometrical isomers, but have different biological activities.

Computational docking of these compounds into *E. coli* GyrB was carried out using AutoDock in an attempt to rationalise the IC₅₀s measured in the enzyme assay, but both compounds had very similar docking scores (compound **40** scored -8.1 and

compound **41** scored -7.9) and were predicted to bind in very similar poses, with the only difference being the orientation of the chloro-substituted phenol ring (Figure 2.7). The imidazole and pyrazole rings are positioned in the part of the binding site which is adjacent to the flexible loop which is disordered in the crystal structures. Computational docking cannot predict interactions between the imidazole or pyrazole ring and the residues in this flexible loop.

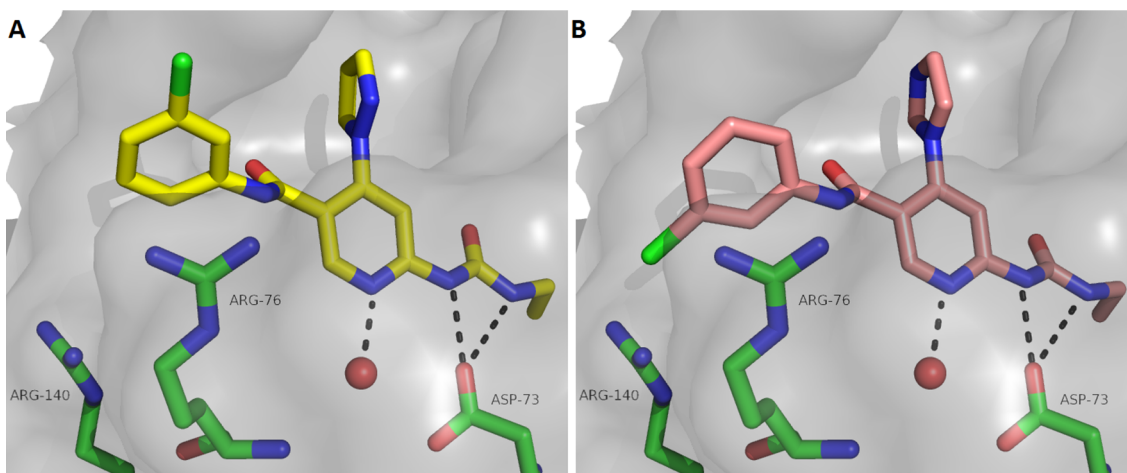


Figure 2.7 Predicted binding poses of compound **40** (A) and compound **41** (B) to *E. coli* GyrB (4HYP) generated using AutoDock.

The differences in these compounds' inhibitory activity against the DNA gyrase enzyme is most likely due to differences in the ways the imidazole and pyrazole rings interact with the flexible loop near the binding site. The differences in these compounds' antibacterial activity could be attributable to a number of different factors: differences in the ability of these compounds to cross the bacterial membrane; differences in their activities against the topoisomerase IV enzyme compared to the DNA gyrase enzyme; different levels of activity against the DNA gyrase enzyme of *S. aureus* compared to the DNA gyrase enzyme from *E. coli* or an unknown off-target effect. Compounds **40** and **41** have different lipophilicities (compound **40** has a clogP of 2.62, whereas **41** has a clogP of 1.86) and this may influence their ability to cross bacterial membranes, but as these effects are difficult to predict, the best way to understand this difference is to make more compounds with similar substitution patterns and test them for their activities.

Based on the observations described above, it was decided to focus synthetic efforts on producing inhibitors of the form **42** in which the substituent in the C-4 position was

varied and the rest of the molecule kept the same as the most potent inhibitor from the series, compound **38** (Figure 2.8). It was assumed that inhibitors with this general structure would maintain the same hydrogen bond contacts to the enzyme as were predicted for compound **38**. The effect of varying the substituent at the C-4 position was difficult to predict computationally, so the only way to determine whether improvements in activity could be achieved by altering this substituent was by making and testing compounds with different substituents at the position. It was decided to synthesise two groups of inhibitors. One in which the R group was an amino aryl substituent, as these had been shown to have the most potent enzyme activities in the previous work. This work will be discussed in Section 2.3. In the second group of inhibitors, R would be a 5-membered heterocycle, as it was hoped synthesising more variants of this type would shed more light on the properties needed for antibacterial activity. This work will be discussed in Section 2.5.

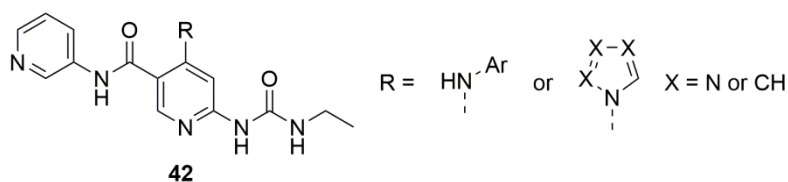


Figure 2.8 General structure of the inhibitors investigated during this project.

It was also decided to produce some derivatives which featured aliphatic substituents in the C4 position. They will be discussed in Section 2.6.

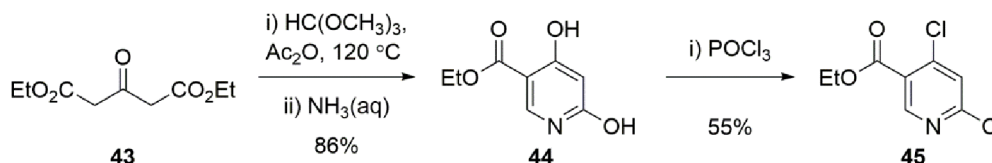
Initial assessment of the *in vitro* ADME properties for compounds in the pyridine 4-carboxamide series will be discussed in Section 2.7.

2.3 C-4 aminoaryl derivatives of the pyridine 3-carboxamide series

A six step synthesis of pyridine-3-carboxamides from acetone dicarboxylate **43** had been developed at the University of Leeds.¹²³ This route was used without modification to synthesise the first pyridine-3-carboxamides in this project.

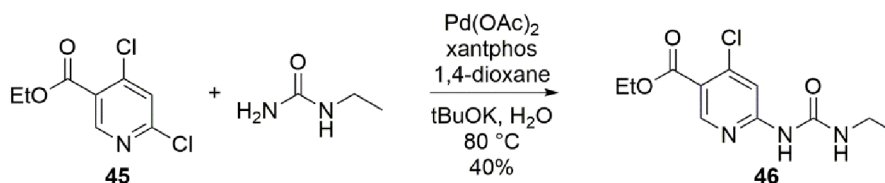
First, an ester of 4,6-dihydroxynicotinate **45** was formed in two steps from diethyl-1,3-acetone dicarboxylate **43**, trimethyl orthoformate and ammonia. This was followed by

chlorination using POCl_3 to give compound **45** (Scheme 2.1). The first step proceeded with a yield of 86% and the second step with a yield of 55%.



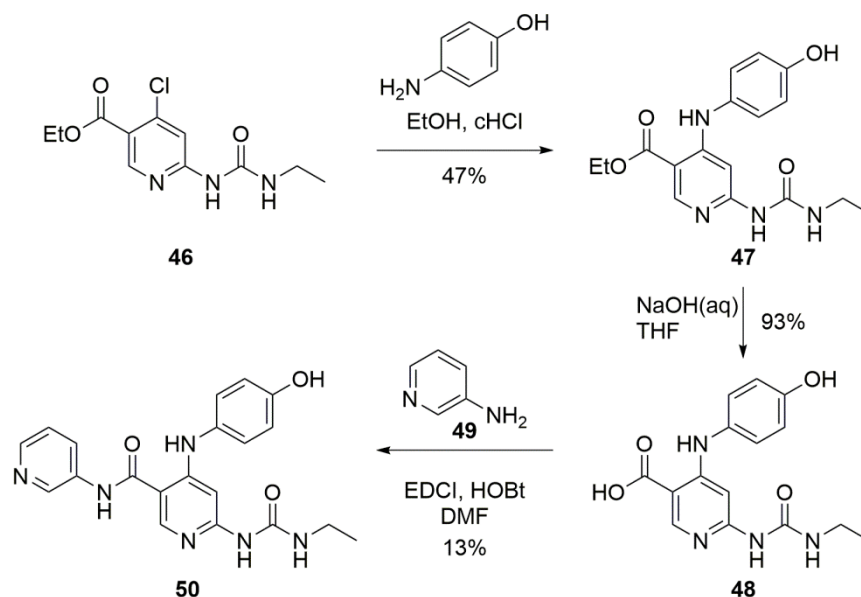
Scheme 2.1 Formation of ethyl- 4,6-dichloronicotinate **45**.

Selective substitution of a chlorine for a urea at the 2-position *via* a Buchwald-Hartwig amination reaction had been reported in the literature.¹²⁷ This reaction was carried out according to the literature conditions. However, at 100 °C the reaction was not selective for the C2 position and a mixture of starting material and mono- and di-substituted material was formed. The selectivity of the reaction was improved by reducing the temperature of the reaction to 80 °C (Scheme 2.2) affording the ethylurea substituted compound **46**.



Scheme 2.2 Selective Buchwald reaction to insert ethyl-urea at the 6-position of ethyl 4,6-dichloronicotinate **47**.

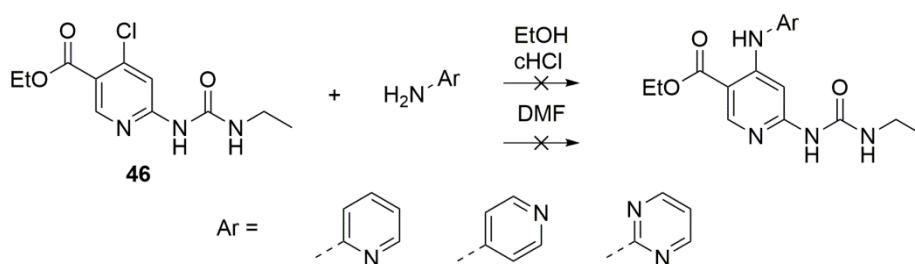
The next step according to the previously established synthetic route was installation of an aniline at the C4 position of the pyridine ring *via* an $\text{S}_{\text{N}}\text{Ar}$ reaction. 4-Hydroxyaniline underwent $\text{S}_{\text{N}}\text{Ar}$ reaction in moderate yield to give **47**. This was followed by hydrolysis which proceeded in good yield to give the carboxylic acid **48** which was coupled to 3-amino pyridine **49** using amide coupling reagents EDC and HOBt to give the final product **50** (Scheme 2.3).



Scheme 2.3 Formation of compound **50**.

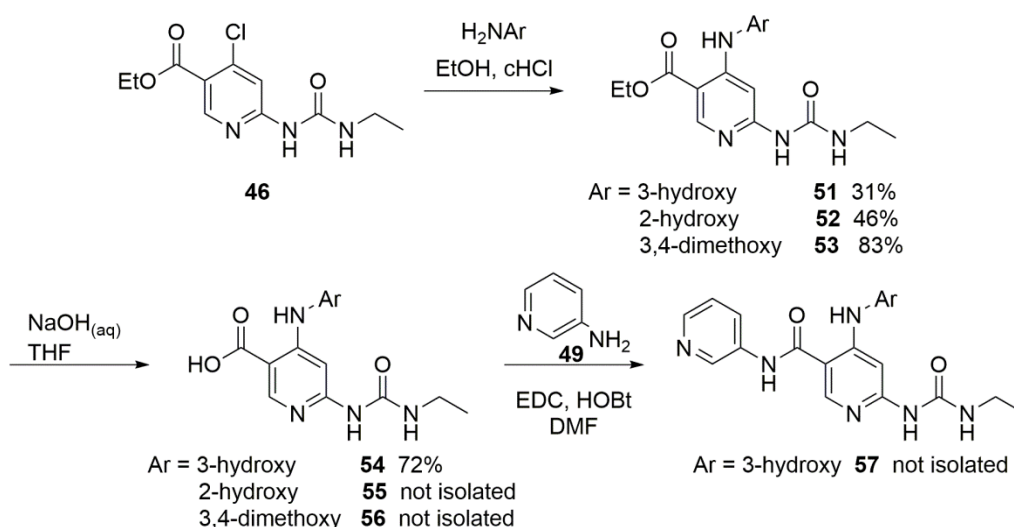
The most potent DNA gyrase inhibitor synthesised as part of the previous work at Leeds was the bis-pyridyl compound **38** (Figure 2.4).⁵⁶ Therefore, 4-aminopyridine, 2-aminopyridine and 2-aminopyrimidine variants were chosen as the next derivatives to make in order to determine whether changing the position of the ring nitrogen would improve the biological activity of the inhibitors.

However, the amino pyridines and amino pyrimidine chosen proved to be unreactive under the previously described S_NAr conditions (Scheme 2.3). The electron deficient nature of the pyridine and pyrimidine rings reduces the nucleophilicity of the amine so that it is unable to attack the Ar-Cl bond of **46** under these conditions. The reaction was then attempted using DMF in place of ethanol, as it is a good solvent for reactions such as nucleophilic aromatic substitutions that follow polar mechanisms. However, no reaction was seen under these conditions (Scheme 2.4).



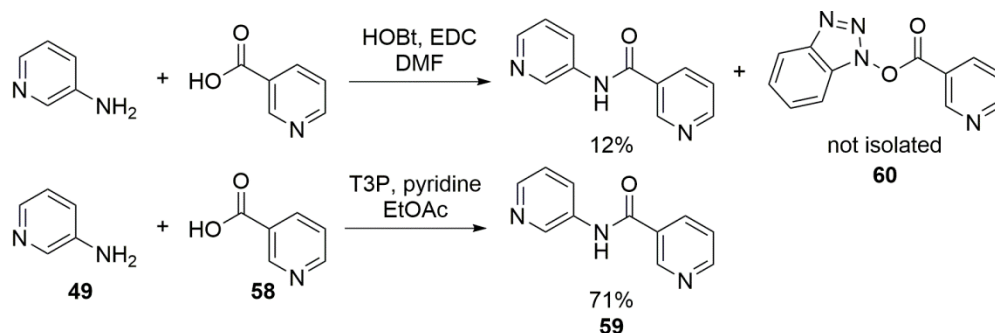
Scheme 2.4 Conditions of attempted S_NAr reactions of amino pyridine and aminopyrimidines.

More activated anilines were investigated, and the S_NAr reaction was successful with 2-hydroxy-, 3-hydroxy- and 3,4-dimethoxyaniline to afford **51**, **52** and **53** respectively. However the reactions were performed on a small scale and following the hydrolysis and amide coupling steps, insufficient material was isolated to allow full characterisation or biological evaluation of the isolated compounds (Scheme 2.5) However, formation of the desired products **55**, **56** and **57** was indicated by LC-MS and NMR of the crude reaction mixture.



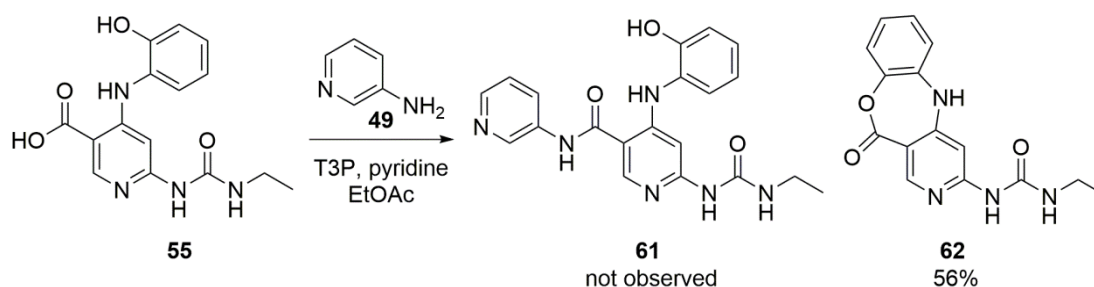
Scheme 2.5 S_NAr , hydrolysis and attempted amide formation using hydroxy- and dimethoxy-substituted anilines.

The major impurity seen in the amide coupling step was the HOBt adduct of the starting material, suggesting that displacement of the HOBt by the aniline was slow. An alternative coupling reagent was sought. Propane phosphonic acid anhydride (T3P) has been shown to be an effective and convenient amide coupling reagent.⁶¹ The reaction of 3-aminopyridine **49** with nicotinic acid **58** to give compound **59** was chosen as a model system to investigate whether switching to T3P as an amide coupling reagent had the potential to give improved yields. When using HOBt and EDC as the amide coupling reagents, a yield of 12% was obtained. The HOBt adduct **60** was detected as a major impurity by NMR of the crude reaction mixture, but was not isolated. Using T3P as the coupling reagent resulted in a significantly higher yield of product which did not require purification using chromatography (Scheme 2.6).



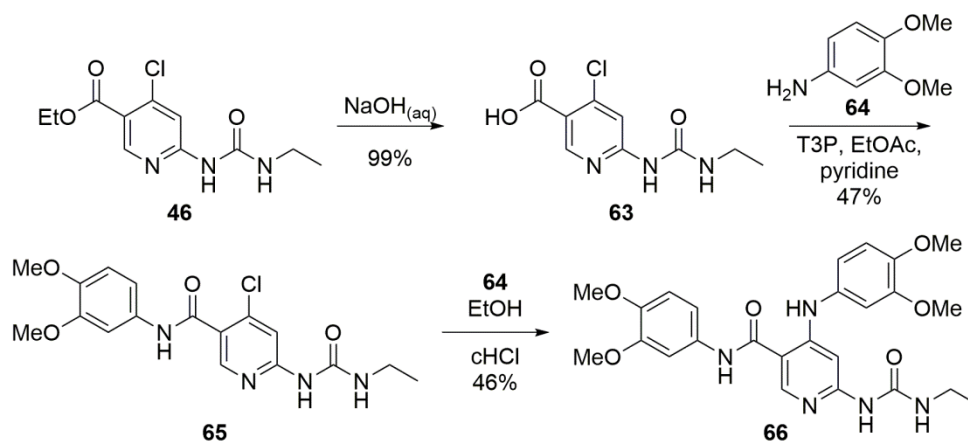
Scheme 2.6 Investigation of T3P as an alternative coupling reagent to HOBt and EDC.

The T3P coupling conditions were then tested using the 2-hydroxyaniline compound **55**, but instead of the expected amide product **61** a lactonisation reaction occurred to give compound **62**, which contained a 7-membered ring lactone, in 56% yield (Scheme 2.7). Although somewhat unexpected, this compound was submitted for biological testing, as it represented an interesting variation of the existing core.



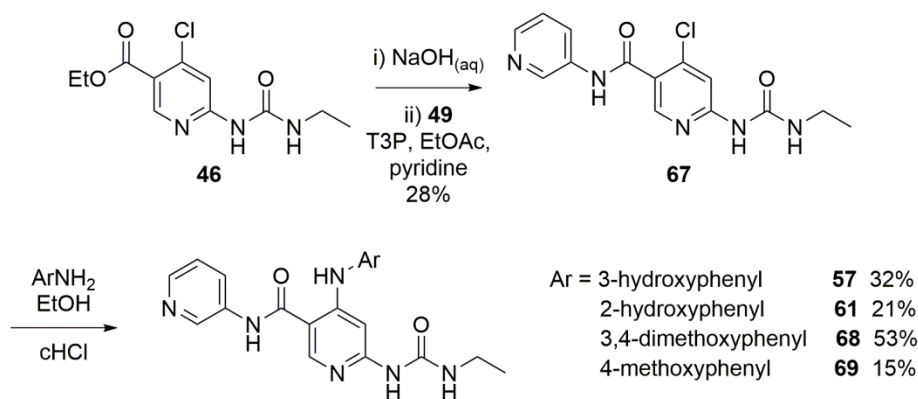
Scheme 2.7 Attempted amide coupling of compound **55** and 3-aminopyridine **49** using T3P.

Re-ordering of the steps in the synthetic route was attempted as a way to improve the efficiency of the synthesis by moving the diversification step to the end of the synthetic route. Hydrolysis of the ester **45** gave the acid **63**. 3,4-dimethoxyaniline **64** was used as the amine in the coupling step for the first attempt at using the new amide coupling conditions in the re-ordered route, as this aniline is more electron rich than 3-aminopyridine and so was expected to react more readily with the activated intermediate derived from compound **63**. The reaction successfully afforded the desired amide **65**. 3,4-dimethoxyaniline **64** was used again to test the S_NAr conditions in the revised synthetic sequence, as use of this amine had been shown previously to give the highest yields of the anilines tried in the earlier version of the synthetic route (Scheme 2.5), and indeed it reacted readily to give the desired product **66** (Scheme 2.8).



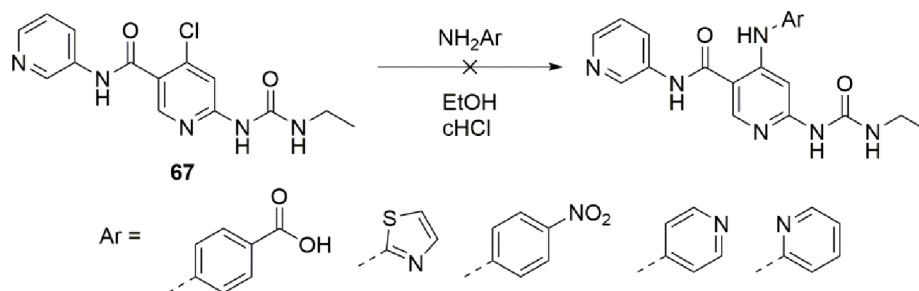
Scheme 2.8 First iteration of a re-ordered synthetic route in which the amide coupling reaction precedes the S_NAr reaction. 3,4-dimethoxy aniline **64** was used as the coupling partner for both reactions due to the high nucleophilicity of its amine.

Having established the re-ordered route and the usefulness of T3P as an amide coupling agent, the ester hydrolysis and amide coupling reactions were repeated using 3-aminopyridine **49** as the amine coupling partner to the acid **63** to give compound **67**. Nucleophilic aromatic substitution of **67** with a number of anilines was then carried out to afford final compounds **57**, **61**, **68** and **69** for biological testing (Scheme 2.9).



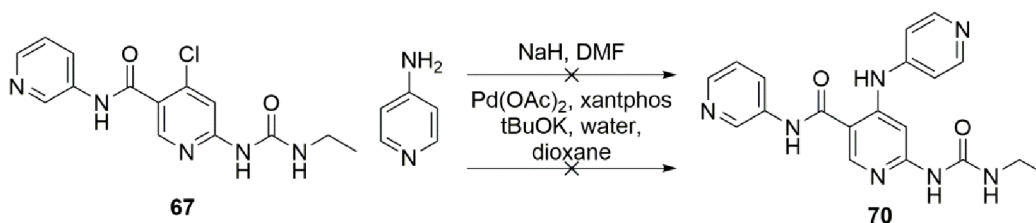
Scheme 2.9 Synthesis of final compounds with 3-pyridyl amide functionality and various arylamine substituents at the C4 position of the central pyridine ring.

Nucleophilic aromatic substitution of **67** with electron deficient anilines was unsuccessful. 4-aminobenzoic acid, 2-aminothiazole, 4-nitroaniline and 4-aminopyridine all proved insufficiently reactive to displace the chlorine of **67** under the established acid catalysed conditions (Scheme 2.10).



Scheme 2.10 S_NAr reactions using electron deficient amines are unsuccessful using the established reaction conditions.

Formation of the 4-aminopyridine-substituted variant **70** was also attempted under base catalysed and Buchwald conditions (Scheme 2.11), but neither of these conditions successfully produced the desired product **70**.



Scheme 2.11 Formation of compound **70** from compound **67** and 4-amino pyridine was unsuccessful under base catalysed, acid catalysed and Buchwald conditions.

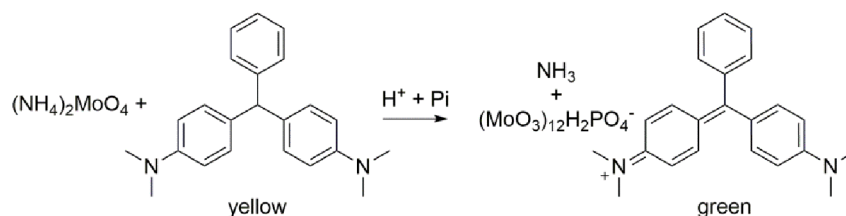
2.4 Biological assessment of inhibitors

Assessment of the biological activity of the inhibitors synthesised during this project was initially carried out by Biota Ltd. in Oxfordshire. Later in the project responsibility for biological evaluation of compounds was transferred to the author. A brief summary of the assays used will be given to explain the different assay protocols used during the project.

The antibacterial activity of inhibitors was determined using standard protocols for the determination of the minimum inhibitory concentration (MIC) as described in Chapter 7, Section 7.2.6 and was performed using comparable protocols both at Biota Ltd at the start of the project and by members of the O'Neill research group at the University of Leeds in the later stages of the project.

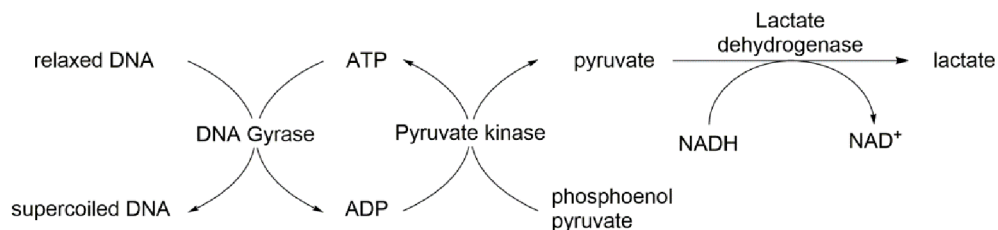
Inhibition of the DNA gyrase and topoisomerase IV enzymes was assayed by Biota Ltd using a malachite green assay which is described in Chapter 7, Section 7.2.4. Use of the

malachite green assay was later investigated at the University of Leeds, but the assay proved to lack robustness and reliability. The malachite green assay is a colourimetric assay which measures the concentration of inorganic phosphate by observing the change in colour of malachite green dye which is added to the assay mixture after a fixed period of incubation (Scheme 2.12). The concentration of inorganic phosphate indicates the amount of ATP which has been converted to ADP and thus the rate of enzyme turnover during the incubation period. However, the malachite green dye is prone to aggregation under the assay conditions making the absorbance measurements unreliable and the activity of the enzyme can only be measured at a single time point.



Scheme 2.12 Reaction of inorganic phosphate with ammonium molybdate under acidic conditions triggers a colour change in malachite green dye from yellow to green.

An alternative assay protocol couples the turnover of ATP with the rate of turnover of NADH, allowing the activity of the enzyme to be monitored continuously by measuring the change in absorbance at 340 nm. This allows enzyme activity to be monitored continuously over a given time period. Pyruvate kinase (PK) and lactate dehydrogenase (LDH) are added to the assay mixture along with phosphoenol pyruvate (PEP) and NADH (Scheme 2.13). This assay protocol is described in Chapter 7, Section 7.2.5.



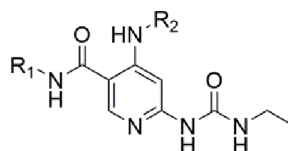
Scheme 2.13 Cascade of reactions in the coupled assay. Turnover of DNA gyrase converts ATP to ADP and Pi which begins a cascade of reactions coupling turnover of DNA gyrase with conversion of NADH to NAD⁺ which can be monitored by measuring absorbance at 340 nm. Compounds whose IC₅₀s had been determined using the malachite green assay at the University of Leeds were had their IC₅₀s re-determined using the “coupled” assay and

the results from the coupled assay are given in the thesis as they were more consistent with previously determined IC₅₀s. Where assays were carried out by Biota Ltd. using the malachite green method it will be indicated.

2.4.1 Biological activity of C-4 aminoaryl pyridines

Table 2.1 shows the activity of the compounds described above against DNA gyrase (GyrB) and topoisomerase IV (ParE) and their antibacterial activity against *S. aureus* and *E. coli*.

Table 2.1



Biological activity of selected pyridine urea carboxamide compounds.

Compound	R ₁	R ₂	clogP	IC ₅₀ s (μM)		MICs (μg/ mL)	
				GyrB	ParE	SA	EC
50			3.15	0.028 ^a	0.94 ^a	8	>64
57			3.15	0.036 ^a	0.78 ^a	n. d.	>64
61			3.15	0.41	0.22 ^a	>64	>64
66			4.04	0.093 ^a	42 ^a	1	>64
68			3.13	0.036 ^a	31 ^a	1	>64
69			3.29	0.019	n/d	4	>64

clogP calculated using the calculator plugins from MarvinSketch¹²⁸; GyrB, *E. coli* DNA gyrase; ParE, *E. coli* topoisomerase IV; SA, *S. aureus* ATCC 29213; EC, *E. coli* ATCC 25922; a assays carried out by Biota Ltd using the Malachite green method.

Several of these compounds are highly potent inhibitors of DNA gyrase, with many of the compounds showing IC₅₀ values lower than 93 nM, which was the IC₅₀ of compound **38**, the most potent pyridine 3-carboxamide DNA gyrase inhibitor synthesised previously at Leeds. However, with the exception of compound **61**, all the compounds were significantly more active against DNA gyrase than topoisomerase IV

and although compound **61** was a little more potent against topoisomerase IV than the other compounds in the series, it was much less active against DNA gyrase.

AutoDock was used to predict the binding poses of the compounds. The binding poses of **50**, **57** and **61** in *E. coli* GyrB and ParE are shown in Figure 2.9. Compounds **50** and **57** were docked in similar poses to the inhibitors already described, but compound **61** was docked in a different pose. This is consistent with the lower activity of this compound. According to the docking model, the *ortho*-hydroxyl substituent present in compound **61** causes a steric clash with the amide carbonyl causing the amide bond to flip into a different orientation. In this conformation compound **61** is less optimally positioned to make hydrogen bond contacts with the protein. The docking model doesn't suggest any obvious cause for the differences in activity between DNA gyrase and topoisomerase IV.

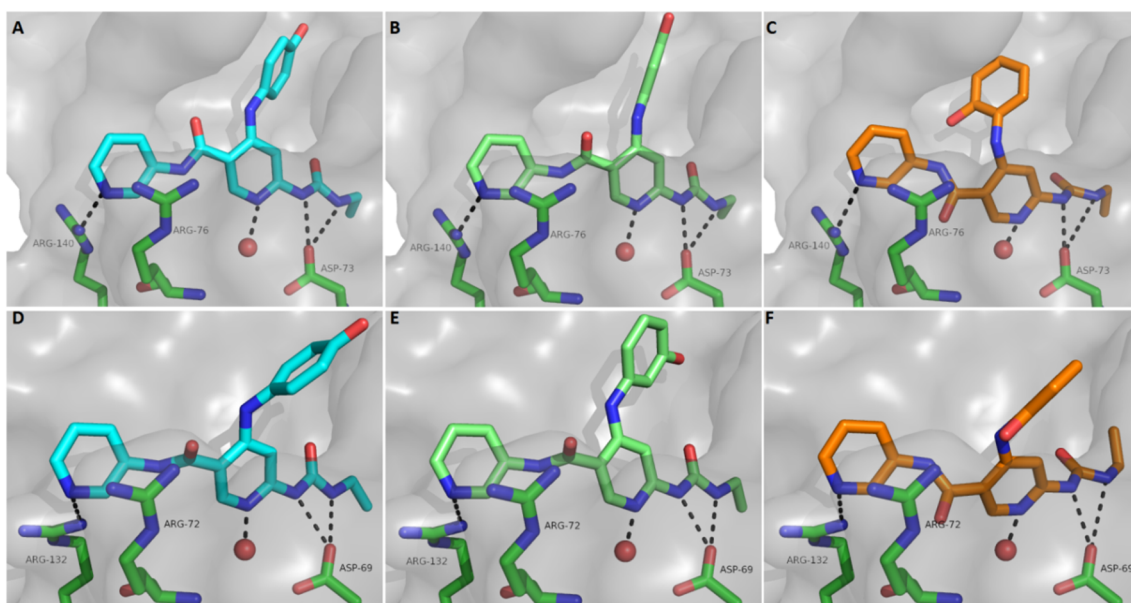


Figure 2.9 Docking poses for compounds **50** (cyan), **57** (green) and **61** (orange) into *E. coli* GyrB (A, B and C) (4HYP) and *E. coli* ParE (D, E and F) (4HZO)⁹².

The greatest selectivity for DNA gyrase over topoisomerase IV was seen with compounds **66** and **68**, both of which have a 3,4-dimethoxyaniline substituent in the C-4 position of the central pyridine ring, this suggests that these larger substituents may disfavour binding to topoisomerase IV. Computational docking predicted the opposite result for these two compounds with both compounds predicted to be unable to adopt favourable binding poses in the GyrB binding site (Figure 2.10). This inconsistency is

likely due to interactions with the flexible loop; in the GyrB crystal structure more of the loop is resolved than in the ParE crystal structure. The docking may predict that the residues from the flexible loop which are present in the GyrB crystal structure would prevent the compounds adopting a conformation that favours binding, when in the enzyme assay the flexible loop would adopt a different conformation allowing the inhibitor to bind.

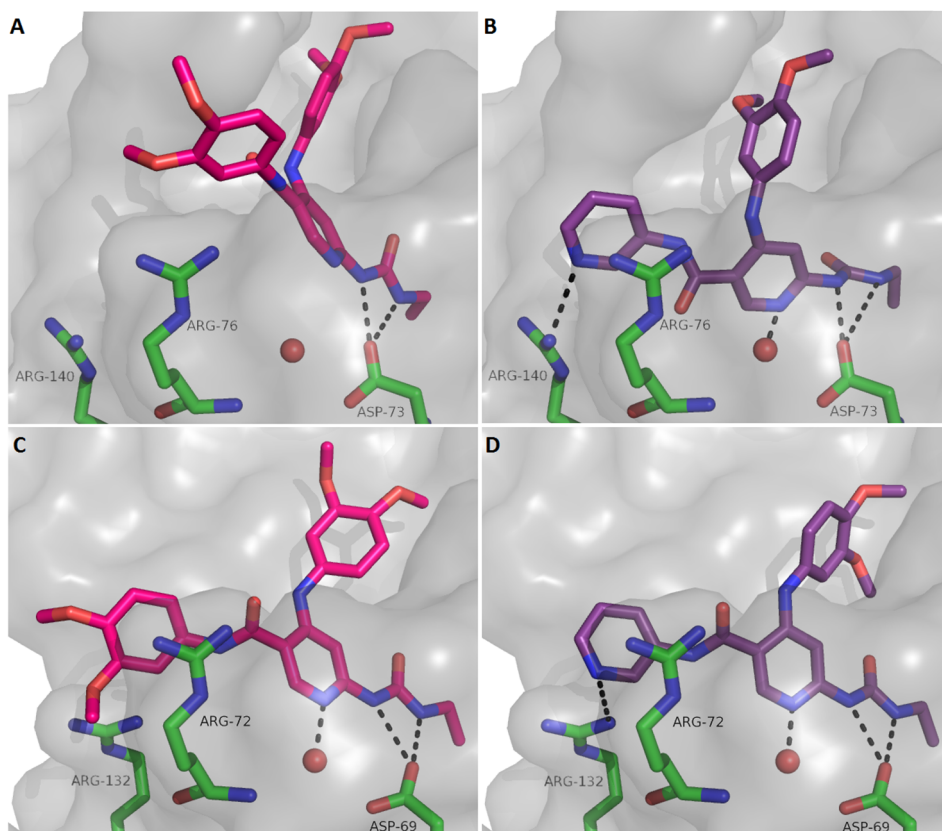


Figure 2.10 Docking poses for compounds **66** (magenta) and **68** (purple) into *E. coli* GyrB (A and B) (4HYP) and *E. coli* ParE (C and D) (4HZ0)⁹².

Despite the high levels of enzyme inhibition exhibited by these compounds, only moderate antibacterial activity was observed. The most potent compounds were **66** and **68** which both exhibited an MIC of 1 $\mu\text{g}/\text{ml}$ against *S. aureus*. These two compounds showed the least activity against topoisomerase IV, which indicates that good activity against DNA gyrase is sufficient for antibacterial activity. Compounds **66** and **68** had the highest and lowest lipophilicities of the compounds tested with clogPs of 4.04 and 3.13 respectively. This is not a very wide range of lipophilicities, so it is hard to say whether the lipophilicity of these compounds has a significant impact on their ability to cross bacterial membranes.

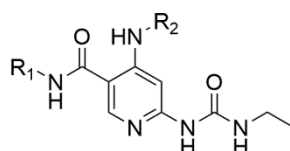
None of the compounds tested showed any activity against *E. coli*. This is most likely to be due to difficulties penetrating the Gram negative outer membrane of *E. coli*.

Compounds **50**, **57**, **66** and **68** were assessed for their antibacterial activity against a wider panel of bacterial species, but showed no activity against *K. pneumoniae*, *A. baumannii* or *P. aeruginosa*.

These compounds were also screened for their inhibitory activity against the DNA gyrase and topoisomerase IV enzymes from *S. aureus* in order to determine whether differences in antibacterial activity could be due to different activities against the enzymes from different bacterial species. These results are given in Table 2.2 along with the selectivity of each compound for GyrB over ParE in each of the two species investigated.

Interestingly, these compounds showed much greater activity against the *S. aureus* topoisomerase IV enzyme than they did against the *E. coli* topoisomerase IV enzyme. This may be one factor which contributes to these compounds having antibacterial activity against *S. aureus* and not *E. coli*, as they are closer to having equal activity against both enzymes in *S. aureus*.

Table 2.2



Biological activity of selected pyridine urea carboxamide compounds.

Cmpd	R ₁	R ₂	<i>E. coli</i>			<i>S. aureus</i>		
			IC _{50s} (μM) GyrB	IC _{50s} (μM) ParE	Selectivity ParE/GyrB	IC _{50s} (μM) GyrB	IC _{50s} (μM) ParE	Selectivity ParE/GyrB
50			0.028	0.94	34	0.024	0.087	3.6
66			0.093	42	450	0.071	0.81	11
68			0.036	31	860	0.041	0.82	20

GyrB, DNA gyrase; ParE, topoisomerase IV; assays carried out by Biota Ltd using the malachite green method.

Compound **62** was also assessed for its biological activity which is shown in Figure 2.11. It exhibited low enzyme activity, particularly against topoisomerase IV and had no

antibacterial activity. This is not unexpected as its structure is significantly different to those of the other inhibitors assayed. Although it is able to form the same hydrogen bond contacts to the aspartate residue and conserved water that are formed by other compounds described in this chapter, it lacks an aromatic group able to form a key π -stacking interaction with an arginine residue in the active site.

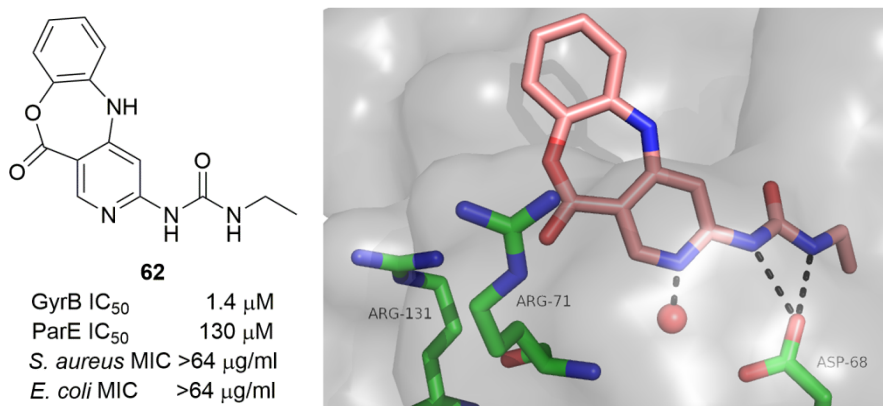
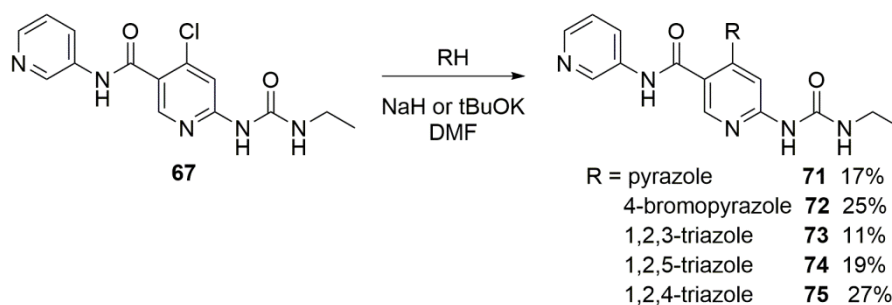


Figure 2.11 Biological activity of compound **62**. GyrB and ParE enzymes from *E. coli* assessed at Biota Ltd. using the malachite green method. Docking pose for compound **64** into *F. tularensis* ParE (4HXZ)⁹².

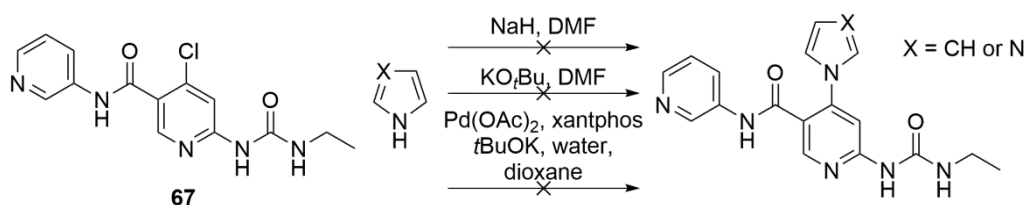
2.5 C-4 heterocyclic derivatives of the pyridine 4-carboxamide series

Synthesis of C-4 heterocycle-substituted derivatives of the pyridine 4-carboxamide compounds began with the same steps described previously in this chapter (Scheme 2.1, Scheme 2.2 and Scheme 2.9) and diverged from the 4-chlorosubstituted intermediate **67**. Installation of 5-membered ring heterocycle units at the C-4 position of the 4-chloro substituted intermediate **67** via S_NAr reaction was carried out successfully with yields of 11-74% (Scheme 2.14). The 1,2,3- and 1,2,5-triazole substituted derivatives **73** and **74** were produced using the same reaction of compound **67** with 1,2,3-triazole and the products separated using column chromatography.



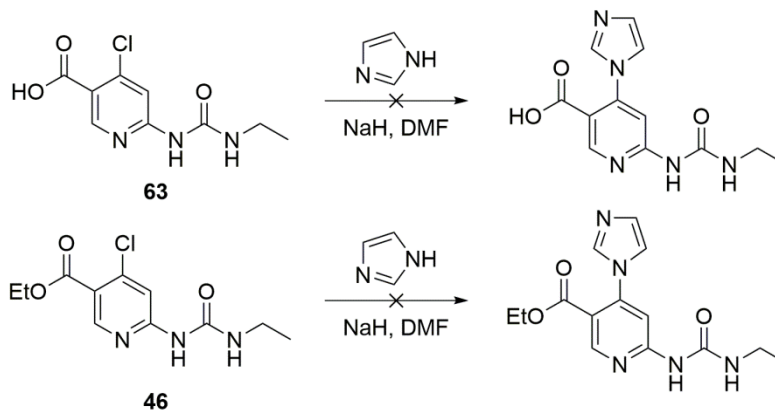
Scheme 2.14 Synthesis of heterocyclic derivatives of the pyridine carboxamide series via S_NAr reaction.

Both pyrrole and imidazole failed to react with compound **67** using the conditions described above. Changing the base from sodium hydride to potassium *tert*-butoxide also failed to give the desired product, as did the use of Buchwald conditions (Scheme 2.15).



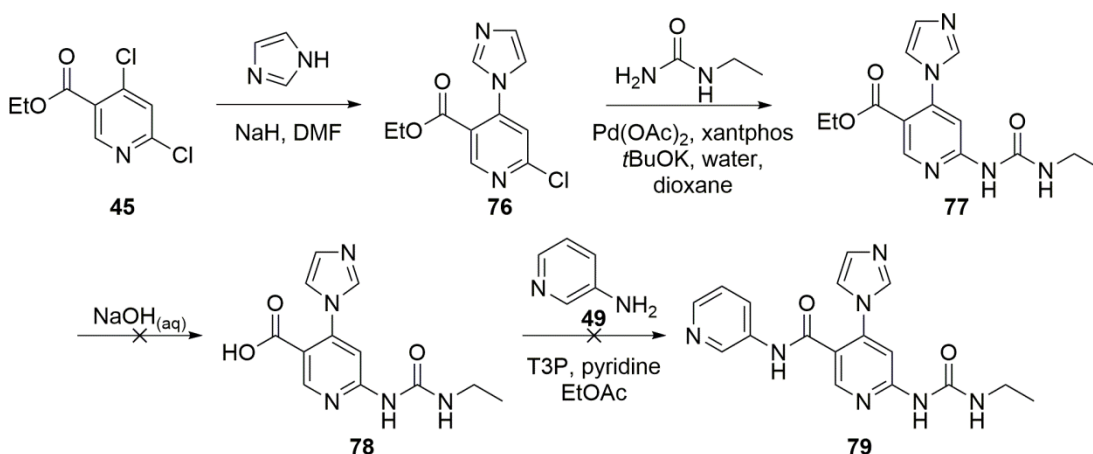
Scheme 2.15 Installation of imidazole and pyrrole using the same conditions as described in Scheme 2.14 was unsuccessful, as were a change of base and the use of Buchwald conditions.

Installation of these moieties at an earlier point in the synthetic route was investigated as a possible way of accessing these compounds. However, neither the carboxylic acid intermediate **63** nor the ester intermediate **46** were able to successfully undergo reaction with imidazole under the conditions investigated (Scheme 2.16).



Scheme 2.16 Attempted installation of imidazole at two earlier points in the synthetic route. Imidazole failed to react with either intermediate.

The reaction of imidazole with the di-chloro substituted intermediate **45** was successful, affording compound **76** and compound **76** was then able to successfully undergo a Buchwald reaction to give the urea substituted intermediate **77**. However, none of the carboxylic acid intermediate **78** was isolated from the hydrolysis reaction and so the amide coupling reaction to give the desired product **79** could not take place (Scheme 2.17).



Scheme 2.17 Attempted synthesis of imidazole substituted derivative **79**. Reaction of imidazole with compound **45** to give compound **76** was successful as was the Buchwald reaction to give compound **77**, but the hydrolysis reaction was unsuccessful.

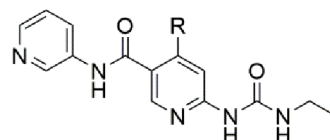
2.5.1 Biological activity of C4-amino heterocyclic pyridines

Biological activities for these compounds are shown in Table 2.3. The bromopyrazole substituted compound **72** had the most potent antibacterial activity with an MIC of 16 $\mu\text{g/ml}$ against *S. aureus*. This compound showed a sub-micromolar level of enzyme inhibition with an IC_{50} of 0.037 μM against DNA gyrase. Compounds **71** and **73** displayed antibacterial activity at 64 $\mu\text{g/ml}$. All of the compounds tested had sub-micromolar enzyme activity. The least potent inhibitors in the series were the 1,2,3- and 1,2,5-triazoles **73** and **74**.

Docking of these compounds to the *E. coli* GyrB protein predicted that they should all bind very similarly in the ATP site (Figure 2.12). The main difference in the predicted poses was that compounds **72** and **73** were predicted to bind with their amide bonds at a tilted angle which positions the pyridine ring in a configuration that prevents the

formation of a hydrogen bond to Arg-140. This may not reflect the true binding poses of these compounds, as this difference doesn't correlate with the IC₅₀s of the compounds.

Table 2.3



Biological activity of selected pyridine urea carboxamide compounds.

Compound	R	clogP	IC ₅₀ s (μM)		MICs (μg/ mL)	
			GyrB	SA	SA	EC
71		0.79	0.086	64	>64	>64
72		1.56	0.037	16	>64	>64
73		-0.02	0.15	64	>64	>64
74		0.41	0.20	n.d.	n.d.	n.d.
75		0.11	0.082	>64	>64	>64

clogP calculated using the calculator plugins from MarvinSketch¹²⁸; GyrB, *E. coli* DNA gyrase; SA, *S. aureus* ATCC 29213; EC, *E. coli* ATCC 25922.

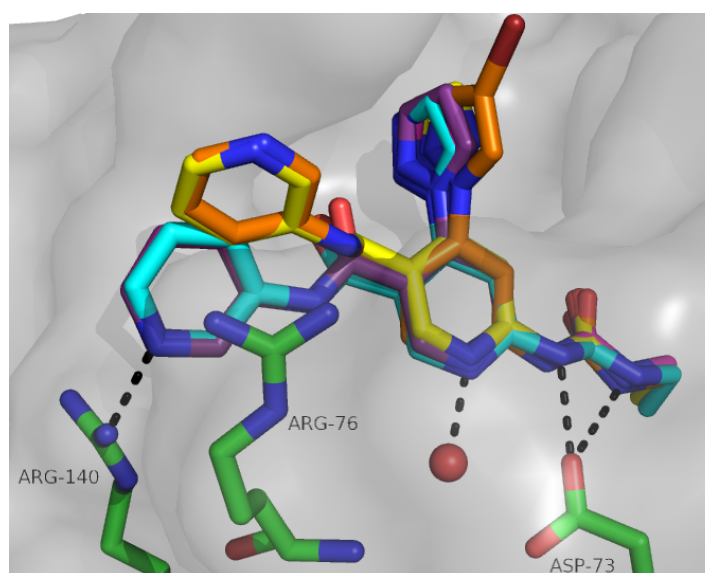
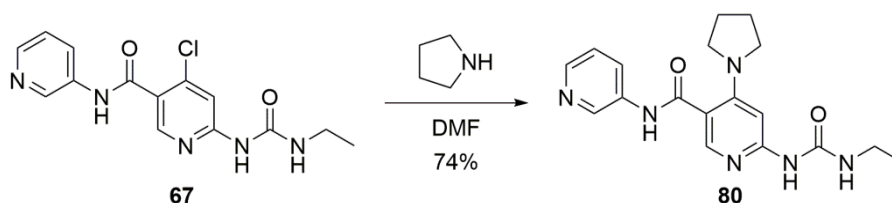


Figure 2.12 Predicted binding poses of compounds **71** (purple), **72** (orange), **73** (yellow), **74** (turquoise) and **75** (magenta) to *E. coli* GyrB (4HYP)⁹².

The IC_{50} s of these compounds don't show any correlation with their clogPs, posing a challenge to the rationalisation of the IC_{50} values of these compounds using computational predictions. The clogPs of these compounds were not particularly well correlated with their antibacterial activity either.

2.6 Pyrrolidine substituents

All of the inhibitors in the series described so far have had a high proportion of aromatic character and a low proportion of sp^3 carbons. It has been shown that the ratio of sp^3 carbons to non- sp^3 carbons in a potential drug molecule correlates with the chance of that molecule successfully progressing towards becoming a drug.¹²⁹ Replacing aromatic rings with aliphatic rings can lead to an increase in solubility for example. It was therefore decided to synthesise a derivative with a higher fraction of sp^3 carbons. Reaction of compound **67** with pyrrolidine furnished compound **80** in good yield (Scheme 2.18).



Scheme 2.18 Reaction of compound **67** with pyrrolidine to afford a derivative with an unsaturated ring substituent at the C4 position **80**.

A series of DNA gyrase inhibitors had been reported by Trius Therapeutics Inc., including compound **33**, which contain a substituted pyrrolidine ring in a position analogous to the C4 substituent in the pyridine carboxamide series (Figure 2.13).¹¹⁹ Having a primary amine which is protonated at biological pH may influence the ability of a compound to penetrate the membranes of bacteria. It has been shown that compounds with activity against Gram negative bacteria tend to have much lower clogPs than compounds which are only active against Gram positive bacteria.³⁴ It was decided to synthesise a variant, **81**, with an analogous aminopyrrolidine substituent. It was decided to synthesise the compound as a racemate in the first instance, as the racemic starting material was more readily available. An asymmetric synthesis could be

carried out later in the case that the racemic compound proved to have particularly promising biological activity.

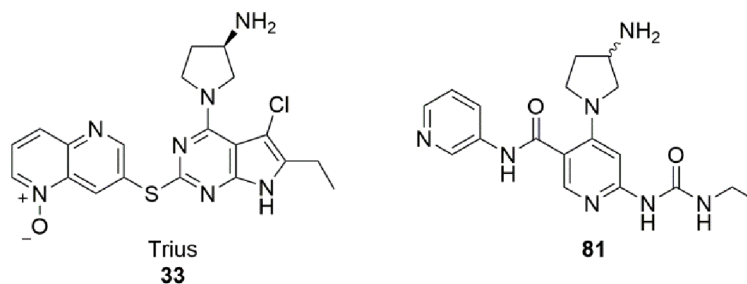
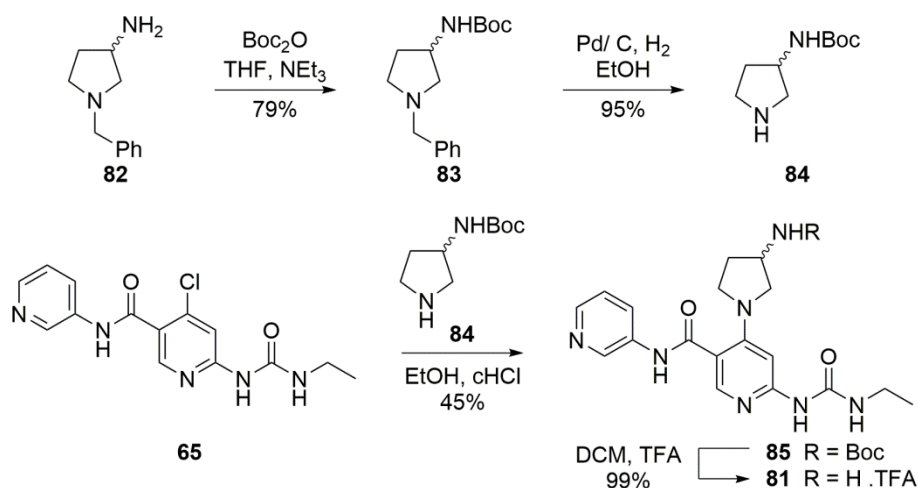


Figure 2.13 An inhibitor containing aminopyrrolidine substituent at the C4 position of the pyridine ring **81** would have a similar substitution pattern to an inhibitor reported by Trius **33**¹¹⁹.

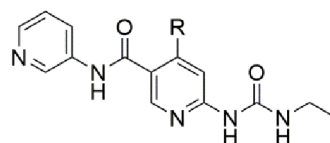
The benzyl protected amino pyrrolidine compound **82** was commercially available and there were literature conditions for the required protection and deprotection steps needed to generate compound **84**¹³⁰. Boc protection of compound **82** to give compound **83** was successful, as was the benzyl deprotection reaction to give compound **84**. Reaction of compound **84** with compound **67** afforded the boc-protected derivative **85** and deprotection with TFA afforded the desired product **81** as a TFA salt (Scheme 2.19).



Scheme 2.19 Change of protection groups afforded the substituted pyrrolidine **84** in two steps from compound **82**. This underwent reaction with compound **67** followed by deprotection to afford the aminopyrrolidine derivative **81**.

The biological activities of compounds **80**, **81** and the boc-protected intermediate **85** along with their clogPs are given in Table 2.4.

Table 2.4



Biological activity of selected pyridine urea carboxamide compounds.

Compound	R	clogP	IC ₅₀ s (μM) GyrB	MICs (μg/ mL)	
				SA	EC
80		1.22	0.12	64	>64
81		-0.03	0.089	>64	>64
85		1.46	0.21	n/d	n/d

clogP calculated using the calculator plugins from MarvinSketch¹²⁸; GyrB, *E. coli* DNA gyrase; SA, *S. aureus* ATCC 29213; EC, *E. coli* ATCC 25922.

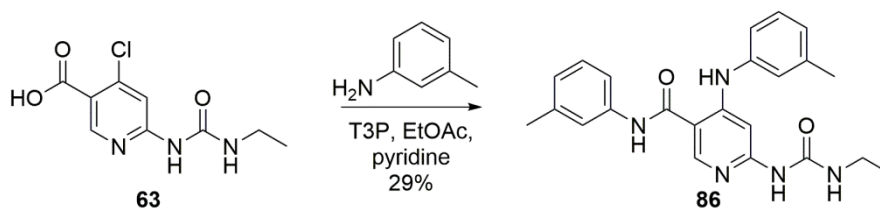
Despite all three compounds showing sub-micromolar enzyme inhibition, only compound **80** showed any antibacterial activity with an MIC of 64 μg/ml against *S. aureus*. Compound **81** had the most potent enzyme activity, but displayed no antibacterial activity at 64 μg/ml against either bacterial strains tested. This suggests that increasing the polarity alone is insufficient to increase antibacterial activity.

2.7 Investigation of ADME

The importance of early determination of the “drug-likeness” of inhibitor compounds has been increasingly highlighted as being of vital importance to the ultimate success of a drug discovery project.¹³¹ The ability of a molecule to be an effective drug depends on many factors; simply being a good inhibitor of the target of interest is not sufficient. A drug molecule must also be able to be easily absorbed in the body, distributed around the body to reach the place that it needs to act, resist metabolism enough to maintain active levels in the blood between doses, and be safely excreted so that it doesn't accumulate to toxic levels in the body. These properties are often referred to

together as ADME (absorption, distribution, metabolism and excretion) and are also often grouped together with toxicity to give ADMET.

There are many assays and experiments that can be carried out to help measure the *in vitro* ADME properties of a potential drug compound at an early stage before it is subjected to any trials in animals. These *in vitro* experiments can be vital in ensuring that resources are not wasted in later parts of a drug discovery project on animal studies that show poor efficacy due to problems with ADME that could have been spotted earlier. Preliminary *in vitro* ADME studies were carried out on four compounds: **69**, **71**, **72** and **86**. The synthesis and biological evaluation of compounds **69**, **71** and **72** was described earlier in this chapter. Compound **86** was originally synthesised as part of previous work at the University of Leeds¹²³ and was resynthesised for these studies in one step from intermediate **65** (Scheme 2.20). The results of the ADME assessments are shown in Table 2.5.



Scheme 2.20 Previously reported DNA gyrase inhibitor **86** was resynthesised in one step from compound **63** by reaction with 2 equivalents of *m*-toluidine.

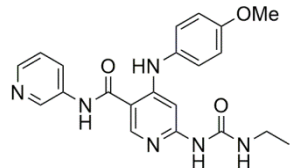
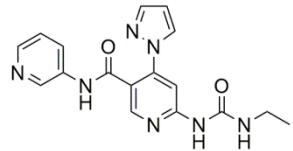
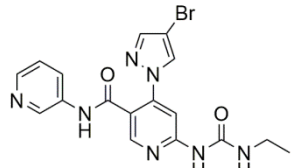
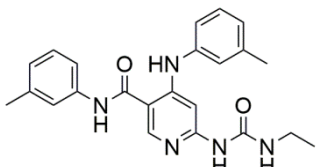
Aqueous solubility is important, as compounds which have low aqueous solubility are hard to administer and will not be able to achieve a high concentration in blood. Additionally, solubility has an impact on the ADME of compounds as increased solubility may improve absorption and distribution. However, compounds with high aqueous solubility are often highly polar and this can increase their rate of metabolism and excretion. The aqueous solubility of compounds **69**, **72** and **86** was very low suggesting they would be challenging to administer orally. This is mirrored by the high levels of plasma protein binding seen for these compounds. However, compound **71** showed a much higher aqueous solubility and correspondingly lower plasma protein binding.

An estimate of the ability of these compounds to cross biological membranes was also carried out using the Caco-2 permeability assay which uses a human intestinal cell line to model absorption of a compound from the gut¹³². The rate of transfer of compound is measured in both directions across the cell membrane. The rate of transfer in the A-B direction (mimicking transfer from the gut to the blood) and the efflux ratio (an indicator that a compound will fail to be absorbed due to efflux) are given in the Table 2.5. Compounds **69** and **71** performed the best in this assay showing a moderate permeability and lower efflux ratios than the other compounds. Compound **72** had a low permeability and a high efflux ratio. Full data are not available for compound **86**, as it was not present in the reservoirs at a high enough concentration for reliable measurements to be made.

Microsomal stability assays were carried out in mice liver microsomes and human liver microsomes. The liver is responsible for metabolism of small molecules so that they can be more easily excreted from the body and liver microsome cells are the cells mostly responsible for this metabolism. These assays give an indication of the speed with which a drug molecule will undergo primary metabolism. The more quickly a drug is metabolised the more frequently it would have to be dosed, so a half-life of several hours is preferred. The half-life ($t_{1/2}$) of a drug molecule is used as a standard measure of metabolic stability. Understanding the difference between rate of metabolism between human and mice cells is useful if a compound is going to be used in a mouse model of the disease in question.

In the human liver microsome assay the most stable compound tested was compound **71** which had a half-life ($t_{1/2}$) of 290 minutes. Compounds **69** and **86** were the least metabolically stable. This suggests that the aryl amine groups are less metabolically stable than the pyrazoles. Addition of functional groups known to slow metabolism, such as CF_3 could increase the half-life of these compounds.¹³³

Table 2.5 Measurements of some ADME properties.

Cmpd	Structure	<i>E. coli</i> GyrB IC ₅₀ (nM)	<i>S. Aureus</i> MIC (µg/ml)	Aqueous solubility ^b (µM)	Human Plasma protein binding ^b (%)	Caco-2 permeability A-B ^b (P _{app} ×10 ⁶ / cm·s ⁻¹)	Caco-2 efflux ratio ^b P _{app} (B-A)/ P _{app} (A-B)	Human liver microsome t _{1/2} ^b (mins)	Mouse liver microsome t _{1/2} ^b (mins)
69		19	4	2.4	97.2	11.83	2.82	20	n/d
71		63	64	88.5	50.2	4.02	2.78	290	n/d
72		27	16	32.6	90.5	1.23	30.8	128	24
86		99 ^a	1	4.26	99.9	<2.67 ^c	n/a	46	58

GyrB, *S. aureus* DNA gyrase; SA, *S. aureus* ATCC 29213; a. assays carried out by Biota Ltd using the Malachite green method; b. assays carried out by Shanghai ChemPartner Ltd. c. P_{app} values were expressed as “<” than the values that were calculated using the minimum concentration of the standards for receiver sides as the concentration in the receivers was below the quantitation limit.

Cytochrome P450 enzymes (CYPs) are the major enzymes involved in drug metabolism as they oxidise small organic molecules allowing them to be more easily excreted from the body.¹³⁴ Inhibition of CYPs can cause adverse drug interactions by preventing the metabolism and clearance of a large number of drug molecules. Molecules which inhibit CYPs may be harder to progress to a successful drug due to their increased chance of adverse interactions. In order to assess the potential of this compound series to inhibit CYPs, compound **86** was assessed against a panel of cytochrome P450s. It showed an IC₅₀ greater than 10 µM against CYP1A2, CYP2C9, CYP2C19 and CYP2D6. These four enzymes are known to be responsible for the primary metabolism of 90% of drugs.¹³⁵

One measurement of toxicity was also carried out. The hERG (human ether a-go-go) gene codes for the α-subunit of a vital ion channel in the heart. Inhibition of this channel causes long QT syndrome, a heart disorder which can lead to dangerous arrhythmias, so compounds which inhibit the channel can cause serious side effects.¹³⁶ Compound **86** was assayed for its inhibition of hERG, but it showed no inhibition at 30 µM which was the highest concentration tested. This suggested that the compounds in this series do not possess a significant hERG liability.

2.8 Summary

Compounds were synthesised and assessed for their antibacterial activity against *S. aureus* and *E. coli* and their inhibitory activity against DNA gyrase. Some compounds were additionally profiled against a broader range of bacterial species and against topoisomerase IV. Four compounds were additionally profiled for their *in vitro* ADME properties.

Several compounds showed more potent activity against DNA gyrase than any inhibitors previously reported in this series, in particular compound **69** which had an IC₅₀ of 19 nM against *E. coli* DNA gyrase. Some compounds showed moderate antibacterial activity against *S. aureus*; the most active compounds were **66** and **68** which had MICs of 1µg/ ml. However, none of the compounds tested showed any activity against *E. coli*.

Despite the highly potent inhibitory activity of these compounds, they show only moderate antibacterial activity. This suggests that the physicochemical properties of these compounds might be reducing the ability of these compounds to reach a sufficiently high concentration within the bacterial cell. This was particularly evident when looking at Gram negative bacteria, against which these compounds showed no activity.

Attempts to prepare compounds with more polar substituents, particularly pyridines, were hampered by the lower reactivity often demonstrated by the heterocyclic molecules.

Preliminary profiling of the *in vitro* ADME properties of these compounds showed some areas of promise and some room for improvement. However, of the four compounds tested for their *in vitro* ADME profiles, the compound with the least potent enzyme and antibacterial activity, compound **71**, proved to have the most promising ADME properties.

2.9 Future work

Chapter 3 details the solution of X-ray crystal structures of these compounds bound to the DNA gyrase protein and discusses their binding mode and the potential to rationally design inhibitors with greater binding affinity. However, as the compounds detailed in this chapter demonstrate, highly potent enzyme activity does not necessarily correlate with potent antibacterial activity and so focusing on improving the physicochemical properties of the compounds rather than their enzyme inhibition might lead to more promising candidates.

The ADME analysis indicated many compounds in this series are not sufficiently soluble and are readily metabolised. Addition of solubilising groups and metabolism blocking groups may improve the properties of these compounds.

Chapter 3 Crystallisation of inhibitor enzyme complexes

3.1 Introduction

The ability of medicinal chemists to rationally design drug molecules, in order to optimise their interactions with a given enzyme or receptor, has been transformed by the development of X-ray crystallography. Rather than blindly investigating SAR by trial and error without being able to explain why one change increases activity while another decreases it, X-ray crystal structures of protein-ligand complexes have allowed scientists to rationalise the binding modes of molecules and therefore make more informed choices about which derivatives to make.¹³⁷

As described in Chapter 1, two truncated versions of the GyrB protein are commonly used in crystallographic experiments. Inhibitor co-crystal structures are most often acquired using the 24 kDa subunit of the protein (GyrB24) which crystallises in a monomeric form, whereas co-crystal structures with ATP and non-hydrolysable analogues of ATP are most often acquired using the 43 kDa subunit of the protein (GyrB43) which crystallises as a protein dimer.

In order to explore the binding mode of the inhibitors described in Chapter 2, it was decided to produce the 24 kDa subunit of GyrB and generate crystal structures of several key inhibitors within the GyrB protein.

3.2 Production of the 24 kDa subunit of GyrB

3.2.1 Cloning of the GyrB24 gene into a vector with a hexahistidine-tag¹

The pAM24 plasmid which codes for the 24 kDa subunit of *E. coli* GyrB was kindly supplied by the Maxwell group at the John Innes Centre. It was decided to transform the gene into a vector with a hexahistidine tag (“his-tag”) for ease of purification. Polyhistidine tags are most frequently added to the N-terminal end of a protein and allow the protein to be purified simply by Ni-resin affinity chromatography.

Ligation independent cloning (LIC) was used to transfer the gene coding for the 24 kDa subunit of GyrB into a pNIC plasmid which includes the his-tag as well as a GB1 tag to

¹ Cloning experiments carried out with the assistance of Dr. Gemma Wildsmith.

increase the solubility of the protein during purification¹³⁸. An overview of the LIC process is given in Figure 3.1. Ligation independent cloning uses the 3' to 5' exonuclease activity of the T4 DNA polymerase to generate long “sticky” ends in both the vector and the insert. Mixing the T4 polymerase treated vector and insert in a 1:2 ratio allows the two to anneal. There is no need to use a DNA ligase, as the sticky ends ensure that the vector and insert remain annealed until they are transformed into ultra-competent *E. coli* cells which will seal the nicks in the plasmid and reproduce it.

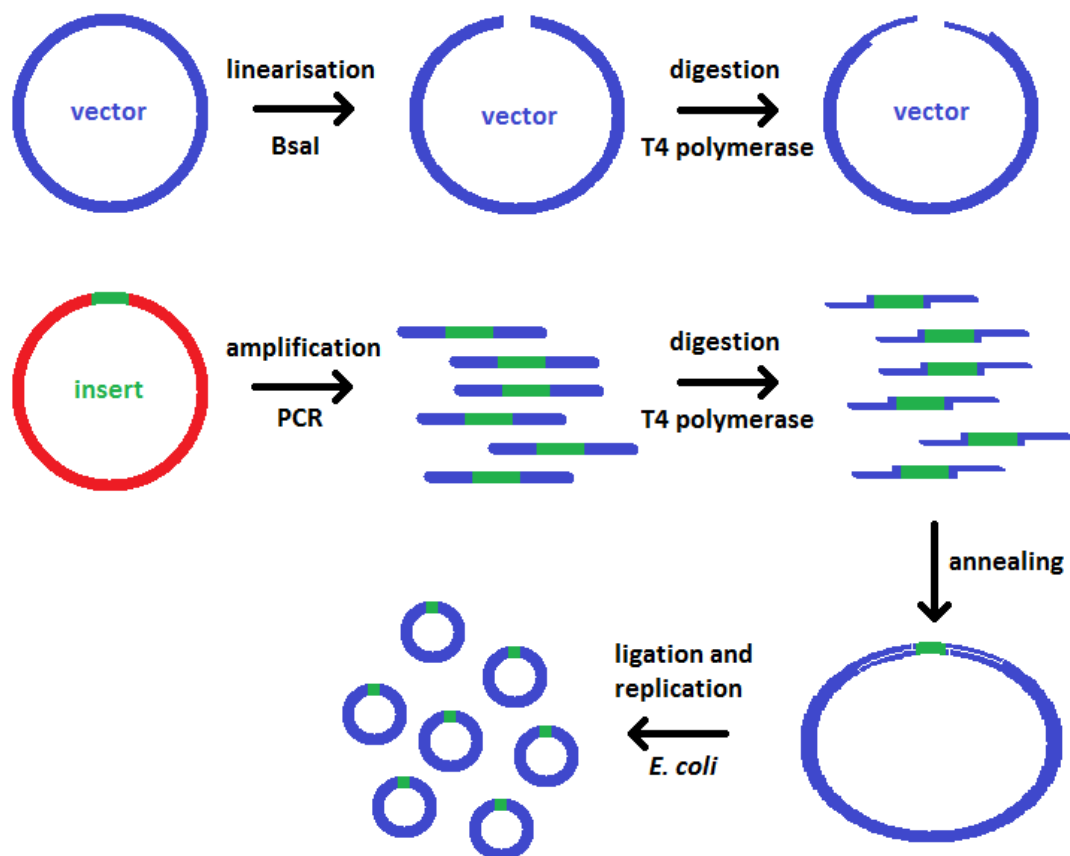


Figure 3.1 Overview of ligation independent cloning (LIC). The vector plasmid is linearised by treatment with BsaI and sticky ends produced by T4 polymerase digestion. The gene of interest is amplified by PCR using primers with complementary sequences to the sticky ends in the vector, so that digestion with T4 polymerase produces complementary sticky ends. When the vector and the insert are mixed they anneal and transformation into *E. coli* cells causes the nicks to be sealed and the plasmid to be replicated.

The pNIC-GB1 vector was linearised by digestion with BsaI and sticky ends generated by treatment with T4 polymerase in the presence of only one deoxynucleotidetriphosphate (dNTP), in this case dGTP (deoxyguanidinetriphosphate). The GyrB24 gene was amplified *via* PCR using primers that contained a complementary

overhang to the pNIC vector and then complementary sticky ends were generated by treatment with T4 polymerase, this time with only dCTP (deoxycytosinetriphosphate). The two components were then mixed in a ratio of 1:2 vector:insert. The annealing product was then transferred into *E. coli* XL10-gold ultracompetent cells which sealed the nicks in the plasmid and were cultured to produce many copies of the plasmid.

Sanger sequencing confirmed the correct sequence in the new plasmid and the DNA was transformed into BL21-Gold (DE3) cells for expression.

3.2.1.1 Production and purification of GyrB24 protein

The histidine residues cause the tagged protein to bind strongly to divalent metal ions. Passing the cell lysate over a resin with appropriate chelating groups bound to nickel ions will cause the protein of interest to be retained on the resin allowing all other proteins from the cell lysate to be washed off the column. The protein of interest can then be eluted using a high imidazole buffer as imidazole will displace the histidines from the nickel on the resin. Figure 3.2 shows a his-tagged protein interacting with a Ni-NTA agarose affinity resin.

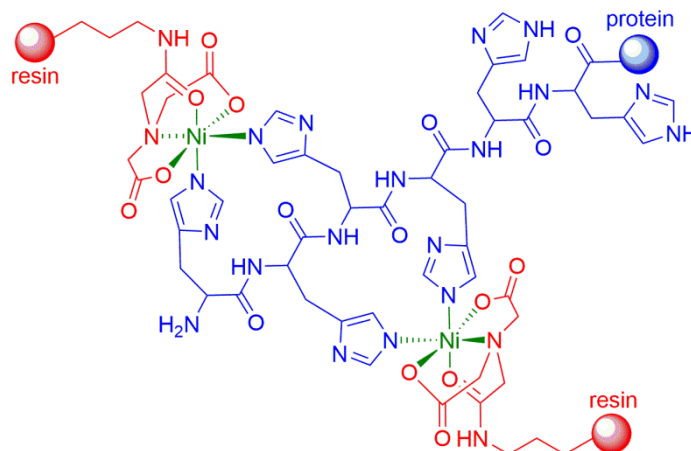


Figure 3.2 Interactions between his-tagged protein and Ni-NTA agarose resin. Agarose resin functionalised with nitrilotriacetic acid (NTA) groups (red) can be loaded with a divalent metal, in this example Ni (green), which will strongly bind to histidine groups in a protein (blue). A chain of adjacent histidine groups ensures a strong interaction with the resin.

Once purified, the his-tag can be removed from the tagged protein using the tobacco etch virus (TEV) protease. This enzyme is a serine protease which recognises the following sequence ENLYFQ\S, where “\” denotes the position of the cleaved peptide bond. Inclusion of this sequence between the his-tag and the GyrB24 protein allows

the his-tag to be removed leaving only the native protein sequence with one extra N-terminal serine residue. There is a large area of contact between the TEV protease and the protein chain being cleaved which allows for a high degree of specificity.¹³⁹

The GyrB24 protein was overexpressed and purified according to the methods described in Chapter 7. The protein was overexpressed and purified using Ni-NTA chromatography and the his-tag cleaved using TEV protease. A second Ni-NTA column separated the cleaved protein from the tag. Size exclusion chromatography was used as a final purification step. The UV trace from the column and an SDS-PAGE gel of the combined protein containing fractions are shown in Figure 3.3.

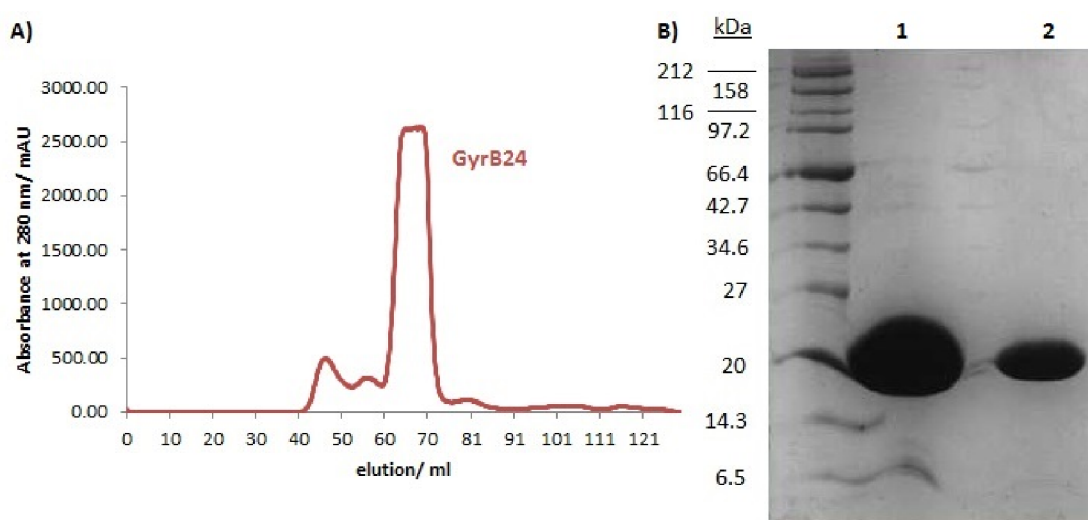


Figure 3.3 Purification of GyB24. A) Size exclusion chromatography trace of fractions containing GyrB24. B) SDS-PAGE gel showing GyrB24 after purification by size exclusion chromatography, lane one is GyrB24 at a concentration of ~12 mg/ml and lane two is diluted to ~4 mg/ml.

A slight impurity was seen at about 8 kDa on the gel at high concentrations of GyrB24 and this was also seen using mass spectroscopy. High resolution mass spectrometry gave a spectrum with a major and a minor peak. Upon deconvolution of the major peak, a mass of 24243 Da, corresponding to the GyrB24 protein, was observed. The minor peak had a mass of 8081 Da corresponding to the cleaved tag (Figure 3.4). As the concentration of the tag was significantly lower than that of the desired protein, it was decided to proceed with this protein in the crystallography experiments. The protein yield was approximately 20 mg L⁻¹ of culture. Aliquots were stored in a high glycerol buffer (Tris pH 7.5 50 mM, EDTA 1 mM, DTT 5 mM, glycerol 30%) at -80 °C.

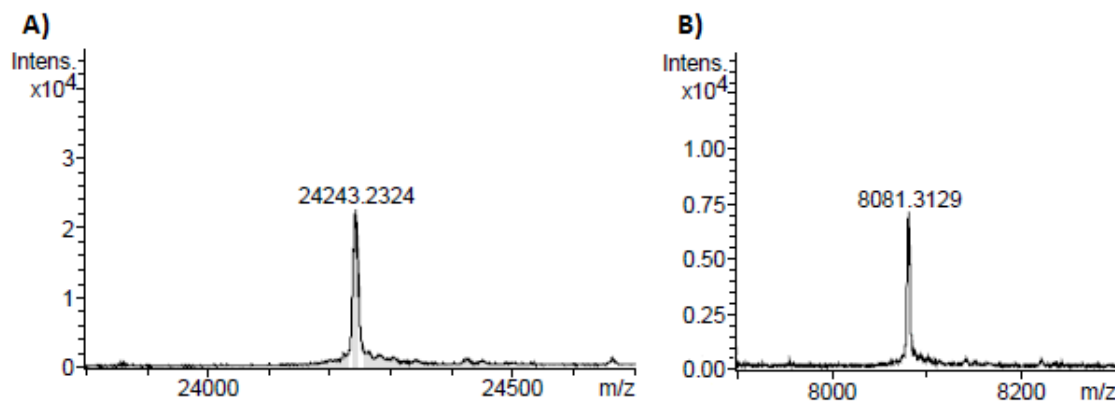


Figure 3.4 Deconvoluted MS peaks from GyrB24 sample. A) major peak corresponding to GyrB24 protein; B) Minor peak corresponding to the cleaved tag.

3.3 Crystallography²

Crystallisation trials of GyrB24 in the presence of four inhibitors were set up. The inhibitors chosen were compounds **69**, **71**, **72** and **86** (Figure 3.5) as they are representative of the main inhibitor groups discussed in Chapter 2 and had been thoroughly characterised in terms of their biological activity.

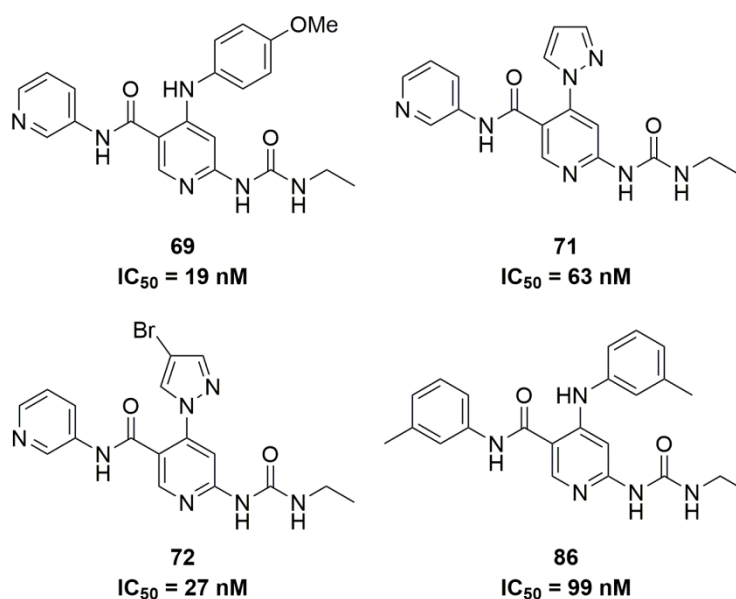


Figure 3.5 Inhibitors chosen for use in crystallisation trials with their IC₅₀s against *E. coli* DNA gyrase.

² The first round of optimisation was carried out by the author with the assistance of Dr. Clare Stevenson at the John Innes Centre. Further rounds of optimisation were carried out by Dr. Clare Stevenson.

Based on previously reported conditions for the crystallisation of GyrB24 in the presence of novobiocin, optimisations were set up using 25-40% PEG400 and 100 mM Hepes pH 6.5 for GyrB24 in the presence of each of the four inhibitors **69**, **71**, **72** and **86**. In the first round of optimisations crystals formed in the presence of compound **72** after a few days. Only microcrystals or spherulites were formed in the presence of the other inhibitors. However, by using a seed stock made from the crystals obtained in the presence of compound **72**, improved crystals were obtained in the presence of the other three inhibitors in similar conditions. The crystals were harvested and X-ray diffraction data recorded at the Diamond Light Source in Oxfordshire.

Figure 3.6 shows a droplet containing protein crystals formed in the presence of compound **72** in a 96 well plate and a crystal in a LithoLoop in the Diamond Light Source beamline, and the resultant diffraction pattern.

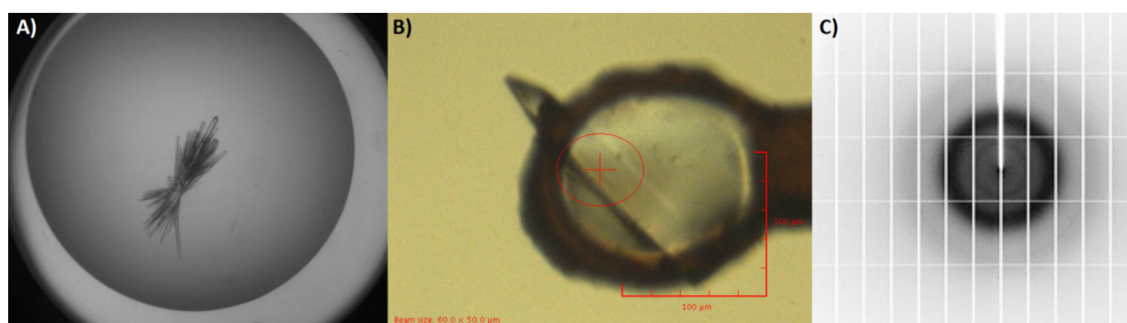


Figure 3.6 A representative example of protein crystals co-crystallised with inhibitors. A) crystals formed in a drop in a 96 well sitting drop plate in the presence of compound **72**; B) A crystal in a LithoLoop photographed in the beamline at the Diamond Light Source C) the diffraction pattern recorded from the crystal.

Diffraction data were collected for several crystals for each inhibitor to find the best dataset. The highest resolution dataset for each inhibitor was chosen that processed with good statistics. Full data collection and refinement statistics for the best dataset for each inhibitor can be found in Chapter 7, Table 7.2.

3.4 Structure solution³

Previously solved crystal structures of GyrB24 in the presence of an inhibitor have been in the $P2_12_12_1$ ^{92,140}, $P12_11$ ^{106,141} and $C121$ ^{87,89,90,116,142,143} space groups. However,

³ Crystal structures were solved by Dr. Clare Stevenson and Dr. David Lawson at the John Innes Centre.

the crystals formed in the presence of compounds **69**, **71**, **72** and **86** were in space group P3₂21. Molecular replacement was used to solve the crystal structure of GyrB24 crystallised with compound **72**. A crystal structure of *S. aureus* GyrB crystallised in the presence of Novobiocin (4URO)¹⁴¹, which was in the P12₁1 space group, was used as the template for molecular replacement. Clear density could be seen for the presence of the inhibitor and the structure of compound **72** was built into the density. Further refinement was carried out using programs from the CCP4 suite¹⁴⁴.

During the model refinement process, difference maps are generated by subtracting the electron density calculated from the model from the “real” electron density from the crystal in order to check that the model has not become biased. Difference maps show electron density for components of the map which have not been accounted for by the model, or that have not been modelled correctly. The presence of specific features, such as inhibitor molecules, can be confirmed using an omit map in which the feature of interest is removed from the model before generating the difference map. The presence of the feature in the omit map confirms that it is not an artefact caused by model bias. Figure 3.7 shows an omit map created by refining the model of the compound **72** crystal structure without including the inhibitor in the model, and the corresponding model with the inhibitor molecule present.

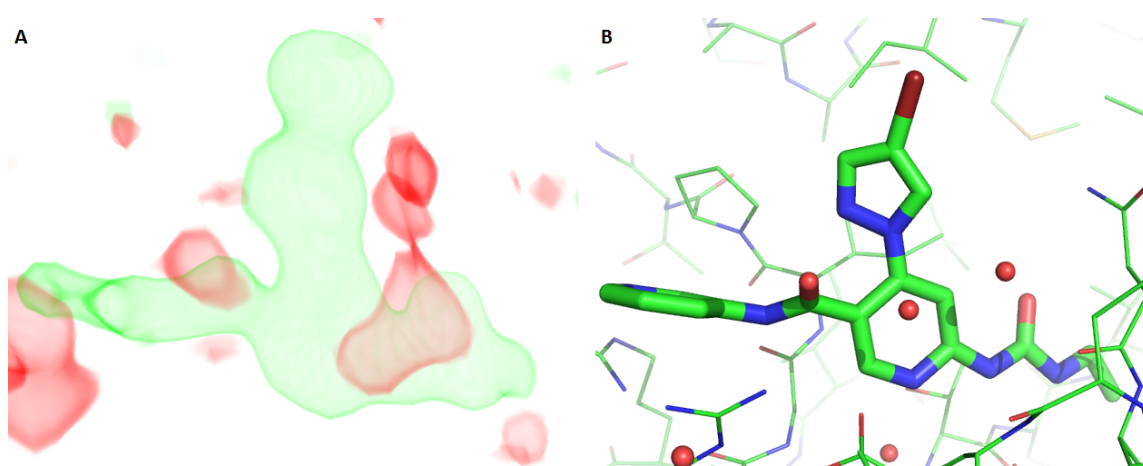


Figure 3.7 A) An omit map generated by refinement of a model of the compound **72** crystal structure in the absence of the inhibitor molecule, showing an area of electron density (green) which corresponds to the missing inhibitor molecule. B) the corresponding model with the inhibitor present.

The structure of the protein with compound **72** bound was then used as the starting model for refinement of the other three structures. All four structures contained

electron density which corresponded to the bound inhibitor. Density maps from the modelled crystal structures are shown in Figure 3.8. The inhibitor binding site is shown with the electron density around the inhibitor molecules.

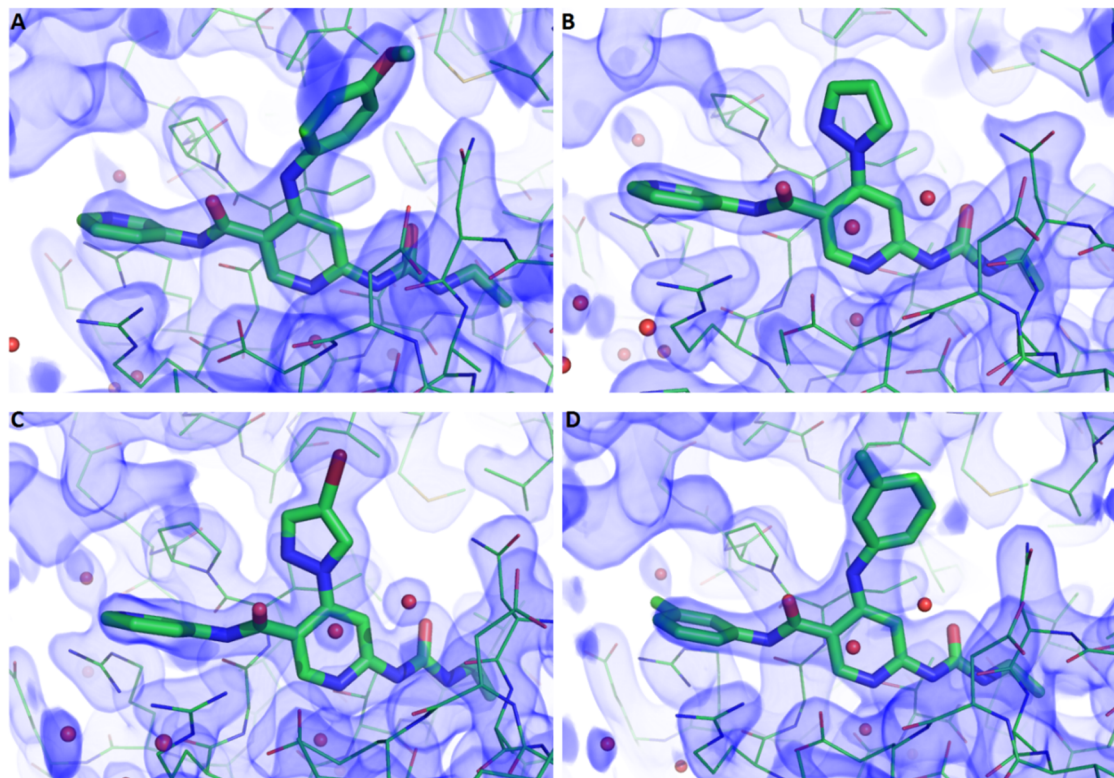


Figure 3.8 Maps of electron density (blue) overlaid with the corresponding model of the crystal structure (green). A) **69**, B) **71**, C) **72** and D) **86**.

The crystal structures of GyrB24 with compounds **69**, **71**, **72** and **86** bound were determined to 1.90, 1.95, 2.35 and 2.50 Å resolution respectively. The models each consisted of one monomer of protein in the asymmetric unit with one molecule of inhibitor bound in the ATP binding site. Each asymmetric unit also contained one PEG molecule and a number of water molecules: 84 in the crystals with compounds **71** and **72** bound, 73 in the crystal with compound **69** bound and 53 in the crystal with compound **86** bound.

3.5 Analysis of crystal structures

All four crystal structures conform to the known structure of this subunit of GyrB with an 8-stranded β -sheet, two relatively long α -helices and three relatively short α -helices, with the ligand bound between two α -helix regions. As with previously

described crystal structures, the loop between Leu-98 and Gly-117, which is adjacent to the inhibitor binding site, is disordered. Figure 3.9 shows a cartoon representation of the crystal structure with compound **72** bound.

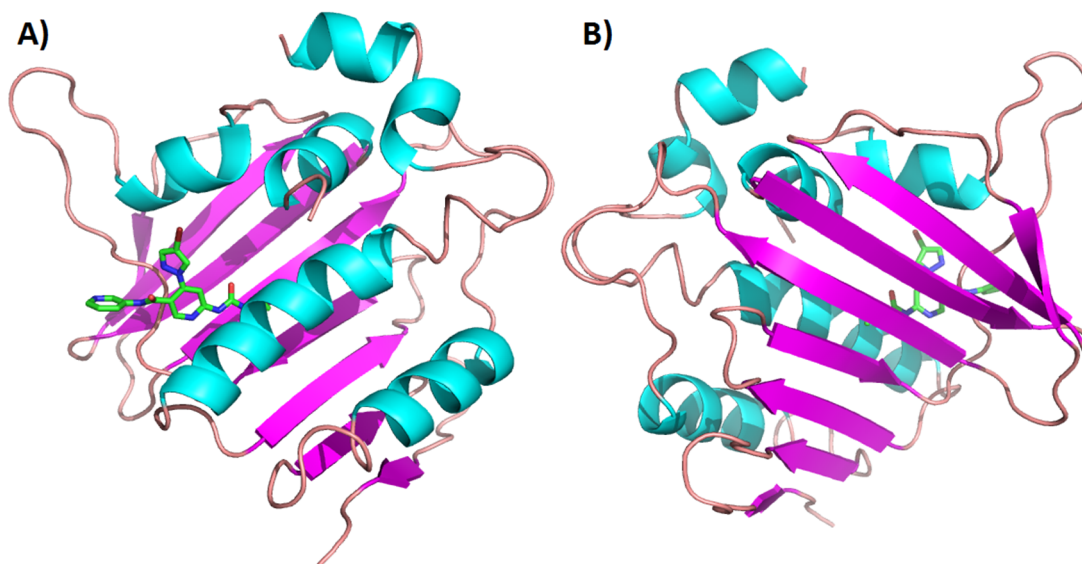


Figure 3.9 Cartoon view of the GyrB24 crystal structure with compound **72** bound (green). A) Binding site between α -helices (cyan) and missing loop region; B) β -sheet region (magenta).

The crystal structures confirmed that the inhibitors were bound in the ATP binding site of the enzyme as had been computationally predicted. Figure 3.10 shows the binding poses from the co-crystal structures (top) and the corresponding docking poses predicted using Glide¹⁴⁵ (bottom) for each of the inhibitors along with the key residues that these inhibitors interact with in the protein.

As with other known inhibitors, a hydrogen bonding network involving Asp-73 and a conserved water molecule in the binding site can be seen. The hydrogen bond donation from the urea moiety and hydrogen bond acceptance from the pyridine rings within the inhibitor molecules closely mirror the poses predicted by computational docking, although the docking predicted a slightly tilted angle for the central pyridine ring in the cases of compounds **69** and **86** and very tilted in the case of compound **72**. This tilt positions the C-4 substituent closer to the hydrophobic region of the binding site, possibly allowing the substituents to interact with hydrophobic residues such as Ile-94.

Computational docking predicted a π -stacking interaction between Arg-76 and the pyridyl rings of compounds **69**, **71** and **72** or the corresponding tolyl ring in compound

86. However, these rings are seen to be tilted in the crystal structures at an angle which would not form an optimal π -stack. Additionally, in the docking model, the amide bond is in the same plane as the central pyridine ring, but in the crystal structure the amide bond has twisted away from the plane of the central pyridine ring in order to form a hydrogen bond with the backbone carbonyl of Gly-77. Formation of this hydrogen bond may compensate for the loss of the π -stacking interaction, especially as the aromatic ring is able to form other interactions. This twist may improve the orientation of the ring nitrogen present in compounds **69**, **71** and **72** to form a hydrogen bond to Arg-134. This is not in the case for compound **86**, as the tolyl ring does not have a nitrogen atom able to form the hydrogen bond.

The tolyl ring of compound **86** is in a different conformation compared to the docked pose with the methyl substituent pointing towards the wall of the cavity rather than up into the solvent exposed region. This may be due to an improved hydrophobic interaction with Pro-79.

The orientations of the C-4 substituents were the least well predicted aspect of the binding poses, except in the case of compound **69** which matches fairly closely. There is an approximately 90° difference in the torsional angle between the pyridine and pyrazole rings of compound **71** and **72** compared to this angle in their docking poses. This may be accounted for by the change in the torsional angle between the pyridine ring and the amide carbonyl. In the docking pose the amide bond is in the same plane as the pyridine ring and the pyrazole ring is twisted to avoid a clash, whereas in the crystal structure the amide bond had moved out of the plane and the pyrazole ring had moved closer to being in the plane.

Of the four compounds investigated, compound **86** was the least active in the enzyme assay. This may be due to the inability of the tolyl ring to form a hydrogen bond to Arg-136. Compound **69** was the most potent inhibitor of *E. coli* DNA gyrase of the compounds described in Chapter 2, this may be due to hydrophobic interactions between the phenyl ring and Ile-94, or unspecific interactions with residues in the disordered loop.

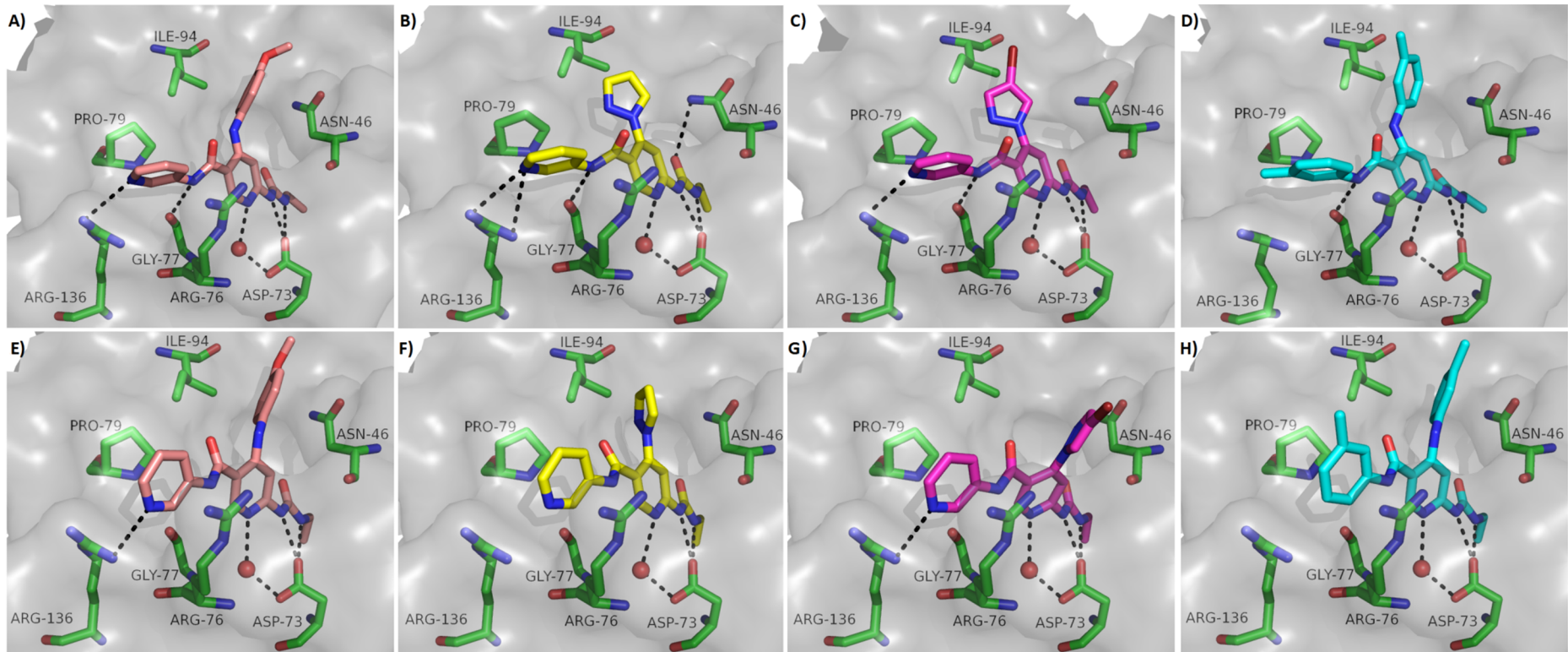


Figure 3.10 Comparison of predicted binding poses of inhibitors in *E. coli* GyrB with X-ray co-crystal structures with the key residues which form interactions with the inhibitors shows in green and the protein surface in grey. Dashed lines indicate a hydrogen bond where the interatomic distance is <3.5 Å. A) compound **69** co-crystallised; B) Compound **71** co-crystallised; C) Compound **72** co-crystallised; D) Compound **86** co-crystallised; E) Compound **69** docked; F) Compound **71** docked; G) Compound **72** docked; H) Compound **86** docked.

3.6 Summary

A variant of the gene for the 24 kDa subunit of *E. coli* GyrB was produced with an N-terminal his-tag for ease of purification, a GB1 tag for increased solubility during purification and a TEV protease cleavage site for removal of the tag following purification. A pNIC vector containing this gene was prepared by ligation independent cloning.

The protein was then produced by growth in *E. coli*. GyrB24 was purified from the soluble fraction of the cell lysate by Ni-resin affinity chromatography and the tag cleaved by incubation with TEV protease. A second Ni-resin column removed the tag and size exclusion chromatography used as a final purification step. Approximately 20 mg of protein were produced per litre of culture.

Protein was crystallised in the presence of four inhibitors: compounds **69**, **71**, **72** and **86**. Crystals formed in the presence of compound **72** under conditions close to those previously established. Crystals formed in the presence of compound **72** were used to seed optimised conditions from which crystals formed in the presence of the other inhibitors. Crystals were harvested and transported to the Diamond Light Source in Oxfordshire.

Diffraction data were collected for a number of crystals formed with each inhibitor and the most promising dataset for each inhibitor was solved to give crystal structures which were resolved to between 1.9 and 2.5 Å. The crystal structures all showed a region of electron density which corresponded to a bound inhibitor molecule.

Analysis of the inhibitor binding poses showed some similarities and some differences when compared to the predicted binding poses. The hydrogen bonding network between the urea nitrogens, the nitrogen of the central pyridine ring, Asp-73 and the conserved water molecule was very similar to the interactions predicted using computational docking. The amide bond was twisted compared with the predicted pose and was thus able to form a hydrogen bond to the carbonyl of Gly-77. The positions of the C-4 substituents of the central pyridine ring were less well modelled

and were angled in a way which may allow them to form hydrophobic interactions with residues in the binding site.

3.7 Future work

The crystal structures described above have shed light on the binding mode of these inhibitors and suggest some potential routes for optimisation of their structures. The urea group, the central pyridine ring and the amide bond all form hydrogen bonds to the protein and modifications of these groups are unlikely to improve the binding of these inhibitors. Some improvements in binding may be seen from optimisation of the aromatic group on the left hand side of the molecule to improve the hydrogen bonding interaction with Arg-136. A different ring system or a substituent extending from the ring may increase the strength of this interaction.

Acquiring crystal structures of these inhibitors bound to the topoisomerase IV enzyme would be a great asset as it would guide the design of inhibitors with less selectivity for DNA gyrase over topoisomerase IV. It would also be useful to acquire crystal structures of inhibitors bound to these proteins from other bacterial species, as the results described in Chapter 2 suggest that these compounds interact less favourably with the topoisomerase IV enzyme from *E. coli* than they do with that from *S. aureus*.

Chapter 4 Use of computational methods for hit identification

4.1 Introduction

Over the last few decades, computational power has increased dramatically. Computational and medicinal chemists have been keen to put this increased calculating ability to good use.¹⁴⁶ While computational methods are not yet capable of fully predicting the complex network of effects a small molecule may have on a living organism, they can increasingly provide approximate guidance for many of the problems encountered in drug discovery. Computational methods are seen as valuable tools to complement the experiments carried out in the lab, and new and improved methods are being continually developed to provide assistance throughout the drug discovery process. This chapter will focus on the computational tools most commonly used at the very start of a medicinal chemistry project to help identify molecules to assess within initial screens against a given biological target.

Over the years, many different computational approaches have been developed to aid in the identification of molecules which are predicted to bind favourably to a specific biological target. Most of the software tools can be grouped into broad classes based on how they search for structures or how they assess the potential of these structures to bind to the target of interest. The two most common approaches to the search for molecular structures are *de novo* design and virtual high throughput screening (vHTS). *De novo* design approaches procedurally generate novel chemical structures that are predicted to interact favourably with the target protein, whereas vHTS approaches search databases of pre-existing small molecules to identify appropriate structures. Ranking or scoring small molecules for their potential to favourably interact with the target of interest can be approached by either ligand-based or target-based methods. Target-based approaches begin with the structure of the target itself and base their assessments on the ways in which a given small molecule might interact with that target. Ligand-based approaches assess the potential of a chemical structure by its similarity to the chemical structure of a known ligand of the target (Figure 4.1).

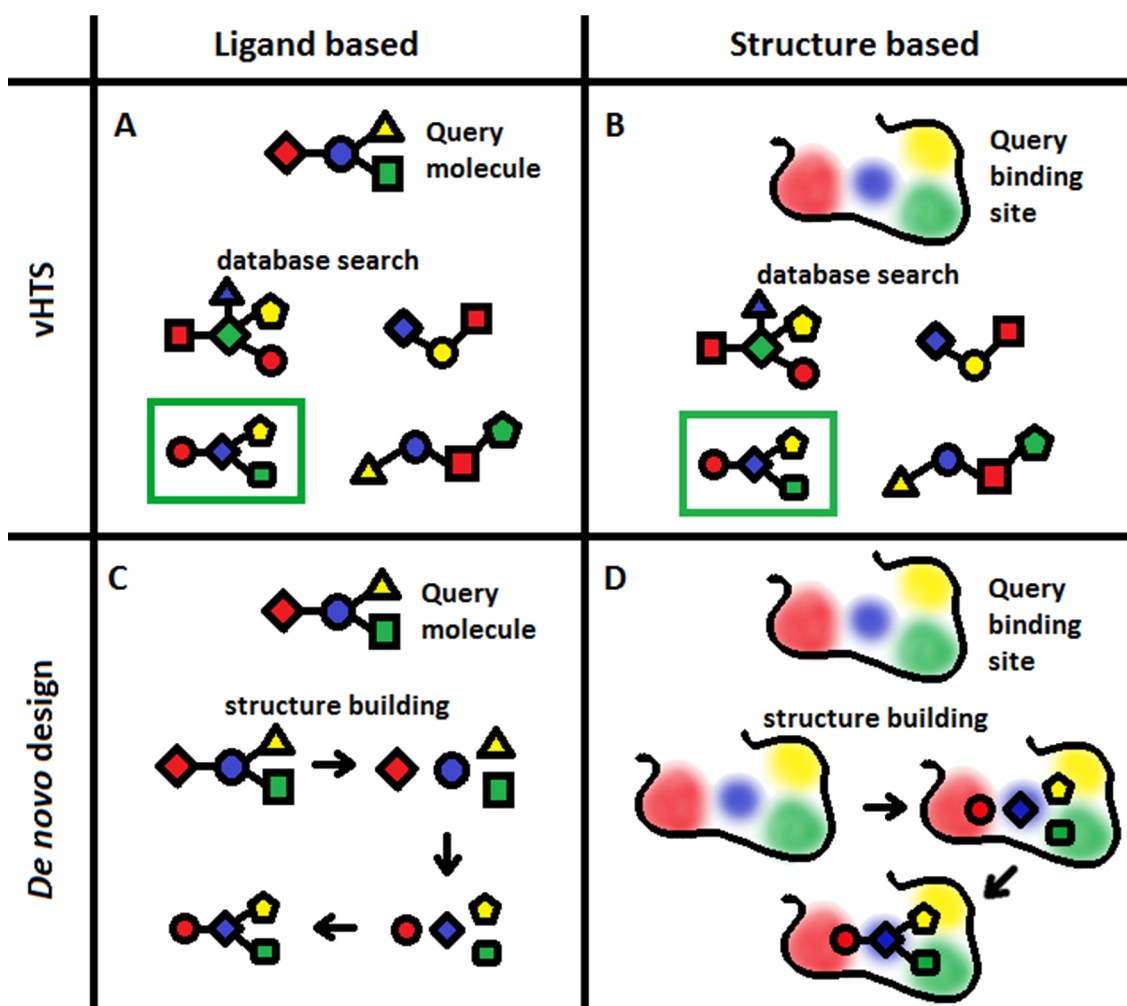


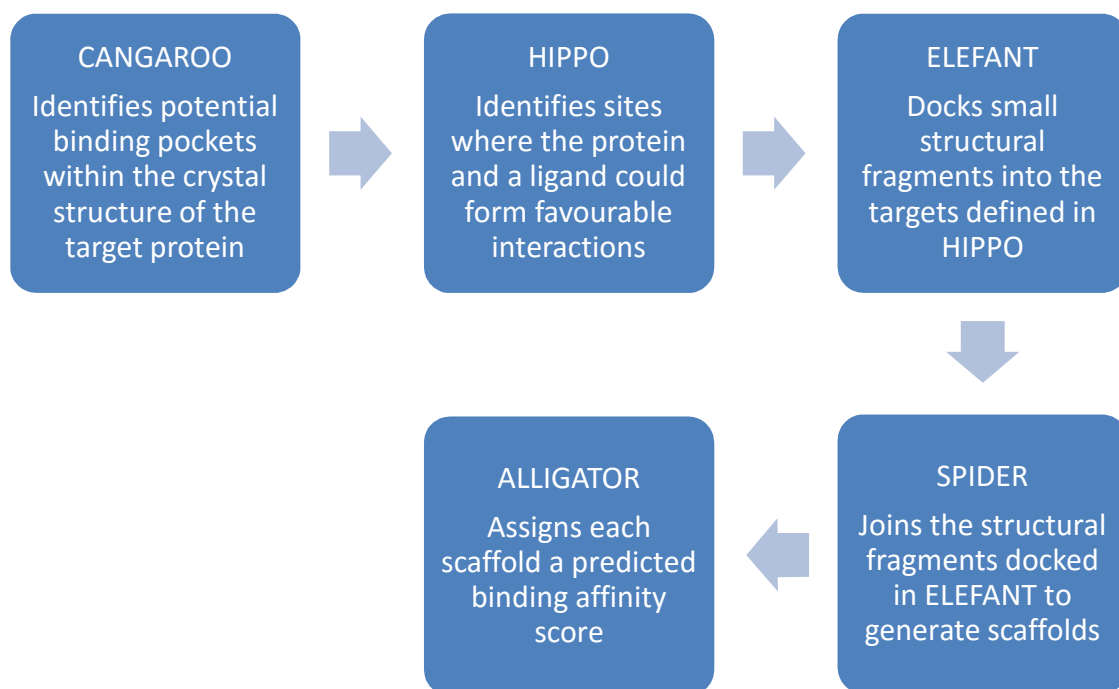
Figure 4.1. Schematic representation of the different approaches to computational hit identification. A) ligand-based vHTS; B) structure-based vHTS; C) ligand-based *de novo* design and D) structure-based *de novo* design. Adapted from Lolli *et. al.* used with permission.¹⁴⁷

In the present work, target-based *de novo* design and both ligand-based and target-based vHTS have been used to search for new chemical structures to investigate as potential inhibitors of DNA gyrase and topoisomerase IV.

4.2 *De novo* design

There are several programs available for *de novo* design¹⁴⁸. In this work, SPROUT has been used¹²⁵. The SPROUT software is comprised of several modules (Scheme 4.1) which are used sequentially: first to define a receptor within the crystal structure of a protein; then to select residues within that receptor in which to bind small structural fragments and finally to connect the fragments to give a series of potential ligand

structures. The program can rank the results by estimated binding affinities, size, ligand efficiency or complexity.



Scheme 4.1 Description of the purpose of each of the modules present in the *de novo* molecular design program SPROUT.

The design of a new series of potential inhibitors of DNA gyrase and topoisomerase IV was attempted using SPROUT with the aim of identifying novel structures. Based on inhibitor structures which have been reported in the literature, three key interactions were chosen as being important to good inhibitor binding: a hydrogen bond acceptor able to interact with the conserved water molecule in the active site; a hydrogen bond donor able to form a hydrogen bond to Asp-82 and an aromatic group able to form a π -stacking interaction with Arg-85. These features are common to almost all of the most active inhibitors reported in the literature including the natural product novobiocin **7**⁵⁰, inhibitors published by Vertex **17**⁸⁷, AstraZeneca **21**¹⁰¹, Evotec **26**¹¹⁴ and Trius **37**⁹², and compounds from the series previously designed at Leeds such as compound **86**¹²³ (Figure 4.2).

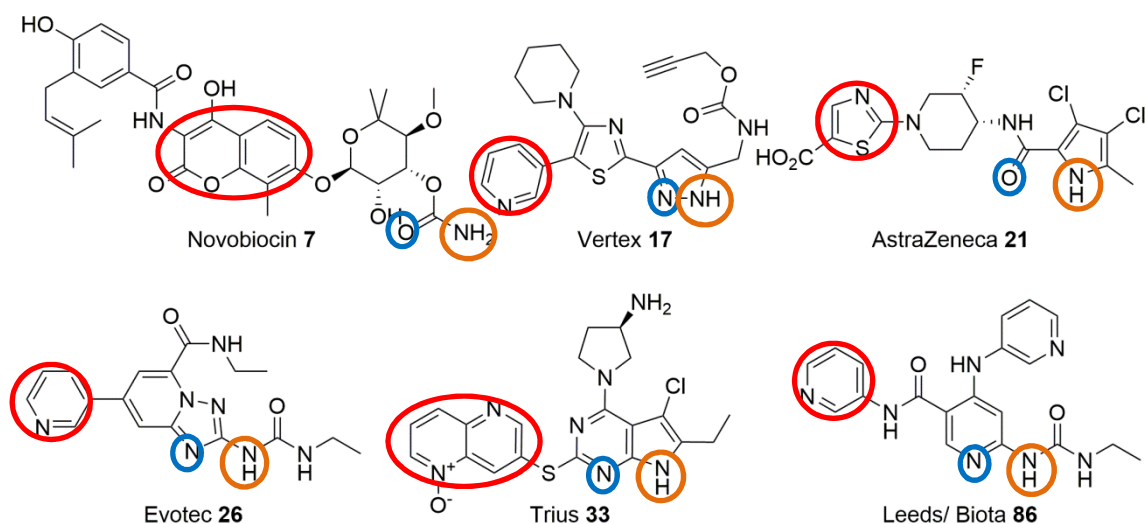


Figure 4.2 Three structural features are common to all reported GyrB/ ParE inhibitors: a hydrogen bond acceptor (blue) which interacts with a conserved water molecule in the active site; a hydrogen bond donor (orange) which interacts with an aspartate residue and an aromatic ring (red) which forms a π -stacking interaction with an arginine residue.

It was chosen to use a crystal structure of ParE from *E. coli* (4HZO⁹²) for the *de novo* design process in SPROUT. Previous inhibitors synthesised at Leeds have been less able to inhibit topoisomerase IV when compared to their activities against DNA gyrase. By beginning the design process with compounds designed to bind well to topoisomerase IV and then assessing designed molecules for their predicted binding to both enzymes it was hoped to design inhibitors with less selectivity for one enzyme over the other.

The Asp-82 residue was selected as one “target site” using the HIPPO module of SPROUT and designated as a hydrogen bond acceptor site. SPROUT can recognise water molecules in the active site of a protein, but does not always predict the optimal hydrogen bonding vector which was the case in this instance. It also isn’t able to recognise sites with the potential to form π -stacking interaction. In order to position fragments to correctly form π -stacking interactions or hydrogen bonds to water if the correct vectors have not been predicted correctly, SPROUT allows the creation of “spheric sites” within the binding site and their designation as hydrogen bond acceptors, donors or hydrophobic sites. Spheric sites were generated at appropriate positions in the binding site to represent the hydrogen bond to the conserved water molecule and the π -stacking interaction to Arg-85. Starting fragments bearing the

appropriate hydrogen bond donors, acceptors and aromatic rings were docked into these “target sites” using the SPIDER module in SPROUT (Figure 4.3).

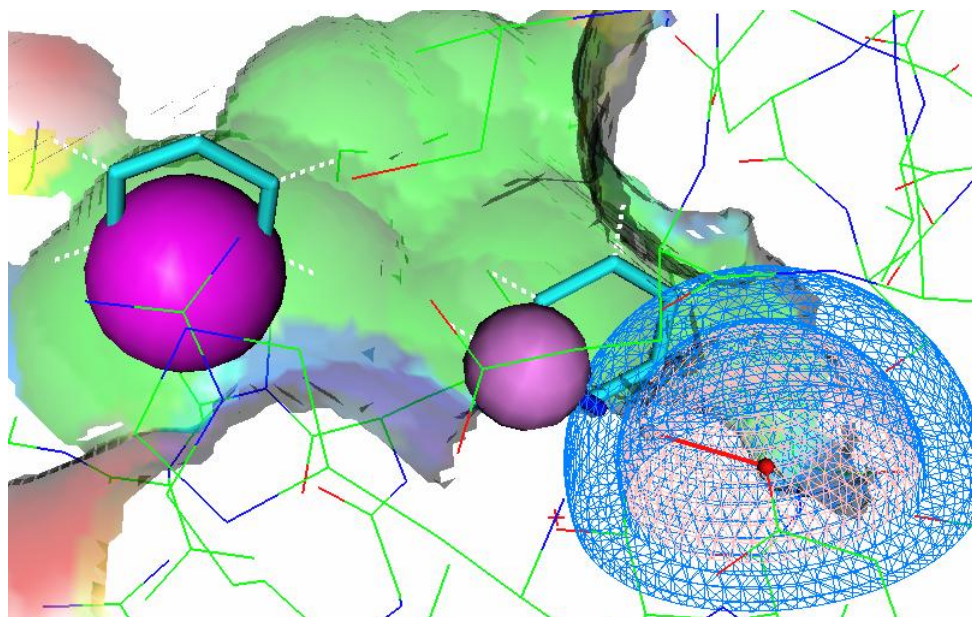


Figure 4.3 Docking of starting fragments into selected “target sites” using SPROUT. Benzene rings (turquoise) have been docked into the spheric sites which are shown in solid purple and an amine (blue) has been docked into the hydrogen bond acceptor site which is shown in blue wireframe.

Thousands of possible scaffolds were generated by connection of these fragments using linkers such as carbon chains, amide bonds and aromatic rings. However SPROUT was unable to connect the desired fragments into any scaffolds that scored higher than the pyridine 3-carboxamide compounds already designed, and upon redocking with AutoDock none of the scaffolds were able to adopt a pose in the active site that would allow the desired interactions to occur. The four scaffolds given the highest scores by SPROUT are shown in Figure 4.4. The hydrogen bond donor and acceptor moieties have been placed too far apart from each other to make the desired contacts and an overly complex ring system is used to connect to the aromatic group that can form a π -stack to Arg85.

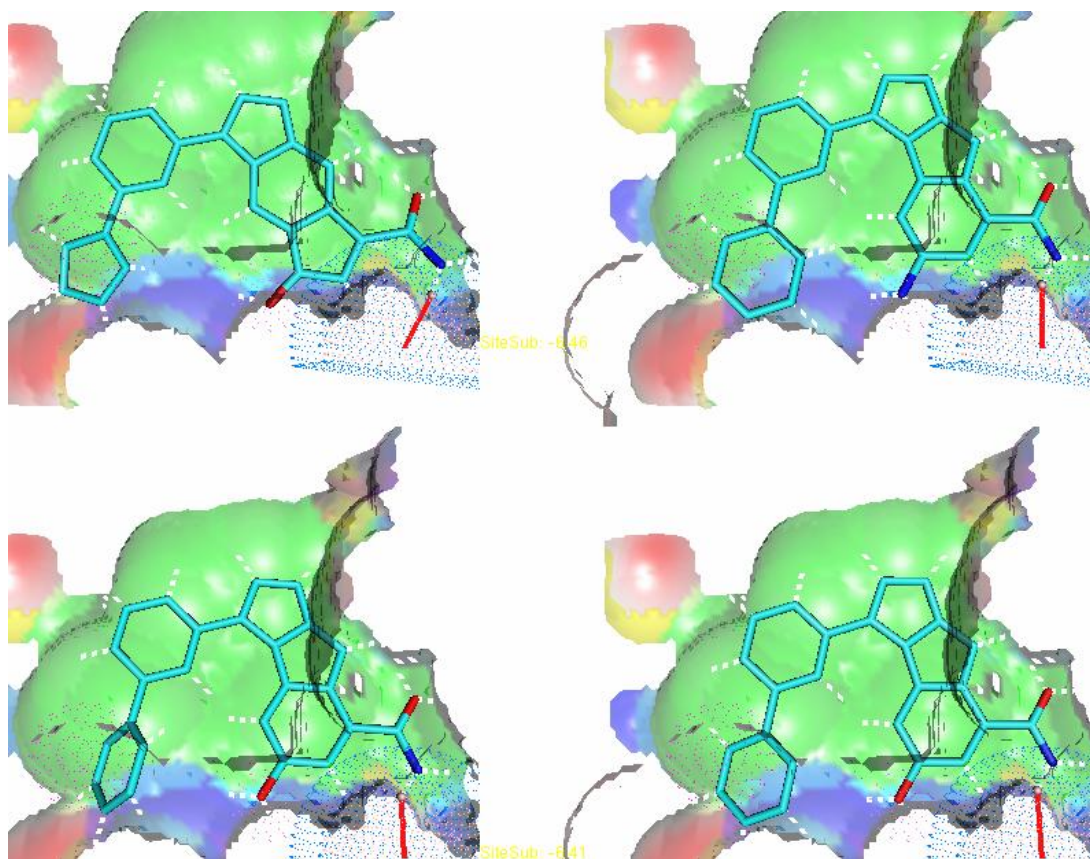


Figure 4.4 The four best scored SPROUT designed scaffolds in the pose predicted by SPROUT. The fragments chosen to form interactions to the protein have been connected *via* complex ring systems which would make them difficult to synthesise and the hydrogen bond donors and acceptors have been placed too far apart to make the desired interactions.

Use of the spheric sites to provide “target sites” for hydrogen bonding to non-protein atoms and π -stacking, did not allow the docked fragments to orient themselves correctly to form the desired interactions, so when connected into a full scaffold the designed structures did not have the desired features. SPROUT was unable to successfully design π -stacking interactions or hydrogen bonds to non-protein atoms and so specifically designing compounds able to form the desired interactions using SPROUT proved challenging. It was decided to focus instead on virtual screening approaches to design novel DNA gyrase and topoisomerase IV inhibitors.

4.3 vHTS

4.3.1 Structure based vHTS

When searching for starting points for a drug discovery project, it is common to screen very large catalogues of small organic molecules using automated assays to look for

any that interact favourably with the biological target of interest. High throughput screening (HTS) of this type can single out a few promising candidates from amongst thousands of compounds and then these “hits” can be followed up with further biological assessment and chemical exploration. However, HTS campaigns are very costly and require a lot of time and resources. An alternative approach to find hit molecules from large compound collections is to utilise molecular docking. Screening large databases for molecules that are predicted to bind well can give a short list of compounds with a higher chance of being active than taking a small sample at random. Screening a small number of compounds is much quicker and cheaper.

Most suppliers of small molecule screening collections provide digital versions of their collections which can be used for vHTS. These databases can be searched individually or combined and searched together. The ZINC database is a combined database containing the compound collections of over 200 commercial suppliers. The database contains almost 100 million unique chemical compounds. This number is too big to be screened in a reasonable time frame, but several subsets of the database are also available that narrow the full compound set based on calculated properties such as size, current availability or “drug likeness” (based on Lipinski’s rule of 5). In this project the “drug-like” subset that contained >10000 compounds was used, but first it was further narrowed down using a diversity filter in Pipeline Pilot to give 10000 compounds.¹⁴⁹

There are a number of docking programs available to assess the binding of a small molecule to a biological target. For this project, Glide, the docking module of Schrodinger’s Maestro software package¹⁴⁵, was chosen to dock the compounds as it was able to exactly reproduce the binding pose of a known inhibitor of DNA Gyrase and topoisomerase IV into its crystal structure (4HZ0, which is ParE from *E. coli*) Figure 4.5. Other features of Glide that were taken into account when choosing it over other docking programs were its speed and the ease with which it can be used in combination with parallel computing resources.

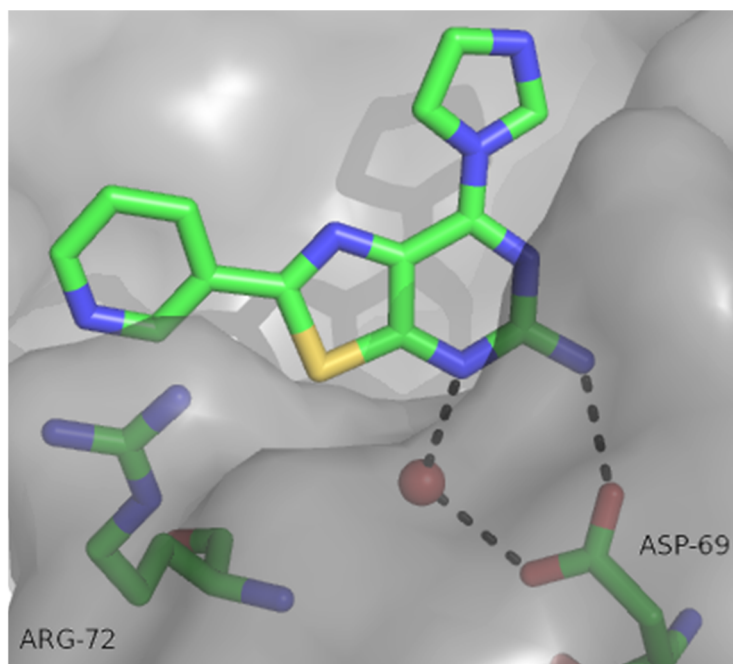


Figure 4.5 Original crystal structure 4HZ0⁹² and docking of the ligand by Glide. The Glide generated pose perfectly overlaps with the pose of the native ligand.

The top 500 ranked docking poses were visually inspected looking for structures which made at least two of the three key binding interactions described earlier in this Chapter. Seven structures, which had high scores and appropriate binding modes, were chosen for purchase. Their scores and binding modes are shown in Table 4.1.

The library was also docked into a crystal structure of DNA gyrase (3G7E, GyrB from *E. coli*) and the top 500 compound were again visually inspected. This time six compounds were selected. Their binding poses and Glide scores are shown in Table 4.2. The Glide scores were higher against this target compared with those docked against topoisomerase IV, and so less emphasis was placed on choosing inhibitors which could make the three desired interactions described earlier.

Table 4.1 Shortlisted compounds from docking of the ZINC database against the topoisomerase IV crystal structure 4HZ0. Binding poses and Glide scores are given.

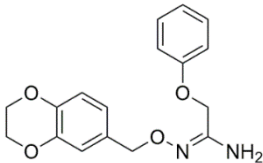
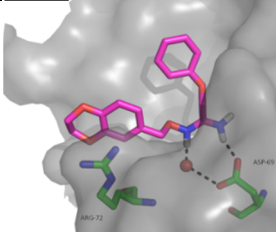
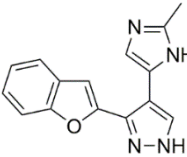
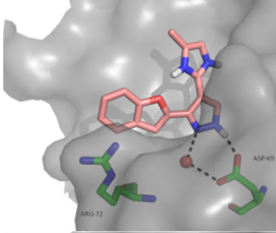
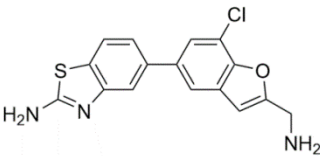
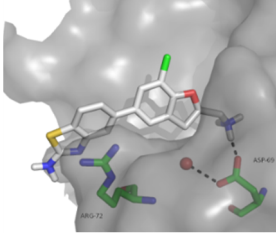
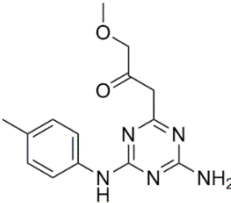
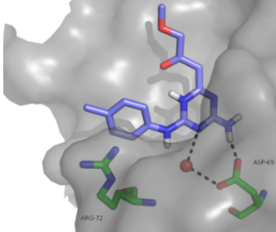
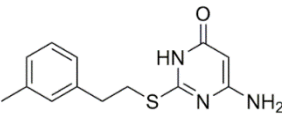
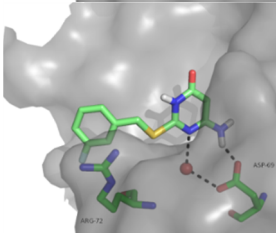
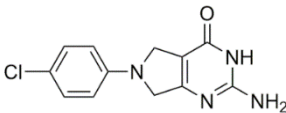
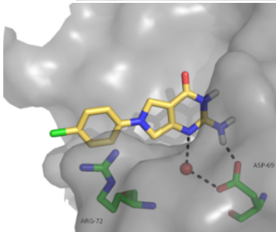
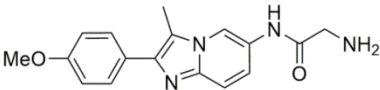
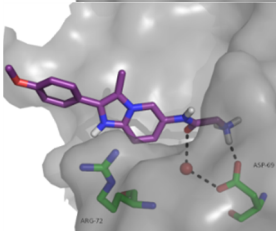
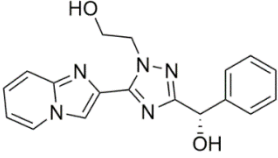
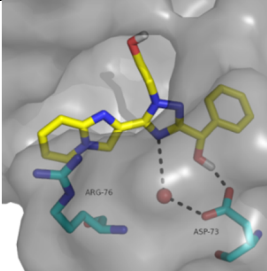
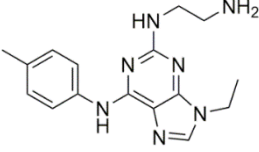
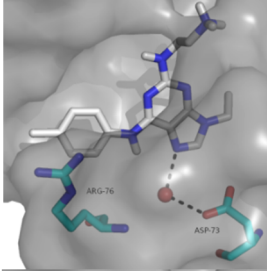
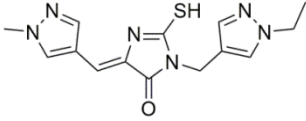
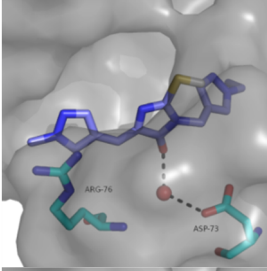
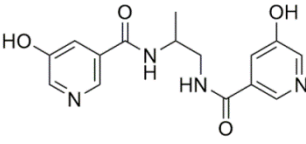
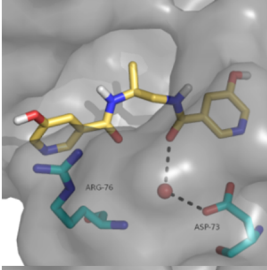
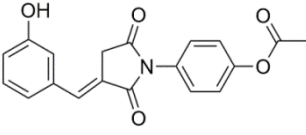
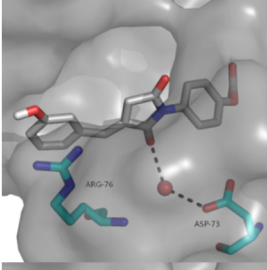
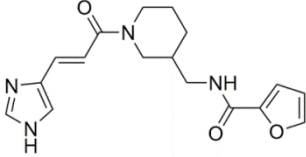
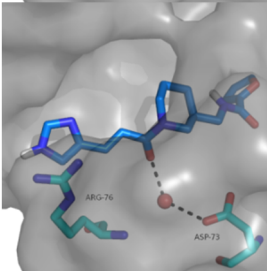
Compound	Compound Structure	Binding pose	Glide Score
87			-8.12
88			-7.58
89			-7.43
90			-7.40
91			-7.38
92			-7.29
93			-7.28

Table 4.2 Shortlisted compounds from docking of the ZINC database against the DNA gyrase crystal structure 3G7E. Binding poses and Glide scores are given.

Compound	Compound Structure	Binding pose	Glide Score
94			-9.63
95			-9.58
96			-9.54
97			-9.49
98			-9.12
99			-9.07

The purchase of the shortlisted compounds is discussed in Section 4.4 and their biological activities are discussed in Section 4.5.

4.3.2 Ligand-based vHTS

Another approach to virtual screening is to look at a known ligand and search for similar molecules. Compounds with similar structural features are more likely to interact well with the biological target than those with very different features. The ROCS (rapid overlay of chemical structures) program provided by OpenEye was used for ligand-based vHTS in this project.¹⁵⁰

The natural product DNA gyrase inhibitors novobiocin **7** and cyclothialidine **10** were used as the initial query molecules and chemical libraries from three suppliers (Maybridge, ChemBridge and Peakdale) were screened against them. However, ROCS was unable to find good shape matches. This is likely due to the size of these molecules, as the average size of molecules in the screening collections was significantly smaller than the natural products. An overlay of the natural products (green) and the highest scoring matches found by ROCS (pink) are shown in Figure 4.6.

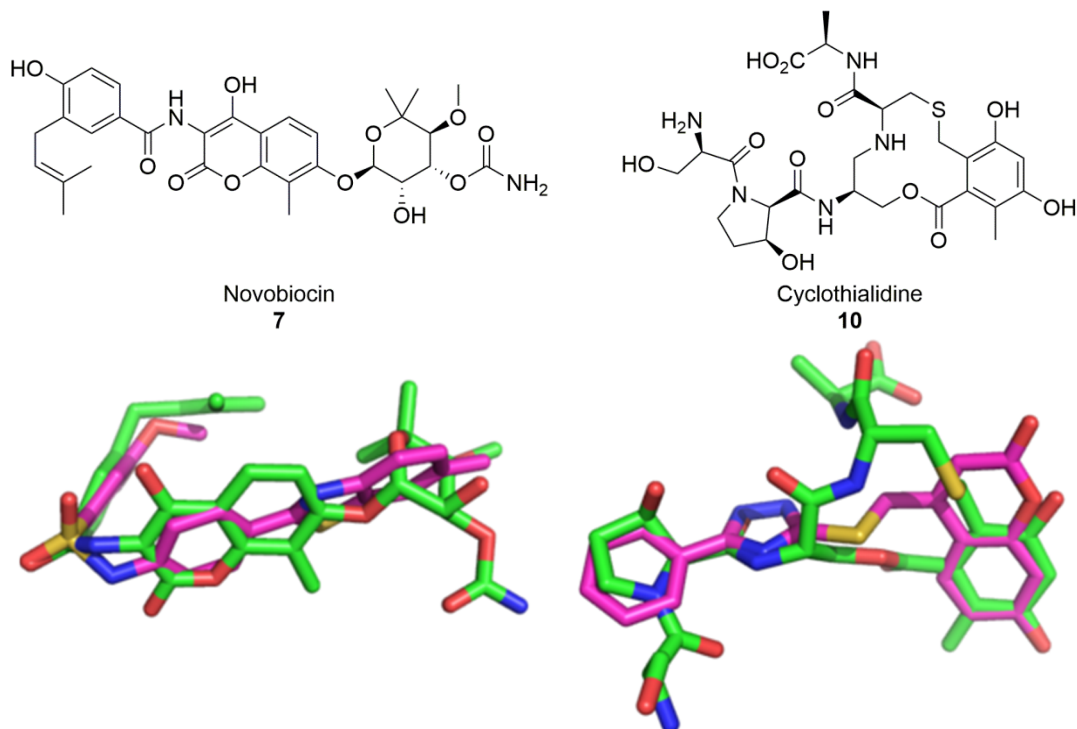


Figure 4.6 The natural products Novobiocin **7** and Cyclothialidine **10** (green) overlaid with the highest scoring matches found by ROCS (pink).

To better match the sizes of molecules present in the compound screening collections a truncated version of novobiocin **100** was tried as an alternative query for ROCS along with the cyclothialidine derivative reported by Roche **11** which was smaller than cyclothialidine⁷⁶. Better shape matches were found for these smaller versions of the natural products as shown in Figure 4.7 and the matches were kept for further analysis.

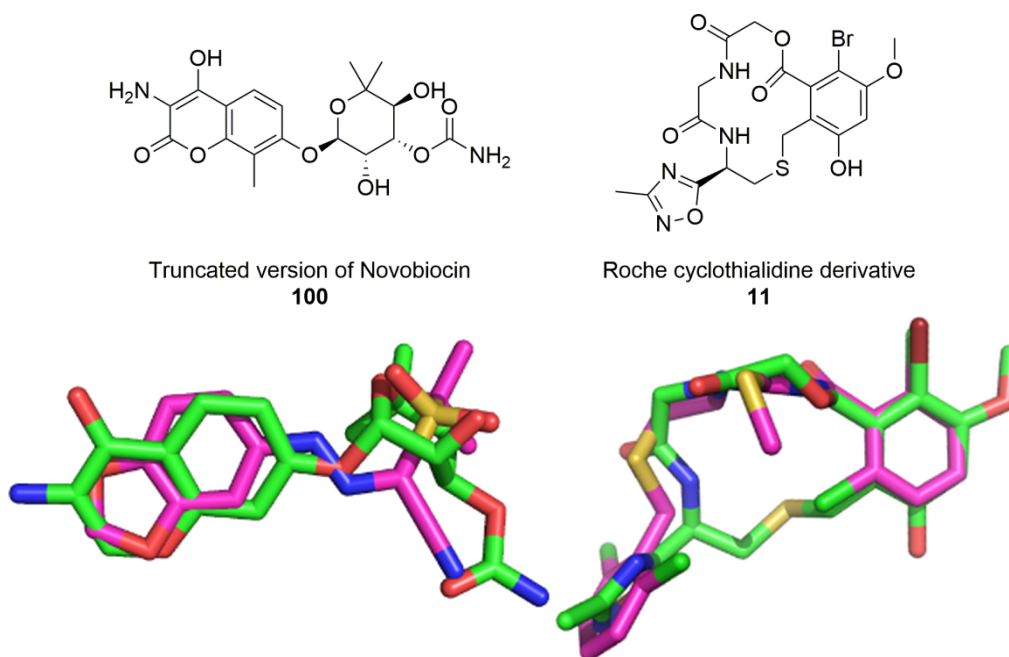


Figure 4.7 A truncated version of Novobiocin **100** and a cyclothialidine derivative reported by Roche **11**⁷⁶ (green) with their highest scoring matches from a ROCS screen of the Peakdale, Maybridge and ChemBridge compound libraries (pink).

Although some structures with good overlap to known natural product inhibitors had been discovered it was decided to also look for matches for some of the many small molecule inhibitors which have been reported in the literature. Six known small molecule inhibitors were chosen to use as queries for the search (Figure 4.8). These inhibitors were chosen as they represented a structurally diverse set of examples from most of the previously described compound series. They all possess the three structural features identified in Section 4.2 as being key to binding. Crystal structures of these inhibitors bound to DNA gyrase were available for all of these compounds with the exception of compound **38**. The structures of the inhibitors in their bound conformation were extracted from the published crystal structures and used for the ROCS search as this allowed the ROCS search to match compounds with the right

shape to fit into the active site in this configuration. The conformation of compound **38** when bound to the enzyme was predicted using docking.

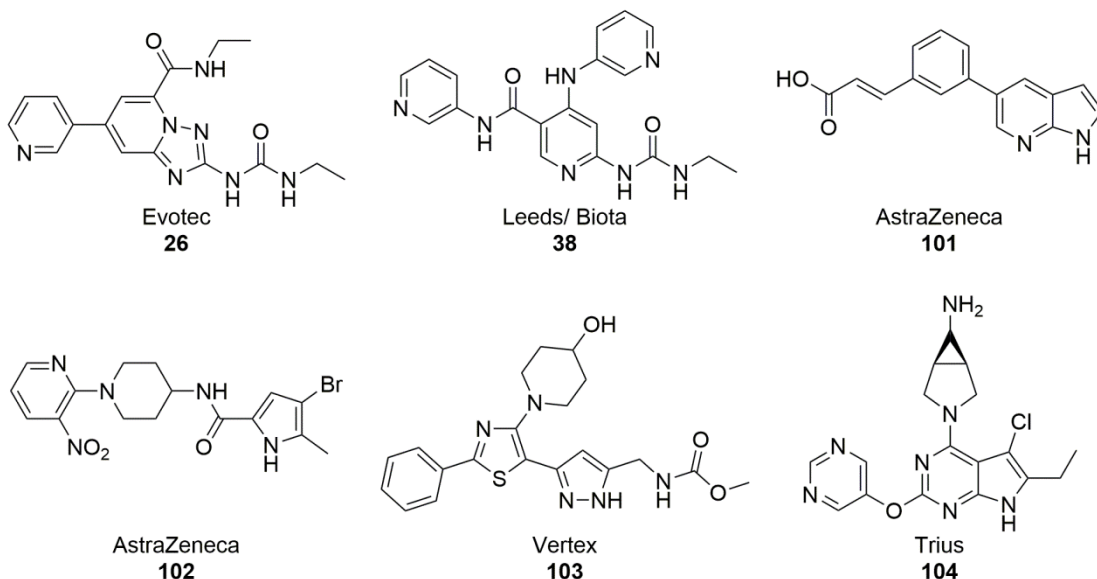


Figure 4.8 Six query molecules from the scientific literature were selected for use in ROCS searches. These compounds were published by Evotec **26**¹¹⁴, Biota and the University of Leeds **38**¹²³, AstraZeneca **101** and **102**^{117,143}, Vertex **103**⁸⁷ and Trius **104**⁹².

Overlays of these structures with their highest scored match from the ROCS search are shown in Figure 4.9 (query structures are shown in green and matches in pink). The program was able to find matches with very similar shapes for each structure. However, key hydrogen bond acceptors and donors were often not matched, as this is not prioritised by the software.

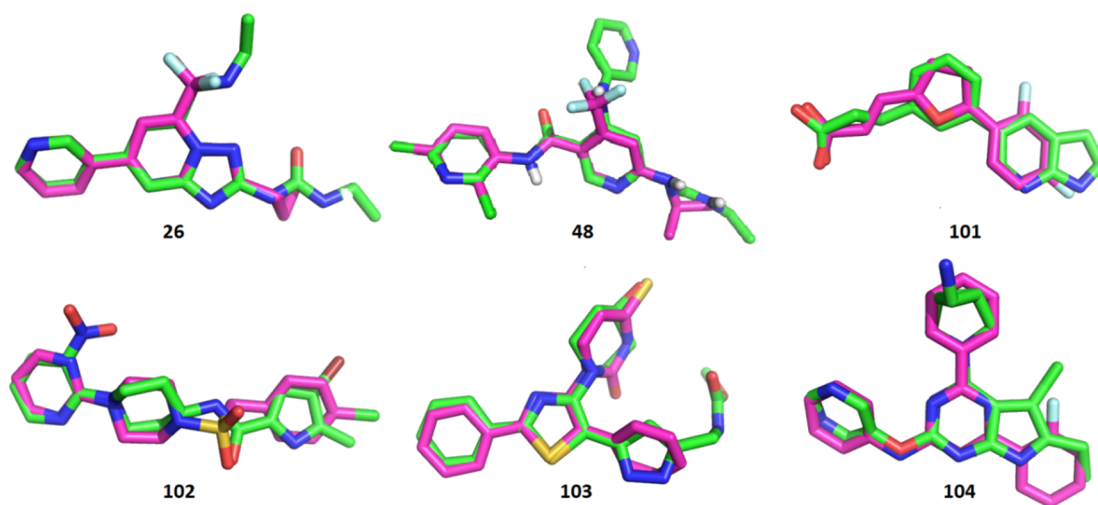
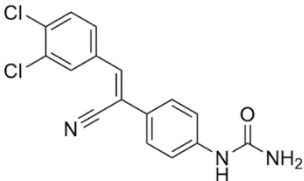
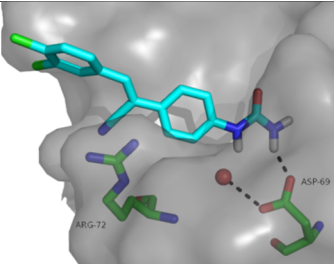
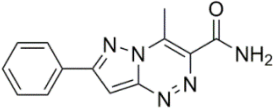
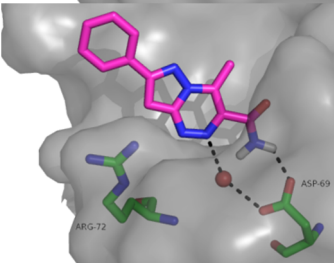
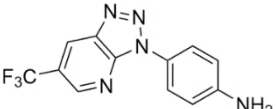
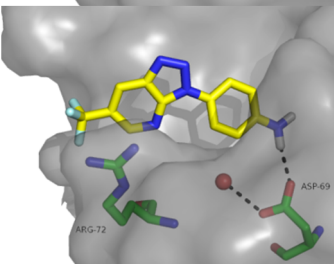
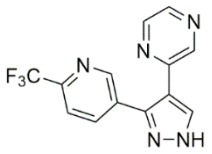
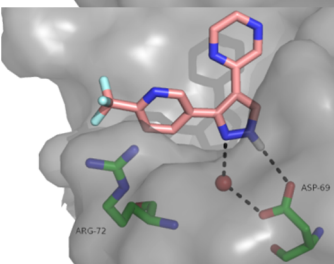


Figure 4.9 Overlays of the six structures chosen as queries for ROCS (green) with their highest scoring matches (pink) from the ChemBridge, Peakdale and Maybridge compound libraries.

The 100 best matches were chosen from each ROCS search. The hits from all the searches were combined and duplicates removed using OpenBabel¹⁵¹ to give a total of 276 compounds. Secondary docking was used to identify which of the best compounds from the ROCS search were likely to form good binding interactions as well as having good shape complementarity with the active site. The compounds were docked into the *E. coli* topoisomerase IV crystal structure (4HZ0) using Glide and the 191 compounds which scored lower than -5 were visually inspected to determine whether they were binding in a favourable conformation. Upon visual inspection the shortlist was narrowed to 4 compounds. Their binding modes and ROCS scores are shown in Table 4.3, along with their Glide scores and the structure they were initially aligned to.

Table 4.3 Shortlisted compounds from a ROCS search of the Maybridge, ChemBridge and Peakdale libraries against six known inhibitors followed by docking into the topoisomerase IV crystal structure 4HZ0⁹² using Glide. Binding poses, ROCS scores and Glide scores are given.

Cmpd	Compound structure	Binding pose	Glide score	ROCS score	Aligned to
105			-6.13	0.930	38
106			-5.60	0.932	26
107			-5.38	1.07	101
108			-5.18	1.13	104

ROCS can also be used to search for molecules that align well with a pharmacophore model rather than an individual inhibitor molecule. Pharmacophore models provide a more general query than searching with a specific inhibitor molecule. vROCS can be used to generate pharmacophore models by combining features of a number of known inhibitors. The pharmacophore model will have a shape that encompasses all of the inhibitors used and will highlight chemical features such as ring systems and hydrogen bond donors and acceptors in order to search for compounds which match these features.

It was decided to carry out a pharmacophore search in addition to the single molecule queries that had been carried out. A pharmacophore model was created using the six inhibitors which had previously been used as individual queries. However, simply aligning the structures and retaining all points at which vROCS suggested a structural alignment could be made gave a pharmacophore model with too many match points (Figure 4.10, A). Docking against this did not give matches which scored highly.

In order to focus the pharmacophore on the key areas of overlap between the inhibitors rather than including the points at which they were less similar, the overlapped inhibitors were truncated leaving only the regions that overlapped well. And only the three key structural features that have been described earlier in the chapter were selected as match points (Figure 4.10, B). However, ROCS was able to find even higher scoring matches if the ring systems were not highlighted as match points for ROCS (Figure 4.10, C). This search was much more closely focused on finding matches with the correct arrangement of hydrogen bond donors and acceptors.

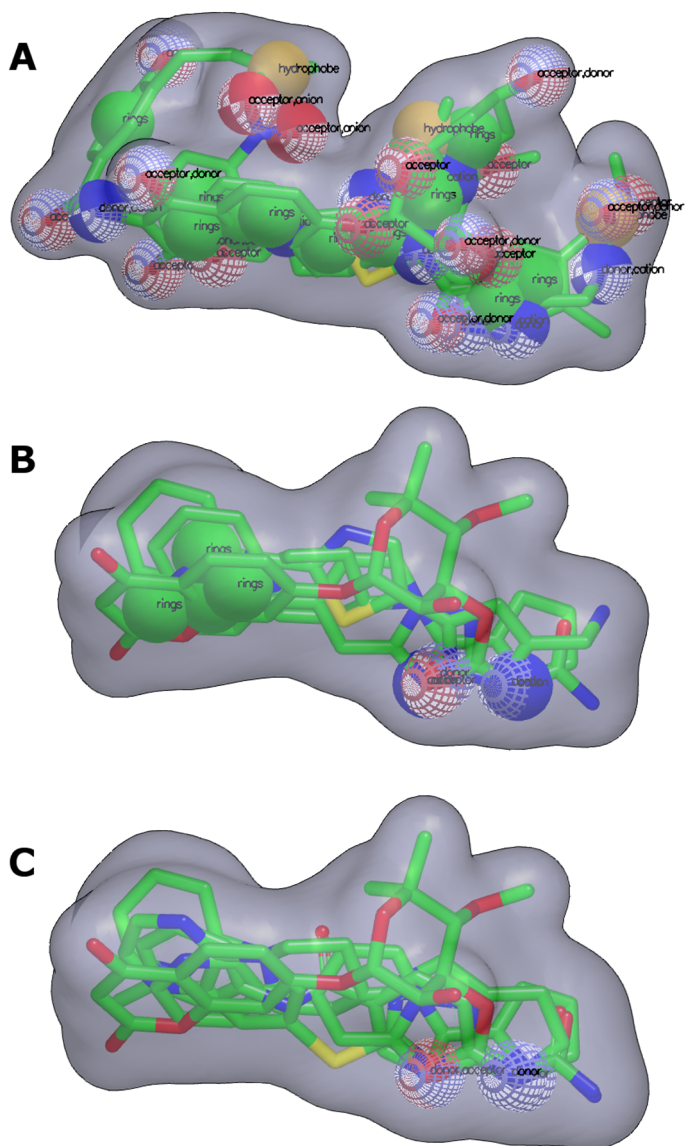
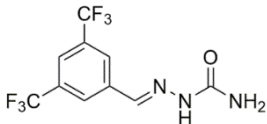
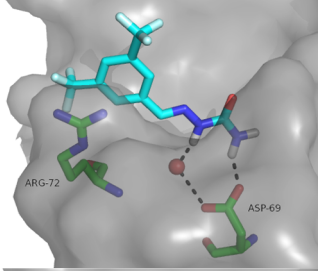
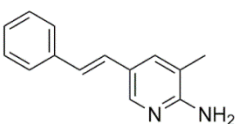
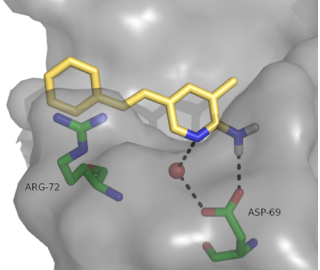
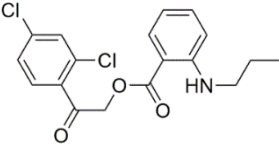
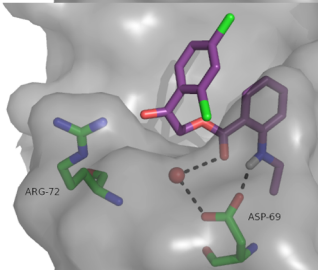
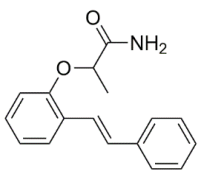
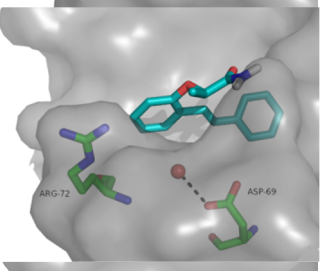
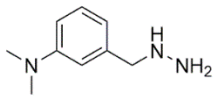
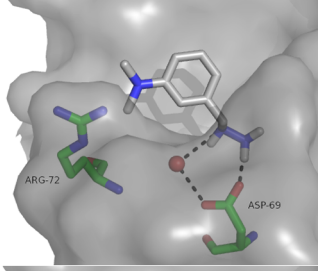
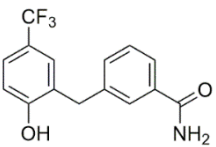
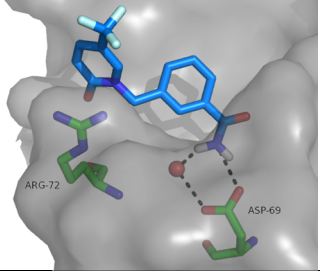


Figure 4.10 Development of a useful pharmacophore model. A model generated by aligning compounds from six different inhibitor classes. B. Model generated by using truncated versions of inhibitors from four known classes, highlighting only the key structural features. C. Model generated using truncated versions of inhibitors from four known compound classes highlighting only the key hydrogen bonding interactions.

As in the previous ROCS searches, the top 100 hits from the ChemBridge, Maybridge and Peakdale libraries were docked with Glide into the *E. coli* ParE crystal structure 4HZ0 and a shortlist selected by visual inspection. The top six hits are shown in Table 4.1 with their binding pose, Glide score and ROCS score. Hits from this search had better Glide scores than the hits from the previous ROCS searches, suggesting that the pharmacophore model was a more useful query than the individual inhibitors.

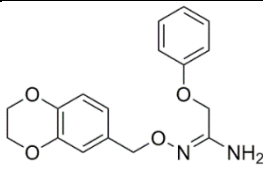
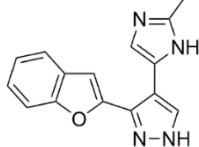
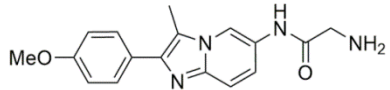
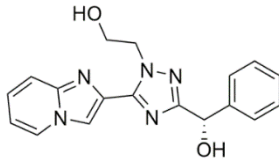
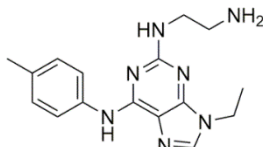
Table 4.4 Shortlisted compounds from a ROCS search of the Maybridge, ChemBridge and Peakdale libraries against a pharmacophore model followed by docking into the topoisomerase IV crystal structure 4HZ0 using Glide. Binding poses, ROCS scores and Glide scores are given.

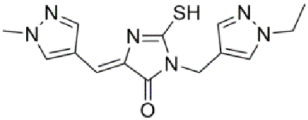
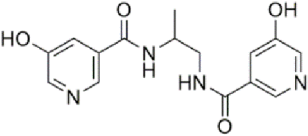
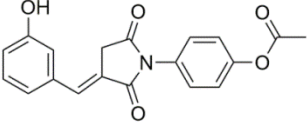
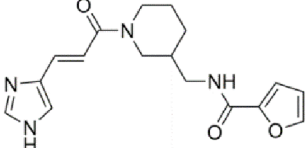
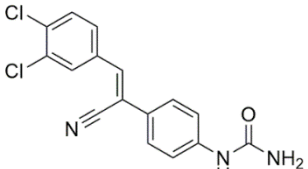
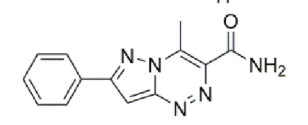
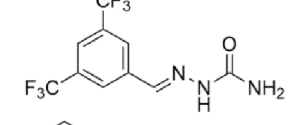
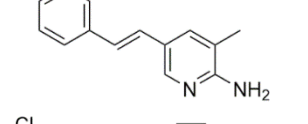
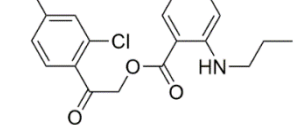
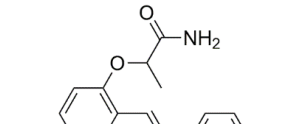
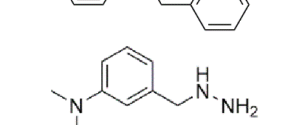
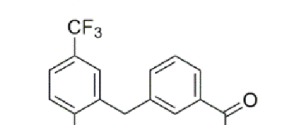
Compound	Compound structure	Binding pose	Glide score	ROCS score
109			-6.68	0.621
110			-6.54	0.629
111			-6.51	0.626
112			-6.53	0.623
113			-7.81	0.591
114			-6.39	0.530

4.4 Choice of ligands for purchase

The most promising structures from both structure-based and ligand-based virtual screening campaigns were combined to give a shortlist of 22 compounds; seven from the target based vHTS screen against ParE; six from the target based vHTS screen against GyrB; four from the ligand based vHTS using individual inhibitor molecules and five from the ligand based vHTS using a pharmacophore model. The availability of these compounds was checked using the eMolecules website which allows ordering of compounds from all of the vendors whose compounds are included in the ZINC database. Of the 22 compounds in the search, only 15 were listed as available. Because structure based vHTS was carried out using a subset of the ZINC database, the shortlist contained molecules from eight different suppliers, as shown in Table 4.5. In order to limit costs, only compounds available from ChemBridge were chosen for purchase as this was the supplier with the most compounds from the list and included compounds from each of the vHTS searches. Six compounds were purchased.

Table 4.5 Availability of shortlisted compounds from computational screens.

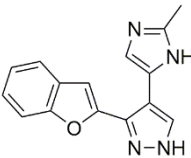
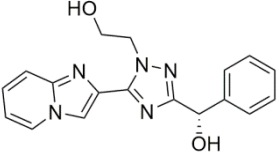
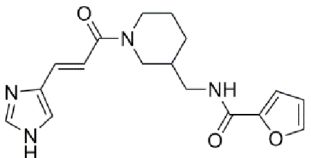
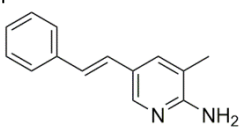
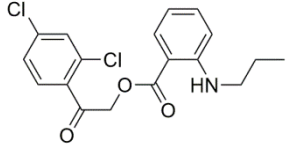
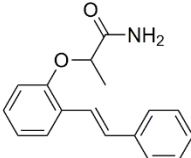
Compound	Structure	Primary computational screen	Supplier
87		Glide docking against topoisomerase IV	Enamine
88		Glide docking against topoisomerase IV	ChemBridge
93		Glide docking against topoisomerase IV	Otava
94		Glide docking against DNA gyrase	ChemBridge
95		Glide docking against DNA gyrase	Otava

96		Glide docking against DNA gyrase	Vitas M labs
97		Glide docking against DNA gyrase	ChemDiv
98		Glide docking against DNA gyrase	InterBioScreen
99		Glide docking against DNA gyrase	ChemBridge
105		ROCS search with query structure 38	Maybridge
106		ROCS search with truncated novobiocin query	Maybridge
109		ROCS search with pharmacophore model query	Maybridge
110		ROCS search with pharmacophore model query	ChemBridge
111		ROCS search with pharmacophore model query	ChemBridge
112		ROCS search with pharmacophore model query	ChemBridge
113		ROCS search with pharmacophore model query	Peakdale
114		ROCS search with pharmacophore model query	Peakdale

4.5 Biological results

The six purchased compounds were initially assessed for their biological activity in an ATPase assay against DNA gyrase. The compounds were screened at a concentration of 100 μM and the activity of the enzyme monitored over half an hour. Novobiocin was used as a control inhibitor. The assay protocol is as described in Chapter 7. The activity of the enzyme in the presence of inhibitor at a concentration of 100 μM relative to its activity in the absence of an inhibitor is shown in Table 4.6. Determination of IC_{50} values for the two most active compounds **110** and **112** was attempted, but the compounds were insoluble at concentrations higher than 100 μM , so an IC_{50} curve could not be recorded.

Table 4.6 Activities of compounds against DNA gyrase.

Compound	Structure	% residual activity at 100 μM
88		93 \pm 1
94		100 \pm 12
99		95 \pm 5
110		66 \pm 11
111		85 \pm 4
112		67 \pm 18

Based on their percentage inhibition at 100 μM it would be expected that the two most active compounds would have IC_{50} values of around 70 μM . This level of activity

was considered too low for it to be worth attempting to optimise their activity through the synthesis of analogues.

4.6 Conclusions and future work

Several different computational methods have been used with the aim of identifying novel inhibitors of DNA gyrase and topoisomerase IV. Use of SPROUT to carry out *de novo* design of inhibitors which would be able to make specific binding interactions within the active site was unsuccessful. vHTS was attempted using both structure-based and ligand-based approaches. A number of compounds which were predicted to bind favourably to DNA Gyrase and topoisomerase IV were identified, but only a small number were purchased and none of those purchased showed sufficiently potent activity to be worth further investigation.

Future computational efforts to identify inhibitors of DNA gyrase and topoisomerase IV should focus on vHTS rather than *de novo* design. As only a small number of compounds were purchased initial efforts could be focused on acquiring and biologically assessing other compounds from the shortlist of compounds chosen from the vHTS studies.

Chapter 5 Rational design of a new inhibitor series using a scaffold-hopping approach

5.1 Introduction

The design of novel inhibitors does not necessarily have to be carried out using computational analysis or searching for hit molecules in high throughput screens to then be optimised. Another approach is to rationally design novel inhibitors based on knowledge of the active site of the enzyme and of the features of known inhibitors. Scaffold-hopping is an approach often used by medicinal chemists to search for compounds which are similar to compounds known to have good activity in the hope that a structurally related molecule may have similar or improved properties. Scaffold-hopping approaches can be grouped into four categories: heterocycle replacement, ring opening or closure, peptidomimetics and topology based hopping.¹⁵²

In this chapter the rational design of three compound series using information gathered from the scientific literature along with knowledge of the features of the binding site of DNA gyrase and topoisomerase IV will be discussed. Additionally, synthetic efforts towards these compounds and initial assessment of their biological activities will be presented.

5.2 Pyrimidines

5.2.1 Background

In 2013, a series of GyrB/ParE inhibitors was published by Trius Therapeutics which showed good activity against Gram negative bacteria (2-64 µg/ml) in addition to potent activity against Gram positive bacteria (<0.06-64 µg/ml). These compounds were among the first inhibitors of the ATP binding sites of DNA gyrase and topoisomerase IV to demonstrate activity in Gram negative bacteria.^{92,118,119} Two of these compounds, **33** and **34**, are shown in Figure 5.1. These compounds were developed from a hit compound derived from a crystallographic screening program, and several co-crystal structures from various points during the project were published.

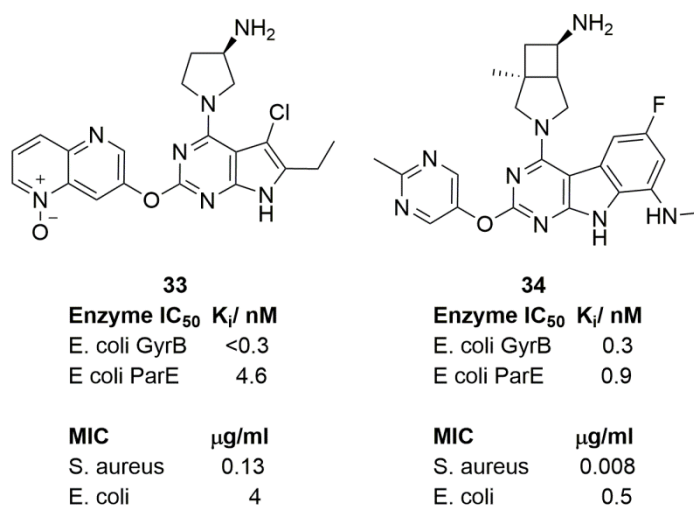


Figure 5.1 Representative examples of a series of GyrB/ParE inhibitors published by Trius Ltd which demonstrated low μg/ml MICs against Gram negative species.^{92,118,119}

5.2.2 Compound design

Based on these compounds a new series of potential GyrB/ ParE inhibitors was designed incorporating some features from the previously discussed pyridine-3-carboxamide series along with features from the Trius compounds giving the general structure **115** (Figure 5.2). It was thought that retaining the *N*-ethyl urea motif and the adjacent nitrogen atom of the pyrimidine ring would allow these compounds to form the same hydrogen bonding network within the ATP binding sites of GyrB and ParE as for compounds from the pyridine-3-carboxamide series. It was hoped that this would result in molecules with similar enzyme potency to compounds from the pyridine-carboxamide series. Furthermore, it was reasoned that incorporating a saturated ring system with a primary “amide substituent” at the C4 position of the central pyrimidine ring, as seen in the Trius compounds, could increase the ability of these compounds to penetrate the membrane of Gram negative cells and thus lead to compounds with antimicrobial activity in Gram negative organisms (Figure 5.2).

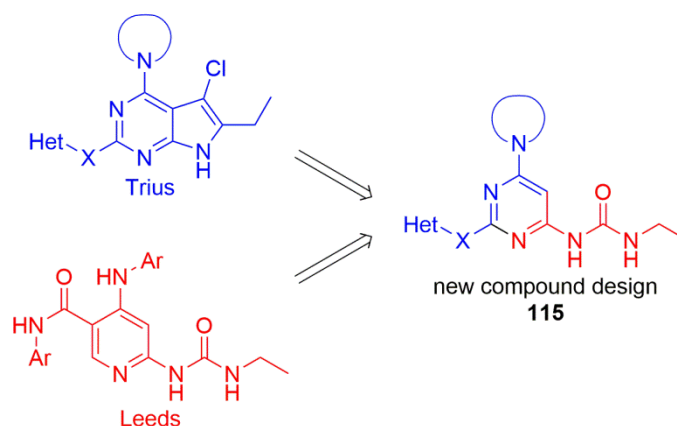


Figure 5.2. A new series of potential GyrB/ParE inhibitors was designed by combining features from the Trius compounds with those from the pyridine carboxamide series.

A small library of compounds corresponding to this designed scaffold was docked into the crystal structure of *E. coli* GyrB using AutoDock, in order to investigate the potential for compounds corresponding to this scaffold to act as inhibitors of these enzymes. The docking pose generated using AutoDock for compound **116**, the lowest scoring compounds from this set, is shown in Figure 5.3. The results for the whole library are shown in Table 5.1 in order of AutoDock score, along with calculated logPs.

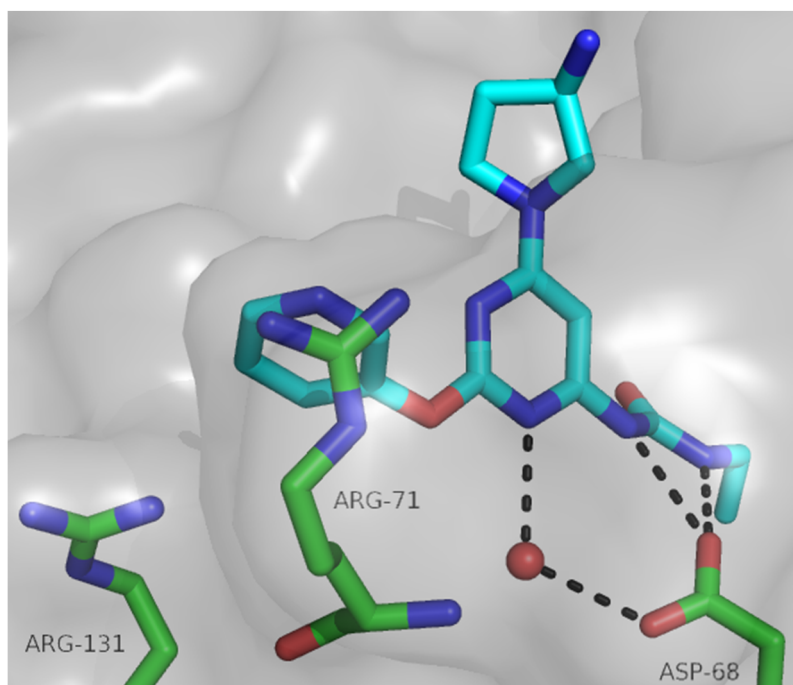
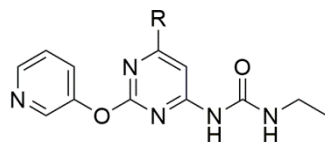


Figure 5.3. Docking pose of compound **116** generated using AutoDock, with the key polar contacts to the GyrB enzyme from *E. coli* (4HXZ)⁹² indicated.

Table 5.1



AutoDock scores and calculated logPs for C4 amino pyrimidine ureas.

Compound	R	AutoDock Score	clogP
116		-8.93	0.94
117		-8.54	1.00
118		-8.35	0.94
119		-8.26	1.26
120		-8.12	1.46
121		-8.04	1.05
122		-7.93	1.05
123		-7.87	2.81
124		-7.70	1.57
125		-7.69	1.77

Docking studies carried out using AutoDock¹²⁶ and logPs calculated using ChemAxon calculator pluggins.¹²⁸

Compounds **116** and **118**, which contain amino pyrrolidine species similar to those seen in the Trius compounds, had the highest AutoDock scores and lowest clogPs. Compounds **117**, **119** and **120**, which also contained protonatable amines, had

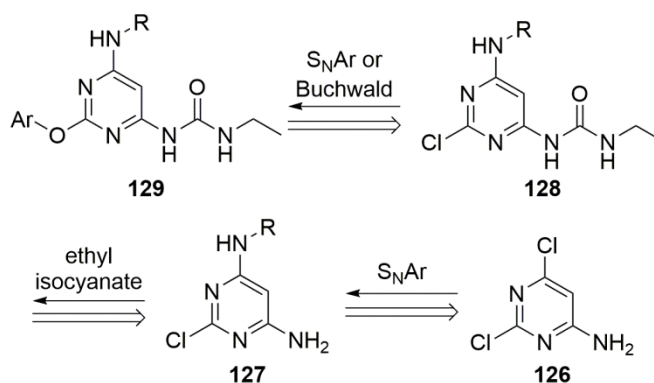
comparable scores. This supports the idea that compounds of this type with protonatable amines could be good inhibitors of the GyrB and ParE enzymes. Slightly lower scores were seen in similar species which contained oxygen in the place of nitrogen, **121**, **122** and **124**. Aromatic groups without a hydrogen bond donor, **123** and **125**, also scored relatively poorly.

The AutoDock scores of these compounds are not as good as the binding scores calculated for compounds from the pyridine-3-carboxamide series (Chapter 2, Table 2), which would suggest that these compounds may exhibit lower enzyme inhibition, but it was hoped that the relative increase in polarity of the compounds in this series will lead to an increase in the antimicrobial activity against Gram negative species.

As the single enantiomers **116** and **118** were both predicted to bind well, it was chosen to first synthesise and test a racemic mixture of the two, with the aim of synthesising the separate enantiomers if the racemate showed sufficient activity. The amino pyrrolidine substituent was chosen as it scored very highly in the docking studies and had a substituent which was analogous to an equivalently positioned substituent seen in some of the Trius compounds, including **35**. Compounds **116** and **118** had a clogP of 0.94, suggesting that a racemate of these compounds might have improved physicochemical properties to enable it to penetrate Gram negative bacteria.

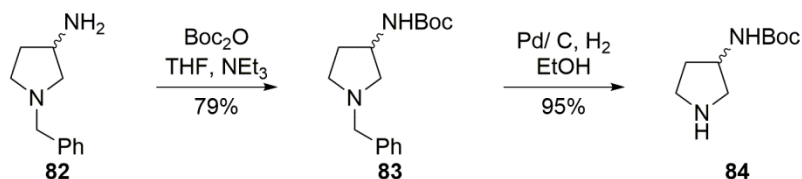
5.2.3 Synthesis

A synthetic route was envisioned (Scheme 5.1) from the commercially available 6-amino-2,4-dichloropyrimidine **126**. It was hoped that S_NAr reactions could be used to insert the substituents at the 2- and 4- positions. Although insertion of the ether linked heterocycle at the 2-position to get from **127** to **128** was expected to be challenging, there was a precedent in the patent literature for carrying out S_NAr reactions using 3-hydroxypyridine as the nucleophile and 2-chloropyrimidine as the electrophile¹⁵³. In the pyridine carboxamide series, formation of the ethyl urea had been carried out successfully by reaction of aminopyridines with ethyl isocyanate,¹²⁴ and it was hoped that this reaction could be carried out using aminopyrimidines to afford **129** from **128**.



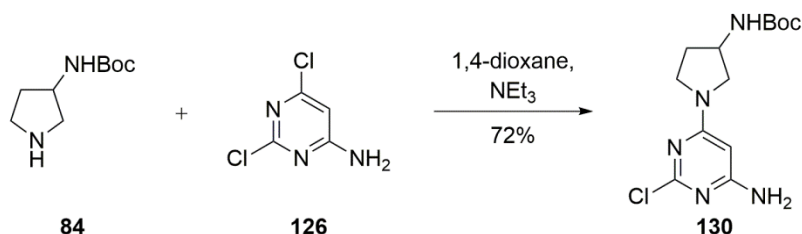
Scheme 5.1 Retrosynthesis of designed pyrimidine compounds from commercially available pyrimidine **126**.

Formation of the boc protected aminopyrrolidine **84** from the commercially available benzyl protected amino pyrrolidine **82** was previously described in Chapter 2 and is shown in Scheme 5.2.



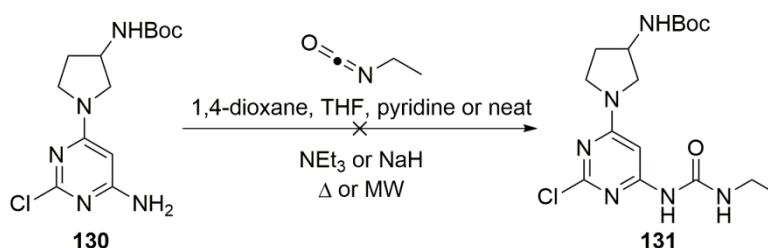
Scheme 5.2 Change of protecting groups on 3-aminopyrrolidine **84** to afford compound **86**.

The Boc protected pyrrolidine **86** was then used in an S_NAr reaction with 6-amino-2,4-dichloropyrimidine **126** to give compound **130**. The reaction occurred in a reasonable yield and was selective for the C-4 position of 6-amino-2,4-dichloropyrimidine (Scheme 5.3).



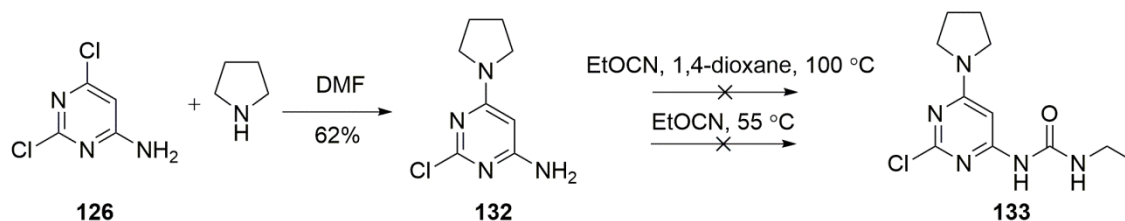
Scheme 5.3 Substitution of the C-4 position of compound **126** with compound **86** via S_NAr to afford compound **130**.

Introduction of the *N*-ethyl urea moiety at the C-6 position of compound **130** was intended to be the next step. Reaction of 6-amino pyridine with ethyl isocyanate had been shown previously to be effective¹²⁴. However, the C-6 amino pyrimidine scaffold proved to be insufficiently reactive under the established conditions and none of urea-substituted compound **131** was formed. The reaction was attempted under microwave conditions and in the presence of several different bases and solvents to no effect (Scheme 5.4).



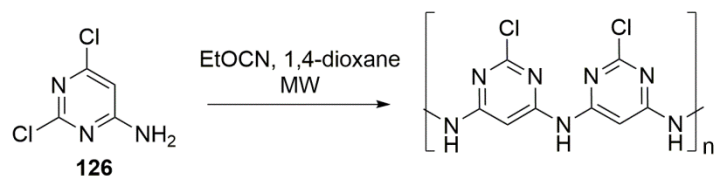
Scheme 5.4 Formation of the ethyl urea **131** by reaction of compound **130** with ethyl isocyanate failed under a range of experimental conditions.

It was thought that the boc-protected amino pyrrolidine moiety might be causing interference in the presence of strong bases, so a simpler variant **132**, which had an unsubstituted pyrrolidine moiety at the C-4 position was synthesised by reaction of compound **126** with pyrrolidine (Scheme 5). Unfortunately, compound **132** failed to react with ethylisocyanate to give compound **133** under a range of conditions.



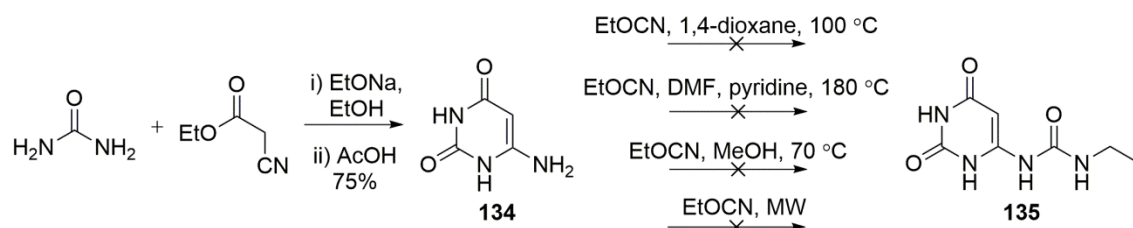
Scheme 5.5 Synthesis of compound **132**, a simpler variant of compound **130** was carried out, but the resulting aminopyrimidine **132** did not undergo successful reaction with ethyl isocyanate to give compound **133** under the conditions tested.

Reaction of ethyl isocyanate with the unsubstituted 2,4-dichloro-6-aminopyrimidine **126** was also attempted, but under the reaction conditions oligomerisation of compound **126**, presumably *via* S_NAr , was observed rather than reaction with ethylisocyanate (Scheme 5.6).



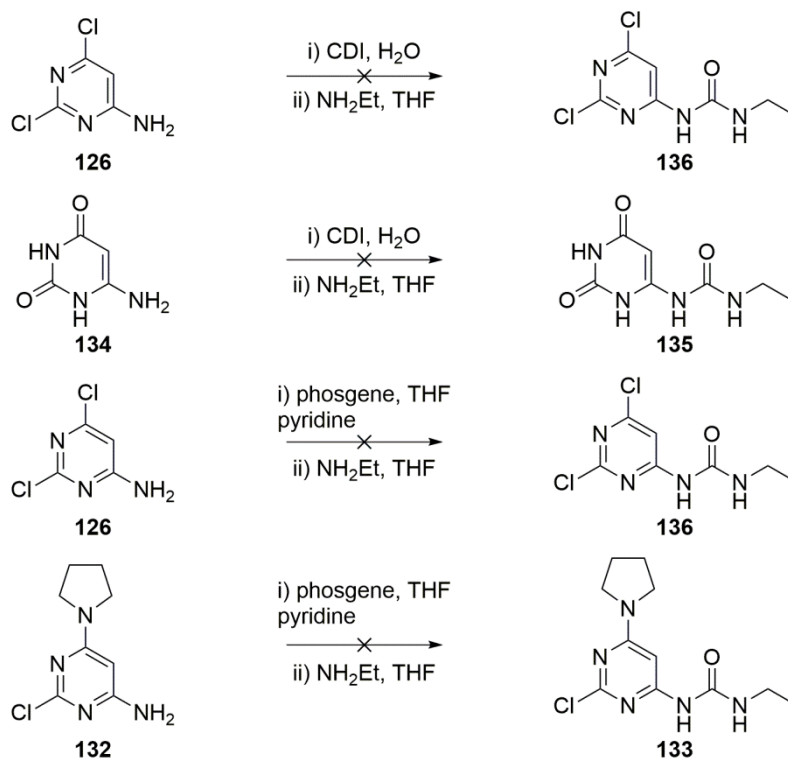
Scheme 5.6 Aminopyrimidine **126** underwent oligomerisation under the reaction conditions.

As reaction at the 4-chloro position of compound **126** was interfering with attempts to form the desired urea, it was thought that compound **134**, a precursor to compound **126** which lacks chlorine substituents, and so was incapable of undergoing an S_NAr reaction, might be able to react with ethyl isocyanate under forcing conditions. It was reasoned that chlorine could be installed in the 2- and 4- positions later in the route *via* reaction with $POCl_3$. Formation of compound **134** from urea and ethylcyanoacetate was carried out in reasonable yield. However, compound **134** was also unreactive under the conditions investigated and none of the urea substituted product **135** was formed (Scheme 5.7).



Scheme 5.7 Synthesis of compound **134** was carried out by reaction of urea with ethyl cyanoacetate, but attempts to form the N-ethyl urea **135** by reaction of compound **134** with ethyl isocyanate were unsuccessful.

As none of the aminopyrimidine variants investigated (**126**, **130**, **132** and **134**) were sufficiently nucleophilic to react with ethylisocyanate, more reactive electrophiles were investigated. Reaction of **126** and **134** with carbonyl diimidazole (CDI) was attempted to no effect, and reaction of **126** and **132** with phosgene was also tried (Scheme 5.8), with none of the desired urea substituted compounds **133**, **135** or **136** were isolated from any of these reactions.



Scheme 5.8 Attempted formation of N-ethyl urea substituted pyrimidines by reaction of compounds **126**, **132** and **134** with CDI and phosgene.

As the installation of the urea group had proved to be a challenge it was decided to focus instead on alternative compound series.

5.3 Triazolopyrimidines

5.3.1 Background

There have been a large number of published GyrB/ParE inhibitors which feature a fused 5,6 heterocycle ring system with *N*-ethyl urea substituent on the 5-membered ring. Examples of these compounds developed by Vertex⁸⁹, Evotec/Prolysis¹¹⁴, Pfizer¹¹³ and Prolysis/Biota¹¹¹ are shown in Figure 5.4. These compounds display a range of activity levels against the topoisomerase enzymes and against bacteria.

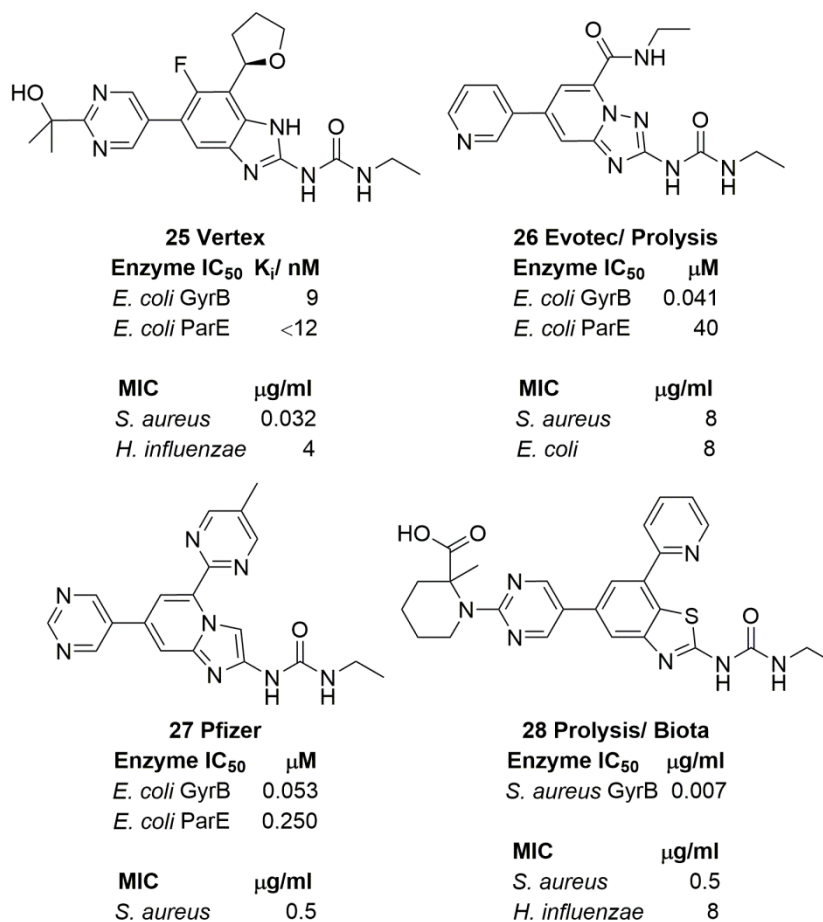


Figure 5.4 DNA Gyrase and topoisomerase IV inhibitors containing an N-ethyl urea substituted, fused-5,6-heterocycle.

AutoDock was used to dock each of the compounds shown in Figure 5.4 to understand the binding poses of these molecules. Their predicted binding poses are shown in Figure 5.5. The compounds are all predicted to bind in approximately the same configuration, making the expected hydrogen bonds to the conserved water molecule and aspartate residue and π -stack to the arginine residue. They all form a hydrogen bond to Arg-132 and compound **25** forms two.

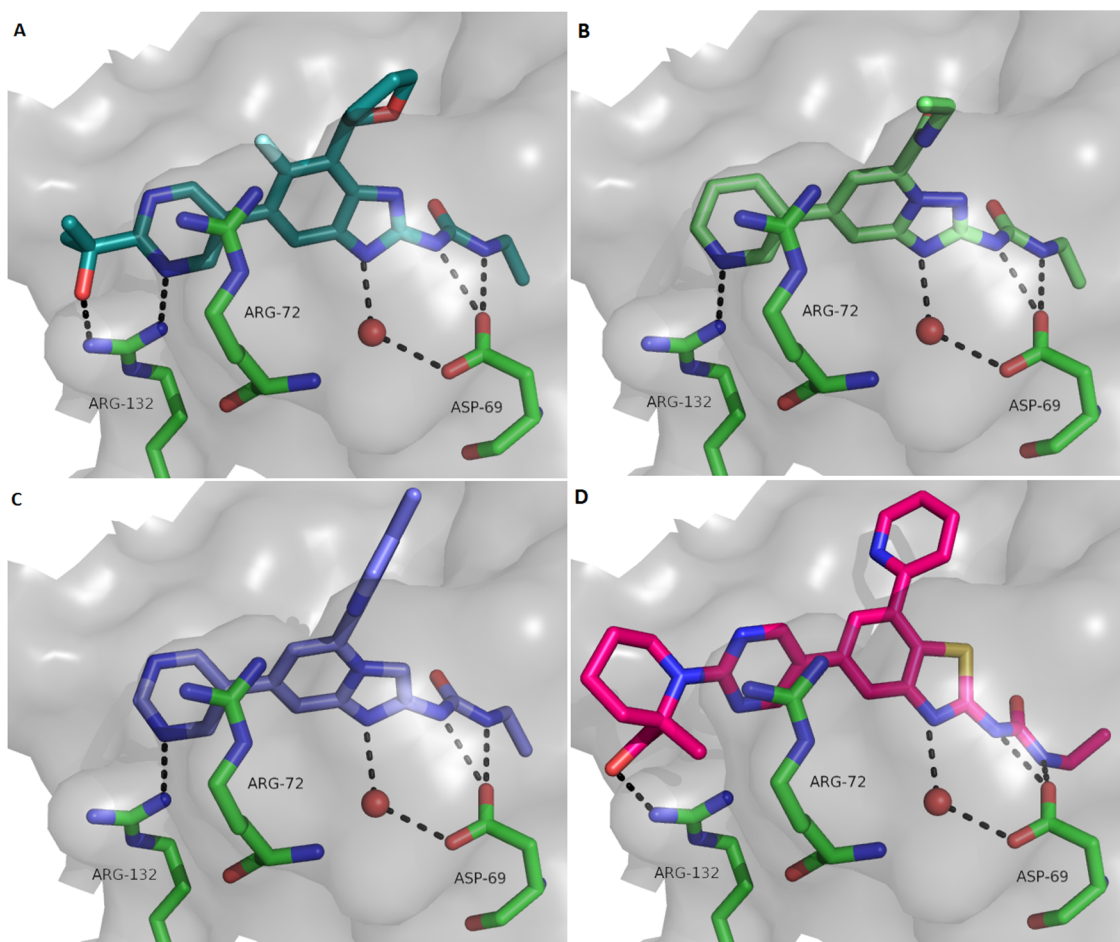
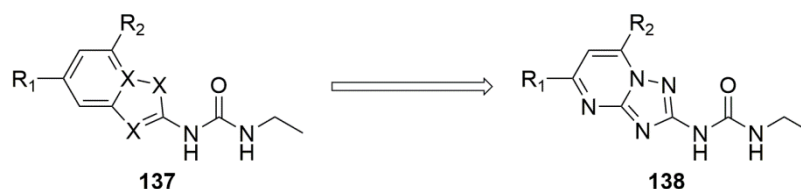


Figure 5.5 Predicted binding poses of inhibitors bearing a urea-substituted fused 5,6 heterocyclic ring to *E. coli* ParE (4HZ0), generated by AutoDock. A) compound **25**, B) compound **26**, C) compound **27**, D) compound **28**.

5.3.2 Compound design

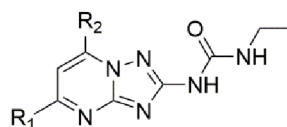
It was decided to investigate a heterocycle replacement approach to generate related compounds. Substitution of an extra nitrogen into the 6-membered ring of **137** (analogous to compound **26**) to give a triazolopyrimidine core **138** (Scheme 5.9) produced compounds which were scored well by AutoDock and had promising clogPs (Table 5.2).



Scheme 5.9 A triazolopyrimidine core **138** was chosen to investigate heterocycle replacement.

When choosing putative inhibitors to dock, R₁ was initially kept as phenyl and a range of heterocycles were investigated as R₂. For the most active compound from the initial docking, R₁ was then varied. All the docked compounds are shown in Table 5.2, in order of docking score.

Table 5.2



AutoDock scores and clogPs for triazolopyrimidine compounds.

Compound	R ₁	R ₂	AutoDock score	clogP
139			-9.55	-0.23
140			-9.02	0.99
141			-8.83	0.16
142			-8.82	-0.23
143			-8.81	0.99
144			-8.12	3.09
145			-8.02	1.3
146			-7.67	2.05
147			-7.34	1.62

Dockings carried out using AutoDock¹²⁶ and logPs calculated using ChemAxon calculator pluggins.¹²⁸

Compound **139** had the best score, but compound **140** was chosen as the first example to be synthesised, as the pyridine ring present in the 5-position of the triazolopyrimidine core in compound **139** was expected to pose a significantly greater

synthetic challenge when compared to the benzene at this position in compound **140** and the AutoDock scores were fairly similar for both compounds. Both compounds also had clogPs close to zero which may increase their chances of being able to penetrate Gram negative bacteria, as high polarity is often associated with compounds able to cross Gram negative membranes.³⁴ The docking pose for compound **140** is shown in Figure 5.6.

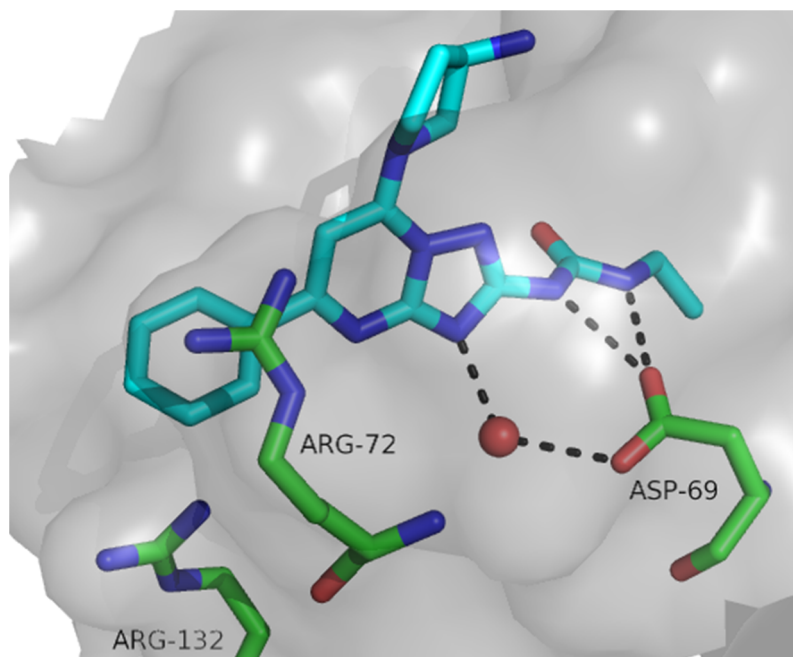
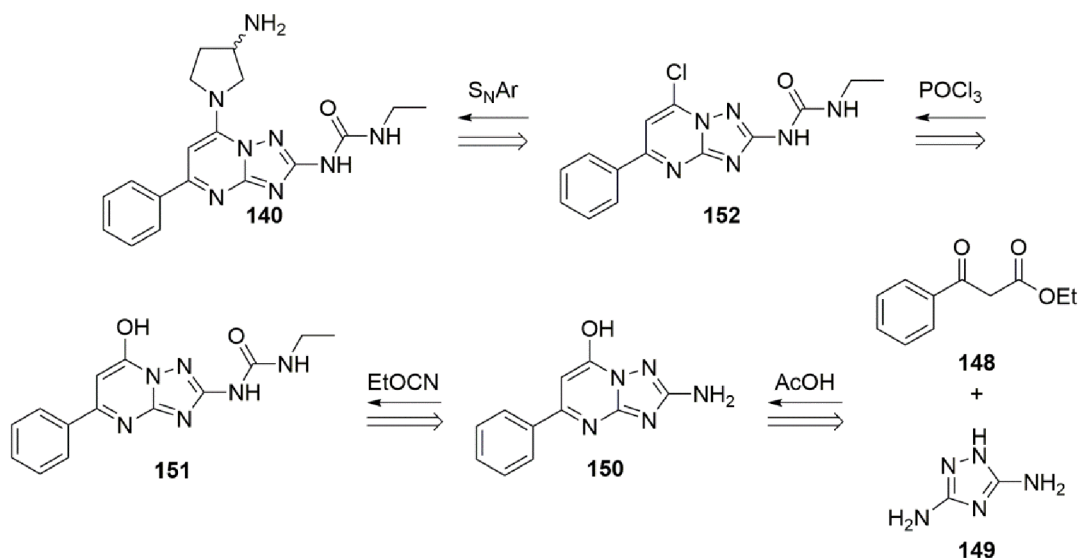


Figure 5.6 Docking pose of compound **140** generated using AutoDock.

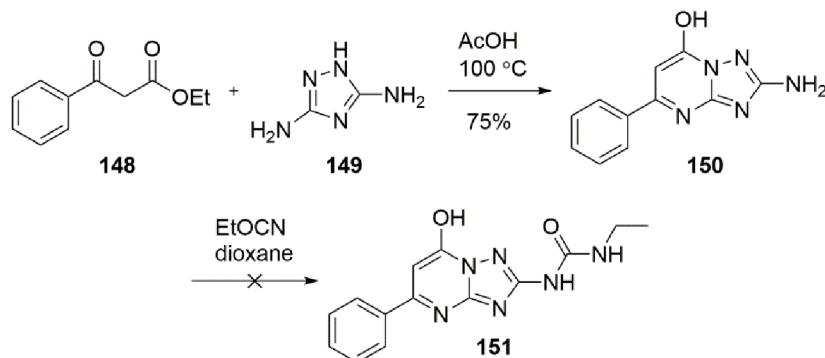
5.3.3 Synthesis

Retrosynthetic analysis of the designed molecular scaffold **140** suggested that synthesis should be able to proceed from initial formation of the triazolopyrimidine ring from ethyl benzoyl acetate **148** and 3,5-diamino-1,2,4-triazole **149** to give compound **150**¹⁵⁴. The ethyl urea could then be inserted by reaction with ethyl isocyanate to give compound **151**. Chlorination of compound **151** using POCl₃ should then provide compound **152** which could furnish the final product **140** *via* nucleophilic substitution of an appropriate group at the C5 position (Scheme 5.10).



Scheme 5.10 Retrosynthetic analysis of designed Triazolopyrimidine compound **143**.

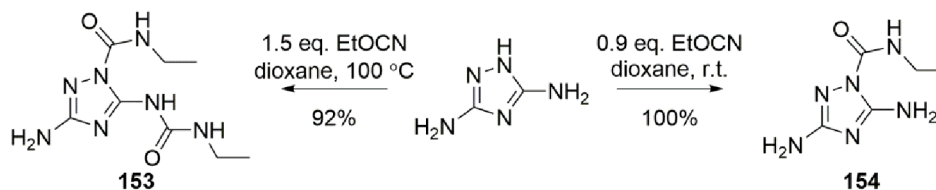
As expected, formation of the triazolopyrimidine **153** from ethyl benzoyl acetate **151** and diaminotriazole **152** was carried out in high yield. However, the subsequent reaction with ethyl isocyanate to give compound **154** was unsuccessful (Scheme 5.11).



Scheme 5.11 Formation of the triazolopyrimidine ring to give compound **150** proceeded in good yield, but formation of the urea substituted compound **151** by reaction with ethyl isocyanate was unsuccessful.

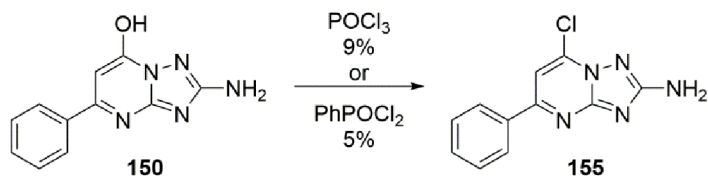
It was hoped that re-ordering the synthetic steps might get around this problem. Formation of the urea prior to the cyclisation reaction *via* reaction of diaminotriazole **149** with ethyl isocyanate was investigated. At first, the reaction of diaminotriazole **149** with ethyl isocyanate was attempted using 1.5 equivalents of ethyl isocyanate and heating. However, only a bis-substituted product **153** was isolated. Repeating the reaction with 0.9 equivalents of ethyl isocyanate and conducting the reaction at room temperature, gave a mono-substituted product **154**. However, substitution occurred

on the ring nitrogen rather than on one of the primary amines (Scheme 5.12) and so this approach could not be progressed forward to form the triazolopyrimidine **150**.



Scheme 5.12 Reaction of 3,5-diamino-1,2,4-triazole **149** with ethyl isocyanate gave a bis-substituted product **153** when 1.5 equivalents were used and substitution occurred on the ring nitrogen to give compound **154** when 0.9 equivalents of isocyanate were used.

Chlorination of the triazolopyrimidine **150** prior to the reaction with ethyl isocyanate to give **155** was attempted. The reaction was low yielding when carried out with phosphorus oxychloride as the chlorinating agent, so phenylphosphonic dichloride was investigated as an alternative chlorinating agent (Scheme 5.13). However, the yield was still very low. The product was highly insoluble which made its purification challenging and precluded the use of any of the usual solvents that might be employed in the subsequent reaction with ethyl isocyanate.



Scheme 5.13 Chlorination of compound **150** was attempted using two chlorinating agents, but the yield was low in both reactions.

No further work was carried out on this series as it was decided to focus on other compound series.

5.4 Quinazolinones

5.4.1 Background

A series of GyrB/ ParE inhibitors was reported by Cubist at the Interscience Conference on Antimicrobial Agents and Chemotherapy (ICAAC) in 2013 which contained a quinazolinone scaffold^{93,100}. An example of these, compound **32** is shown in Figure 5.7. Although this series was in the early stages of development, compound **32** showed

very promising biological activity, including moderate activity against *E. coli*. The quinazolinone core represents a novel way of providing the desired pattern of hydrogen bond donors and acceptors to bind tightly to the enzyme active site. Little has been published or patented on this compound series other than the report at ICAAC. A crystal structure was reported at ICAAC, but is not available online, so the compound was docked into the active site of *E. coli* ParE using AutoDock, so that its binding mode could be visualised. It was given a score of -8.02 by the program. The predicted binding pose is given in Figure 5.7.

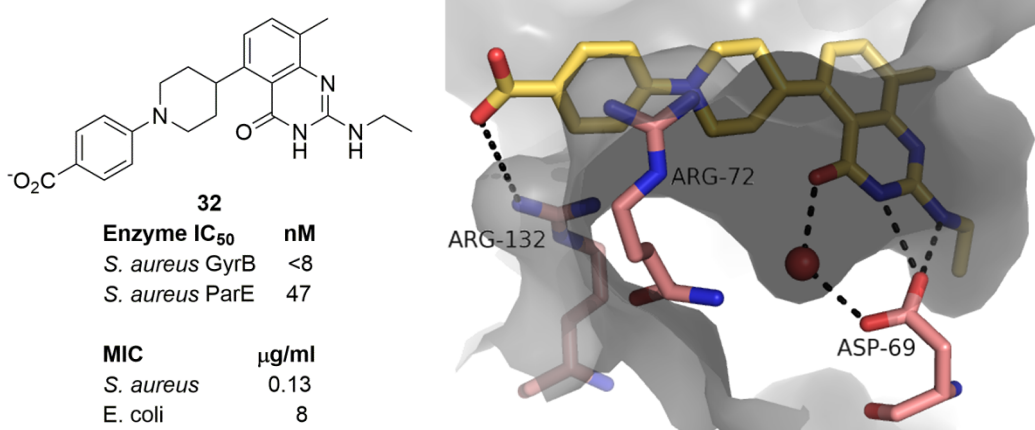
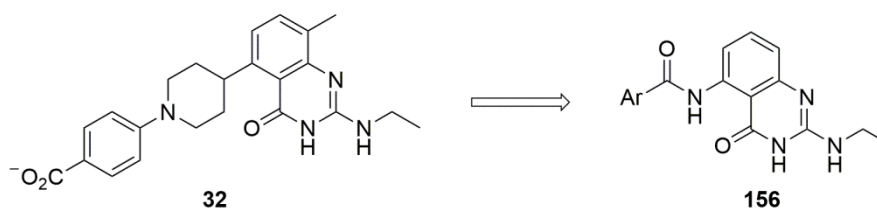


Figure 5.7 Structure and activity of a quinazolinone inhibitor **32** reported by Cubist at ICAAC in 2013 (left). And its binding pose in *E. coli* ParE (4HZ0) as modelled using AutoDock (right).

The binding pose shows that compound **32** is able to form the key interactions which have been described previously (hydrogen bonds to a conserved water and an aspartate residue and a π -stack to an arginine residue), as well as an additional hydrogen bond to another arginine residue near the entrance of the binding pocket.

5.4.2 Compound design

An alternative linking group to connect the quinazolinone core to an aromatic group capable of forming the desired π -stacking interaction was sought. An amide linkage was used in the pyridine carboxamide series, so replacement of the piperidine linker of **32** with an amide was contemplated which gave the general structure **156** (Scheme 5.14). Variation of the aromatic group was prioritised for the initial investigation, but further derivatives could be substituted at the 7- position of the quinazolinone ring, which projects into a solvent exposed area of the binding site analogous to substituents at the C4 position in the pyridine carboxamide series.



Scheme 5.14 Design of a series of compounds with a quinazolinone core analogous to an inhibitor series published by Cubist, but with an amide linkage rather than a piperidine linker.

A selection of potential inhibitor structures containing a quinazolinone ring with an amide linked aromatic group was docked using AutoDock (Table 5.3). The amide was in the reverse conformation compared to the pyridine carboxamide series, as docking of a variant with the amide bond the other way around indicated that the compound would be unlikely to adopt a binding pose which would make analogous contacts to the Cubist compounds (Figure 5.8).

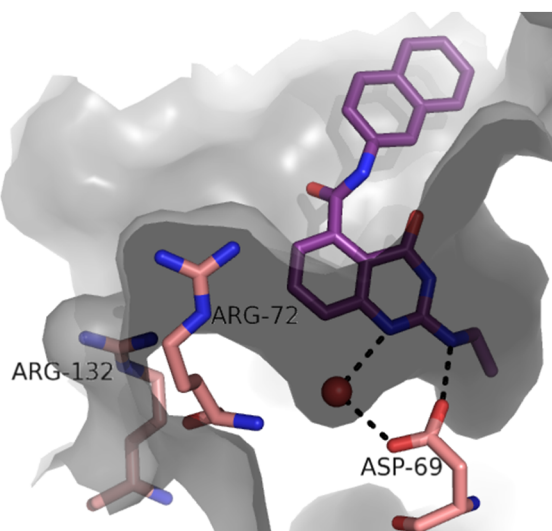
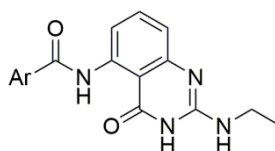


Figure 5.8 Binding pose of quinazolinone compound with reversed amide bond. The docking pose is different to that seen for the Cubist compounds.

The compound with the best AutoDock score was **157** and docking indicated that it would be able to form the additional hydrogen bond to arginine-132 as well as forming the hydrogen bonding network with Aps-69 and the conserved water molecule in the active site. The docking poses for compounds **157** and **158** are shown in Figure 5.9. The compounds are predicted to bind similarly to the Cubist compounds. An initial library of five compounds **158**, **161**, **162**, **163** and **164** were chosen for synthesis as they gave a broad sampling of different sized groups and a range of clogPs.

Table 5.3



AutoDock scores and calculated logPs for amino ethyl quinazolinones.

Compound	R	AutoDock Score	clogP
157		-8.65	-0.77
158		-8.25	4.52
159		-8.17	3.86
160		-7.51	1.66
161		-7.50	3.42
162		-7.50	4.37
163		-7.45	1.66
164		-7.42	2.87
165		-7.30	2.85
166		-6.93	2.04

Dockings carried out using AutoDock⁵⁹ and logPs calculated using Marvin beans.⁵⁸

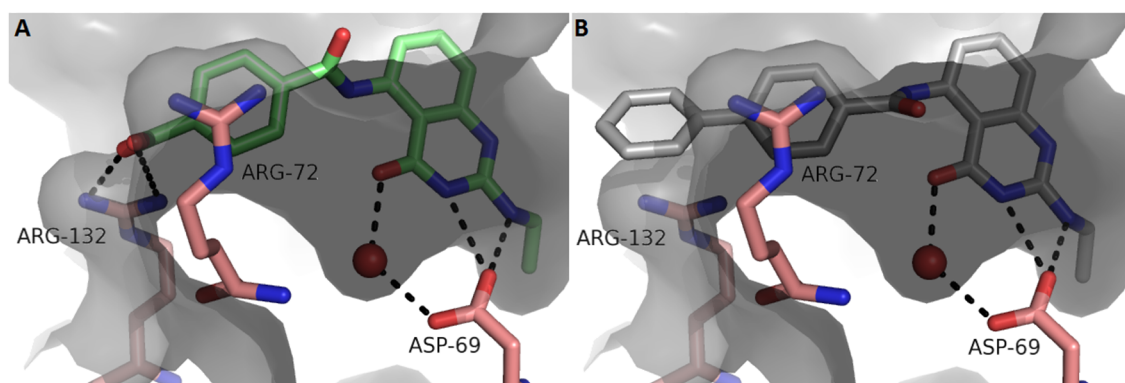
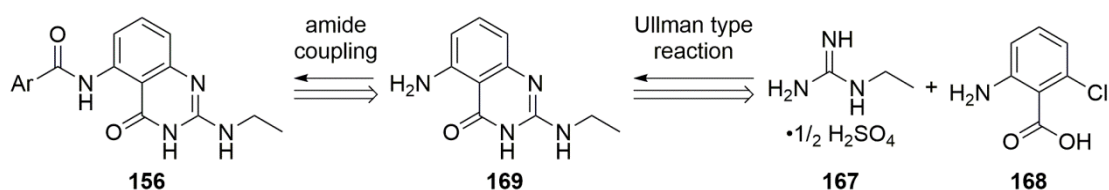


Figure 5.9 AutoDock poses for compounds **157** and **158** showing key binding interactions to the ATP binding site of *E. coli* ParE (4HZ0)⁹².

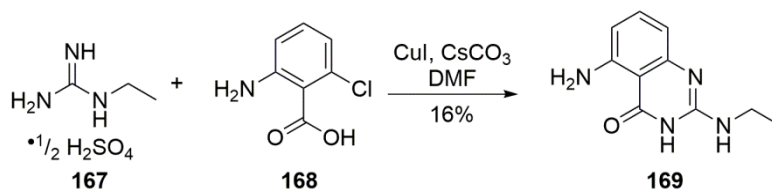
5.4.3 Synthesis

There are a number of published methods for the synthesis of 2-alkylaminoquinazolinones¹⁵⁵, but the most useful in terms of the requirements of this synthetic route was a modification of the Ullman reaction, using ethyl guanidine sulphate **167** and a 2-chlorobenzoic acid compound, reported by Huang *et. al.*¹⁵⁶ It was hoped that this reaction would be compatible with 2-amino-5-chlorobenzoic acid **168** and allow access to compound **167** which bears an amine substituent at the 5-position of the resulting quinazolinone ring, thus allowing access to the desired inhibitor structures **156** *via* an amide coupling reaction (Scheme 5.15).



Scheme 5.15 Retrosynthesis of quinazolinone compounds **156**.

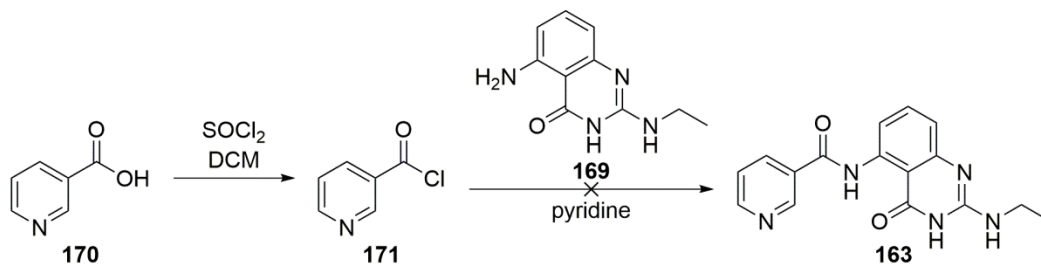
2-amino-5-chlorobenzoic acid **168** was commercially available and reaction of this with ethyl guanidine sulphate **167** under the conditions described successfully afforded the quinazolinone **169**¹⁵⁶, although the yield was fairly low (16%) (Scheme 5.16). The low yield was partly attributed to the presence of the primary amine which likely gave challenges to isolation and purification of the product. The reaction was also attempted under microwave conditions, but very little of the desired product was detected in the crude reaction mixture, and so microwave conditions were not investigated further.



Scheme 5.16 Formation of quinazolinone **169** *via* a copper catalysed reaction between 2-amino-6-chlorobenzoic acid **168** and ethyl guanidine sulfate **167**.

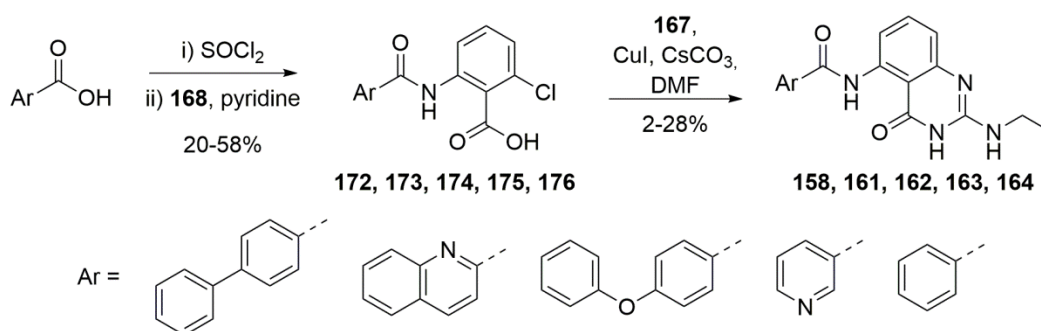
Compound **163** was chosen as the first inhibitor to synthesise in this series. Nicotinic acid **170** was reacted with thionyl chloride to afford nicotiny chloride **171** which was

used immediately in a reaction with aminoquinazolinone **169**. However, none of the desired product **163** could be isolated (Scheme 5.17).



Scheme 5.17 Attempted coupling between 5-aminoquinazolinone compound **169** and nicotinyl chloride **171** which was generated immediately prior to the reaction from nicotinic acid **170**.

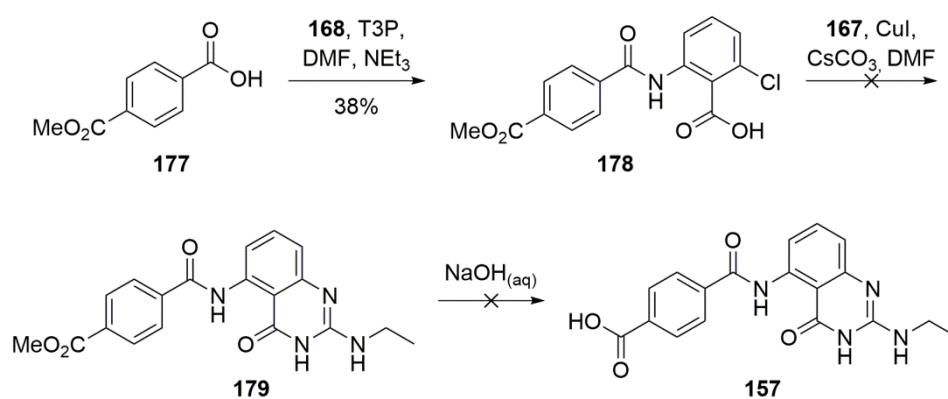
Reordering of the steps, so that the amide coupling reaction was carried out first was then attempted. Amide coupling reactions between 2-amino-6-chlorobenzoic acid **168** and an appropriate acid chloride, which was generated immediately prior to use, generally proceeded in moderate to good yield (Scheme 5.18) giving amides **172**, **173**, **174**, **175** and **176**. The cyclisation reaction to generate the quinazolinone ring proceeded in generally higher yield following the amide coupling reaction than it had done with 2-amino-6-chlorobenzoic acid **168** and successfully furnished the small library of compounds **158**, **161**, **162**, **163** and **164** which had been chosen following the computational docking studies (Scheme 5.18).



Scheme 5.18 Formation of a small library of compounds *via* an amide coupling reaction followed by cyclisation with ethyl guanidine sulfate **167** to give quinazolinones **158**, **161**, **162**, **163** and **164**.

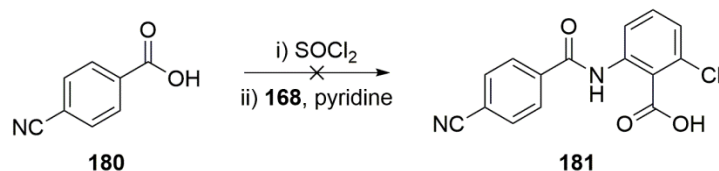
Synthesis of **157**, a derivative with an acidic group in the position predicted to mimic that within the Cubist compound **32**, was also attempted. Initially, monomethylterephthalate **177** was chosen as the starting material. This was coupled

to 2-amino-6-chlorobenzoic acid **168** using T3P as an amide coupling reagent rather than forming an acid chloride. This was based upon the expectation that reaction of compound **177** with thionyl chloride would not be selective for the carboxylic acid and there would also be reaction with the methyl ester. This reaction proceeded in moderate yield to give compound **178**. However, the Ullman-like reaction with ethyl guanidine sulfate **167** which followed did not afford a sufficient quantity of compound **179** to allow full characterisation, although its formation was confirmed using LC-MS. Therefore, hydrolysis of the ester **179** to give compound **157** could not be attempted (Scheme 5.1).



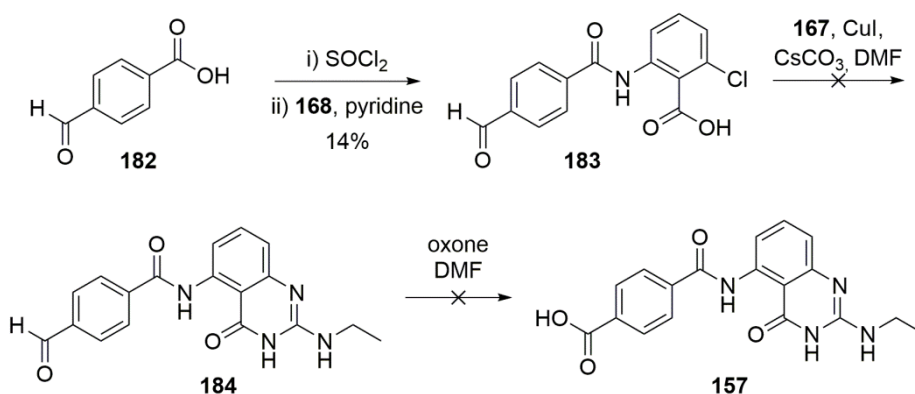
Scheme 5.19 Amide coupling between monomethyl terephthalate **177** and 2-amino-6-chlorobenzoic acid **168** gave compound **178**. However, formation of the quinazolinone ring to give compound **179** was unsuccessful and ester hydrolysis to afford compound **157** could not be attempted.

An alternative route to this product was envisioned wherein the final step would involve hydrolysis of a nitrile group rather than an ester. However, the synthesis of the desired amide precursor proved challenging. Formation of an acid chloride from 4-cyanobenzoic acid **180** followed by reaction with 2-amino-6-chlorobenzoic acid **168** was attempted as these conditions had been used successfully with other derivatives (Scheme 5.18). However, the reaction gave a mixture of products with very little of the desired amide **181** present (Scheme 5.20) and it was decided to focus efforts on a different route to the desired compound.



Scheme 5.20 Attempted formation of nitrile substituted compound **181** gave a mixture of products.

Finally, oxidation of an aldehyde was considered as a method for accessing the desired carboxylic acid functionality. Reaction of 4-formyl benzoic acid **182** with 2-amino-6-chlorobenzoic acid **168** was carried out successfully to give compound **183**. However, the subsequent Ullman-type reaction to generate the quinazolinone intermediate **184** was unsuccessful, and therefore oxidation of **184** to give the desired carboxylic acid substituted derivative **157** could not be carried out.



Scheme 5.21 Amide coupling between 4-formylbenzoic acid **182** and 2-amino-6-chlorobenzoic acid **168** via an acid chloride intermediate gave compound **183**. However, formation of the quinazolinone ring to give compound **184** was unsuccessful and oxidation to afford compound **157** could not be attempted.

No further attempts to form the carboxylic acid derivative were made.

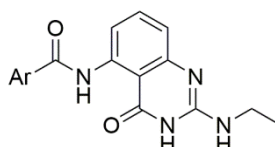
5.4.4 Biological evaluation of initial compound library

The results from the biological evaluation of compounds **158**, **161**, **162**, **163** and **164** are shown in Table 5.4. These compounds were assessed for their enzyme inhibition using an ATPase assay against the *E. coli* DNA gyrase enzyme and for antibacterial activity against *S. aureus* and *E. coli*.

These compounds all showed activity against the enzyme in the low μM range, with the exception of **161**, which suggests that either the quinoline ring system does not fit

well into the ATP binding site of GyrB, or the presence of the nitrogen atom in the ring favours a different conformation of the inhibitor which doesn't bind as efficiently. The most potent inhibitors were **163** and **164** which possess a simple six membered ring. This suggests further optimisation should focus on substituted phenyl and pyridyl rings at this position. Unfortunately, none of these compounds showed antibacterial activity against *S. aureus* or *E. coli*. This may be due to their low aqueous solubility. The addition of solubilising groups may provide compounds with antibacterial activity.

Table 5.4



Biological activity of substituted quinazolinones

Compound	Ar	clogP ^a	DNA gyrase IC ₅₀ μM	<i>S. aureus</i> MIC μg/μl	<i>E. Coli</i> MIC μg/μl
158		4.52	20	>256	>256
161		3.42	900	>256	>256
162		4.37	33	>256	>256
163		1.66	3.3	>256	>256
164		2.87	1.1	>256	>256

a. clogP calculated using the calculator plugins from MarvinSketch¹²⁸; *S. aureus* SH1000 and *E. coli* BW25113

5.4.5 Efforts towards the synthesis of quinazolinone derivatives with improved solubility

Morpholine rings are commonly used in medicinal chemistry as solubilising groups and it was decided to attempt the synthesis of a quinazolinone derivative containing a morpholine substituent at the 7- position of the quinazolinone ring **180**. Docking of this derivative into the ParE binding site indicated that the morpholine ring would be positioned in the solvent-exposed portion of the binding site and should not disrupt the hydrogen bonding interactions formed by the rest of the molecule to the protein (Figure 5.10).

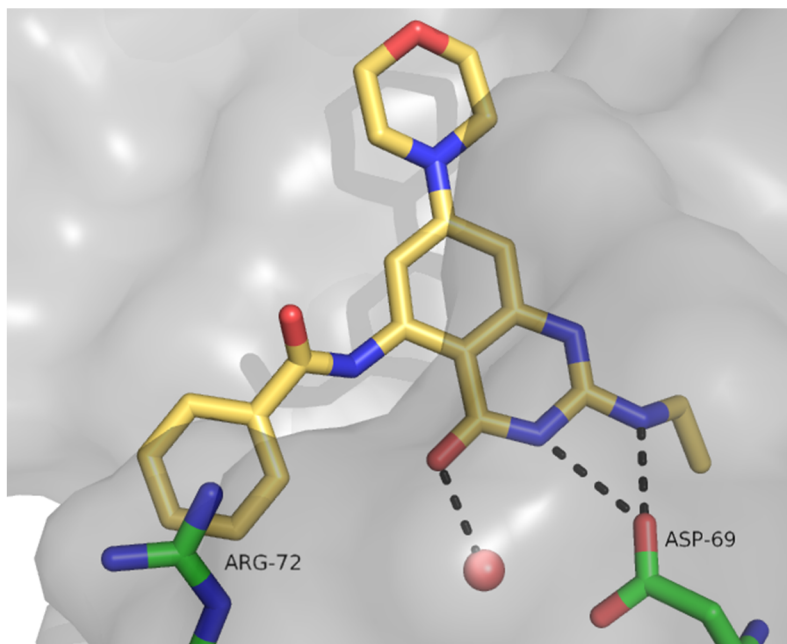
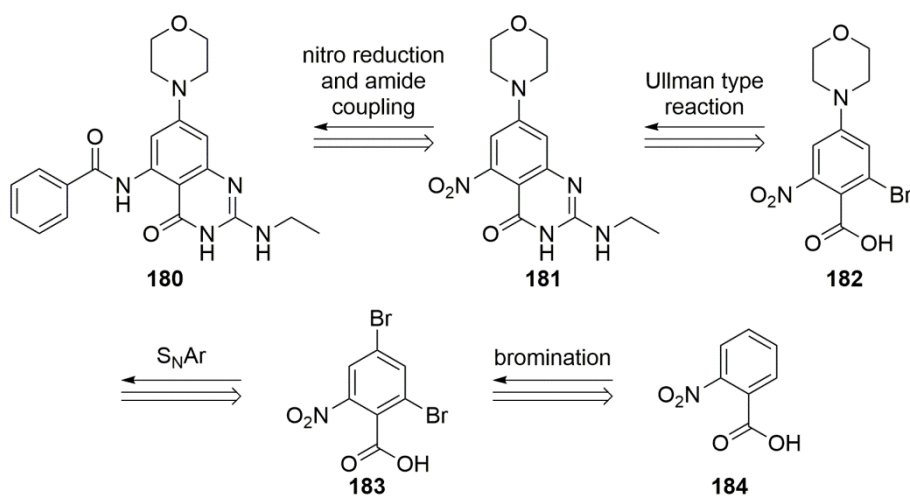


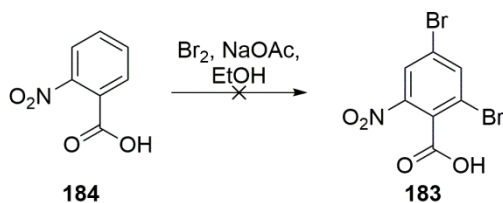
Figure 5.10 Predicted binding pose of compound **180** bound to *E. coli* ParE generated using AutoDock.

A retrosynthetic analysis of compound **180** was performed. Amide coupling would be a potential final step in this synthesis after reduction of a nitro group in intermediate **181**. The Ullman-type reaction to generate the quinazolinone ring would precede this step from bromo-substituted compound **182**. The morpholine ring would be installed relatively early in the route *via* an S_NAr reaction from the dibromo compound **183** which could be formed by the bromination of the commercially available compound **184** (Scheme 5.22).



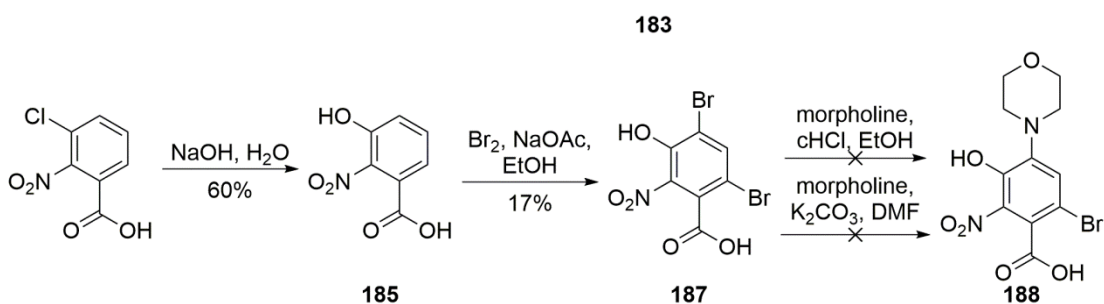
Scheme 5.22 Retrosynthetic analysis of morpholine substituted compound **180** from the commercially available 2-nitrobenzoic acid **184** in five steps.

Unfortunately, compound **184** failed to undergo bromination under standard bromination conditions, most likely due to the electron poor nature of the ring (Scheme 5.23).



Scheme 5.23 Attempted bromination of compound **184** under standard conditions did not produce the desired compound **183**.

Bromination of a more electron-rich phenolic variant of compound **184** had been reported in the literature and so the phenolic variant **185** was produced using an S_NAr reaction from the chloro-substituted variant **186** and brominated under standard conditions to give compound **187** (Scheme 5.24).¹⁵⁷ Reaction of compound **187** with morpholine was attempted, but the substitution was unsuccessful under acid catalysed and base catalysed conditions investigated, and no formation of compound **188** was detected.



Scheme 5.24 The dibromo-substituted compound **187** was produced in two steps from **186**. However, reaction of compound **187** with morpholine to give compound **188** was unsuccessful under the conditions investigated.

Due to time constraints, this avenue of investigation was not pursued any further.

5.5 Conclusions and future work

Three novel inhibitor scaffolds were designed and attempts were made to synthesise all three. The pyrimidine and triazolopyrimidine scaffolds proved to be synthetically intractable, but an exploratory library of quinazolinones were produced and

biologically assessed. Several of the synthesised compounds showed promising enzyme activity, but the compounds were not antibacterial at low concentrations and were insoluble at higher concentrations.

Several synthetic routes to compound **157**, which was predicted to have the best binding of the designed quinazolinone compounds, were investigated, but none were successful. Further optimisation of the Ullman-like quinazolinone ring forming reaction may facilitate the production of compound **157**, as this step was low yielding and in several cases did not produce enough material for isolation and characterisation.

Variants of the quinazolinone compounds bearing a solubilising group were designed, but there was not time to fully investigate synthetic approaches to these compounds. Further investigation of this synthetic route could furnish quinazolinone compounds with improved properties.

Chapter 6 Conclusions and Future Work

This project was broadly divided into two sections. Firstly, further exploration of the pyridine 3-carboxamide inhibitors which had been previously discovered at the University of Leeds and, secondly, efforts to identify a novel series of DNA gyrase and topoisomerase IV inhibitors.

6.1 Development of Pyridine-3-carboxamides as inhibitors of DNA gyrase and topoisomerase IV

6.1.1 Summary

A library of pyridine 3-carboxamide derivatives were synthesised and assessed for their biological activity. All of the synthesised inhibitors had IC_{50} s of ≤ 210 nM against *E. coli* DNA gyrase. Several compounds showed antibacterial activity against *S. aureus*, but none were active against *E. coli*. The structures of some representative DNA gyrase inhibitors are shown in Figure 6.1 along with their biological activities. These compounds are highly potent inhibitors of DNA gyrase and topoisomerase IV, but their antibacterial activities were not as good as might be hoped for such potent enzyme inhibitors. This suggests that the physicochemical properties of these compounds might be reducing their ability to reach a sufficiently high concentration within the bacterial cell. Alternatively, the lower activity of these compounds against the topoisomerase IV enzyme from *E. coli* relative to the same enzyme from *S. aureus* may be a factor in the different activities of the compounds against the different bacterial strains.

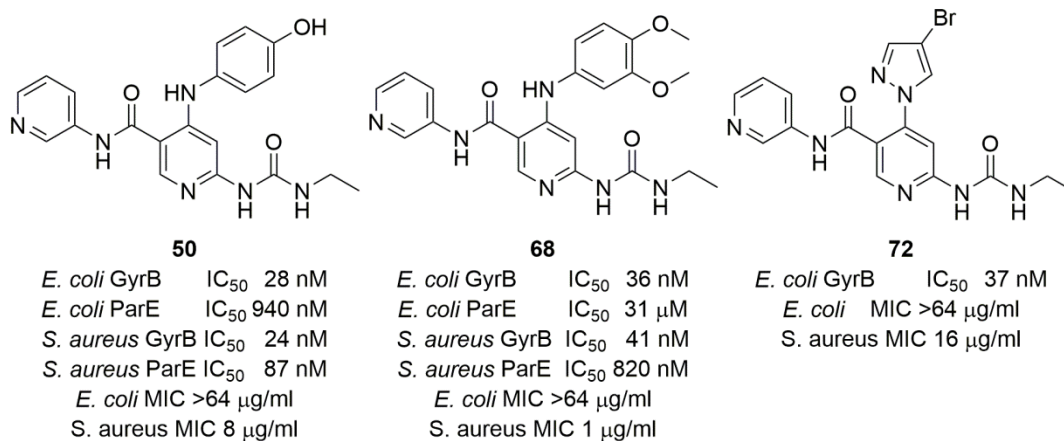


Figure 6.1 Structures of some representative pyridine 3-carboxamide compounds which exhibit potent inhibition of DNA gyrase and topoisomerase IV.

Four compounds were assessed for a number of *in vitro* ADME properties. Three of which were synthesised as part of this project, and one which was produced originally as part of previous work at the University of Leeds and which was resynthesised for this project. The compounds produced for this project generally had more favourable *in vitro* ADME properties than the compound which was designed prior to the commencement of the project. Two of the compounds had low aqueous solubility, but the other two were moderately soluble. The compound with the lowest aqueous solubility had very high levels of plasma protein binding and performed very poorly in the Caco-2 membrane permeability assay. The other compounds performed better in the Caco-2 assay, but the compounds were not predicted to have a very strong ability to be taken up from the gut. The metabolic stability of these compounds was assessed using a liver microsome assay. They displayed moderate metabolic stability, but would benefit from increased stability going forward. Unfortunately, the compound with the most favourable ADME profile was the compound with the least potent antibacterial activity.

In order to assess the binding mode of these compounds and also to confirm that they definitely bind to the ATP site of DNA gyrase, crystallography experiments were carried out. The 24 kDa construct of GyrB which is often used for crystallographic experiments in the presence of inhibitors was produced and crystallisation experiments produced crystals with all four inhibitors which were selected for this study. The crystals

diffracted well and all showed electron density corresponding to the inhibitor they were crystallised with. The structures were solved using molecular replacement to a good resolution.

The hydrogen bond contacts which had been predicted using computational docking were all shown to be in the expected configuration. The configuration of the substituent at the C-4 position of the central pyridine ring was not as closely matched to the poses predicted by computational docking, but this was not unexpected as this region of the protein is flexible when ATP is not bound. The residues in the flexible loop are usually disordered in crystal structures. This makes computational docking less able to predict interactions in this region of the binding site.

6.1.2 Future work

The results from the *in vitro* ADME profiling of these compounds and from the crystallographic experiments suggest a number of additional avenues to explore. Improvements in the metabolic stability of these compounds would be highly beneficial, so the addition of functional groups known to increase metabolic stability, such as fluorine or trifluoromethane, should be investigated.

Synthesis of the pyrrole and imidazole derivatives which was not completed during this project should be carried out, along with other similar derivatives in order to explore a range of compounds with very similar shapes, but different polarities. Assessment of the biological activities of these compounds will help in understanding the relationship between hydrophilicity and antibacterial activity in this series. A wider range of derivatives bearing primary amines, and derivatives bearing carboxylic acid groups should be produced in order to further understand the effects of charged groups.

Additional antibacterial screening against a wider range of Gram negative and Gram positive bacterial species, in particular the ESKAPE pathogens (*E. faecium*, *S. aureus*, *K. pneumoniae*, *A. baumannii*, *P. aeruginosa*, and *Enterobacter* species) which are the most clinically relevant strains¹⁵⁸, should be carried out. It would also be of interest to determine the activity of these compounds against strains of Gram negative bacteria

which have impaired efflux pumps in order to determine the degree to which these compounds lack activity against these species due to active efflux.

Compounds bearing aniline substituents have a high propensity to be mutagenic when tested *in vivo*. The Ames test is an *in vitro* model for mutagenicity. At least one member of the series which contains an aniline substituent should be subjected to the Ames test in order to establish whether the aniline is likely to pose a mutagenic risk, and if so, further investigation of derivatives with an aniline substituent should be avoided.

Co-crystal structures are very useful to guide design of compound structures. It would be useful to compare the binding of inhibitors into the ATP site of ParE with their binding mode in GyrB. Therefore production of the 24 kDa subunit of ParE should be carried out in order to compare the binding poses of these compounds in both proteins.

6.2 Design of novel chemical series as inhibitors of DNA Gyrase and Topoisomerase IV

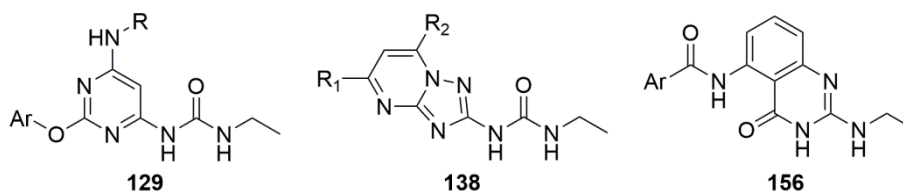
6.2.1 Summary

De novo design using SPROUT was carried out with the aim of designing novel inhibitor scaffolds with an appropriate acceptor/donor motif to form hydrogen bonds to the conserved water molecule and aspartate residue in the ATP binding site of the DNA gyrase and topoisomerase IV enzymes. However, in the searches which were carried out, SPROUT did not find solutions which linked the hydrogen bond donor and acceptor groups in a configuration which would allow them to form the desired interactions, and the designed scaffolds were too complex to be synthetically tractable.

Two vHTS approaches were used to search commercial databases for potential inhibitors of the DNA gyrase and topoisomerase IV enzymes. Glide was used to carry out structure based vHTS screening of the ZINC database using GyrB (3G7E) and ParE (4HZ0) crystal structures. ROCS was used to carry out ligand based vHTS screening

using a diverse selection of known DNA gyrase and topoisomerase IV inhibitors as queries. A pharmacophore model was also generated using vROCS and used as the query for a further ROCS search. The hits from all of the vHTS searches were visually assessed and a shortlist of potential inhibitors generated. This shortlist comprised compounds from a number of suppliers, and the compounds which were available from ChemBridge were purchased and assayed for their inhibition of DNA gyrase. Two of the compounds displayed some activity at a concentration of 100 μ M, but this was not considered sufficient to be worth investigating the SAR of these compounds.

Rational design was also carried out. A scaffold hopping approach was used to design analogues of known inhibitor series. Pyrimidines **129**, triazolopyrimidines **138**, and quinazolinones **156** were designed which were predicted to form binding interactions with the GyrB and ParE ATP binding sites and synthesis was carried out towards the production of these compounds.



The quinazolinone compounds proved to be the most synthetically tractable and a small library of compounds was produced and the compounds assessed for their inhibition of the DNA gyrase enzyme. The most potent compound had an IC_{50} of 1.1 μ M, but none of the compounds displayed antibacterial activity against *E. coli* or *S. aureus*. The compounds which had been synthesised had very low aqueous solubility, so a variant was designed with a morpholine substituent in the hope it would demonstrate improved solubility, but only a preliminary effort towards its synthesis was carried out.

6.2.2 Future work

The shortlisted hits from the vHTS studies were available from a number of different suppliers and only those available from ChemBridge were purchased and biologically assessed. The purchase of a wider selection of molecules would allow a better assessment of the effectiveness of the different vHTS approaches used and provide

additional opportunities to identify a hit molecule with sufficient activity against the DNA gyrase and topoisomerase IV enzymes to be worth carrying out an SAR study.

The pyrimidine and triazolopyrimidine compounds which were designed proved to be synthetically intractable. The design of variants of these compounds with improved synthetic tractability might prove to be a source of potent inhibitors.

Only a few examples of the quinazolinone inhibitor series were synthesised. The copper catalysed, Ullman-like reaction used to form the quinazolinone ring was low yielding and posed a challenge to the production of a number of derivatives. Optimisation of this reaction or the identification of an alternative route to this scaffold would likely enable the production of a larger library of quinazolinones in order to establish more of the SAR of these compounds.

The quinazolinone inhibitors synthesised to date have had insufficient aqueous solubility for the successful formation of an inhibitor-protein co-crystal for X-ray crystallography. The synthesis of derivatives with improved aqueous solubility would facilitate the acquisition of an X-ray crystal structure of a quinazolinone inhibitor bound in the ATP binding site of GyrB or ParE. The acquisition of a crystal structure would guide further optimisation of these inhibitors.

Chapter 7 Experimental

7.1 Chemical methods

7.1.1 Instrumentation and General Methods

All reagents were obtained commercially and used directly without further purification. Petrol refers to petroleum ether (bp. 40-60 °C). Solvents were removed under reduced pressure using an aspirator pump connected to a Buchi rotary evaporator; this was followed by drying under high vacuum at 0.5 mmHg using a rotary oil pump. Flash chromatography was performed using geduran silica gel 60 (particle size 40-63 μm) supplied by Merck. Thin layer chromatography (TLC) was performed using aluminium precoated silica plates (Machery–Nagek 818133, 0.20 mm thickness) supplied by Merck. Infrared (IR) spectra were recorded on a Perkin Elmer Spectrum One FT–IR spectrometer or on a Bruker Alpha Platinum ATR, as solid samples unless stated. Vibrational frequencies are reported in wavenumbers (cm^{-1}). Melting point determination was carried out on a Reichert Hot Stage apparatus and are reported uncorrected. High–resolution mass spectrometry was carried out using a Bruker MaXis Impact Time of Flight spectrometer using ESI. Elemental analysis was carried out using a Carlo Erba 1108 Elemental Analyzer. HPLC analyses were carried out on a Dionex HPLC system using a Thermo Electron Corporation Hyperprep HS C18 column (8 μm , 250 \times 4.6 mm) and a diode array as a detector. A gradient of water and acetonitrile (5-95%) was used as solvent at a flow rate of 1 ml/min for 40 mins. ^1H and ^{13}C NMR spectra are recorded on a 300 / 75 MHz Bruker DPX300 spectrometer, a 400 / 100 MHz Bruker AV3-400 spectrometer or a 500 / 125 MHz Bruker Advance 500 spectrometer as indicated, using an internal deuterium lock. Chemical shifts were recorded with reference to tetramethylsilane (TMS) as an internal standard. Coupling constants are given in Hertz (Hz). Proton and carbon assignment has been carried out based on HMBC and HMQC spectra analysis where appropriate.

7.1.2 General Methods

The general methods described below exemplify frequently performed reactions. The molarities are representative of a specific example and where referenced are scaled accordingly.

General method A – Acid catalysed nucleophilic aromatic substitution

The appropriate aryl chloride (40 mg, 0.13 mmol, 1.0 eq) and amine (19 mg, 0.13 mmol, 1.0 eq) were dissolved in EtOH (2 ml) and cHCl (1 drop) was added. The resulting solution was heated to 80 °C overnight and then cooled to 0 °C and basified to pH 4 by careful addition of aqueous NaOH (2M). The resulting precipitate was collected using filtration and purified as specified.

General method B – Base catalysed nucleophilic aromatic substitution

The appropriate heterocycle (55 mg, 0.38 mmol, 1.2 eq) was dissolved in DMF (2 ml) and cooled to 0 °C. NaH (60% suspension in oil, 19 mg, 0.47 mmol, 1.5 eq) was added portion wise and the mixture stirred for 1 h under N₂. The appropriate aryl chloride (100 mg, 0.31 mmol, 1.0 eq) was added and the reaction mixture heated to 70 °C for 18 h. The reaction mixture was allowed to cool to room temperature, quenched by addition of water (10 ml) and purified as specified.

General method C – amide coupling using T3P

The appropriate carboxylic acid (100 mg, 0.41 mmol, 1.0 eq) and amine (85 mg, 0.91 mmol, 2.2 eq) were suspended in pyridine (5 ml) and T3P solution (50% in EtOAc, 0.50 ml, 0.82 mmol, 1.2 eq) added. The reaction was stirred for 18 hours and the concentration reduced *in vacuo*. Water (5 ml) was added and the reaction stirred for 15 minutes. The resultant precipitate was collected by filtration and purified as specified.

General method D – amide coupling *via* an acid chloride intermediate

The appropriate carboxylic acid (1.44 g, 11.7 mmol, 2.00 eq) was suspended in thionyl chloride (10 ml). The reaction mixture was heated to 70 °C until the carboxylic acid was no longer detected by TLC. Thionyl chloride was removed *in vacuo* and the appropriate amine (1 g, 5.84 mmol, 1.00 eq) and pyridine (5 ml) added and the reaction heated to

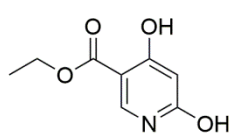
80 °C for 16 hours. The pyridine was removed in *vacuo* and the resulting residue acidified by addition of HCl (2 M, 20 ml) and extracted into EtOAc (3 x 20 ml). The combined organics were dried over MgSO₄ and concentrated *in vacuo*. The resulting residue was purified as specified.

General method E – quinazolinone formation

The appropriate 2-chlorobenzoic acid (200 mg, 0.727 mmol, 1.00 eq), ethyl guanidine sulfate (396 mg, 1.45 mmol, 2.00 eq) and caesium carbonate (145 mg, 2.91 mmol, 4.00 eq) were suspended in DMF (4 ml) under nitrogen and stirred for 5 minutes. Copper iodide (28.0 mg, 0.147 mmol, 0.200 eq) was added and the reaction heated to reflux for the specified time. The reaction was allowed to cool and filtered through celite. The filtrate was concentrated *in vacuo* and purified as specified.

7.1.3 Preparative procedures

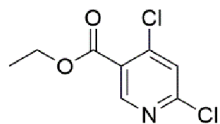
Ethyl 4,6-dihydroxynicotinate¹²³ 44



Diethyl 1,3-acetonedicarboxylate (6.5 ml, 29 mmol) was dissolved in acetic anhydride (5.5 ml, 61 mmol) and trimethylorthoformate (8.6 ml, 43 mmol) added. The resulting colourless mixture was heated to 120 °C for 3 hours during which time the solution developed an orange colour. The reaction mixture was allowed to cool to room temperature and excess acetic acid removed *in vacuo*. The resulting dark orange liquid was cooled to 0 °C and aqueous NH₃ (33% solution, 5.3 ml) added dropwise over half an hour. A yellow precipitate formed. The resulting mixture was acidified to pH1 by addition of cHCl and the resulting off-white precipitate collected by filtration to afford the title compound (5.2 g, 28 mmol, 96%) as colourless microcrystals, m.p. 215.9-218.4 °C (from EtOH-water, lit.¹²³ m.p. 200-204 °C); *R*_f 0.34 (EtOAc); δ_H (300 MHz, DMSO-*d*₆) 13.35 (br. s., 1 H, 4-OH), 10.95 (br. s., 1 H, 6-OH), 8.21 (s, 1 H, 2-H), 5.95 (s, 1 H, 5-H), 4.38 (q, *J* 7.1 Hz, 2 H, 3-CO₂CH₂CH₃), 1.38 (t, *J* 7.1 Hz, 3 H, CO₂CH₂CH₃); δ_C (75 MHz, DMSO-*d*₆) 168.2 (3-CO₂CH₂CH₃), 168.0 (6-C), 167.2 (4-C), 141.4 (2-C), 100.8 (5-C), 99.7 (3-C), 61.9 (3-CO₂CH₂CH₃), 14.1 (3-CO₂CH₂CH₃); (Found C, 52.6; H, 4.90; N, 7.5; C₈H₇NO₄ requires C, 52.5; H, 4.95; N, 7.7%); ν_{max} / cm⁻¹ (solid) 2671, 1662, 1573, 1403; *m/z* (ESI⁺) found MH⁺

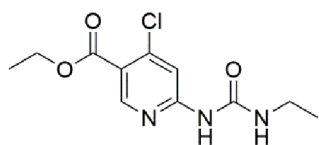
184.0605, $C_8H_{10}NO_4$ *MH* requires 184.0604; HPLC = 1.30 mins. Spectroscopic data consistent with literature values.¹²³

Ethyl 4,6-dichloronicotinate¹²³ **45**



Compound **44** (5.0 g, 27 mmol) was suspended in $POCl_3$ (25 ml) and the reaction heated to 80 °C for 18 hours. A further portion of $POCl_3$ was then added and the reaction mixture stirred at 80 °C for a further 4 hours. The reaction was allowed to cool and the volume reduced *in vacuo* and the resulting brown oil added carefully to a mixture of ice and water and allowed to warm to room temperature. The aqueous portion was extracted into DCM (6 × 20 ml), the combined organic extracts were then washed with brine (30 ml), dried over $MgSO_4$ and concentrated *in vacuo* to give a brown oil. Purification of this oil using column chromatography (1:15 EtOAc–Petrol) afforded the title compound (3.4 g, 15 mmol, 57%) as colourless crystals, m.p. 31.1–31.3 °C; R_f 0.68 (1:9 EtOAc–Pet); δ_H (300 MHz, $DMSO-d_6$) 8.85 (s, 1 H, 2-H), 7.47 (s, 1 H, 5-H), 4.44 (q, J 7.0 Hz, 2 H, 3- $CO_2CH_2CH_3$), 1.42 (t, 3 H, J 7.0 Hz, 3- $CO_2CH_2CH_3$); δ_C (75 MHz, $DMSO-d_6$) 163.1 (3- $CO_2CH_2CH_3$), 154.6 (6-C), 152.3 (2-C), 145.9 (4-C), 126.0 (5-C), 124.9 (3-C), 62.2 (3- $CO_2CH_2CH_3$), 14.2 (3- $CO_2CH_2CH_3$); (Found C, 43.8; H, 3.15; N, 6.3; $C_8H_7Cl_2NO_2$ requires C, 43.7; H, 3.20; N, 6.4%); ν_{max} / cm^{-1} (solid) 3091, 2977, 1732, 1570, 1538, 1448; m/z (ESI⁺) found MH^+ 219.9924, $C_8H_8Cl_2NO_2$ *MH* requires 219.9927; HPLC RT = 3.05 mins. Spectroscopic data consistent with literature values.¹²³

4-chloro-6-[(ethylcarbamoyl)amino]pyridine-3-carboxylate¹²³ **46**

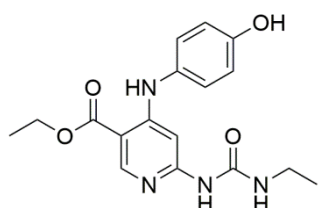


Palladium (II) acetate (203 mg, 0.908 mmol) was added to a solution of xantphos (653 mg, 1.14 mmol) in degassed, anhydrous 1,4-dioxane (20.0 ml) at room temperature. The mixture was stirred under nitrogen for 1 hour and treated with compound **45** (1.00 g, 4.54 mmol), *N*-ethylurea (359 mg, 4.08 mmol), potassium *tert*-butoxide (763 mg, 6.81 mmol) and degassed water (0.6 ml, 6.8 mmol). The mixture was heated under nitrogen to 80 °C for 2 hours and then cooled to room temperature, diluted with water (15 ml)

and extracted with EtOAc (3 × 20 ml). The combined organic extracts were then washed with brine (15 ml), dried with MgSO₄ and concentrated *in vacuo* to give the crude product as an orange solid. Purification of this solid using column chromatography (1:2 EtOAc–Petrol) afforded the title compound (460 mg, 1.69 mmol, 41%) as colourless crystals, m.p. 163.8-164.3 °C; *R*_f 0.29 (1:2 EtOAc–Petrol); δ_H (300 MHz, CDCl₃) 9.02 (br. s., 1 H, 6-NHCONHCH₂CH₃), 8.77 (s, 1 H, 5-H), 8.39 (s, 1 H 6-NHCONHCH₂CH₃), 6.88 (s, 1 H, 2-H), 4.40 (q, *J* 7.2 Hz, 2 H, 3-CO₂CH₂CH₃), 3.43 (qd, *J* 7.1, 5.5 Hz, 2 H, 6-NHCONHCH₂CH₃), 1.41 (t, *J* 7.2 Hz, 3 H, 3-CO₂CH₂CH₃), 1.26 (t, *J* 7.3 Hz, 3 H, 6-NHCONHCH₂CH₃); δ_C (75 MHz, CDCl₃) 163.6 (3-CO₂CH₂CH₃), 156.1 (6-NHCONHCH₂CH₃), 155.7 (2-C), 150.9 (6-C), 145.5 (4-C), 118.4 (5-C), 113.3 (3-C), 61.5 (3-CO₂CH₂CH₃), 34.9 (6-NHCONHCH₂CH₃), 15.2 (6-NHCONHCH₂CH₃), 14.2 (3-CO₂CH₂CH₃); (Found C, 48.9; H, 5.00; N, 14.7; C₁₁H₁₄ClN₃O₃ requires C, 48.6; H, 5.19; N, 15.5%); ν_{max} / cm⁻¹ (solid) 1688, 1549; *m/z* (ESI⁺) found MH⁺ 272.0789, C₁₁H₁₅ClN₃O₃ *MH* requires 272.0796; HPLC RT = 1.29 mins. Spectroscopic data consistent with literature values.¹²³

ethyl 6-[(ethylcarbamoyl)amino]-4-[(4-hydroxyphenyl)amino]pyridine-3-carboxylate

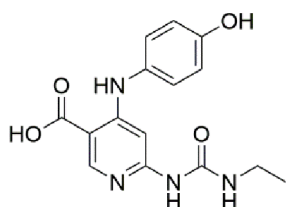
47



General method A using compound **46** (100 mg, 0.368 mmols) and 2-aminophenol (36 mg, 0.331 mmol). The reaction mixture was concentrated *in vacuo* to afford a yellow oil. Purification using column chromatography (EtOAc–Petrol–NEt₃ 1:1:0.001) afforded the title compound (54 mg, 0.16 mmol, 47%) as colourless microcrystals, m.p. 227.3-224.7 °C (from EtOH); *R*_f 0.48 (3:1 EtOAc–Petrol); δ_H (300MHz, DMSO-*d*₆) 9.54 (s, 1 H, 6-NHCONHCH₂CH₃), 9.35 (s, 1 H, OH), 9.06 (s, 1 H, 4-NH), 8.56 (s, 1 H, 2-H), 7.73 (br. s., 1 H, 6-NHCONHCH₂CH₃), 7.07 (d, *J* 8.6 Hz, 2 H, 4-phenyl 2-H), 6.95 (s, 1 H, 5-H), 6.81 (d, *J* 8.6 Hz, 2 H, 4-phenyl 3-H), 4.29 (q, *J* 7.1 Hz, 2 H, 3-CO₂CH₂CH₃), 3.10 (qd, *J* 7.2, 5.8 Hz, 2 H, 6-NHCONHCH₂CH₃), 1.32 (t, *J* 7.1 Hz, 3 H, 3-CO₂CH₂CH₃), 1.03 (t, *J* 7.2 Hz, 3 H, 6-NHCONHCH₂CH₃); δ_C (75 MHz, DMSO-*d*₆) 166.9 (3-CO₂CH₂CH₃), 160.5 (6-NHCONHCH₂CH₃), 155.3 (4-phenyl 4-C), 154.5 (6-C or 4-C), 154.1 (6-C or 4-C), 151.7 (2-C), 129.1 (4-phenyl 1-C), 126.3 (2-phenyl 2-C), 116.0 (4-phenyl 3-C), 102.6 (3-C), 90.9 (5-C), 60.3 (3-CO₂CH₂CH₃), 33.7 (6-

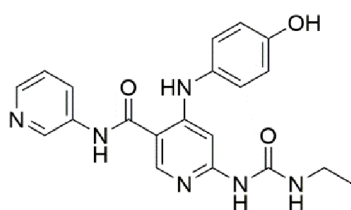
NHCONHCH₂CH₃), 15.2 (6-NHCONHCH₂CH₃), 14.1 (3-CO₂CH₂CH₃); ν_{\max} / cm⁻¹ (solid) 2973, 1687, 1562, 1513, 1487; m/z (ESI⁺) found MH⁺ 345.1562, C₁₇H₂₀N₄O₄ MH requires 345.1557; HPLC RT = 2.62 min.

6-[(ethylcarbamoyl)amino]-4-[(4-hydroxyphenyl)amino]pyridine-3-carboxylic acid **48**



Compound **47** (100 mg, 0.291 mmol) was dissolved in THF (3 ml) and NaOH_(aq) (2 M, 3 ml) was added. The reaction mixture was heated to 90 °C for 18 hours. The reaction was allowed to cool to room temperature and then THF was removed *in vacuo*. The resulting aqueous solution was acidified to pH4 by the dropwise addition of HCl (2 M). The resulting precipitate was collected by filtration to afford the title compound (86 mg, 0.27 mmol, 93%) as off-white microcrystals, m.p. > 250 °C; R_f 0.13 (1:9 MeOH–EtOAc); δ_H (300 MHz, DMSO-*d*₆) 12.82 (br. s., 1 H, 3-CO₂H), 9.57-9.90 (m, 2 H, 2 × NH or NH and OH), 9.19 (br. s., 1 H, NH or OH), 8.51 (s, 1 H, 2-H), 7.91 (br. s., 1 H, 6-NHCONHCH₂CH₃), 7.06 (d, J 8.8 Hz, 2 H, 4-phenyl 2-H), 6.93 (s, 1 H, 5-H), 6.83 (d, J 8.8 Hz, 2 H, 4-phenyl 3-H), 3.10 (qd, J 7.1, 6.0 Hz, 2 H, 6-NHCONHCH₂CH₃), 1.03 (t, J 7.1 Hz, 3 H, 6-NHCONHCH₂CH₃); δ_C (75 MHz, DMSO-*d*₆) 169.1 (3-CO₂H), 155.3 (6-C), 154.8 (4-phenyl 4-C), 154.3 (6-NHCONHCH₂CH₃), 151.4 (2-C), 129.2 (4-phenyl 1-C), 126.3 (4-C), 126.0 (4-phenyl 2-C), 116.0 (4-phenyl 3-C), 104.1 (3-C), 90.7 (5-C), 33.7 (6-NHCONHCH₂CH₃), 15.25 (6-NHCONHCH₂CH₃); ν_{\max} / cm⁻¹ (solid) 3135, 1661, 1597, 1554, 1519; m/z (ESI⁺) found MH⁺ 317.1230, C₁₅H₁₇N₄O₄ MH requires 317.1244; HPLC RT = 3.07 min, (92%).

6-[(ethylcarbamoyl)amino]-4-[(4-hydroxyphenyl)amino]-N-(pyridin-3-yl)pyridine-3-carboxamide **50**

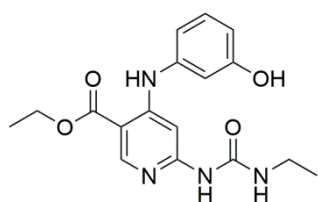


Compound **48** (60 mg, 0.18 mmol) was dissolved in DMF and HOBT·H₂O (35 mg, 0.29 mmol) and EDC (54 mg, 0.29 mmol) were added. The resulting mixture was stirred for 30 minutes and then 3-aminopyridine (20 mg, 0.21 mmol) was added. The reaction was stirred at room temperature for 16 hours and then

heated to 40 °C for 1 hour before being cooled to room temperature, diluted with water (10 ml) and extracted into EtOAc (3 × 10 ml). The combined organic extracts were washed with NaHCO₃ (10 ml), water (10 ml) and brine (10 ml), dried over MgSO₄ and concentrated *in vacuo* to give an orange oil. Purification of this oil using column chromatography (1:9 MeOH–EtOAc) afforded a pale yellow oil. Recrystallisation from MeOH afforded the title compound (9.4 mg, 0.024 mmol, 13%) as colourless crystals, m.p. 110.1-114.4 °C (from MeOH); *R_f* 0.45 (EtOAc); δ_H (300 MHz, MeOD) 8.85-8.90 (m, 1 H, 3-pyridyl 2-*H*), 8.53 (s, 1 H, 2-*H*), 8.29 (d, *J* 4.9, 1 H, 3-pyridyl 6-*H*), 8.22 (d, *J* 8.5, 1 H, 3-pyridyl 4-*H*), 7.42 (dd, *J* 8.1, 4.5 Hz, 1 H, 3-pyridyl 5-*H*), 7.08 (d, *J* 8.8 Hz, 2 H, 4-phenyl 2-*H*), 6.85 (d, *J* 8.8 Hz, 2 H, 4-phenyl 3-*H*), 6.55 (s, 1 H, 5-*H*), 3.28 (q, *J* 6.9 Hz, 3 H, 6-NHCONHCH₂CH₃), 1.18 (t, *J* 7.3 Hz, 3 H, 6-NHCONHCH₂CH₃); δ_C (125 MHz, DMSO-*d*₆) 166.9 (3-CONH), 155.8 (4-phenyl 4-C), 154.9 (4-C, 6-C or 6-NHCONHCH₂CH₃), 154.2 (4-C, 6-C or 6-NHCONHCH₂CH₃), 153.8 (4-C, 6-C or 6-NHCONHCH₂CH₃), 149.0 (2-C), 144.5 (3-pyridyl 6-C), 142.3 (3-pyridyl 2-C), 135.5 (3-pyridyl 3-C), 129.5 (4-phenyl 1-C), 127.7 (3-pyridyl 4-C), 125.7 (4-phenyl 2-C), 123.5 (3-pyridyl 5-C), 115.9 (4-phenyl 3-C), 106.9 (3-C), 91.2 (5-C), 33.7 (6-NHCONHCH₂CH₃), 15.3 (6-NHCONHCH₂CH₃); ν_{max} / cm⁻¹ (solid) 3324, 2963, 2854, 1638, 1560, 1488; *m/z* (ESI⁺) found MH⁺ 393.1668, C₂₀H₂₁N₆O₃ *MH* requires 393.1670; HPLC RT = 1.29.

ethyl 6-[(ethylcarbamoyl)amino]-4-[(3-hydroxyphenyl)amino]pyridine-3-carboxylate

51

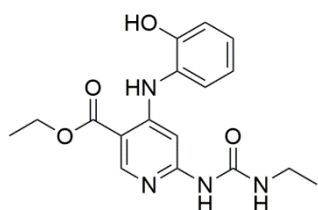


General method A using compound **46** (250 mg, 0.919 mmols) and 3-aminophenol (100 mg, 0.919 mmol) afforded the title compound (184 mg, 0.534 mmol, 58%) as colourless crystals, m.p. 185.1-188.7 °C; *R_f* 0.45 (3:1 EtOAc–Petrol); δ_H (300 MHz, DMSO-*d*₆) 9.64 (s, 1 H, 6-NHCONHCH₂CH₃), 9.56 (s, 1 H, 4-NH), 9.19 (br. s., 1 H, OH), 8.60 (s, 1 H, 2-*H*), 7.75 (br. s., 1 H, 6-NHCONHCH₂CH₃), 7.27 (s, 1 H, 4-phenyl 2-*H*), 7.21 (t, *J* 8.0 Hz, 1 H, 4-phenyl 5-*H*), 6.71 (d, *J* 7.7 Hz, 1 H, 4-phenyl 6-*H*), 6.66 (s, 1 H, 5-*H*), 6.62 (d, *J* 8.2 Hz, 1 H, 4-phenyl 4-*H*), 4.30 (q, *J* 7.1 Hz, 2 H, 3-CO₂CH₂CH₃), 3.12 (dq, *J* 7.3, 6.0 Hz, 2 H, 6-NHCONHCH₂CH₃), 1.33 (t, *J* 7.0 Hz, 3 H, 3-CO₂CH₂CH₃), 1.05 (t, *J* 7.1 Hz, 3 H, 6-NHCONHCH₂CH₃); δ_C (75 MHz, DMSO-*d*₆) 166.9 (3-CO₂CH₂CH₃), 158.3 (6-

NHCONHCH₂CH₃), 154.1 (4-phenyl 3-C), 152.9 (2-C), 139.3 (4-phenyl 1-C), 130.2 (4-phenyl 5-C), 113.7 (4-phenyl 6-C), 112.1 (4-phenyl 4-C), 110.0 (4-C), 103.1 (4-phenyl 2-C), 91.5 (2-C), 60.4 (3-CO₂CH₂CH₃), 33.8 (6-NHCONHCH₂CH₃), 15.2 (6-NHCONHCH₂CH₃), 14.1 (3-CO₂CH₂CH₃), 3-C and 6-C not resolved; ν_{\max} / cm⁻¹ (solid) 3269, 1688, 1583, 1489, 764, 751, 692; m/z (ESI⁺) found MH⁺ 345.1571, C₁₇H₂₀N₄O₄ MH⁺ requires 345.1557; HPLC RT = 2.00 mins.

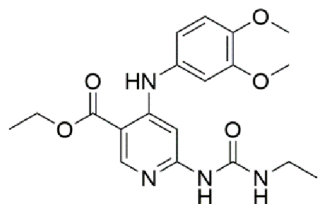
ethyl 6-[(ethylcarbamoyl)amino]-4-[(2-hydroxyphenyl)amino]pyridine-3-carboxylate

52



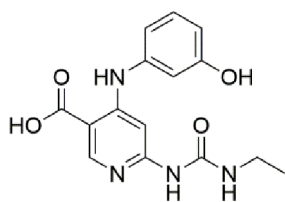
General method A using compound **46** (100 mg, 0.368 mmols) and 2-aminophenol (36 mg, 0.33 mmol) afforded an off-white solid. The material was purified using column chromatography (1:1 EtOAc–Petrol) to afford the title compound (156 mg, 0.455, 50%) as colourless crystals, m.p. 206.7–209.7 °C; R_f 0.52 (3:1 EtOAc–Petrol); δ_H (300 MHz, DMSO-*d*₆) 10.19 (br. s, 1 H, 6-NHCONHCH₂CH₃), 9.99 (br. s, 1 H, 4-NH), 8.61 (s, 1 H, 2-H), 7.36 (br. s, 1 H, OH), 7.31 (dd, J 8.0, 1.4 Hz, 1 H, 4-phenyl 6-H), 7.18 (t, J 7.0 Hz, 1 H, 4-phenyl 4-H), 7.04 (dd, J 8.2, 0.8 Hz, 1 H, 4-phenyl 3-H), 6.91 (td, J 8.2, 0.8 Hz, 1 H, 4-phenyl 5-H), 6.57 (br. s, 1 H, 6-NHCONHCH₂CH₃), 4.37 (q, J 6.9 Hz, 2 H, 3-CO₂CH₂CH₃), 3.15 (qd, J 7.4, 5.8 Hz, 2 H, 6-NHCONHCH₂CH₃), 1.35 (t, J 7.1 Hz, 3 H, 3-CO₂CH₂CH₃), 1.06 (t, J 7.1 Hz, 3 H, 6-NHCONHCH₂CH₃); δ_C (125 MHz, DMSO-*d*₆) 164.9 (3-CO₂CH₂CH₃), 154.7 (6-NHCONHCH₂CH₃), 154.0 (6-C), 151.2 (2-C), 150.1 (4-phenyl 2-C), 143.7 (4-C), 127.9 (4-phenyl 1-C), 125.1 (4-phenyl 4-C), 123.8 (4-phenyl 5-C), 119.4 (4-phenyl 6-C), 116.6 (4-phenyl 3-C), 104.8 (3-C), 91.5 (5-C), 61.7 (3-CO₂CH₂CH₃), 34.1 (6-NHCONHCH₂CH₃), 14.9 (6-NHCONHCH₂CH₃), 14.0 (3-CO₂CH₂CH₃); ν_{\max} / cm⁻¹ (solid) 2925, 2854, 1705, 1651, 1544; m/z (ESI⁺) found MH⁺ 345.1558, C₁₇H₂₀N₄O₄ MH requires 345.1557; HPLC RT = 2.04 min.

ethyl 4-[(3,4-dimethoxyphenyl)amino]-6-[(ethylcarbamoyl)amino]pyridine-3-carboxylate 53



General method A using compound **46** (100 mg, 0.368 mmol) and 4-aminobenzoic acid (73 mg, 0.33 mmol) afforded the title compound (264 mg, 0.680 mmol, 82%) as colourless microcrystals, m.p. 206.4-207.3 °C; R_f 0.10 (1:2 EtOAc–Petrol); δ_H (300 MHz, DMSO- d_6) 9.52 (s, 1 H, 4-NH), 9.24 (br. s., 1 H, 6-NHCONHCH₂CH₃), 8.60 (s, 1 H, 2-H), 7.79 (br. s., 1 H, 6-NHCONHCH₂CH₃), 7.15 (s, 1 H, 5-H), 7.01 (d, J 8.7 Hz, 2 H, 4-phenyl 6-H), 6.94 (d, J 2.5 Hz, 1 H, 4-phenyl 2-H), 6.82 (dd, J 8.7, 2.5 Hz, 1 H, 4-phenyl 5-H), 4.32 (q, J 7.0 Hz, 2 H, 3-CO₂CH₂CH₃), 3.79 (m, 6 H, OCH₃), 3.12 (qd, J 7.1, 5.3 Hz, 2 H, 6-NHCONHCH₂CH₃), 1.34 (t, J 7.0 Hz, 3 H, 3-CO₂CH₂CH₃), 1.05 (t, J 7.1 Hz, 3 H, 6-NHCONHCH₂CH₃); δ_C (125 MHz, DMSO- d_6) 166.1 (3-CO₂CH₂CH₃), 154.4 (6-NHCONHCH₂CH₃ or 6-C), 154.2 (6-NHCONHCH₂CH₃ or 6-C), 149.3 (2-C), 147.0 (4-phenyl 3-C), 130.5 (4-phenyl 4-C), 116.4 (4-phenyl 5-C), 112.3 (4-phenyl 6-C), 108.9 (4-phenyl 2-C), 103.5 (3-C), 91.2 (5-C), 60.9 (3-CO₂CH₂CH₃), 55.7 (OCH₃), 55.6 (OCH₃), 33.9 (6-NHCONHCH₂CH₃), 15.1 (5-NHCONHCH₂CH₃), 14.1 (3-CO₂CH₂CH₃) 4-C and 4-phenyl 1-C not resolved; ν_{max} / cm⁻¹ (solid) 2925, 2854, 1704, 1650, 1588, 1546; m/z (ESI⁺) found MH⁺ 389.1833, C₁₉H₂₅N₄O₅ MH requires 389.1820; HPLC RT = 2.49 min.

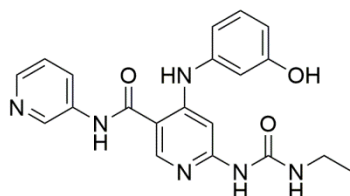
6-[(ethylcarbamoyl)amino]-4-[(3-hydroxyphenyl)amino]pyridine-3-carboxylic acid 54



Compound **51** (177 mg, 0.515 mmol) was dissolved in THF (2 ml) and NaOH_(aq) (2 M, 2 ml) was added. The reaction mixture was heated to 80 °C for 18 hours and then cooled to 0 °C. The reaction mixture was acidified to pH 4 by the dropwise addition of HCl (2 M). The resulting precipitate was collected by filtration to afford the title compound (23 mg, 0.071 mmol, 93%) as dark red microcrystals, m.p. 248.8-250.3 °C; R_f 0.13 (1:9 MeOH–EtOAc); δ_H (300 MHz, DMSO- d_6) 9.87 (br. s., 1 H, 6-NHCONHCH₂CH₃), 9.62 (s, 1 H, 2-H), 9.13 (br. s., 1H, 4-NH), 8.57 (s, 1 H, 5-H), 7.84 (br. s., 1 H, OH), 7.25 (s, 1 H, 4-phenyl 2-H), 7.20 (t, J 8.2 Hz, 1 H, 4-phenyl 5-H), 6.70 (d, J

8.2 Hz, 1 H, 4-phenyl 2-H), 6.65 (br. s, 1 H, 6-NHCONHCH₂CH₃), 6.60 (d, *J* 8.2 Hz, 1 H, 4-phenyl 4-H), 3.13 (qd, *J* 7.1, 5.8 Hz, 2 H, 6-NHCONHCH₂CH₃), 1.05 (t, *J* 7.1 Hz, 3 H, 6-NHCONHCH₂CH₃); δ_c 168.7 (3-CO₂H), 158.4 (6-NHCONHCH₂CH₃), 154.2 (2-C), 153.6 (4-phenyl 3-C), 139.2 (4-phenyl 1-C) 130.3 (4-phenyl 5-C), 113.8 (3-C), 112.4 (4-phenyl 6-C), 110.2 (4-phenyl 6-C), 104.1 (4-phenyl 2-C), 91.5 (5-C), 33.9 (6-NHCONHCH₂CH₃), 15.2 (6-NHCONHCH₂CH₃); ν_{\max} / cm⁻¹ (solid) 2973.1, 2882.9, 1703.7, 1667.2, 1584.3, 1542.7; *m/z* (ESI⁺) found MH⁺ 317.1255, C₁₅H₁₆N₄O₄ *MH* requires 317.1244; HPLC RT = 2.58 mins.

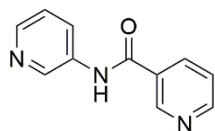
6-[(ethylcarbamoyl)amino]-4-[(3-hydroxyphenyl)amino]-N-(pyridin-3-yl)pyridine-3-carboxamide 57



Compound **67** (50 mg, 0.157 mmol) and 3-hydroxyaniline (17 mg, 0.157 mmol) were suspended in EtOH and cHCl (1 drop) was added. The reaction was heated to 80 °C for 16 hours before being cooled to 0 °C and neutralised to pH 7 by careful addition of aqueous NaOH (2M). The reaction mixture was concentrated *in vacuo* and the resulting orange solid washed with water and dried under the air. Recrystallisation from EtOH afforded the title compound (20 mg, 0.051 mmol, 32%) as pale orange microcrystals. m.p. 238.2-242.1 (EtOH); *R_f* 0.03 (EtOAc); δ_H (500 MHz, DMSO-*d*₆) 10.45 (s, 1 H, 6-NHCONHCH₂CH₃), 9.79 (s, 1 H, 3-CONH), 9.57 (s, 1 H, 4-NH), 8.88 (s, 1 H, 3-pyridyl 2-H), 8.62 (s, 1 H, 2-H), 8.33 (d, *J* 4.3 Hz, 1 H, 3-pyridyl 6-H), 8.13 (d, *J* 8.1 Hz, 1 H, 3-pyridyl 4-H), 7.97 (br. s., 1 H, 4-phenyl-OH), 7.41 (dd, *J* 8.1 and 4.3 Hz, 1 H, 3-pyridyl 5-H), 7.30 (s, 1 H, 5-H), 7.20 (t, *J* 7.8 Hz, 1 H, 4-phenyl 5-H), 6.71 (d, *J* 7.8 Hz, 1 H, 4-phenyl 6-H), 6.67 (s, 1 H, 4-phenyl 2-H), 6.59 (d, *J* 7.8 Hz, 1 H, 4-phenyl 4-H), 4.35 (t, *J* 4.6 Hz, 1 H, 6-NHCONHCH₂CH₃), 4.36 (qd, *J* 4.6 and 7.1 Hz, 2 H, 6-NHCONHCH₂CH₃), 1.07 (t, *J* 7.1 Hz, 3 H, 6-NHCONHCH₂CH₃); δ_c (125 MHz, DMSO-*d*₆) 166.9 (3-CONH), 158.3 (6-NHCONHCH₂CH₃), 155.9 (4-phenyl 3-C), 154.3 (6-C), 152.2 (4-C), 149.1 (5-C), 144.7 (3-pyridyl 2-C), 142.3 (3-pyridyl 6-C), 139.9 (3-pyridyl 3-C), 135.4 (4-phenyl 1-C), 130.2 (4-phenyl 5-C), 127.8 (3-pyridyl 4-C), 123.5 (3-pyridyl 5-C), 113.0 (4-phenyl 6-C), 111.5 (4-phenyl 4-C), 109.3 (4-phenyl 2-C), 107.7 (3-C), 92.3 (2-C), 33.8 (6-NHCONHCH₂CH₃), 15.3 (6-NHCONHCH₂CH₃); ν_{\max} / cm⁻¹ (solid) 3414, 1731, 1628 and

1509; m/z (ESI⁺) found MH⁺ 393.1676, C₂₀H₂₀N₆O₃ MH requires 393.1670; HPLC RT = 1.34 min.

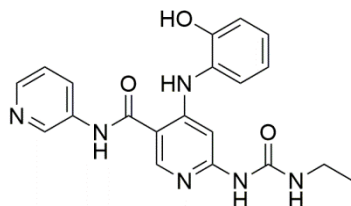
N-(pyridin-3-yl)nicotinamide 59



Either: General method C using nicotinic acid (100 mg, 0.813 mmol) and 3-aminopyridine (84 mg, 0.89 mmol) afforded the title compound (115 mg, 0.578 mmol, 71%) as colourless microcrystals.

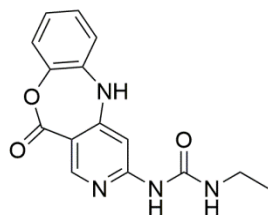
Or: Nicotinic acid (100 mg, 0.813 mmol) was dissolved in DMF (5 ml) and HOBT.H₂O (165 mg, 1.22 mmol) and EDC (233 mg, 1.22 mmol) were added. The resulting solution was stirred for 20 minutes and then 3-aminopyridine (84 mg, 0.89 mmol) was added. The reaction mixture was stirred at room temperature overnight. The reaction mixture was then diluted with water (5 ml), extracted with EtOAc (3 × 10 ml) and the combined organic extracts were washed with NaHCO₃ (10 ml), water (10 ml) and brine (10 ml), dried over MgSO₄ and concentrated *in vacuo* to give a tan gum. Purification of this gum using column chromatography (1:1 EtOAc–Petrol) afforded the title compound (10 mg, 0.050 mmol, 12%) as colourless microcrystals, m.p. 192.9–193.5 °C; R_f 0.29 (1:1 EtOAc–Pet); δ_H (300 MHz, DMSO-*d*₆) 10.67 (s, 1 H, 3-CONH), 9.13 (dd, J 2.2, 0.8 Hz, 1 H, 6-H), 8.94 (d, J 2.2 Hz, 1 H, 3-pyridyl 5-H), 8.79 (dd, J 4.7, 1.6 Hz, 1 H, 2-H), 8.28–8.39 (m, 2 H, 4-H and 3-pyridyl 6-H), 8.20 (ddd, J 8.2, 2.5, 1.6 Hz, 1 H, 3-pyridyl 4-H), 7.60 (ddd, J 8.1, 4.8, 0.8 Hz, 1 H, 5-H), 7.43 (dd, J 8.2, 4.7 Hz, 1 H, 3-pyridyl 5-H); δ_C (75 MHz, MeOD-*d*₄) 166.7 (3-CONH), 153.8 (6-C), 149.6 (2-C), 145.9 (3-pyridyl 6-C), 142.9 (3-pyridyl 5-C), 137.5 (4-C or 3-pyridyl 3-C), 137.4 (4-C or 3-pyridyl 3-C), 132.2 (3-C), 130.1 (3-pyridyl 4-C), 125.4 (5-C), 125.3 (3-pyridyl 5-C); (Found C, 66.2; H, 4.45; N, 20.7; C₁₁H₉N₃O requires C, 66.3; H, 4.55; N, 21.1%); ν_{max} / cm⁻¹ (solid) 1679, 1588, 1548; m/z (ESI⁺) found MH⁺ 200.0819, C₁₁H₁₀N₃O MH requires 200.0818; HPLC RT = 0.663 mins. Spectroscopic data consistent with literature values.¹⁵⁹

6-[(ethylcarbamoyl)amino]-4-[(2-hydroxyphenyl)amino]-N-(pyridin-3-yl)pyridine-3-carboxamide 61



Compound **67** (30 mg, 0.09 mmol) and 2-hydroxyaniline (30 mg, 0.09 mmol) were dissolved in ethanol (2 ml) and NEt_3 (5 drops) was added. The reaction was heated to 80 °C for 3 hours. The reaction was then allowed to cool to room temperature and the solvent removed *in vacuo*. The resulting off white residue was taken up in EtOAc (10 ml), washed with water (3 × 10 ml) and brine (10 ml), the volume reduced *in vacuo* and the product collected by filtration to afford the title compound (7.5 mg, 0.191 mmol, 21%) as pale red microcrystals, R_f 0.03 (EtOAc); δ_H (500 MHz, $\text{DMSO-}d_6$) 10.43 (br. s., 1 H, 3-CONH), 9.85 (s, 1 H, 6-NHCONHCH₂CH₃), 9.77 (s, 1 H, 4-NH), 9.14 (s, 1 H, 4-phenyl 6-H), 8.88 (s, 1 H, 3-pyridyl 2-H), 8.61 (s, 1 H, 2-H), 8.33 (d, 1 H, J 4.6 Hz, 3-pyridyl 6-H), 8.14 (d, J 7.8 Hz, 1 H, 3-pyridyl 4-H), 8.00 (br. s., 1 H, 4-phenyl OH), 7.41 (dd, J 8.5, 4.8 Hz, 1 H, 3-pyridyl 5-H), 7.32 (d, J 7.8 Hz, 1 H, 4-phenyl 3-H), 7.23 (s, 1 H, 5-H), 6.91 - 7.03 (m overlapping, 2 H, 4-phenyl 4-H and 5-H), 6.86 (t, J 6.9 Hz, 1 H, 6-NHCONHCH₂CH₃), 3.17 (qd, J 7.1, 6.9 Hz, 2 H, 6-NHCONHCH₂CH₃), 1.09 (t, J 7.1 Hz, 3 H, 6-NHCONHCH₂CH₃); δ_C (500 MHz, $\text{DMSO-}d_6$) 166.9 (3-CONH), 155.9 (4-phenyl 2-C), 154.4 (6-C), 152.1 (4-C), 149.6 (6-NHCONHCH₂CH₃), 149.0 (5-C), 144.6 (3-pyridyl 2-C), 142.2 (3-pyridyl 6-C), 127.7 (3-pyridyl 4-C), 126.5 (4-phenyl 1-C), 124.7 (4-phenyl 4-C), 123.5 (3-pyridyl 5-C), 122.1 (4-phenyl 5-C), 119.2 (4-phenyl 6-C), 115.8 (4-phenyl 3-C), 108.0 (3-C), 92.0 (2-C), 33.8 (6-NHCONHCH₂CH₃), 15.3 (6-NHCONHCH₂CH₃); $\nu_{\text{max}} / \text{cm}^{-1}$ (solid) 2969, 2811, 1698, 1642, 1543, 1517; m/z (ESI⁺) found MH^+ 393.1673, $\text{C}_{20}\text{H}_{20}\text{N}_6\text{O}_3$ MH requires 393.1670; HPLC RT = 1.38 mins.

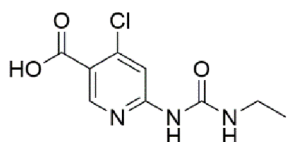
3-ethyl-1-{9-oxo-10-oxa-2,6-diazatricyclo[9.4.0.0^{3,8}]pentadeca-1(15),3(8),4,6,11,13-hexaen-5-yl}urea 62



Compound **52** (150 mg, 0.436 mmol) was suspended in THF (2.5 ml) and NaOH_(aq) (2 M, 2 ml) was added. The reaction mixture was heated to 80 °C for 18 hours and then cooled to 0 °C. The reaction mixture was acidified to pH4 by the dropwise addition of HCl (2 M). The resulting precipitate was collected by filtration to afford 6-[(ethylcarbamoyl) amino]-4-[(2-hydroxyphenyl) amino] pyridine-3-carboxylic acid (25 mg, 0.078 mmol, 90%) as a dark red solid. δ_{H} (300 MHz, DMSO-*d*₆) 9.99 (br. s., 1 H, 6-NHCONHCH₂CH₃), 8.57 (s, 1 H, 2-H), 7.70 (br. s., 1 H, 4-NH), 7.58 (br. s., 1 H, 6-NHCONHCH₂CH₃), 7.32 (d, *J* 6.3 Hz, 1 H, 4-phenyl 6-H), 7.16 (t, 1 H, 4-phenyl 4-H), 7.09-6.84 (m, 4 H, 5-H, 4-phenyl 3-H, 5-H, OH), 3.15 (qd, *J* 6.9, 5.8 Hz, 2 H, 6-NHCONHCH₂CH₃), 1.05 (t, *J* 7.3 Hz, 3 H, 6-NHCONHCH₂CH₃). ¹H NMR indicated that the material was sufficiently pure and the material was carried through to the next step without further analysis. General method C using 6-[(ethylcarbamoyl)amino]-4-[(2-hydroxyphenyl) amino]pyridine-3-carboxylic acid (110 mg, 0.348 mmol) and 3-amino pyridine (36 mg, 0.38 mmol) After 16 hours, a further 5 equivalents of T3P (1 ml) was added and to the reaction mixture and the reaction mixture was stirred for a further 48 hours. After this time no starting material was observed using TLC. The reaction mixture was basified to pH 11 by careful addition of aqueous NaOH (1 M) and stirred for 20 minutes during which time a precipitate formed. The precipitate was collected using filtration and washed with water to afford the title compound (56 mg, 0.19 mmol, 56%) as yellow microcrystals, m.p. >250 °C; *R*_f 0.28 (1:1 EtOAc–Pet); δ_{H} (300 MHz, DMSO-*d*₆) 9.65 (s, 1 H, 6-NHCONHCH₂CH₃), 9.35 (s, 1 H, 4-NH), 8.63 (s, 1 H, 2-H), 7.41 (s, 1 H, 5-H), 7.27 (t, *J* 5.9 Hz, 1 H, 6-NHCONHCH₂CH₃), 7.07-7.21 (m, 4 H, ArH), 3.16 (qd, *J* 7.0, 5.9 Hz, 2 H, 6-NHCONHCH₂CH₃), 1.08 (t, *J* 7.0 Hz, 3 H, 6-NHCONHCH₂CH₃); (75 MHz, DMSO-*d*₆) δ_{C} 163.9 (6-NHCONHCH₂CH₃), 156.6 (2-C), 156.0 (3-CO₂), 154.6 (4-C or 6-C), 154.0 (4-C or 6-C), 141.3 (4-phenyl 2-C), 134.5 (4-phenyl 1-C), 126.2 (4-phenyl 4-C or 4-phenyl 5-C), 124.6 (4-phenyl 4-C or 4-phenyl 5-C), 122.2 (4-phenyl 3-C or 4-phenyl 6-C), 120.35 (4-phenyl 3-C or 4-phenyl 6-C), 105.5 (3-C), 96.2 (5-C), 33.9 (6-NHCONHCH₂CH₃), 15.2 (6-NHCONHCH₂CH₃); ν_{max} / cm⁻¹ (solid) 3107, 1696,

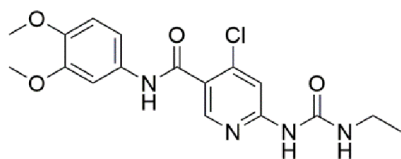
1571, 1513; m/z (ESI⁺) found MH⁺ 299.1146, C₁₅H₁₅N₄O₃ requires 299.1139; HPLC RT = 3.14 mins.

4-chloro-6-[(ethylcarbamoyl)amino]pyridine-3-carboxylic acid¹²³ **63**



Compound **46** (700 mg, 2.57 mmol) was suspended in NaOH (2 M, 30 ml) and heated to 80 °C for 16 hours. The reaction mixture was then cooled to 0 °C and acidified to pH 4 by dropwise addition of HCl. The resulting precipitate was collected using filtration, washed with water and dried under air to afford the title compound (516 mg, 2.12 mmol, 83%) as pale yellow microcrystals, R_f 0.05 (1:9 MeOH–EtOAc); δ_H (300 MHz, DMSO-*d*₆) 9.60 (1H, br. s., 6-NHCONHCH₂CH₃), 8.63 (s, 1 H, 2-H), 7.72 (s, 1 H, 5-H), 7.44 (t, J 5.2 Hz, 1 H, 6-NHCONHCH₂CH₃), 3.12 (qd, J 7.1 and 5.2 Hz, 2 H, 6-NHCONHCH₂CH₃), 1.03 (t, J 7.1 Hz, 3 H, 6-NHCONHCH₂CH₃); δ_C (75 MHz, DMSO-*d*₆) 164.6 (3-CO₂H), 155.9 (6-NHCONHCH₂CH₃), 153.9 (6-C), 151.4 (2-C), 143.9 (4-C), 111.8 (5-C), 102.6 (3-C), 33.9 (6-NHCONHCH₂CH₃), 15.1 (6-NHCONHCH₂CH₃); ν_{max} / cm⁻¹ (solid) 2927, 1698, 1586, 1542; m/z (ESI⁺) found MH⁺ 244.0483, C₉H₁₁ClN₃O₃ *MH* requires 244.0483; HPLC RT = 1.38 min. Spectroscopic data consistent with literature values.¹²³

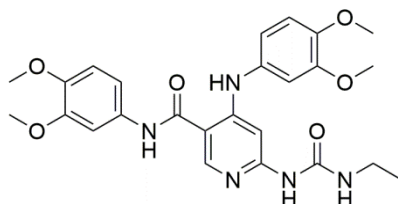
4-chloro-N-(3,4-dimethoxyphenyl)-6-[(ethylcarbamoyl)amino]pyridine-3-carboxamide **65**



General method C using compound **63** (100 mg, 0.411 mmol) and 3,4-dimethoxyaniline (138 mg, 0.905 mmol) afford the title compound (89 mg, 0.24, 57%) as off-white microcrystals, m.p. >250 °C; R_f 0.19 (1:1 EtOAc–Pet); δ^H (300 MHz, DMSO-*d*₆) 10.35 (br. s, 1 H, 3-CONH), 9.57 (br. s, 1 H, 6-NHCONHCH₂CH₃), 8.40 (s, 1 H, 2-H), 7.79 (s, 1 H, 5-H), 7.42 (d, J 2.4 Hz, 1 H, 3-phenyl 2-H), 7.23 (dd, J 8.6, 2.5 Hz, 1 H, 3-phenyl 6-H), 6.93 (d, J 8.6 Hz, 1 H, 3-phenyl 5-H), 3.75 (s, 3 H, 3-phenyl 3-OCH₃), 3.74 (s, 3 H, 3-phenyl 4-OCH₃), 3.18 (q, J 7.2 Hz, 2 H, 6-NHCONHCH₂CH₃), 1.09 (t, J 7.2 Hz, 3 H, 6-NHCONHCH₂CH₃); δ_C (75 MHz, DMSO-*d*₆) 162.6 (6-C), 155.0 (3-CONH), 148.5 (5-phenyl 3-C), 147.3 (2-C), 145.3 (5-phenyl 4-C), 142.1 (4-C), 132.4 (5-phenyl 1-C), 125.8

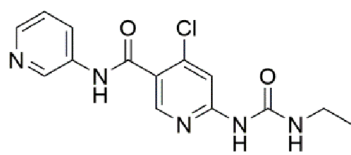
(C-3), 112.0 (3-phenyl 5-C), 111.4 (3-phenyl 6-C), 111.0 (5-C), 104.5 (3-phenyl 2-C), 55.7 (3-phenyl 3-OCH₃ or 4-OCH₃), 55.4 (3-phenyl 3-OCH₃ or 4-OCH₃), 33.8 (6-NHCONHCH₂CH₃), 15.12 (6-NHCONHCH₂CH₃); ν_{\max} / cm⁻¹ (solid) 3266, 1691, 1642, 1538; m/z (ESI⁺) found MH⁺ 379.1171, C₁₇H₂₄ClN₄O₄ MH requires 379.1168; HPLC RT = 2.05 mins.

N-(3,4-dimethoxyphenyl)-4-[(3,4-dimethoxyphenyl)amino]-6-[(ethylcarbamoyl)amino]pyridine-3-carboxamide 66

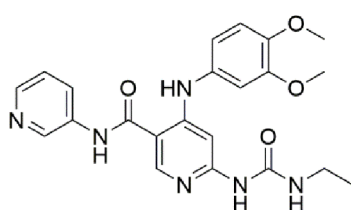


General method A using compound **65** (66 mg, 0.18 mmol) and 3,4-dimethoxyaniline (29 mg, 0.19 mmol) afforded the title compound (40 mg, 0.080 mmol, 46%) as pale pink microcrystals, m.p. 224.9-227.2 °C;

R_f 0.16 (1:1 EtOAc–Pet); δ_H (500 MHz, DMSO-*d*₆) 10.09 (s, 1 H, 4-NH), 9.82 (br. s., 1 H, 6-NHCONHCH₂CH₃), 9.06 (s, 1 H, 3-CONH), 8.53 (s, 1 H, 2-H), 8.06 (br. s, 1 H, 6-NHCONHCH₂CH₃), 7.39 (d, J 2.6 Hz, 1 H 3-phenyl 2-H), 7.25 (dd, J 8.5, 2.1 Hz, 1 H, 3-phenyl 5-H), 7.10 (s, 1 H, 5-H), 6.96 (d, J 8.5 Hz, 1 H, 3-phenyl or 4-phenyl 6-H), 6.91 (d, J 8.5 Hz, 1 H, 3-phenyl or 4-phenyl 6-H), 6.88 (d, J 2.6 Hz, 1 H, 4-phenyl 2-H), 6.76 (dd, J 8.5, 2.6 Hz, 1 H, 4-phenyl 5-H), 3.77 (s, 3 H, OCH₃), 3.76 (s, 3 H, OCH₃), 3.74 (s, 3 H, OCH₃), 3.73 (s, 3 H, OCH₃), 3.14 (qd, J 7.3, 6.0, 2 H, 6-NHCONHCH₂CH₃), 1.06 (t, J 7.3 Hz, 3 H, 6-NHCONHCH₂CH₃); δ_C (125 MHz, DMSO-*d*₆) 166.2 (3-CONH), 155.6 (6-NHCONHCH₂CH₃), 154.4 (6-C), 149.2 (2-C), 148.5 (3-phenyl or 4-phenyl 4-C), 148.4 (3-phenyl or 4-phenyl 4-C), 145.9 (4-C), 145.3 (4-phenyl 1-C), 114.9 (4-phenyl 5-C), 112.7 (4-phenyl 2-C), 112.4 (3-phenyl 5-C), 111.8 (3-phenyl or 4-phenyl 6-C), 107.8 (3-phenyl or 4-phenyl 6-C), 105.9 (3-C), 91.5 (5-C), 55.7 (OCH₃), 55.6 (OCH₃), 55.4 (OCH₃), 55.3 (OCH₃), 33.6 (6-NHCONHCH₂CH₃), 15.3 (6-NHCONHCH₂CH₃); ν_{\max} / cm⁻¹ (solid) 3287, 1686, 1633, 1582, 1509; m/z (ESI⁺) found MNa⁺ 518.2016, C₂₅H₂₉N₅O₆ MNa requires 518.2010; HPLC RT = 2.21 min.

4-chloro-6-[(ethylcarbamoyl)amino]-N-(pyridin-3-yl)pyridine-3-carboxamide 67

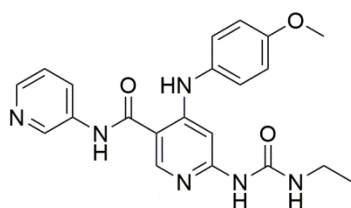
Compound **63** (100 mg, 0.411 mmol) and 3-amino pyridine (85 mg, 0.91 mmol) were dissolved in EtOAc (1 ml), and pyridine (0.1 ml) and T3P (1 ml, 1.64 mmol, 50% solution in EtOAc) were added. The reaction mixture was stirred at room temperature for 18 hours and then basified to pH 10 by addition of aqueous NaOH (2M). The mixture was then stirred for 20 minutes and the product collected by filtration to afford the title compound (45 mg, 0.14 mmol, 34%) as pale orange microcrystals, m.p. 210.4-215.6 °C; R_f 0.24 (1:1 EtOAc–Pet); δ_H (300 MHz, DMSO- d_6) 10.74 (s, 1 H, 4-NH), 9.57 (s, 1 H, 6-NHCONHCH₂CH₃), 8.84 (d, J 2.2 Hz, 1 H, 3-pyridyl 2-H), 8.47 (s, 1 H, 2-H), 8.33 (d, 1 H, J 3.8 Hz, 3-pyridyl 6-H), 8.15 (d, J 8.8 Hz, 1 H, 3-pyridyl 4-H), 7.80 (s, 1 H, 5-H), 7.31-7.50 (m, 2 H, 3-pyridyl 5-H and 6-NHCONHCH₂CH₃), 3.18 (qd, J 7.2 and 5.5 Hz, 2 H, 6-NHCONHCH₂CH₃), 1.09 (t, J 7.2 Hz, 3 H, 6-NHCONHCH₂CH₃); δ_C (125 MHz DMSO- d_6) 163.1 (3-CONH), 155.0 (6-C), 154.0 (6-NHCONHCH₂CH₃), 148.0 (2-C), 144.8 (3-pyridyl 6-C), 141.6 (3-pyridyl 2-C), 141.2 (3-pyridyl 3-C), 135.5 (4-C), 126.5 (3-pyridyl 4-C), 124.8 (3-C), 123.7 (3-pyridyl 5-C), 111.2 (5-C), 33.9 (6-NHCONHCH₂CH₃), 15.2 (6-NHCONHCH₂CH₃); ν_{max} / cm⁻¹ (solid) 3179, 1669, 1548; m/z (ES⁺) found MH⁺ 320.0912 C₁₄H₁₄ClN₅O₂ MH requires 320.0909; HPLC RT = 0.99 mins.

4-[(3,4-dimethoxyphenyl)amino]-6-[(ethylcarbamoyl)amino]-N-(pyridin-3-yl)pyridine-3-carboxamide 68

General method A using compound **67** (40 mg, 0.13 mmol) and 3,4-dimethoxyaniline (19 mg, 0.13 mmol) afforded the title compound (29 mg, 0.066 mmol, 53%) as pale pink microcrystals, m.p. >250 °C; R_f 0.13 (1:1 EtOAc–Pet); δ_H (300 MHz, DMSO- d_6) 10.43 (s, 1 H 3-CONH), 9.73 (s, 1 H, 4-NH), 9.13 (s, 1 H, 6-NHCONHCH₂CH₃), 8.87 (d, J 2.4, 1 H, 3-pyridyl 2-H), 8.60 (s, 1 H, 2-H), 8.31 (dd, J 4.6, 1.4 Hz, 1 H, 3-pyridyl 6-H), 8.12 (ddd, J 8.3, 2.4, 1.4, 1 H, 3-pyridyl 5-H), 7.98 (br. s., 1 H, 6-NHCONHCH₂CH₃), 7.39 (dd, J 8.3, 4.6 Hz, 1 H, 3-pyridyl 4-H), 7.15 (s, 1 H, 5-H), 6.98 (d, J 8.7 Hz, 1 H, 4-phenyl 2-H), 6.90 (d, J 2.3 Hz, 1 H, 4-phenyl 5-H), 6.79 (dd, J 8.7,

2.3 Hz, 1 H, 4-phenyl 6-H), 3.74 - 3.86 (overlapping singlets 2 H, 2 × OCH₃), 3.15 (dq, *J* 7.1, 5.9 Hz, 2 H, 6-NHCONHCH₂CH₃), 1.06 (t, *J* 7.1 Hz, 3 H, 6-NHCONHCH₂CH₃); δ_c (75 MHz, DMSO-*d*₆) 166.9 (3-CONH), 155.9 (6-NHCONHCH₂CH₃), 154.3 (4-C), 153.0 (6-C), 149.1 (2-C), 146.0 (4-phenyl 5-C), 145.3 (3-pyridyl 6-C), 144.6 (4-phenyl 4-C), 142.3 (3-pyridyl 2-C), 135.5 (4-phenyl 1-C), 131.6 (3-pyridyl 3-C), 127.7 (3-pyridyl 5-C), 123.5 (3-pyridyl 4-C), 115.2 (4-phenyl 6-C), 112.2 (4-phenyl 2-C), 108.0 (4-phenyl 5-C), 107.1 (3-C), 91.5 (5-C), 55.7 (OCH₃), 55.4 (OCH₃), 33.8 (6-NHCONHCH₂CH₃), 15.3 (6-NHCONHCH₂CH₃); ν_{max} / cm⁻¹ (solid) 3264, 1708, 1653, 1513, 1484, 1325; *m/z* (ESI⁺) found MH⁺ 437.194286 C₂₂H₂₅N₆O₄ *MH* requires 437.193180; HPLC RT = 2.83 mins.

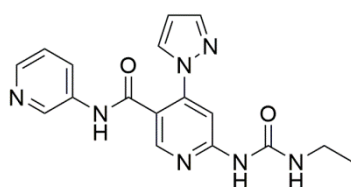
6-[(ethylcarbamoyl)amino]-4-[(4-methoxyphenyl)amino]-N-(pyridin-3-yl)pyridine-3-carboxamide 69



Compound **67** (50 mg, 0.16 mmol) and *p*-anisidine (23 mg, 0.18 mmol) were dissolved in EtOH (2 ml) and 1 drop of 2 M HCl was added. The reaction was heated to 70 °C for 18 hours. The reaction was then allowed to cool and neutralised by addition of NaOH (2M aqueous solution). The reaction mixture was concentrated *in vacuo*. Trituration with MeOH followed by recrystallisation from EtOH afforded the title compound (10 mg, 0.025 mmol, 15%) as colourless microcrystals, m.p. >250 °C; *R*_f 0.08 (EtOAc); δ_H (300 MHz, DMSO-*d*₆) 12.22 (br. s, 1 H, 3-CONH), 11.05 (br. s., 1 H, 4-NH), 10.00 (br. s, 1 H, 6-NHCONHCH₂CH₃), 9.33 (d, *J* 2.3 Hz, 1 H, 3-pyridyl 2-H), 8.78 (d, *J* 8.7 Hz, 1 H, 3-pyridyl 6-H), 8.61 - 8.73 (m, 2 H, 2-H and 3-pyridyl 5-H), 8.02 (dd, *J* 8.7, 5.3 Hz, 1 H, 3-pyridyl 4-H), 7.46 (t, *J* 5.5 Hz, 1 H, 6-NHCONHCH₂CH₃), 7.30 (d, *J* 8.7 Hz, 2 H, 4-phenyl 2-H), 7.05 (d, *J* 8.7 Hz, 2 H, 4-phenyl 3-H), 6.55 (s, 1 H, 5-H), 3.80 (s, 3 H, 4-phenyl 4-OCH₃), 3.15 (qd, *J* 7.2, 5.5 Hz, 2 H, 6-NHCONHCH₂CH₃), 1.07 (t, *J* 7.2 Hz, 3 H, 6-NHCONHCH₂CH₃); δ_c (75 MHz, DMSO-*d*₆) 164.3 (3-CONH), 158.0 (6-NHCONHCH₂CH₃), 155.4 (4-phenyl 4-C), 153.8 (6-C), 148.8 (4-phenyl 1-C), 140.4 (2-C), 138.1 (3-pyridyl 5-C), 137.7 (4-C), 134.8 (3-pyridyl 6-C), 134.6 (3-pyridyl 2-C), 129.4 (3-pyridyl 3-C), 126.8 (4-phenyl 2-C and 3-pyridyl 4-C), 115.0 (4-phenyl 3-C), 109.3 (3-C), 91.2 (5-C), 55.4 (4-phenyl 4-OCH₃), 34.1 (NHCONHCH₂CH₃), 14.8 (6-NHCONHCH₂CH₃);

ν_{\max} / cm^{-1} (solid) 2977.0, 1768.7, 1698.1; m/z (ESI⁺) found MH^+ 407.1825, $\text{C}_{21}\text{H}_{23}\text{N}_6\text{O}_3$
MH requires 407.1826; HPLC RT = 1.51 mins.

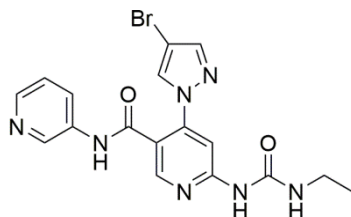
6-[(ethylcarbamoyl)amino]-4-(1H-pyrazol-1-yl)-N-(pyridin-3-yl)pyridine-3-carboxamide 71



Pyrazole (23.0 mg, 0.344 mmol) was dissolved in DMF (2 ml) and the resulting solution was cooled to 0 °C. Potassium *tert*-butoxide (42.1 mg, 0.376 mmol) was added and the reaction stirred at 0 °C for 1 hour.

Compound **67** (84 mg, 0.263 mmol) was added to the reaction mixture and the reaction mixture was heated to 70 °C for 18 hours. The reaction mixture was allowed to cool to room temperature, diluted with water (10 ml) and extracted into DCM (4 × 10 ml). The combined organic extracts were dried over MgSO_4 and concentrated *in vacuo* to afford a yellow oil. Trituration with CHCl_3 afforded the title compound (23 mg, 0.066 mmol, 17%) as off-white microcrystals. m.p. 225.4 – 228.7 °C; R_f 0.04 (EtOAc); δ_{H} (500 MHz, $\text{DMSO}-d_6$) 10.59 (s, 1 H, 3-CONH) 9.49 (s, 1 H, 6-NHCONHCH₂CH₃), 8.72 (d, J 2.6 Hz, 1 H, 3-pyridyl 2-H) 8.44 (s, 1 H, 2-H), 8.28 (dd, J 4.7, 1.3 Hz, 1 H, 3-pyridyl 6-H), 8.14 (d, J 2.1 Hz, 1 H, 4-pyrazolyl 5-H), 8.03 (d, J 8.3 Hz, 1 H, 3-pyridyl 4-H), 7.90 (s, 1 H, 5-H), 7.73 (d, J 1.7 Hz, 1 H, 4-pyrazolyl 3-H), 7.49 (t, J 5.4 Hz, 1 H, 6-NHCONHCH₂CH₃), 7.35 (dd, J 8.3, 4.7 Hz, 1 H, 3-pyridyl 5-H), 6.53 (dd, J 1.7, 2.1 Hz, 1 H, 4-pyrazolyl 4-H), 3.19 (qd, J 7.2, 5.4 Hz, 3 H, 6-NHCONHCH₂CH₃), 1.09 (t, J 7.2 Hz, 3 H, 6-NHCONHCH₂CH₃); δ_{C} (125 MHz, $\text{DMSO}-d_6$) 164.4 (3-CONH), 155.3 (6-NHCONHCH₂CH₃), 154.1 (6-C), 148.3 (2-C), 145.2 (3-pyridyl 6-C), 144.5 (4-pyrazolyl 5-C), 142.1 (4-pyrazolyl 3-C), 141.2 (3-pyridyl 2-C), 135.8 (4-C), 130.0 (4-pyrazolyl 5-C), 126.5 (3-pyridyl 4-C), 123.6 (3-pyridyl 5-C), 119.2 (3-C), 108.6 (4-pyrazolyl 4-C), 103.4 (5-C), 33.9 (6-NHCONHCH₂CH₃), 15.23 (6-NHCONHCH₂CH₃); ν_{\max} / cm^{-1} (solid) 3209, 3120, 3042, 2973, 1668, 1656, 1585, 1527, 1480, 1419; m/z (ESI⁺) found MH^+ 352.1532, $\text{C}_{17}\text{H}_{18}\text{N}_7\text{O}_2$
MH requires 352.1516; HPLC RT = 1.19 mins.

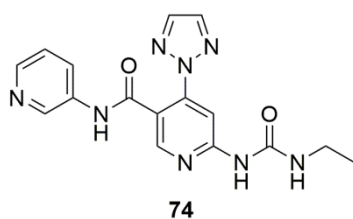
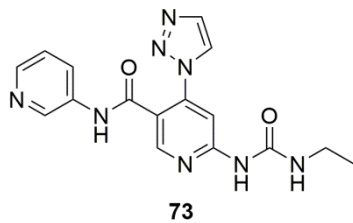
4-(4-bromo-1H-pyrazol-1-yl)-6-[(ethylcarbamoyl)amino]-N-(pyridin-3-yl)pyridine-3-carboxamide 72



General method B using 4-bromopyrazole (18.8 mg, 0.470 mmol) and compound **67** (100 mg, 0.313 mmol). The reaction mixture was diluted with water (10 ml) and extracted into DCM (3 × 10 ml). The combined organic

extracts were washed with brine (10 ml), dried over MgSO₄ and concentrated *in vacuo* to afford an off-white solid. Recrystallisation from EtOH afforded the title compound (34 mg, 0.079 mmol, 25%) as colourless microcrystals, m.p. 239.4-241.8 °C; *R*_f 0.05 (EtOAc); δ_H (500 MHz, DMSO-*d*₆) 10.61 (s, 1 H, 3-CONH), 9.55 (s, 1 H, 6-NHCONHCH₂CH₃), 8.72 (s, 1 H, 3-pyridyl 2-*H*), 8.49 (s, 1 H, 2-*H* or 4-pyrazolidyl 5-*H*), 8.48 (s, 1 H, 2-*H* or 4-pyrazolidyl 5-*H*), 8.29 (dd, *J* 4.5, 1.1 Hz, 1 H, 3-pyridyl 6-*H*), 8.02 (d, *J* 8.5 Hz, 1 H, 3-pyridyl 4-*H*), 7.87 (s, 1 H, 5-*H*), 7.87 (s, 1 H, 4-pyrazolidyl 3-*H*), 7.41 (t, *J* 4.8 Hz, 1 H, 6-NHCONHCH₂CH₃), 7.36 (dd, *J* 8.1, 4.7 Hz, 1 H, 3-pyridyl 5-*H*), 3.19 (qd, *J* 7.2, 4.8 Hz, 2 H, 6-NHCONHCH₂CH₃), 1.08 (t, *J* 7.2 Hz, 1 H, 6-NHCONHCH₂CH₃); δ_C (125 MHz, DMSO-*d*₆) 163.9 (3-CONH), 155.4 (6-NHCONHCH₂CH₃), 154.1 (6-C), 148.6 (5-C), 144.9 (3-pyridyl 6-C), 144.6 (3-pyridyl 2-C), 142.3 (4-pyrazolyl 3-C), 141.2 (2-C), 135.7 (4-C), 130.5 (4-pyrazolyl 5-C), 126.5 (3-pyridyl 4-C), 123.6 (3-pyridyl 5-C), 119.3 (3-C), 104.0 (5-C), 95.5 (4-pyrazolyl 4-C), 34.0 (6-NHCONHCH₂CH₃), 15.2 (6-NHCONHCH₂CH₃); ν_{max} / cm⁻¹ (solid) 3307, 2975, 1667, 1607, 1589, 1518, 1480; *m/z* (ESI⁺) found MH⁺ 430.0625, C₁₇H₁₇BrN₇O₂ *MH* requires 430.0622; HPLC RT = 1.79.

6-[(ethylcarbamoyl)amino]-N-(pyridin-3-yl)-4-(2H-1,2,3-triazol-2-yl)pyridine-3-carboxamide **73 and 6-[(ethylcarbamoyl)amino]-N-(pyridin-3-yl)-4-(1H-1,2,3-triazol-1-yl)pyridine-3-carboxamide **74****

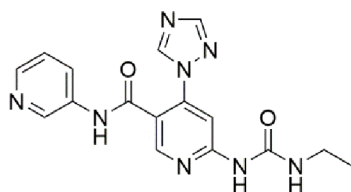


General method B using compound **67** (100 mg, 0.313 mmol) and 1,2,3-triazole (20 μ l, 0.345 mmol). The reaction mixture was diluted with water (10 ml) and the resulting precipitate was collected by filtration as colourless microcrystals which consisted of a mixture of the geometric isomers **73** and **74**. Purification using column chromatography (1:19 MeOH–EtOAc) afforded both of the title compounds **73** (10 mg, 0.027 mmol, 9%)

and **74** (21 mg, 0.060 mmol, 19%) as colourless microcrystals. **73**: m.p. >250 °C; R_f 0.18 (5% MeOH in EtOAc); δ_H (500 MHz, MeOD) 8.74 (br. s., 1 H, NH), 8.68 (s, 1 H, 3-pyridyl 2-H), 8.50 (s, 1 H, 2-H), 8.33 (d, J 4.4 Hz, 1 H, 3-pyridyl 6-H), 8.14 (d, J 8.1 Hz, 1 H, 3-pyridyl 4-H), 7.93 (d, J 0.9 Hz, 1 H, 4-triazolyl 4-H), 7.84 (s, 1 H, 5-H), 7.71 (d, J 0.9, 1 H, 4-triazolyl 5-H), 7.45 (dd, J 8.1, 4.4 Hz, 1 H, 3-pyridyl 5-H), 3.38 (q, J 7.3 Hz, 2 H, 6-NHCONHCH₂CH₃), 1.26 (t, J 7.3 Hz, 2 H, 6-NHCONHCH₂CH₃); δ_C (125 MHz, DMSO-*d*₆) 163.2 (4-CONH), 155.6 (6-NHCONHCH₂CH₃), 154.0 (6-C), 148.8 (3-pyridyl 6-C), 144.7 (3-pyridyl 4-C), 142.6 (3-pyridyl 3-C), 141.2 (3-pyridyl 2-C), 137.6 (4-triazolyl 4-C), 126.6 (3-pyridyl 4-C), 125.7 (4-triazolyl 5-C), 123.6 (3-pyridyl 5-C), 119.9 (3-C), 105.5 (5-C), 34.0 (6-NHCONHCH₂CH₃), 15.2 (6-NHCONHCH₂CH₃); ν_{max} / cm⁻¹ (solid) 2966, 2667, 1750, 1680, 1604, 1483; m/z (ESI⁺) found MH⁺ 353.1469, C₁₆H₁₇N₈O₃ MH requires 353.1469; HPLC RT = 1.12 mins. **74**: m.p. >250 °C; R_f 0.48 (5% MeOH in EtOAc); δ_H (500 MHz, MeOD) 8.78 (d, J 2.3 Hz, 1 H, 3-pyridyl 2-H), 8.52 (s, 1 H, 2-H), 8.35 (d, J 6.0 Hz, 1 H, 3-pyridyl 6-H), 8.18 - 8.22 (m, 1 H, 3-pyridyl 4-H), 8.01 (s, 2 H, 4-triazolyl 3-H), 7.48 (dd, J 8.5, 4.8 Hz, 1 H, 3-pyridyl 5-H), 3.39 (q, J 7.0 Hz, 2 H, 6-NHCONHCH₂CH₃), 1.26 (t, J 7.3 Hz, 3 H, 6-NHCONHCH₂CH₃); δ_C (75 Hz, DMSO-*d*₆) 164.2 (3-CONH), 155.2 (6-NHCONHCH₂CH₃), 154.1 (6-C), 148.4 (3-pyridyl 6-C), 144.5 (2-C), 143.7 (3-pyridyl 3-C), 141.1 (3-pyridyl 2-C), 137.6 (4-triazolyl 3-C), 135.9 (4-C), 126.4 (3-pyridyl 4-C), 123.6 (3-pyridyl 5-C), 118.5 (3-C), 102.2 (5-C), 33.9 (6-NHCONHCH₂CH₃), 15.2 (6-NHCONHCH₂CH₃); ν_{max} / cm⁻¹ (solid) 3305, 3114, 2976, 1686, 1644, 1608, 1584, 1557,

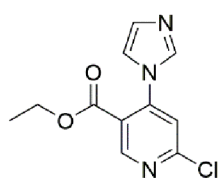
1528; m/z (ESI⁺) found MH⁺ 353.1471, C₁₆H₁₇N₈O₂ MH requires 353.1469; HPLC RT = 1.23 mins.

6-[(ethylcarbamoyl)amino]-N-(pyridin-3-yl)-4-(1H-1,2,4-triazol-1-yl)pyridine-3-carboxamide 75



General method B using 1,2,4-triazole (19 mg, 0.28 mmol) and compound **67** (80 mg, 0.25 mmol). The reaction mixture was diluted with water (10 ml) and extracted into DCM (5 × 10 ml). The combined organic extracts washed with water (2 × 10 ml) and brine (2 × 10 ml), dried over MgSO₄, concentrated *in vacuo* and triturated with Et₂O to afford a pale yellow solid. Recrystallisation from MeOH afforded the title compound (12 mg, 0.034 mmol, 14%) as colourless microcrystals, m.p. 232.5-235.5 °C; *R_f* 0.20 (5% MeOH in EtOAc); δ_H (500 MHz, DMSO-*d*₆) 10.69 (s, 1 H, 3-CONH), 9.67 (s, 1 H, 4-triazolyl 5-H), 9.06 (s, 1 H, 6-NHCONHCH₂CH₃), 8.74 (s, 1 H, 3-pyridyl 2-H), 8.61 (s, 1 H, 2-H), 8.32 (dd, *J* 4.4, 1.1 Hz, 1 H, 3-pyridyl 6-H), 8.23 (s, 1 H, 4-triazolyl 3-H), 8.05 (d, *J* 8.2 Hz, 1 H, 3-pyridyl 4-H), 7.98 (d, *J* 1.8 Hz, 1 H, 5-H), 7.42 (br. s., 1 H, 6-NHCONHCH₂CH₃), 7.39 (dd, *J* 8.2, 5.0 Hz, 1 H, 3-pyridyl 5-H), 3.21 (q, *J* 7.1 Hz, 2 H, 6-NHCONHCH₂CH₃), 1.12 (t, *J* 7.1 Hz, 3 H, 6-NHCONHCH₂CH₃); δ_C (125 MHz, DMSO-*d*₆) 163.3 (3-CONH), 155.6 (6-NHCONHCH₂CH₃), 153.9 (6-C), 152.6 (5-triazolyl 3-C), 148.8 (2-C), 144.7 (3-pyridyl 5-C), 142.7 (3-pyridyl 6-C), 141.3 (3-pyridyl 2-C), 135.5 (4-C), 126.6 (3-pyridyl 4-C), 123.6 (5-C), 119.4 (3-C), 105.0 (5-C), 33.8 (6-NHCONHCH₂CH₃), 15.1 (6-NHCONHCH₂CH₃); ν_{max} / cm⁻¹ (solid) 3094, 2925, 2379, 2343, 1682, 1650, 1611, 1530; m/z (ESI⁺) found MH⁺ 353.1471, C₁₆H₁₇N₈O₃ MH requires 353.1469; HPLC RT = 1.10 mins.

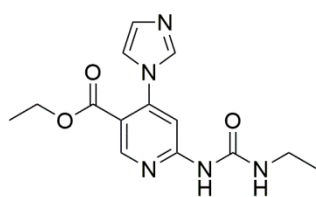
ethyl 6-chloro-4-(1H-imidazol-1-yl)pyridine-3-carboxylate 76



General method B using imidazole (340 mg, 5.0 mmol) and compound **45** (1.0 g, 4.5 mmol). An off-white solid was collected by filtration and extracted into EtOAc (3 × 10 ml). The combined organic extracts were washed with brine (10 ml), dried over Na₂SO₄

and concentrated *in vacuo* to an off-white residue. Purification using column chromatography (1:1 EtOAc–Pet) afforded the title compound (400 mg, 1.6 mmol, 36%) as colourless microcrystals, m.p. 139.0–144.1 °C; R_f 0.4 (EtOAc); δ_H (400 MHz, $CDCl_3$) 8.96 (s, 1 H, 2-H), 8.41 (s, 1 H, 4-imidazolyl 2-H), 7.64 (s, 1 H, 4-imidazolyl 5-H), 7.44 (s, 1 H, 5-H), 7.23 (s, 1 H, 4-imidazolyl 4-H), 4.45 (q, J 7.1 Hz, 2 H, 3-CO₂CH₂CH₃), 1.44 (t, J 7.1 Hz, 3 H, 3-CO₂CH₂CH₃); δ_C (100 MHz, $CDCl_3$) 163.1 (3-CO₂CH₂CH₃), 152.6 (2-C), 151.1 (6-C), 146.9 (4-C), 135.4 (4-imidazolyl 2-C), 131.6 (4-imidazolyl 4-C), 123.8 (3-C), 116.1 (4-imidazolyl 5-C), 113.7 (5-C), 62.1 (3-CO₂CH₂CH₃), 14.2 (3-CO₂CH₂CH₃); ν_{max} / cm^{-1} (solid) 3126, 2991, 1712, 1579; m/z (ESI⁺) found MNa^+ 274.0351, $C_{11}H_{10}ClN_3O_2$ MNa requires 274.0354; HPLC RT = 1.20 mins.

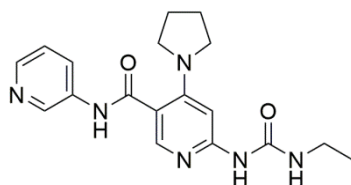
Ethyl 6-[(ethylcarbamoyl)amino-4-(1H-imidazol-1-yl)pyridine-3-carboxylate 77



Palladium acetate (64 mg, 0.29 mmol) and xantphos (248 mg, 0.429 mmol) were dissolved in degassed, anhydrous 1,4-dioxane (5 ml) and the resulting solution was stirred under N₂ for 20 minutes. N-Ethyl urea (189 mg, 2.15 mmol), compound **76** (360 mg, 1.43 mmol) and potassium *tert*-butoxide (240 mg, 2.15 mmol) were then added to the reaction mixture and the reaction mixture was heated to 100 °C for 4 hours. The reaction mixture was then allowed to cool, filtered through celite and extracted into EtOAc (3 × 10 ml). The combined organic extracts were washed with water (10 ml), dried over MgSO₄ and concentrated *in vacuo* to afford an orange residue. Purification using column chromatography (3:97 MeOH–DCM) afforded the title compound (62.7 mg, 0.206 mmol, 14%) as colourless microcrystals. m.p. 200–202 °C (EtOH); R_f 0.06 (EtOAc); δ_H (500 MHz, $CDCl_3$) 9.95 (br. s., 1 H, 6-NHCONHCH₂CH₃), 9.05 (br. s., 1 H, 6-NHCONHCH₂CH₃), 8.84 (s, 1 H, 2-H), 7.67 (s, 1 H, 4-imidazolyl 2-H), 7.20 (s, 1 H, 4-imidazolyl 5-H), 7.12 (s, 1 H, 4-imidazolyl 4-H), 6.90 (s, 1 H, 5-H), 4.23 (q, J 7.33 Hz, 2 H, 3-CO₂CH₂CH₃), 3.42 (qd, J 7.30, 5.50 Hz, 2 H, 6-NHCONHCH₂CH₃), 1.25 (t, J 7.30 Hz, 3 H, 3-CO₂CH₂CH₃), 1.20 (t, J 7.30 Hz, 3 H, 6-NHCONHCH₂CH₃); δ_C (100 MHz, $CDCl_3$) 163.7 (3-CO₂CH₂CH₃), 156.0 (6-NHCONHCH₂CH₃), 155.5 (6-C), 151.7 (2-C), 145.7 (4-C), 137.2 (4-imidazolyl 2-C), 129.9 (4-imidazolyl 5-C), 120.1 (4-imidazolyl 4-C), 115.5 (3-C), 108.4 (5-C), 61.7 (3-CO₂CH₂CH₃), 35.0 (6-NHCONHCH₂CH₃), 15.2 (3-CO₂CH₂CH₃),

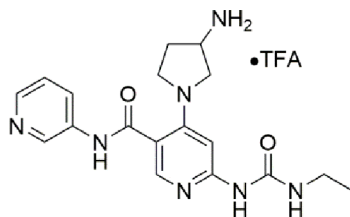
13.9 (6-NHCONHCH₂CH₃); ν_{\max} / cm⁻¹ (solid) 3214, 3120, 3136, 1725, 1686; m/z (ESI⁺) found MH⁺ 304.1416 C₁₄H₁₇N₅O₃ MH⁺ requires 304.0104; HPLC RT = 1.33 mins.

6-[(ethylcarbamoyl)amino]-N-(pyridin-3-yl)-4-(pyrrolidin-1-yl)pyridine-3-carboxamide 80



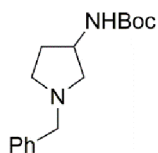
Compound **67** (50 mg, 0.157 mmol) was dissolved in DMF (2 ml) and pyrrolidine (8.5 μ l, 0.172 mmol) was added. The reaction was heated to 70 °C for 90 minutes and then stirred at room temperature for 18 hours. The reaction mixture was then diluted with water (5 ml) and the resulting precipitate collected by filtration to afford the title compound (40.9 mg, 0.116 mmol, 74%) as colourless microcrystals, m.p. 237.4-240.2 °C; R_f 0.18 (5% MeOH in EtOAc); δ_H (500 MHz, DMSO-*d*₆) 10.51 (s, 1 H, 3-CONH), 8.91 (s, 1 H, 6-NHCONHCH₂CH₃), 8.83 (d, *J* 2.6 Hz, 1 H, 3-pyridyl 2-H), 8.27 (dd, 1 H, *J* 4.7, 1.7 Hz, 3-pyridyl 6-H), 8.21 (br. s., 1 H, 6-NHCONHCH₂CH₃), 8.12 (d, *J* 8.5 Hz, 1 H, 3-pyridyl 4-H), 7.99 (s, 1 H, 5-H), 7.36 (dd, *J* 8.5, 4.7 Hz, 1 H, 3-pyridyl 5-H), 6.64 (s, 1 H, 2-H), 3.20 - 3.27 (m, 2 H, 4-pyrrolidyl 2-H₂), 3.16 (qd, *J* 7.2, 5.8 Hz, 2 H, 6-NHCONHCH₂CH₃), 1.73 - 1.91 (m, 2 H, 4-pyrrolydyl 3-H₂), 1.07 (t, *J* 7.2 Hz, 3 H, 6-NHCONHCH₂CH₃); δ_C (125 MHz, DMSO-*d*₆) 166.9 (3-CONH), 154.7 (6-NHCONHCH₂CH₃), 154.5 (C-4), 151.2 (C-6), 147.2 (5-C), 144.3 (3-pyridyl 6-C), 141.1 (3-pyridyl 2-C), 136.0 (3-pyridyl 3-C), 126.3 (3-pyridyl 4-C), 123.6 (3-pyridyl 5-C), 113.8 (3-C), 93.1 (2-C), 49.2 (4-pyrrolidyl 2-C), 33.7 (6-NHCONHCH₂CH₃), 25.1 (4-pyrrolidyl 3-C), 15.4 (6-NHCONHCH₂CH₃); ν_{\max} / cm⁻¹ (solid) 3229, 3034, 2949, 1655, 1601, 1567, 1525; m/z (ESI⁺) found MH⁺ 355.1895, C₁₈H₂₂N₆O₂ MH⁺ requires 355.1877; HPLC RT = 1.14 mins.

1-{2-[(ethylcarbamoyl)amino]-5-[(pyridin-3-yl)carbamoyl]pyridin-4-yl}pyrrolidin-3-aminium trifluoroacetate **81**



Compound **85** (50 mg, 0.12 mmol) was dissolved in DCM (2 ml) and TFA (2 ml) was added. The reaction mixture was stirred at room temperature for 3 hours and then concentrated *in vacuo* to afford the title compound (49 mg, 0.11 mmol, 98%) as a yellow glass. m.p. 138.9-141.0 °C; R_f 0.01 (EtOAc); δ_H (500 MHz, MeOD) 8.94 - 9.02 (m, 1 H, 3-pyridyl 2-H), 8.36 (app. d, J 4.8 Hz, 1 H, 3-pyridyl 6-H), 8.26 (app. d, J 6.0 Hz, 1 H, 3-pyridyl 4-H), 8.08 (s, 1 H, 2-H), 7.58 (dt, J 8.5, 4.8 Hz, 1 H, 3-pyridyl 5-H), 6.32 (s, 1 H, 5-H), 3.95 (quin, J 5.4 Hz, 1 H, 4-pyrrolidyl 2-H), 3.83 (dd, J 12.0, 6.4 Hz, 1 H, 4-pyrrolidyl 2-H), 3.71 (dt, J 12.0, 7.5 Hz, 1 H, 4-pyrrolidyl 5-H), 3.59 (dtd, J 8.1, 5.6, 5.6, 2.1 Hz, 1 H, 4-pyrrolidyl 5-H), 3.54 (dd, J 12.0, 4.3 Hz, 1 H, 4-pyrrolidyl 3-H), 3.18 (q, J 7.2 Hz, 2 H, 6-NHCONHCH₂CH₃), 2.39 (qt, J 7.5, 6.0 Hz, 1 H, 4-pyrrolidyl 4-H), 2.13 (td, J 12.9, 5.8 Hz, 1 H, 4-pyrrolidyl 4-H), 1.14 (t, J 7.2 Hz, 1 H, 6-NHCONHCH₂CH₃); δ_C (125 MHz, MeOD) 165.6 (3-CONH), 156.3 (6-NHCONHCH₂CH₃), 154.7 (6-C), 150.2 (4-C), 144.2 (3-pyridyl 6-C), 140.1 (3-pyridyl 1-C), 139.1 (3-pyridyl 2-C), 137.7 (C-2), 131.2 (3-pyridyl C-4), 126.3 (3-pyridyl C-5), 115.8 (C-3), 94.7 (5-C), 54.6 (4-pyrrolidyl 2-C), 49.6 (4-pyrrolidyl 3-C), 35.7 (6-NHCONHCH₂CH₃), 29.9 (4-pyrrolidyl 4-C), 15.1 (6-NHCONHCH₂CH₃). (4-pyrrolidyl 5-C under solvent peak). ν_{max} / cm⁻¹ (solid) 2981.9, 1673.1, 1650.51; m/z (ESI⁺) found MH⁺ 370.1990, C₁₈H₂₃N₇O₂ *MH* requires 370.1986; HPLC RT = 0.77 mins.

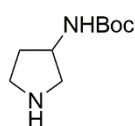
tert-butyl N-(1-benzylpyrrolidin-3-yl)carbamate¹³⁰ **83**



Boc anhydride (1.36 mg, 6.25 mmol) was dissolved in THF (10 ml) and 1-benzyl-3-aminopyrrolidine (1.00 g, 5.68 mmol) and NEt₃ (0.95 ml, 6.8 mmol) were added. The reaction mixture was stirred at room temperature for 18 hours and then concentrated *in vacuo*. The resulting off-white residue was taken up into EtOAc (20 ml) and washed with NaOH_(aq) (1 M, 20 ml). The combined organic extracts were dried over MgSO₄, and concentrated *in vacuo* to afford a pale yellow solid. Recrystallisation from EtOAc afforded the title compound

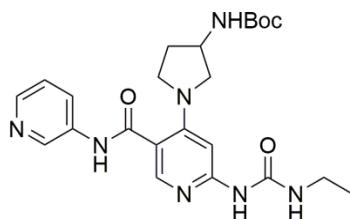
(1.06 g, 3.83 mmol, 67%) as colourless needles, m.p. 108.1- 114.0 °C; R_f 0.14 (1:1 EtOAc–Pet); δ_H (300 MHz, $CDCl_3$) 7.16 - 7.37 (m, 5 H, 1-benzyl CH), 4.88 - 5.04 (m, 1 H, NH), 4.05 - 4.25 (m, 1 H, CH), 3.58 (s, 2 H, 1-benzyl CH_2), 2.68 - 2.86 (m, 1 H, CH), 2.45 - 2.66 (m, 2 H, CH_2), 2.13 - 2.36 (m, 2 H, CH_2), 1.48 - 1.69 (m, 1 H, CH), 1.43 (s, 9 H, CH_3); δ_C (150 Hz, $CDCl_3$) 155.4 (3- $NHCO_2$), 138.8 (1-benzyl 1-C), 128.8 (1-benzyl 3-C), 128.3 (1-benzyl 2-C), 127.0 (1-benzyl 4-C), 79.2 ($OC(CH_3)_3$), 61.0 (1-C), 60.2 (1-benzyl CH_2), 52.6 (5-C), 49.9 (3-C), 32.7 (4-C), 28.4 (CH_3); (Found C, 69.6; H, 8.90; N, 10.1; $C_{16}H_{24}N_2O_2$ requires C, 69.5; H, 8.75; N, 10.1%); ν_{max} / cm^{-1} (solid) 3199, 2969, 2810, 1699, 1538, 1493; m/z (ES^+) found MH^+ 277.1909, $C_{16}H_{25}N_2O_2$ MH requires 277.1911; HPLC RT = 1.78 mins. Spectroscopic data consistent with literature values.¹³⁰

tert-butyl N-(pyrrolidin-3-yl)carbamate¹³⁰ 84



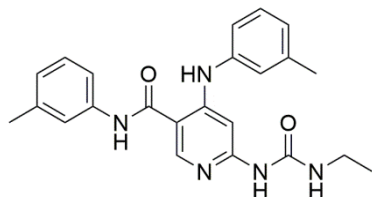
Compound **83** (1.00 g, 3.62 mmol) was dissolved in EtOH (10 ml) and THF (5 ml) and activated Pd on charcoal (100 mg) were added. The mixture was stirred under an atmosphere of H_2 for 72 hours. The reaction mixture was then filtered through celite and the celite washed with EtOAc. The filtrate was concentrated *in vacuo* to afford the title compound (670 mg, 3.60 mmol, 97%) as colourless microcrystals, m.p. 76.4-78.9 °C; R_f 0.02 (EtOAc); δ_H (300 MHz, $CDCl_3$) 4.82 (br. s., 1 H, 3- $NHCO_2$), 4.09 (br. s., 1 H, CH), 3.59 (s, 1 H, 3-H), 2.84 - 3.15 (m overlapping, 3 H, 3 \times CH), 2.76 (dd, J 11.3, 3.8 Hz, 1 H, CH), 2.45 - 2.52 (m, 1 H, CH), 2.10 (br. s., 1 H, NH), 1.63 - 1.73 (m, 1 H, CH), 1.44 (s, 9 H, CH_3); δ_C (125 MHz, $CDCl_3$) 155.5 (3- $NHCO_2$), 79.3 ($OC(CH_3)_3$), 62.9 (3-C), 60.8 (2-C), 45.5 (C-5), 32.3 (C-4), 28.4 (CH_3); ν_{max} / cm^{-1} (solid) 3308, 2974, 1683, 1520; m/z (ESI^+) found MH^+ 187.1442, $C_9H_{19}N_2O_2$ MH requires 187.1441. Spectroscopic data consistent with literature values.¹³⁰

tert-butyl N-(1-(2-[(ethylcarbamoyl)amino]-5-[(pyridin-3-yl)carbamoyl]pyridin-4-yl)pyrrolidine-3-yl)carbamate **85**

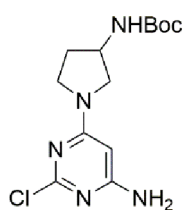


Compound **67** (100 mg, 0.313 mmol) and compound **84** (96 mg, 0.51 mmol) were dissolved in EtOH (4 ml) and the resulting solution was heated to 70 °C for 18 hours. 1 drop of 2M HCl was added to the reaction mixture and the reaction mixture was then stirred for a further 72 hours. The reaction mixture was allowed to cool and concentrated *in vacuo* to afford an off-white residue. Purification using column chromatography (4% MeOH–EtOAc) afforded the title compound (66 mg, 0.14 mmol, 45%) as a colourless glass, R_f 0.05 (EtOAc); δ_H (500 MHz, MeOD) 8.74 (br. s., 1 H, 3-pyridyl 2-H), 8.20 (dd, J 4.7, 1.3 Hz, 1 H, 3-pyridyl 6-H), 8.13 (d, J 7.7 Hz, 1 H, 3-pyridyl 6-H), 7.99 (s, 1 H, 2-H), 7.34 (dd, J 8.1, 4.7 Hz, 1 H, 3-pyridyl 5-H), 6.30 (s, 1 H, 5-H), 4.04 (br. s., 1 H, 4-pyrrolidyl 2-H), 3.44–3.52 (m, 1 H, 4-pyrrolidyl 2-H), 3.35–3.44 (m, 1 H, 4-pyrrolidyl 5-H), 3.24–3.31 (m, 1 H, 5-H), 3.16–3.24 (m, 4 H, 6-NHCONHCH₂CH₃, 4-pyrrolidyl 3-H and 5-H), 3.12 (dd, J 10.3, 4.7 Hz, 1 H, 4-pyrrolidyl 4-H), 2.07 (dq, J 12.5, 6.4 Hz, 1 H, 4-pyrrolidyl 4-H), 1.83 (dq, J 12.5, 6.4 Hz, 1 H, 4-pyrrolidyl 4-H), 1.30 (s, 9 H, 3 × CH₃), 1.09 (t, J 7.1 Hz, 3 H, 6-NHCONHCH₂CH₃); δ_C (125 MHz, MeOD) 169.7 (3-CONH), 158.0 (4-pyrrolidyl 3-NHCO₂C(CH₃)₃), 157.7 (6-NHCONHCH₂CH₃), 156.0 (6-C), 153.3 (4-C), 148.4 (3-pyridyl 6-C), 145.5 (6-pyridyl 1-C), 142.1 (3-pyridyl 2-C), 137.5 (C-2), 129.2 (3-pyridyl 4-C), 125.3 (3-pyridyl 5-C), 115.2 (3-C), 94.7 (5-C), 80.3 (4-pyrrolidyl 3-NHCO₂C(CH₃)₃), 56.1 (4-pyrrolidyl 3-C), 51.5 (4-pyrrolidyl 2-C), 35.4 (6-NHCONHCH₂CH₃), 31.8 (4-pyrrolidyl 4-C), 28.6 (4-pyrrolidyl 3-NHCO₂C(CH₃)₃), 15.5 (6-NHCONHCH₂CH₃), (4-pyrrolidyl 5-C under solvent peak); ν_{max} / cm⁻¹ (solid) 3221, 2973, 1662, 1603; m/z (ESI⁺) found MH⁺ 470.2519, C₂₃H₃₂N₇O₄ MH requires 470.2510; HPLC RT = 1.45 mins.

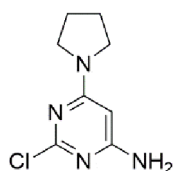
6-[(ethylcarbamoyl)amino]-N-(3-methylphenyl)-4-[(3-methylphenyl)amino]pyridine-3-carboxamide 86



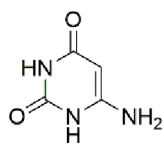
Compound **63** (152 mg, 0.559 mmol) was suspended in pyridine (2 ml) and *m*-toluidine (0.133 ml, 1.23 mmol) and T3P solution (50% in EtOAc, 0.67 ml, 1.8 mmol) were added. The reaction mixture was heated to 70 °C for 18 hours. Further portions of T3P solution (0.26 ml, 0.67 mmol) and *m*-toluidine (0.133 ml, 1.23 mmol) were then added and the reaction mixture was heated to 90 °C for a further 10 hours. The reaction mixture was then allowed to cool to room temperature and concentrated *in vacuo* to afford an off-white solid. Trituration with Et₂O afforded the title compound (65.4 mg, 0.161 mmol, 29%) as colourless microcrystals. m.p. 235.4-238.8; *R*_f 0.17 (1:1 EtOAc-Pet); δ_H (500 MHz, DMSO-*d*₆) 10.18 (br. s, 1 H, 3-CONH), 9.91 (br. s, 1 H, 6-NHCONHCH₂CH₃), 9.11 (br. s, 1 H, 4-NH), 8.55 (s, 1 H, 2-H), 8.09 (br. s., 1 H, 6-NHCONHCH₂CH₃), 7.55 (s, 1 H, 3-phenyl 2-H), 7.46 (d, *J* 8.1 Hz, 1 H, 3-phenyl 6-H), 7.27 (t, *J* 7.7 Hz, 1 H, 3-phenyl 5-H), 7.02 - 7.10 (m, 2 H, 5-H and 4-phenyl 5-H), 7.02 - 7.10 (m, 2 H, 4-phenyl 2-H and 4-phenyl 6-H), 6.95 (d, *J* 7.7 Hz, 1 H, 4-phenyl 4-H), 6.92 (d, *J* 7.7 Hz, 1 H, 3-phenyl 4-H), 3.15 (qd, *J* 7.1, 5.6 Hz, 2 H, 6-NHCONHCH₂CH₃), 2.31 (s, 3 H, CH₃), 2.30 (s, 3 H, CH₃), 1.06 (t, *J* 7.1 Hz, 3 H, 6-NHCONHCH₂CH₃); δ_C (125 MHz, DMSO-*d*₆) 166.5 (3-CONH), 155.8 (6-C), 154.4 (6-NHCONHCH₂CH₃), 152.0 (4-C), 148.8 (2-C), 138.9 (4-phenyl 1-C), 138.8 (3-phenyl 1-C), 138.6 (4-phenyl 3-C), 137.7 (3-phenyl 3-C), 129.2 (4-phenyl 5-C), 128.4 (3-phenyl 5-C), 124.8 (4-phenyl 2-C), 124.5 (3-phenyl 2-C), 122.7 (4-phenyl 6-C), 121.3 (3-phenyl 6-C), 119.9 (4-phenyl 4-C), 118.0 (3-phenyl 4-C), 108.3 (3-C), 92.0 (5-C), 33.8 (6-NHCONHCH₂CH₃), 21.2 (4-phenyl CH₃), 21.0 (3-phenyl CH₃), 15.3 (6-NHCONHCH₂CH₃); ν_{max} / cm⁻¹ (solid) 3395, 3341, 2968, 2860, 1713, 1682; *m/z* (ESI⁺) found MNa⁺ 426.1906, C₂₃H₂₅N₅O₂ *MNa* requires 426.1900; HPLC RT = 3.43 mins.

tert-butyl N-[1-(6-amino-2-chloropyrimidin-4-yl)pyrrolidin-3-yl]carbamate 130

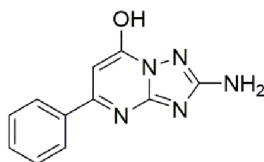
Compound **84** (640 mg, 3.46 mmol) and 4-amino-2,6-dichloropyridine (567 mg, 3.46 mmol) were suspended in 1,4-dioxane (15 ml) and NEt_3 (0.96 ml, 6.92 mmol) was added. The reaction mixture was heated to 100 °C for 3 hours and then allowed to cool to room temperature. The reaction mixture was concentrated *in vacuo* and the resulting off-white residue was purified using column chromatography (5:1 to 1:1 Pet–EtOAc) to afford the title compound (780 mg, 2.49 mmol, 73%) as colourless microcrystals. R_f 0.26 (2:5 EtOAc–Pet); δ_H (300 MHz, CDCl_3) 5.79 (s, 1 H, 1-pyrimidinyl C5-H), 4.81 (br. s, 2 H, NH_2), 4.75 (br. s, 1 H, NH), 4.27 (m, 1 H, CH), 3.76 (dd, J 11.8, 6.0 Hz, 1 H, C5-H), 3.52 - 3.65 (m, 2 H, C5-H and), 3.41 (dd, J 11.5, 2.7 Hz, 1 H, CH), 2.11 - 2.28 (m, 1 H, C4-H), 1.79 - 1.97 (m, 1 H, C4-H), 1.44 (s, 9 H, CH_3); δ_C (125 MHz, CDCl_3) 164.1 (1-pyrimidinyl 6-C), 160.1 (4-C), 159.9 (1-pyrimidinyl 2-C), 155.3 (3- NHCO_2), 92.6 (1-pyrimidinyl 5-C), 79.74 ($\text{CO}_2\text{C}(\text{CH}_3)_3$), 52.5 (5-C), 50.2 (2-C), 44.6 (3-C), 31.7 (4-C), 28.4 (CH_3); $\nu_{\text{max}}/\text{cm}^{-1}$ (solid) 3338, 3223, 2872, 1688, 1623; m/z (ESI^+) found MH^+ 314.1383, $\text{C}_{13}\text{H}_{21}\text{ClN}_5\text{O}_2$ MH requires 314.1378; HPLC RT = 1.88 mins.

2-chloro-6-(pyrrolidin-1-yl)pyrimidin-4-amine 132

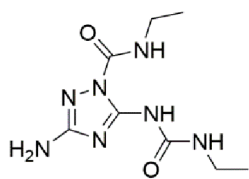
4-amino-2,6-dichloropyrimidine (1.1 g, 6.1 mmol) was dissolved in 1,4-dioxane (10 ml) and pyrrolidine (0.30 ml, 6.1 mmol) was added. The reaction mixture was heated to 100 °C for 5 hours and then allowed to cool. The reaction mixture was concentrated *in vacuo* to afford a colourless solid. Purification using column chromatography (1:1 EtOAc–Pet) afforded the title compound (750 mg, 3.79 mmol, 62%) as colourless microcrystals, R_f 0.25 (1:1 EtOAc–Pet); δ_H (300 MHz, CDCl_3) 5.76 (s, 1 H, 5- H), 4.64 (br. s., 2 H, NH_2), 3.52 (br. s., 4 H, 4-pyrrolidyl 2- H and 5- H) 1.82 - 2.10 (m, 4 H, 4-pyrrolidyl 3- H and 4- H); δ_C (500 MHz, CDCl_3) 164.0 (4-C), 160.1 (2-C), 159.9 (6-C), 91.9 (5-C), 46.7 (4-pyrrolidyl 2-C), 25.4 (4-pyrrolidyl 3-C); $\nu_{\text{max}}/\text{cm}^{-1}$ (solid) 3322, 3179, 2970, 2858, 163, 1547, 1510; m/z (ESI^+) found MH^+ 199.0750, $\text{C}_8\text{H}_{12}\text{ClN}_4$ MH requires 199.0745; HPLC RT = 1.23 mins.

6-amino-1,2,3,4-tetrahydropyrimidine-2,4-dione¹⁶⁰ 134

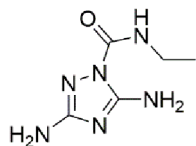
Sodium (3.9 g, 170 mmol) was added to EtOH (100 ml) under N₂. When the sodium was fully dissolved urea (5.15 g, 86 mmol) and ethyl cyanoacetate (9.15 ml, 86 mmol) were added to the solution and the reaction mixture was then heated to reflux for 18 hours. Hot water (100 ml) was then added to the reaction mixture. Once the precipitate had fully dissolved, the reaction was neutralised to pH 7 by addition of glacial acetic acid. The reaction mixture was then cooled to 0 °C and the precipitate collected by filtration to afford the title compound (5.56 g, 43.7 mmol, 51%) as pale yellow microcrystals, m.p. >250 °C; *R_f* 0.04 (EtOAc); δ_H (500 MHz, DMSO-*d*₆) 10.09 (br. s, 2 H, 1-NH and 3-NH), 6.21 (br. s., 2 H, NH₂), 4.43 (s, 1 H, 5-H); δ_C (150 Hz, DMSO-*d*₆) 164.3 (C-4), 155.2 (6-C), 151.1 (C-2), 74.1 (5-C); ν_{max}/cm⁻¹ (solid) 3398, 3117, 2954, 2833, 1696, 16223, 1575, 1530, 1468; *m/z* (ESI⁺) found MH⁺ 128.0455, C₄H₆N₃O₂ *MH* requires 128.0455; HPLC RT = 0.83 mins. Spectroscopic data consistent with literature values.¹⁶⁰

2-amino-5-phenyl-4H,7H-[1,2,4]triazolo[1,5-a]pyrimidin-7-one 150

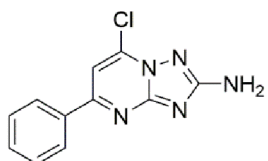
Ethyl benzoylacetate (874 μl, 5.05 mmol) and 2,5-diaminotriazole (500 mg, 5.05 mmol) were suspended in AcOH (10 ml) and the reaction mixture was heated to 100 °C for 72 hours. The reaction was then allowed to cool to room temperature and the resulting precipitate was collected by filtration and washed with methanol to afford the title compound (850 mg, 3.75 mmol, 74%) as colourless microcrystals. m.p. >250 °C; *R_f* 0.04 (EtOAc); δ_H (500 MHz, DMSO-*d*₆) 7.88 (s, 2 H, 5-phenyl 2-H), 7.46 - 7.57 (m, 3 H, 5-phenyl 3-H and 4-H), 6.33 (br. s., 2 H, 2-NH₂), 6.25 (s, 1 H, 6-H), 2.06 (br. s., 1 H, 4-NH); δ_C (125 MHz, DMSO-*d*₆) 155.3 (7-C), 150.3 (5-C), 130.4 (5-phenyl 4-C), 128.8 (5-phenyl 3-C), 127.1 (5-phenyl 2-C), 97.9 (6-C); ν_{max} / cm⁻¹ (solid) 3306, 3178, 3080, 2590, 1673; *m/z* (ESI⁺) found MH⁺ 228.0881, C₁₁H₁₀N₅O *MH* requires 228.0880; HPLC RT = 1.38 mins.

3-amino-N-ethyl-5-[(ethylcarbamoyl)amino]-1H-1,2,4-triazole-1-carboxamide 153

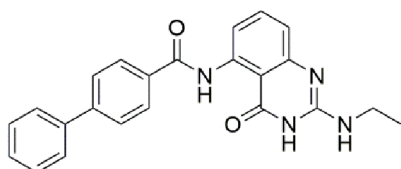
2,5-diaminotriazole (200 mg, 2.02 mmol) was suspended in 1,4-dioxane (6 ml) and ethyl isocyanate (240 μ l, 3.03 mmol) was added. The reaction mixture was stirred at room temperature for 40 hours and the resulting precipitate was collected by filtration to afford the title compound (338 mg, 1.40 mmol, 92%) as colourless microcrystals, m.p. >250 °C; R_f 0.05 (1:1 EtOAc-Pet); δ_H (300 MHz, DMSO- d_6) 9.33 (br. s., 1 H, 5-NHCONHCH₂CH₃), 8.14 (t, J 5.9 Hz, 1 H, 1-CONHCH₂CH₃), 7.84 (t, J 5.8 Hz, 1 H, 5-NHCONHCH₂CH₃), 7.33 (br. s., 2 H, 3-NH₂), 3.21 (m, 4 H, 1-CONHCH₂CH₃ and 5-NHCONHCH₂CH₃), 1.11 (m, 6 H, 1-CONHCH₂CH₃ and 5-NHCONHCH₂CH₃); δ_C (125 MHz, MeOD) 157.4 (3-C), 156.4 (1-CONHCH₂CH₃ or 5-NHCONHCH₂CH₃), 156.1 (1-CONHCH₂CH₃ or 5-NHCONHCH₂CH₃), 152.7 (5-C), 35.7 (1-CONHCH₂CH₃ or 5-NHCONHCH₂CH₃), 35.7 (1-CONHCH₂CH₃ or 5-NHCONHCH₂CH₃), 15.6 (1-CONHCH₂CH₃), 15.1 (5-NHCONHCH₂CH₃); ν_{max} / cm^{-1} (solid) 3395, 3341, 2968, 2860, 1713, 1682; m/z (ESI⁺) found MH⁺ 242.1362, C₈H₁₅N₇O₂ MH requires 242.1360;

3,5-diamino-N-ethyl-1H-1,2,4-triazole-1-carboxamide 154

2,5-diaminotriazole (200 mg, 2.02 mmol) was suspended in 1,4-dioxane (5 ml) and ethyl isocyanate (186 μ l, 1.83 mmol) was added. The reaction mixture was then stirred at room temperature for 48 hours and the resulting precipitate was collected by filtration to afford the title compound (316 mg, 1.86 mmol, 100%) as colourless microcrystals, m.p. 121.7-124.8 °C; R_f 0.19 (EtOAc); δ_H (500 MHz, MeOD) 3.33 (q, J 7.20 Hz, 1 H, 1-CONHCH₂CH₃), 1.22 (t, J 7.10 Hz, 3 H, 1-NHCH₂CH₃); δ_C (125 MHz, MeOD) 161.9 (C-3), 157.9 (C-5), 153.1 (1-CONHCH₂CH₃), 35.6 (1-CONHCH₂CH₃), 15.2 (1-CONHCH₂CH₃); ν_{max} / cm^{-1} (solid) 3419, 3332, 3203, 2974, 1712, 1687 m/z (ESI⁺) found MH⁺ 171.0989, C₅H₁₁N₆O MH requires 171.0989; HPLC RT = 1.78 mins. Spectroscopic data consistent with literature values.¹⁶¹

7-chloro-5-phenyl-[1,2,4]triazolo[1,5-a]pyrimidin-2-amine 155

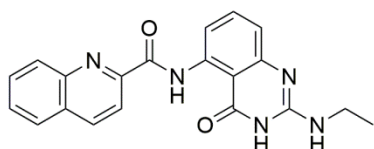
Either: compound **150** (180 mg, 0.79 mmol) was suspended in POCl₃ (4 ml) and heated to 100 °C for 4 hours. The resulting reaction mixture was then poured onto a mixture of ice and water and neutralised by the addition of K₂CO₃. The resulting aqueous mixture was extracted into DCM (4 × 10 ml). The combined organic extracts were washed with brine (10 ml), dried over Na₂SO₄ and concentrated *in vacuo* to afford a dark orange residue. Purification by column chromatography (1:2 Pet–EtOAc) afforded the title compound (18 mg, 0.078 mmol, 10%) as off-white microcrystals. Or: compound **150** (180 mg, 0.79 mmol) was suspended in phenyl phosphonic anhydride (4 ml) and heated to 140 °C for 4 hours. The resulting reaction mixture was then poured onto a mixture of ice and water and neutralised by the addition of K₂CO₃. The resulting aqueous mixture was extracted into DCM (4 × 10 ml). The combined organic extracts were washed with brine (10 ml), dried over Na₂SO₄ and concentrated *in vacuo* to afford a dark orange residue. Purification by column chromatography (1:2 Pet–EtOAc) afforded the title compound (11 mg, 0.043, 5%) as off-white microcrystals. *R*_f 0.2 (1:1 EtOAc–Pet); δ_H (300 MHz, CDCl₃) 8.14 (dd, *J* 6.9, 3.0 Hz, 2 H, 5-phenyl 2-H), 7.49 - 7.59 (m, 3 H, 5-phenyl 3-H and 5-phenyl 4-H), 7.47 (s, 1 H, 6-H), 4.84 (br. s., 2 H, 2-NH₂); δ_C (75 MHz, DMSO-*d*₆) 167.7 (2-C), 157.5 (5-C), 155.5 (3'-C), 136.2 (5-phenyl 1-C), 135.8 (7-C), 130.9 (5-phenyl 4-C), 128.9 (5-phenyl 3-C), 127.3 (5-phenyl 2-C), 105.1 (6-C); ν_{max} / cm⁻¹ (solid) 3317, 3174, 1645; *m/z* (ESI⁺) found MH⁺ 246.0544, C₁₁H₉ClN₅ *MH* requires 246.0541; HPLC RT = 1.93 mins.

N-[2-(ethylamino)-4-oxo-3,4-dihydroquinazolin-5-yl]-4-phenylbenzamide 158

General method E using compound **172** (350 mg, 0.98 mmol). Purification using column chromatography (1:1 Pet–EtOAc to EtOAc) followed by recrystallization from EtOAc afforded the title compound (12 mg, 0.032 mmol, 3%) as colourless microcrystals. m.p. >250 °C; *R*_f 0.62 (1:1 EtOAc–Pet); δ_H (500 MHz, DMSO-*d*₆) 8.51 (br. s., 1 H, 3-NH), 8.41 (d, *J* 8.7 Hz, 1 H, 5-NHCO), 8.01 - 8.18 (m, 2 H, 5-phenyl 3-H), 7.92

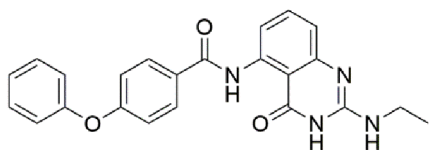
(d, J 8.2 Hz, 2 H, 4-phenyl 2-H), 7.80 (d, J 7.3 Hz, 2 H, 5-phenyl 2-H), 7.59 (t, J 8.0 Hz, 1 H, 4-phenyl 4-H), 7.54 (t, J 7.6 Hz, 2 H, 4-phenyl 3-H), 7.45 (t, J 7.3 Hz, 1 H, 7-H), 7.01 (d, J 8.2 Hz, 1 H, 6-H), 6.39 (br. s., 1 H, 8-H), 5.77 (s, 1 H, 2-NHCH₂CH₃), 3.38 (qd, J 7.3, 6.8 Hz, 2 H, 2-NHCH₂CH₃), 1.18 (t, J 7.3 Hz, 3 H, 2-NHCH₂CH₃); δ_c (100 MHz, DMSO-*d*₆) 165.8 (5-NHCO), 164.7 (4-C), 153.0 (2-C), 130.4 (8'-C), 144.1 (5-phenyl 4-C), 141.0 (5-C), 139.4 (4-phenyl 1-C), 135.7 (7-C), 133.8 (5-phenyl 1-C), 129.6 (4-phenyl 3-C), 128.7 (4'-C), 128.1 (5-phenyl 3-C), 127.7 (5-phenyl 2-C), 127.6 (4-phenyl 2-C), 127.5 (4-phenyl 4-C), 119.8 (6-C), 111.3 (8-C), 35.6 (2-NHCH₂CH₃), 15.1 (2-NHCH₂CH₃); ν_{\max} / cm⁻¹ (solid) 3246, 3117, 3029, 1671, 1607; m/z (ESI⁺) found MH⁺ 385.1672, C₂₃H₂₀N₄O₂ *MH* requires 385.1659; HPLC RT = 2.83 mins.

N-[2-(ethylamino)-4-oxo-3,4-dihydroquinazolin-5-yl]quinoline-2-carboxamide **161**



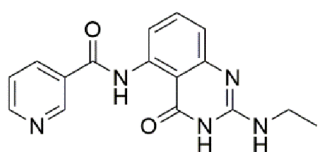
General method E using compound **173** (235 mg, 0.721 mmol). Purification using column chromatography (7:1 EtOAc–Pet) afforded the title compound (6.1 mg, 0.017

mmol, 2%) as pale yellow microcrystals. m.p. >250 °C; R_f 0.40 (1:7 EtOAc–Pet); δ_H (500 MHz, DMSO-*d*₆) 11.17 (br. s., 1 H, NH), 8.63 (d, J 8.1 Hz, 1 H, quinoline 4-H), 8.51 (d, J 8.1 Hz, 1 H, quinazolinone 6-H), 8.28 (d, J 8.5 Hz, 1 H, quinoline 3-H), 8.15 (d, J 8.5 Hz, 1 H, quinoline 8-H), 8.12 (d, J 8.5 Hz, 1 H, quinoline 5-H), 7.91 (t, J 7.7 Hz, 1 H, quinoline 7-H), 7.76 (t, J 7.5 Hz, 1 H, quinoline 6-H), 7.58 (t, J 8.1 Hz, 1 H, quinazolinone 7-H), 7.00 (d, J 8.1 Hz, 1 H, quinazolinone 8-H), 6.34 (br. s., 1 H, NHCH₂CH₃), 3.36 (qd, J 7.1, 5.0 Hz, 2 H, NHCH₂CH₃), 1.16 (t, J 7.1 Hz, 3 H, NHCH₂CH₃), 3-NH not resolved; δ_c (125 MHz, DMSO-*d*₆) 164.5 (quinazolinone 4-C), 163.1 (ArCONHAr), 152.6 (quinazolinone 2-C), 150.0 (quinazolinone C-8'), 145.9 (quinoline C-8'), 139.7 (quinazolinone C-5), 138.2 (quinoline 4-C), 134.8 (quinazolinone 7-C), 130.7 (quinoline C-4'), 129.3 (quinoline C-2 or C-8), 129.0 (quinoline C-2 or C-8), 128.4 (quinoline C-5 or C-6), 128.1 (quinoline C-5 or C-6), 119.6 (quinazolinone C-8), 118.7 (quinoline C-3), 111.2 (quinazolinone C-6), 105.3 (quinazolinone C-4'), 35.1 (NHCH₂CH₃), 14.7 (NHCH₂CH₃); ν_{\max} / cm⁻¹ (solid) 2959, 2929, 2860, 1726; m/z (ESI⁺) found MH⁺ 360.1459, C₂₀H₁₇N₅O₂ *MH* requires 360.1455; HPLC RT = 2.27 mins.

N-[2-(ethylamino)-4-oxo-3,4-dihydroquinazolin-5-yl]-4-phenoxybenzamide 162

General method E using compound **174** (193 mg, 0.53 mmol). Purification using column chromatography (1:1 EtOAc–Pet to EtOAc) afforded

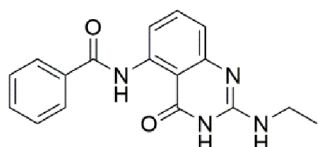
the title compound (38 mg, 0.095 mmol, 18%), as colourless microcrystals, m.p. 233.9–235.6; R_f 0.55 (EtOAc); δ_H (500 MHz, DMSO- d_6) 11.13 (br. s., 1 H, 3-NH), 8.38 (br. s., 1 H, 5-NHCO), 8.02 (d, J 7.3 Hz, 2 H, 6-benzamido 2-H), 7.56 (t, J 7.9 Hz, 1 H, 7-H), 7.48 (m, 2 H, 4-phenoxy 3-H), 7.26 (t, J 7.3 Hz, 1 H, 8-H), 7.16 (d, J 8.7 Hz, 4 H, 6-benzamido 3-H and 4-phenoxy 2-H), 6.99 (d, J 7.8 Hz, 1 H, 6-H), 6.39 (br. s., 1 H, 2-NHCH₂CH₃) 3.35 - 3.42 (m, 2 H, overlapped with H₂O signal, 2-NHCH₂CH₃), 1.17 (t, J 7.1 Hz, 3 H, 2-NHCH₂CH₃); δ_C (125 MHz, DMSO- d_6) 163.9 (5-NHCO), 163.6 (4-C), 160.2 (6-benzamido 4-C), 155.5 (4-phenoxy 1-C), 154.0 (2-C), 142.5 (8'-C), 140.6 (5-C), 130.2 (6-benzamido 2-C), 130.1 (6-benzamido 1-C), 129.4 (7-C), 129.2 (4-phenoxy 3-C), 124.4 (8-C), 124.3 (4-phenoxy 4-C), 119.6 (4-phenoxy 2-C), 117.9 (6-C), 104.6 (6-benzamido 3-C), 35.1 (2-NHCH₂CH₃), 14.6 (2-NHCH₂CH₃), 4'-C not resolved; ν_{max} / cm⁻¹ (solid) 3251, 3068, 2978, 1674, 1607; m/z (ESI⁺) found MH⁺ 401.1624, C₂₃H₂₀N₄O₂ MH requires 401.1608; HPLC RT = 2.69 mins.

N-[2-(ethylamino)-4-oxo-3,4-dihydroquinazolin-5-yl]pyridine-3-carboxamide 163

General method E using compound **175** (100 mg, 1.17 mmol). Purification using column chromatography (5% MeOH in CHCl₃) afforded the title compound (37 mg, 0.18 mmol, 16%) as colourless microcrystals. m.p. >250 °C; R_f 0.09 (EtOAc); δ_H (500 MHz, DMSO- d_6) 11.20 (br. s., 1 H, quinazolinone 3-NH), 9.82 (br. s., 1 H, 5-NHCO) 9.15 (s, 1 H, pyridyl 2-H), 8.80 (d, J 4.7 Hz, 1 H, pyridyl 6-H), 8.32 - 8.42 (m, 1 H, quinazolinone 6-H), 8.30 (d, J 7.7 Hz, 1 H, pyridyl 4-H), 7.63 (dd, J 7.7, 4.7 Hz, 1 H, pyridyl 5-H), 7.56 (app. t, J 8.1 Hz, 1 H, quinazolinone 7-H), 7.00 (d, J 8.1 Hz, 1 H, quinazolinone 8-H), 6.45 (br. s., 1H, 2-NHCH₂CH₃), 3.35 (qd, J 7.1, 5.6 Hz, 2 H, 2-NHCH₂CH₃), 1.15 (t, J 7.1 Hz, 3 H, 3-NHCH₂CH₃); δ_C (125 MHz, DMSO- d_6) 163.1 (5-NHCO), 152.6 (pyridyl 6-C), 148.1 (pyridyl 2-C), 140.1 (quinazolinone 5-C), 134.9 (quinazolinone 7-C), 134.8 (pyridyl 4-C),

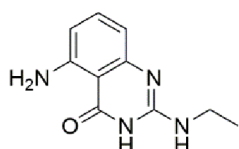
130.2 (quinazolinone C-4'), 124.1 (pyridyl 3-C), 124.0 (pyridyl 5-C), 118.8 (quinazolinone 8-C), 111.0 (quinazolinone 6-C) 104.5, 35.1 (2-NHCH₂CH₃), 14.6 (2-NHCH₂CH₃); ν_{\max} / cm⁻¹ (solid) 3029, 1674, 1643; m/z (ESI⁺) found MH⁺ 310.1302, C₁₆H₁₅N₅O₂ *MH* requires 310.1299; HPLC RT = 0.83 mins.

N-[2-(ethylamino)-4-oxo-3,4-dihydroquinazolin-5-yl]benzamide 164



General method E using compound **176** (200 mg, 0.727 mmol). Purification using column chromatography (1:1 to 7:3 EtOAc–Pet) followed by recrystallisation from EtOH afforded the title compound (34 mg, 0.11 mmol, 15%), as colourless microcrystals m.p. >250 °C; R_f 0.29 (1:1 EtOAc–Pet); δ_H (300 MHz, DMSO-*d*₆) 11.12 (br. s., 1 H, 3-H), 8.41 (d, J 7.9 Hz, 1 H, 5-NHCO), 8.00 (d, J 6.8 Hz, 2 H, 5-phenyl 2-H), 7.45 - 7.74 (m, 4 H, 7-H, 5-phenyl 3-H and 5-phenyl 4-H), 6.99 (d, J 7.9 Hz, 1 H, 6-H), 6.43 (br. s., 1 H, 2-NHCH₂CH₃, 8-H), 3.33 - 3.57 (m, 2 H, overlapped with H₂O signal, 2-NHCH₂CH₃), 1.17 (t, J 7.2 Hz, 3 H, 2-NHCH₂CH₃); δ_C (100 MHz, DMSO-*d*₆) 165.1 (C-4), 155.8 (2-C), 150.3 (8'C), 140.9 (5-C), 135.6 (5-phenyl 1-C), 135.1 (7-C), 132.6 (5-phenyl 4-C), 129.5 (4-phenyl 3-C), 127.5 (4'-C), 127.4 (4-phenyl 2-C), 119.8 (6-C), 111.3 (8-C), 35.6 (2-NHCH₂CH₃), 15.1 (2-NHCH₂CH₃) 5-NHCO not resolved; ν_{\max} / cm⁻¹ (solid) 3469, 3241, 3024, 1682, 1612; m/z (ESI⁺) found MH⁺ 309.1353, C₁₇H₁₆N₄O₂ *MH* requires 309.1346; HPLC RT = 2.06 mins.

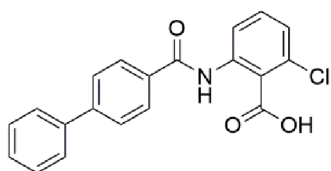
5-amino-2-(ethylamino)-1,4-dihydroquinazolin-4-one 169



General method E using 2-amino-6-chloro benzoic acid (200 mg, 1.17 mmol). Purification using column chromatography (5% MeOH in CHCl₃) afforded the title compound (37 mg, 0.18 mmol, 16%) as colourless microcrystals. m.p. 158.2 – 162.5 °C; R_f 0.25 (EtOAc); δ^H (500 MHz, DMSO-*d*₆) 10.41 (br. s., 1 H, 1-H), 7.11 (t, J 7.9 Hz, 1 H, 7-H), 6.89 (br. s., 2 H, 5-NH₂), 6.26 (d, J 7.7 Hz, 1 H, 8-H), 6.20 (d, J 8.1 Hz, 1 H, 6-H), 6.05 (br. s., 1 H, 2-NHCH₂CH₃), 3.16 - 3.30 (m, 2 H, 2-NHCH₂CH₃, overlapped with H₂O signal), 1.11 (t, J 7.1 Hz, 3 H, 2-NHCH₂CH₃); δ_C (100 MHz, DMSO-*d*₆) 162.8 (4-C), 151.3 (2-C), 135.0 (7-C), 110.6 (4'-C), 107.0 (6-C),

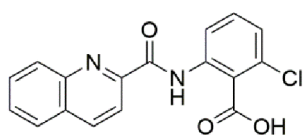
102.2 (8-C), 35.5 (2-NHCH₂CH₃), 15.2 (2-NHCH₂CH₃); ν_{\max} / cm⁻¹ (solid) 3409, 3040, 2870, 1673, 1603; m/z (ESI⁺) found MNa⁺ 277.0901, C₁₀H₁₂N₄O MNa requires 277.0903; HPLC RT = 1.36 mins.

2-chloro-6-(4-phenylbenzamido)benzoic acid 172



General method D using 4-phenyl benzoic acid (317 mg, 1.61 mmol) and 2-amino-6-chlorobenzoic acid (250 mg, 1.46 mmol). Purification using column chromatography (toluene) afforded the title compound (143 mg, 0.35 mmol, 24%) as colourless microcrystals, m.p. 227.6-231.3; R_f 0.57 (EtOAc); δ_H (500 MHz, CDCl₃) 8.30 (dt, J 8.7, 1.7 Hz, 2 H, 6-phenyl 3-H), 7.68 (dt, J 8.7, 1.7 Hz, 2 H, 4-phenyl 2-H), 7.51 - 7.65 (m, 4 H, 6-phenyl 2-H, 4-phenyl 4-H and 4-H), 7.30 - 7.48 (m, 4 H, 4-phenyl 3-H, 3-H and 5-H); δ_C (75 MHz, DMSO-*d*₆) 206.4 (1-CO₂H), 156.9 (6-NHCO), 155.7 (6-phenyl 4-C), 144.3 (4-phenyl 1-C), 136.6 (6-phenyl 1-C), 130.5 (6-C), 129.1 (4-C), 128.6 (2-C), 127.2 (1-C), 126.9 (4-phenyl 2-C), 126.3 (4-phenyl 3-C), 114.8 (5-C); ν_{\max} / cm⁻¹ (solid) 2836, 2545, 1675, 1606; m/z (ESI⁺) found MH⁺ 374.0549, C₂₀H₁₄ClNO₃ MNa⁺ requires 374.0554; HPLC RT = 3.35 mins.

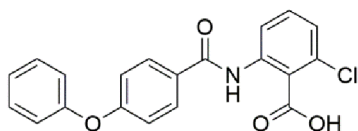
2-chloro-6-(quinoline-2-amido)benzoic acid 173



General method D using quinaldic acid (227 mg, 1.61 mmol) and 2-amino-6-chlorobenzoic acid (250 mg, 1.46 mmol). Purification using column chromatography (0.5% AcOH in EtOAc) afforded the title compound (227 mg, 0.85 mmol, 58%) as pale yellow microcrystals. m.p. 238.1-242.1 °C; R_f 0.40 (1:7 EtOAc-Pet); δ_H (500 MHz, DMSO-*d*₆) 11.46 (br. s, 1 H, COOH), 8.66 (d, J 8.5 Hz, 1 H, 6-quinoline 4-H), 8.41 (d, J 8.5 Hz, 1 H, 5-H), 8.26 (d, J 8.5 Hz, 1 H, 6-quinoline 3-H), 8.17 (d, J 8.5 Hz, 1 H, 6-quinoline 8-H), 8.13 (d, J 8.1 Hz, 1 H, 6-quinoline 5-H), 7.93 (app t, J 7.7 Hz, 1 H, 6-quinoline 7-H), 7.77 (app t, J 7.5 Hz, 1 H, 6-quinoline 6-H), 7.55 (t, J 8.1 Hz, 1 H, 4-H), 7.35 (d, J 7.7 Hz, 1 H, 3-H); δ_C (125 MHz, DMSO-*d*₆) 166.5 (1-CO₂H), 162.1 (6-NHCO), 148.8 (6-quinoline 2-C), 145.6 (6-quinoline 8-C'), 138.7 (6-quinoline 4-C), 136.8 (6-C), 131.5 (4-C), 131.5 (2-C), 131.0

(6-quinoline 7-C), 130.9 (1-C), 129.3 (6-quinoline 8-C or 6-C), 129.2 (6-quinoline 8-C or 6-C), 128.7 (6-quinoline 5-C), 128.2 (6-quinoline 4-C'), 125.5 (3-C), 119.8 (5-C), 118.4 (6-quinoline 3-C); ν_{\max} / cm^{-1} (solid) 3279, 2855, 1679, 1594; m/z (ESI⁺) found MH⁺ 327.0539, C₁₇H₁₁ClN₂O₃ MH requires 327.0531; HPLC RT = 2.91 mins.

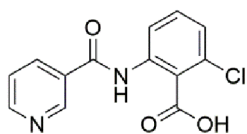
2-chloro-6-(4-phenoxybenzamido)benzoic acid 174



General method D using 4-phenyl benzoic acid (289 mg, 1.35 mmol) and 2-amino-6-chloro benzoic acid (250 mg, 1.46 mmol). MeOH (50 ml) was added to reaction

mixture and the resulting precipitate was collected by filtration to afford the title compound (106 mg, 0.289 mmol, 21%) as colourless microcrystals, m.p. 165.7-168.4; R_f 0.39 (toluene); δ_H (500 MHz, CDCl₃) 8.19 (dt, J 8.8, 2.0 Hz, 2 H, 6-benzamido 2-H), 7.60 (t, J 7.9 Hz, 1 H, 4-H), 7.50 (dd, J 7.9, 1.1 Hz, 1 H, 3-H), 7.43 (dd, J 7.9, 1.1 Hz, 1 H, 5-H), 7.35 (tt, J 7.8, 1.7 Hz, 2 H, 4-phenoxy 3-H), 7.15 (tt, J 7.9, 1.7 Hz, 1 H, 4-phenoxy 4-H), 6.96 - 7.06 (m, 4 H, 6-benzamido 3-H and 4-phenoxy 2-H); δ_C (125 MHz, DMSO- d_6) 161.7 (6-NHCO), 161.2 (1-CO₂H), 156.7 (6-benzamido 4-C), 155.7 (4-phenoxy 1-C), 155.0 (6-C), 149.0 (6-benzamido 1-C), 136.6 (4-C), 134.1 (2-C), 130.4 (6-benzamido 6-C), 130.3 (4-phenoxy 3-C), 126.2 (1-C), 124.9 (3-C), 124.0 (5-C), 120.0 (4-phenoxy 2-C), 117.7 (6-benzamido 3-C), 114.5 (4-phenoxy 4-C); ν_{\max} / cm^{-1} (solid) 3071, 2923, 1756, 1623; HPLC RT = 4.11 mins.

2-chloro-6-(pyridine-3-amido)benzoic acid 175

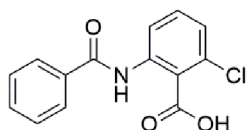


General method D using nicotinic acid (1.44 g, 11.7 mmol) and 2-amino-6-chloro benzoic acid (1 g, 5.84 mmol). Purification using column chromatography (DCM–MeOH 99:1) afforded the title compound

(341 mg, 1.24 mmol, 21%) as colourless microcrystals, m.p. 153.4-154.2 °C; R_f 0.18 (1:1 EtOAc–Pet); δ_H (500 MHz, DMSO- d_6) 9.31 (d, J 1.4 Hz, 1 H, 6-pyridyl 2-H), 8.85 (dd, J 4.6, 1.4 Hz, 1 H, 6-pyridyl 6-H), 8.49 (d, J 8.2 Hz, 1 H, 6-pyridyl 4-H), 7.90 (t, J 8.2 Hz, 1 H, 6-pyridyl 5-H), 7.68 - 7.76 (m, 2 H, 3-H and 4-H), 7.66 (dd, J 8.0, 4.8 Hz, 1 H, 5-H); δ_C (125 MHz, DMSO- d_6) 155.8 (1-CO₂H), 155.3 (6-NHCO), 153.13 (6-pyridyl 6-C),

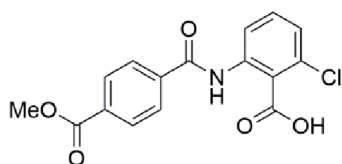
148.7 (6-pyridyl 2-C), 148.4 (6-pyridyl 3-C), 136.7 (6-pyridyl 6-C), 135.4 (6-pyridyl 4-C), 134.1 (6-C), 130.9 (4-C), 126.4 (3-C), 125.9 (2-C), 124.1 (5-C), 115.0 (1-C); ν_{\max} / cm^{-1} (solid) 3090, 1779, 1626; m/z (ESI⁻) found M-H 275.0220, $\text{C}_{12}\text{H}_9\text{ClN}_2\text{O}_3$ M-H requires 275.0229; HPLC RT = 1.96 mins.

2-benzamido-6-chlorobenzoic acid 176



General method D using benzoic acid (227 mg, 2.27 mmol) and 2-amino-6-chloro benzoic acid (250 mg, 1.46 mmol). Purification using column chromatography (toluene) afforded the title compound (213 mg, 0.775 mmol, 37%) as colourless microcrystals, m.p. 154.3-155.2 °C; R_f 0.59 (1:4 EtOAc-Pet); δ_{H} (300 MHz, CDCl_3) 8.25 - 8.38 (m, 2 H, 2-phenyl 2-H), 7.71 (t, J 7.9 Hz, 1 H, 4-H), 7.58 - 7.66 (m, 2 H, 2-phenyl 3-H), 7.48 - 7.58 (m, 3 H, 2-NHCO, 3-H and 5-H); δ_{C} (100 MHz, $\text{DMSO}-d_6$) 159.4 (CONH), 137.9 (2-C), 137.1 (4-C), 134.6 (2-phenyl 1-C), 133.5 (3-C), 131.0 (1-C), 130.1 (6-C), 129.6 (2-phenyl 4-C), 128.4 (2-phenyl 3-C), 127.9 (2-phenyl 2-C), 126.8 (5-C), 1-C not resolved; ν_{\max} / cm^{-1} (solid) 3065, 1755, 1625; m/z (ESI⁺) found MNa^+ 298.0204, $\text{C}_{14}\text{H}_{10}\text{ClNO}_3$ MNa requires 298.0241; HPLC RT = 3.60 mins.

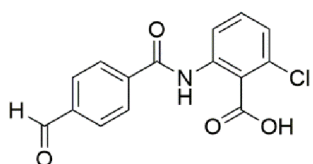
2-chloro-6-[4-(methoxycarbonyl)benzamido]benzoic acid 178



Monomethyl terephthalate (1.00 g, 5.56 mmol) was suspended in DMF under N_2 and NEt_3 (2.31 ml, 16.7 mmol) and T3P solution (50% in DMF, 6.5 ml, 11 mmol) were added. The reaction mixture was stirred at room temperature for two hours and then 2-amino-6-chlorobenzoic acid (613 mg, 5.56 mmol) was added. The reaction mixture was stirred for a further 18 hours and then a further 0.5 equivalents of T3P solution were added and the reaction mixture was heated to 75 °C for 18 hours. A further equivalent of NEt_3 was then added and the reaction mixture was heated to 100 °C for three hours before being allowed to cool to room temperature. Water (5 ml) was added and the resulting precipitate was collected by filtration to afford the title compound (700 mg, 2.10 mmol, 38%) as colourless needles. m.p. 198.2-201.3; R_f 0.5

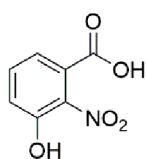
(1:4 EtOAc-Pet); δ_{H} (500 MHz, CDCl_3) 8.38 (d, J 8.55 Hz, 2 H, 6-benzamido 2-H), 8.19 (d, J 8.55 Hz, 2 H, 6-benzamido 3-H), 7.72 (t, J 7.69 Hz, 1 H, 4-H), 7.64 (dd, J 7.70, 1.00 Hz, 1 H, 3-H), 7.57 (dd, J 7.70, 1.07 Hz, 1 H, 5-H), 3.98 (s, 3 H, 6-benzamido-4- CO_2CH_3); δ_{C} (125 MHz, CDCl_3) 156.9 (6-NHCO), 155.7 (1- CO_2H), 149.0 (6-benzamido-4- CO_2CH_3), 136.2 (2-C), 136.0 (4-C), 133.8 (6-C or 6-benzamido 1-C), 133.6 (6-C or 6-benzamido 1-C), 131.2 (5-C), 129.9 (6-benzamido 3-C), 128.4 (6-benzamido 2-C), 126.5 (3-C), 114.9 (6-benzamido 4-C), 52.5 (6-benzamido-4- CO_2CH_3); ν_{max} / cm^{-1} (solid) 3039, 1767, 1725, 1631; HPLC RT = 3.63 mins.

2-chloro-6-(4-formylbenzamido)benzoic acid 183



General method C using 4-formyl benzoic acid (1.00 g, 6.67 mmol) and 2-amino-6-chlorobenzoic acid (1.04 g, 6.06 mmol). A pale yellow precipitate was removed from the reaction mixture by filtration. The filtrate was concentrated *in vacuo* to afford a yellow solid. Recrystallisation from toluene afforded the title compound (263 mg, 0.888 mmol, 14%) as pale yellow microcrystals. m.p. 207.4-210.2 °C; R_f 0.13 (EtOAc); δ_{H} (400 MHz, $\text{DMSO-}d_6$) 10.14 (s, 1 H, 6-phenyl 4-CHO), 8.38 (d, J 8.40 Hz, 2 H, 6-phenyl 3-H), 8.12 (d, J 8.40 Hz, 2 H, 6-phenyl 2-H), 7.90 (t, J 7.80 Hz, 1 H, 4-H), 7.72 (d, J 7.82 Hz, 2 H, 3-H and 5-H); δ_{C} (100 MHz, $\text{DMSO-}d_6$) 193.4 (6-phenyl 4-CHO), 156.6 (6-NHCO), 155.9, (1- CO_2H), 149.0 (6-phenyl 1-C), 139.2 (6-C), 137.2 (4-C), 135.1 (6-phenyl 4-C), 134.6 (2-C), 131.6 (5-C), 130.4 (6-phenyl 2-C), 129.4 (1-C), 129.0 (6-phenyl 3-C), 127.0 (3-C); ν_{max} / cm^{-1} (solid) 3085, 2820, 2736, 1760, 1697; m/z (ESI⁺) found MH^+ 304.0375, $\text{C}_{15}\text{H}_{11}\text{ClNO}_4$ MH requires 304.0371; HPLC RT = 2.49 mins.

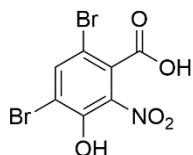
3-hydroxy-2-nitrobenzoic acid 185



3-chloro-2-nitrobenzoic acid (1.0g, 5.0 mmol) and NaOH (2.0g, 60 mmol) were dissolved in water (10 ml) and the reaction mixture was heated to reflux for 40 hours. The reaction mixture was then allowed to cool to room temperature and acidified to pH 3 by dropwise addition of HCl . The reaction mixture was extracted into EtOAc (4 × 30 ml) and the combined organic extracts were

washed with brine (20 ml), dried over MgSO_4 and concentrated *in vacuo* to afford an orange residue. Recrystallisation from EtOAc afforded the title compound (492 mg, 3.02 mmol, 60%) as pale yellow microcrystals. m.p. 163.5-165.8 °C; R_f 0.16 (EtOAc); δ_H (500 MHz, $\text{DMSO-}d_6$) 11.22 (s, 1 H, 3-OH), 7.49 (t, J 8.00 Hz, 1 H, 5-H), 7.41 (dd, J 7.79, 0.92 Hz, 1 H, 6-H), 7.31 (dd, J 8.25, 0.92 Hz, 1 H, 4-H); δ_C (125 MHz, $\text{DMSO-}d_6$) 163.6 (1- CO_2H), 148.1 (3-C), 138.5 (2-C), 129.3 (6-C), 123.5 (1-C), 119.9 (4-C), 119.5 (5-C); ν_{max} / cm^{-1} (solid) 3298, 3091, 2835, 2578, 1689; m/z (ESI⁺) found MNa^+ 227.9875, $\text{C}_7\text{H}_5\text{NO}_5$ MNa requires 227.9879; HPLC RT = 1.19 mins. Spectroscopic data consistent with literature values.¹⁵⁷

4,6-dibromo-3-hydroxy-2-nitrobenzoic acid **187**



Compound **185** (1.23 g, 6.72 mmol) was dissolved in EtOH (10 ml) and cooled to 0 °C, sodium acetate trihydrate (3.06 g, 2.25 mmol) and bromine (0.85 ml, 16 mmol) were then added to the solution. The reaction mixture was stirred at room temperature for 4 hours. The reaction mixture was concentrated *in vacuo* and the resulting pale orange residue was purified by trituration with Et_2O to afford the title compound (705 mg, 2.08 mmol, 31%) as pale orange microcrystals. m.p. 195.0-198.5 °C; R_f 0.10 (EtOAc); δ_H (500 MHz, $\text{DMSO-}d_6$) 8.50 (s, 1 H, 5-H); δ_C (75 MHz, $\text{DMSO-}d_6$) 165.2 (1- CO_2H), 158.1 (3-C), 136.2 (2-C), 134.2 (1-C), 128.8 (5-C), 110.9 (6-C), 109.6 (4-C); ν_{max} / cm^{-1} (solid) 3362, 3085, 2865, 1703, 1522; m/z (ESI⁻) found M-H 339.8288, $\text{C}_7\text{H}_3\text{Br}_2\text{NO}_5$ M-H requires 339.8285; HPLC RT = 3.19 mins. Spectroscopic data consistent with literature values.¹⁵⁷

7.2 Biological Methods

7.2.1 Instrumentation

Media, buffer and other equipment were sterilised using either a Prestige Medical bench top autoclave or an LTE Touchclave-R autoclave. All contaminated glassware, plastic-ware and media containing genetically modified bacteria was disposed of by bleaching, using either Virkon or Presept for 24 h or autoclaved (120 °C for 20 min) before disposal as aqueous waste or for incineration. Bacterial cultures were incubated in a Kuhner ShakerX ISF1-X or a Stuart orbital incubator. LB Agar plates and 96 well assay plates were incubated in a Binder BD23 incubator at 37°C. Centrifugation was carried out in a Beckman Coulter Avanti J-301 centrifuge and in bench-top centrifuges Pico and Fresco 17/21 from Thermo electron corporation. Cells were disrupted using a Constant Systems Cell Disrupter (T2/40/AA/AA). Size exclusion chromatography was performed using an Äkta Purifier FPLC from GE Healthcare. Protein and DNA concentrations were determined using a Nanodrop2000 UV/Vis spectrophotometer (Thermo Scientific). SDS-PAGE electrophoresis was carried out using a Bio-Rad mini-protean 3 apparatus and the polyacrylamide gels were imaged with both UV and white light using a Bio-Rad molecular imager Gel Doc XR. Broad range (2-212 kDa) protein marker from New England Biolabs (NEB) was used as a reference. Water was purified before use to 15 Mq using an ELGA PURLAB Classic purification system. Protein mass spectrometry was performed in original buffers on a Bruker MaXis impact spectrometer and the raw mass spectra were deconvoluted using a maximum entropy algorithm part of Bruker data analysis. Results are quoted as mass-charge ratios (m/z). Spectrophotometry of 96 well plates was carried out using a Perkin Elmer EnVision plate reader.

7.2.2 Materials

Analytical grade reagents were purchased from Sigma Aldrich, VWR International, Fisher Scientific and Alfa Aesar unless otherwise stated. Ni-NTA agarose was purchased from Qiagen. Enzymes, buffers and molecular weight markers were supplied by New

England Biolabs. DNase I recombinant and Protease inhibitor cocktail (cOmplete™) were purchased from Roche Diagnostics.

Media

Lysogeny Broth (LB): LB pre-mix freeze dried powder (consisting of tryptone (10 g/L), yeast extract (5 g/L), NaCl (10 g/L)) was made up with purified water to a quantity of 25 g/L, autoclaved at 121 °C for 20 minutes as required and allowed to cool before use.

Agar

Agar plates were made with agar (15 g/L) and LB (25 g/L) before being autoclaved at 121 °C for 20 minutes and stored at 60 °C. Agar was allowed to cool for 15 minutes before being inoculated with the desired antibiotic, poured onto Petri dishes in 20 ml portions and left to set in a sterile environment. Plates were stored at 4 °C prior to use.

Plasmids

Plasmids used during the project are given in Table 7.1.

Table 7.1 Plasmids used during the project

Name	Resistance	Promotor	Genes encoded
pAM24 JM109	Ampicilin	T7	GyrB24
pAG111	Ampicilin	T7	GyrB
pPH3 JM109	Ampicilin	T7	GyrA
pNIC-GB1	Kanamycin	T7	His ₆ -GB1
pNIC-GB1-GyrB24	Kanamycin	T7	His ₆ -GB1-GyrB24
pNIC-GB1-GyrA	Kanamycin	T7	His ₆ -GB1-GyrA
pNIC-GB1-GyrB	Kanamycin	T7	His ₆ -GB1-GyrB

pAM24, pAG111 and pPH3 were generously provided to us by the Maxwell group at the John Innes centre. pNIC vectors were a kind gift from Dr. Charles Allerston and Dr. Opher Gileadi, at the Oxford site of the Structural Genomics Consortium (www.addgene.org/Opher_Gileadi/), to the Driscoll group at the NIMR, London. pNIC-GB1 was constructed at the NIMR from pNIC-GST by Dr. TJ. Ragan. All other pNIC plasmids were produced with the assistance of Gemma Wildsmith at the University of Leeds according to the procedure described in Section 7.2.7.

Buffers and Stains

Buffers for size exclusion chromatography were vacuum filtered through a 0.22 μM membrane prior to use. Buffers used in the manipulation of DNA described in section 7.2.7 were purchased from New England Biolabs (NEB) or EMD Millipore as stated.

5X assay buffer for coupled assay: 250 mM Tris pH 7.5, 5 mM EDTA, 25 mM MgCl_2 , 25 mM DTT, 50% glycerol

Dilution buffer for coupled assay: 50 mM Tris pH 7.5, 100 mM KCl, 2 mM DTT, 1 mM EDTA, 50% glycerol

TGED buffer: 50 mM Tris pH 7.5, 10% glycerol, 1mM EDTA, 5 mM DTT

High glycerol TGED: 50 mM Tris pH 7.5, 30% glycerol, 1mM EDTA, 5 mM DTT

SDS-PAGE loading buffer: 100 mM Tris pH 6.8, 4% SDS, 400 mM DTT, 20% glycerol, 0.6 mM bromophenol blue

5 \times SDS-PAGE running Buffer: 125 mM Tris, 960 mM glycine, 0.5% SDS

Coomassie Stain: 0.25% Coomassie blue R-250, 40% methanol, 10% acetic acid

Coomassie Destain: 40% methanol, 10% acetic acid

Lysis buffer: 50 mM Tris pH 8, 500 mM NaCl

Wash buffer: 50 mM Tris pH 8, 500 mM NaCl, 50 mM imidazole

Elution buffer: 50 mM Tris pH 8, 500 mM NaCl, 300 mM imidazole

7.2.3 Methods

7.2.4 Malachite green assay⁴

Gyrase converts ATP into ADP and inorganic phosphate. The released phosphate can be detected by the addition of malachite green solution and measured by monitoring the increase in absorbance at 600 nm. The ATPase assay measures the amount of ATP being cleaved to ADP and P_i by reaction of the P_i with malachite green dye. For IC_{50} determinations each compound was tested once at multiple concentrations. Singlicate

⁴ Malachite green assay was performed at **Biota Europe Ltd.**, Begbroke Business & Science Park, Sandy Lane, Yarnton, Oxfordshire, OX5 1PF.

samples were taken after 60 minutes and IC_{50} values were determined. Enzyme supplied by Inspiralis was used in all assays.

The ATPase assay was carried out in a buffer containing 2 mU/ μ l Gyrase enzyme (A_2B_2 complex from *S. aureus*), 0.08 mg/ml double stranded DNA, 8 mM HEPES.KOH pH 7.6, 100 mM potassium glutamate, 2 mM magnesium acetate, 2 mM DTT, 0.01 mg/ml BSA, and 5% DMSO solution containing the inhibitor. Alternatively, the ATPase assay was carried out in a buffer containing 4.8 μ g/ml Gyrase enzyme (A_2B_2 complex from *E. coli*), 0.08 μ g/ml ssDNA, 35 mM Tris pH 7.5, 24 mM KCl, 2 mM $MgCl_2$, 6.5% Glycerol, 2 mM DTT, 1.8 mM Spermidine, 0.5 mg/ml BSA and 5% DMSO solution containing the inhibitor. The reaction is started by adding ATP to a final concentration of 1 mM and allowed to incubate at 30 °C for 60 minutes. The reaction was stopped by adding 200 μ l of malachite green solution (0.034% malachite green, 10 mM ammonium molybdate, 1 M HCl, 3.4% ethanol, 0.01% tween 20). Colour was allowed to develop for 5 minutes and the absorbance at 600 nm was measured spectrophotometrically. The IC_{50} values were determined from the absorbance readings using no compound and no enzyme controls.

7.2.5 Coupled assay

The coupled enzyme ATPase assay is based on the conversion of phosphoenolpyruvate (PEP) to pyruvate by pyruvate kinase (PK) coupled to the conversion of pyruvate to lactate by lactate dehydrogenase (LDH). This step requires NADH which is oxidized to NAD^+ . NADH absorbs strongly at 340 nm but NAD^+ does not, enabling the reduction of NADH over time to be followed by monitoring the decrease in absorbance at 340 nm (A_{340}).

A typical 96 well plate set-up would contain 3 repeats of each of the following conditions: a no-enzyme control containing all components of the assay except the Gyrase or topoisomerase IV enzyme; a no-compound control containing water instead of an inhibitor. Four dilution series comprising seven concentrations of inhibitor (novobiocin was always used as one of the four as a control, as it is a commercially available inhibitor of known activity). The six remaining wells in the plate could be used to measure activity of two inhibitors at a single concentration.

An assay mix was prepared immediately prior to use; components of the assay mix and quantities needed are given in Table 7.2. Stock solutions were stored at $-20\text{ }^{\circ}\text{C}$ until needed. PK/LDH solution purchased from Aldrich as a buffered aqueous glycerol solution containing 900-1400 units/ml of LDH and 600-1000 units/ml of PK from rabbit muscle. NADH solutions were made up fresh immediately prior to each assay and kept in the dark on ice until all other preparations were complete. NADH was the last component added to the assay mix and was only added immediately prior to use.

Table 7.2 Components of a typical assay mix with quantities needed per well and per 96 well plate.

Component	Quantity required per well/ μL	Quantity needed to provide sufficient mixture for a 96 well plate/ μL
5X assay buffer	20	2000
2 mg/ ml DNA solution	3	300
80 mM PEP solution	1	100
PK/LDH solution	1.5	150
10 mM NADH	2	200
water	47.5	4750
total	75	7500

To each well of a 96 well plate 10 μL of water or an inhibitor solution at the appropriate concentration, 75 μL of assay mix and 10 μL of enzyme solution (500 nM in dilution buffer) (or dilution buffer in the case of the no-enzyme control) was added and the contents of each well mixed. Absorbance at 340 nm was monitored once per minute for 5 minutes and then 5 μL of ATP solution (40 mM) added to each well. Absorbance at 340 nm was monitored once per minute for 20-30 minutes as required to see a significant decrease in absorbance in all wells except the no-enzyme control.

IC_{50} curves were plotted using GraphPad Prism 6¹⁶² and are shown in Figure 7.1 and Figure 7.2.

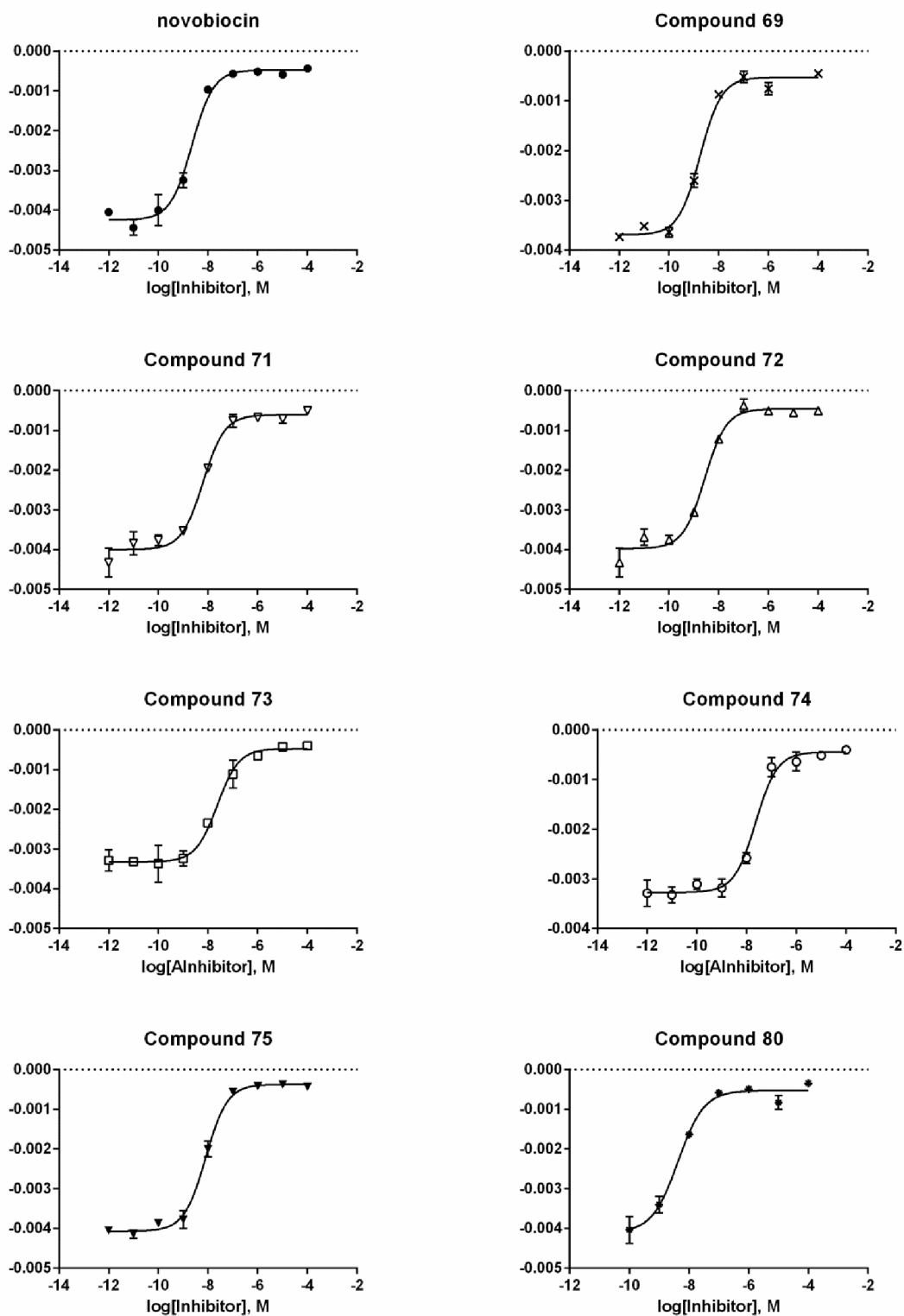


Figure 7.1 IC_{50} curves for novobiocin and compounds 69, 71, 72, 73, 74, 75 and 80.

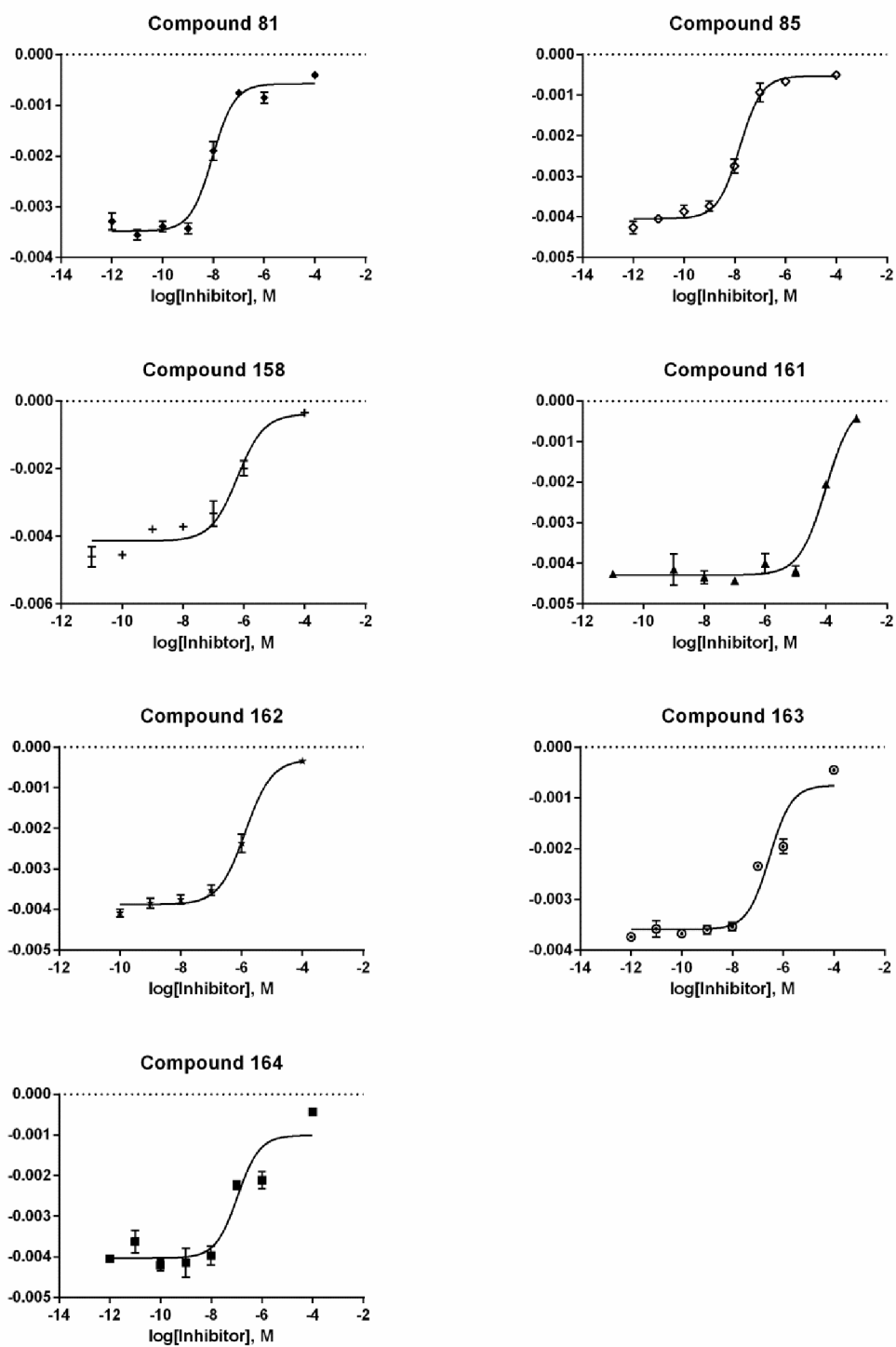


Figure 7.2 IC_{50} curves for compounds 81, 85, 158, 161, 162, 163 and 164.

7.2.6 MIC determination⁵

The minimal inhibitory concentration (MIC) is the lowest compound concentration needed to inhibit visible bacteria growth or to inhibit growth based on absorbance readings. The bacterial strains tested were: *Klebsiella pneumoniae* ATCC 13882; *Acinetobacter baumannii* ATCC 19606; *Pseudomonas aeruginosa* ATCC 27853, *Escherichia coli* ATCC 25922 and *Staphylococcus aureus* ATCC 29213. All strains were grown in Müller-Hinton (MH) broth. Compounds were tested by doubling dilutions over the concentration range: 0.12-64 µg/ml. Compounds were tested for antimicrobial activity by susceptibility testing in liquid media. MICs for compounds against each strain were determined by the broth microdilution method according to the guidelines of the Clinical Laboratories and Standards Institute (CLSI) Methods for Dilution Antimicrobial Susceptibility Tests for Bacteria That Grow Aerobically¹⁶³.

7.2.7 Cloning of DNA gyrase genes into pNIC

The GyrB24, GyrB and GyrA genes were subcloned from the pAM24, pAG111 and pPH3 plasmids generously provided by the Maxwell group at the John Innes Centre into a pNIC plasmid using ligation independent cloning (LIC).

7.2.7.1 Linearisation of vector by digestion with BsaI

The pNIC vector (5 µg) was combined with 5 µl of 10× NEB buffer 4, 1 µl of BSA and 3 µl of BsaI-HF (10 units/ µl) and the volume made up to 50 µl with water. The digestion mix was incubated for 2 hours at 37 °C and the digested DNA isolated by agarose gel electrophoresis and purified using a QIAquick gel extraction kit.

7.2.7.2 T4 DNA polymerase treatment of the vector

The vector was then treated with T4 polymerase to generate sticky ends. 600 ng of the linearised vector were added to a 1.5 ml Eppendorf tube along with 2 µl of 10× NEB buffer 2, 2 µl of 25 mM dGTP, 2 µl of 50 mM DTT, 0.5 µl of BSA and 0.5 µl of T4 DNA polymerase (3 units/µl) and the volume made up to 20 µl with water. The digestion mix was incubated for 30 minutes at 22 °C and 20 minutes at 75 °C.

⁵ MIC determination was initially performed at Biota Europe Ltd., Begbroke Business & Science Park, Sandy Lane, Yarnton, Oxfordshire, OX5 1PF and later at the University of Leeds by Anna Lipell or Victoria Lee.

7.2.7.3 PCR amplification of the Insert

DNA for the proteins of interest was amplified from an expression plasmid: pAM24, pAG111 and pPH3 were the plasmid containing the GyrB24, GyrB and GyrA genes respectively. PCR reactions were prepared in thin walled PCR tubes on ice using the KOD Hotstart Polymerase Kit (Novagen). An example of a typical PCR reaction is shown in Table 7.3, a typical PCR program is shown in Table 7.4.

Table 7.3 PCR reaction for insert preparation in 100 μ l

Reagent	Final Concentration	Volume
Template DNA	20 ng	Up to 1 μ l
KOD Hotstart buffer	1x	10 μ l
dNTP mix	200 μ M	10 μ l
MgSO ₄	1.5 mM	6 μ l
Forward primer	0.5 μ M	5 μ l of 10 μ M stock
Reverse primer	0.5 μ M	5 μ l of 10 μ M stock
KOD enzyme	1 U	2 μ l
H ₂ O	N/A	Up to 100 μ l

Table 7.4 A typical PCR program for insert preparation

Step	Time	Temperature (°C)	Cycles
Denaturation	2 min	95	1
Denaturation	30 sec	95	30
Annealing	30 sec	56	
Extension	30 sec ^a	72	
Extension	10 min	72	1
Hold		4	1

a) one minute per 1 kb.

Clean amplification of the insert was checked by agarose gel electrophoresis and the DNA purified using a Qiagen PCR clean-up kit.

7.2.7.4 T4 polymerase treatment of the insert

The insert was then treated with T4 polymerase to generate sticky ends. 0.2 pmol of the insert were added to a 0.5 ml Eppendorf tube along with 2 μ l of 10 \times NEB buffer 2, 2 μ l of 25 mM dCTP, 2 μ l of 50 mM DTT, 0.5 μ l of BSA and 0.5 μ l of T4 DNA polymerase (3 units/ μ l) and the volume made up to 20 μ l with water. The digestion mix was incubated for 30 minutes at 22 °C and 20 minutes at 75 °C.

7.2.7.5 Annealing of the vector and insert

The concentration of the vector and the insert were determined using a Nanodrop2000 UV/Vis spectrophotometer (Thermo Scientific) at measuring absorbance at 260 nm and 320 nm and the following equations:

$$\text{Concentration } (\mu\text{g ml}^{-1}) = (A_{260} - A_{320}) \times 50 \mu\text{g ml}^{-1}$$

$$\text{Yield } (\mu\text{g}) = \text{Concentration } (\mu\text{g ml}^{-1}) \times \text{volume (ml)}$$

$$\text{Yield (nmoles)} = \frac{\text{yield } (\mu\text{g})}{\text{number of base pairs} \times 0.65}$$

0.1 pmol of the vector and 0.2 pmol of the insert were combined and incubated at room temperature for 20 minutes.

7.2.7.6 Transformation of the annealing product into ultracompetent *E. coli*

A tube of XL10-gold ultracompetent cells (Agilent) was thawed on ice for 10 minutes. 20 μl of cells were added to 2 μl of the annealing mixture and gently mixed. The cells were incubated for 30 minutes on ice and then heat shocked for 30 seconds at 42 °C. The cells were immediately cooled on ice for 5 minutes and then 950 μl of SOC medium added to the tube and the tubes incubated in a shaking incubator at 37 °C for an hour. The tubes were centrifuged at 5000 rpm for 2 minutes and 850 μl of the supernatant removed. The cells were resuspended in the remaining supernatant and plated onto LB agar plates containing 50 $\mu\text{g/ml}$ kanamycin pre-warmed to 37 °C. The plates were incubated at 37 °C overnight.

7.2.7.7 DNA purification and sequence determination

Two colonies were chosen to confirm that subcloning had occurred successfully. The colonies were used to inoculate 10 ml of sterile LB medium containing kanamycin and grown overnight at 37 °C in a shaking incubator. Plasmid DNA was purified from overnight cultures using the Qiaprep miniprep kit and purified plasmids sent to GATC Biotech for Sanger sequencing. Plasmid DNA was sent away at the concentration of 30-75 ng/ μl in 30 μl aliquots. Sequencing confirmed the presence of the desired gene in the pNIC plasmid.

7.2.7.8 Preparation of *E. coli* glycerol stocks

The plasmid was extracted from the frozen cell stock and transformed into BL21-Gold (DE3) (Agilent) cells for protein expression using the method described in Section 7.2.7.6. A well isolated colony from a fresh transformation was used to inoculate 10 ml of sterile LB medium containing kanamycin in a 50 ml Falcon tube. The culture was grown in a shaking incubator at 37 °C for 4-6 hours until the optical density at 600 nm had reached 0.6, 1 ml of culture was mixed vigorously with 400 µl of sterile glycerol (40% w/v) in 1.5 ml cryovials and stored at -80 °C.

7.2.8 Production and purification of GyrB24, GyrB and GyrA proteins

A starter culture was produced by inoculation of 2 × 20 ml of sterile LB media in a 50 ml falcon tube with cells from a frozen glycerol stock. Kanamycin was added and the culture was incubated over night at 37 °C with shaking at 230 rpm.

The starter culture was pelleted at 3000 rpm for 10 minutes and the supernatant discarded. The cell pellets were resuspended in sterile LB media and added to 0.5 L of LB media containing kanamycin (60 µg/ml). The cell culture was incubated at 37 °C with shaking at 200 rpm and 1 ml aliquots taken at regular intervals to measure the optical density at 600 nm (OD₆₀₀). Once the OD₆₀₀ reached ~0.6, protein expression was induced by the addition of IPTG to a concentration of 0.5 mM. The cell culture was incubated at 20 °C for 18 hours with shaking at 200 rpm and the cells harvested by centrifugation at 6000 rpm at 4 °C for 10 minutes.

The supernatant was decanted and the cell pellets resuspended in lysis buffer (50 ml per litre of cell culture). Protease inhibitor cocktail was added prior to cell lysis. Cells were lysed using a constant cell disrupter (20 psi, 5 ml injections). Cell lysate was clarified by centrifugation at 16000 rpm for 30 minutes at 4 °C. The supernatant was decanted and DNase (Roche) added.

Hexahistidine-tagged proteins were purified by Ni-NTA (Qiagen) chromatography. 4 ml of Ni-NTA resin was packed into a gravity-driven column (BioRad Econopac) and equilibrated with 10 column volumes (CV) of lysis buffer. The supernatant was applied to the column and the flow-through loaded onto the column a second time. The resin

was washed with 5 CV of lysis buffer followed by 5 CV of wash buffer and eluted with elution buffer. Elution was monitored using the Bio-rad Bradford protein assay. Elution buffer was applied until protein was no longer detected. 15 µl of each step was collected and analysed by SDS-PAGE. Fractions containing the desired protein were concentrated by centrifugal concentration to a volume of <10 ml using Amicon Ultra-15 centrifugal filter devices (Millipore) with a 10000 Da molecular weight cut off.

After every four uses of the column the column was stripped and regenerated by washing with the following sequence of solutions: 5 CV of 0.1% SDS, 5 CV of 0.1 M NaOH, 5 CV of 10 mM EDTA, 20 CV water, 2 CV 500 mM NiSO₄ and 20 CV of water. The column was stored in 20% EtOH at 4 °C between uses.

The pNIC-GB1 plasmid contains a tobacco etch virus (TEV) cleavage site (ENLYFQ*S) to enable removal of the H6 and GB1 tags. Treatment with TEV protease yields a non-native N-terminal serine. Recombinant H₆-TEV protease was prepared in-house.

TEV protease was added to the concentrated eluate obtained from the Ni-NTA column at an approximate ratio of 1:100 by volume. The eluate was then dialysed for 18 hours at 5 °C into 200× the sample volume of 20 mM Tris-HCl, 300 mM NaCl, 1 mM DTT pH 8. The dialysis bag was then transferred into 200× the sample volume of 20 mM Tris-HCl, 150 mM NaCl, pH 8 and dialysed at 4 °C for 18-24 hours. The TEV-cleaved sample was then loaded into a pre-equilibrated Ni-NTA column and washed with lysis buffer. Samples of the flow-through and wash were analysed by SDS-PAGE. Fractions containing the desired protein were combined and concentrated by centrifugal concentration to a volume <10 ml.

Size exclusion chromatography was carried out as a final purification step using an AKTA purifier chromatography system (GE Healthcare) with a prepacked HiLoad 26/60 Superdex 200 or HiLoad 16/60 Superdex 75 prep grade column (GE healthcare) equilibrated with the appropriate buffer. Fractions were analysed by SDS-PAGE and fractions containing the desired protein were concentrated to the desired volume by centrifugal concentration.

Protein concentration was determined using a Nanodrop2000 UV/Vis spectrophotometer (Thermo Scientific). Absorbance at 280 nm is measured and the

Beer-Lambert Law ($A=\epsilon CL$) used to calculate concentration. A is the absorbance at 280 nm, C is the protein concentration (M), ϵ is the molar extinction coefficient ($M^{-1} \text{ cm}^{-1}$) and L is the path length (cm). Molar extinction coefficients for each protein constructs were predicted using the Expasy ProtParam server.

To produce the full DNA gyrase protein for use in assays, equimolar portions of the GyrB and GyrA proteins were combined in high glycerol TGED buffer and placed on a shaker at room temperature for half an hour. The mixture was then divided into aliquots and flash frozen. Enzyme activity was measured using the coupled assay (as described in Section 7.2.5) and was consistent with reported values. DNA gyrase protein was stored at $-80\text{ }^{\circ}\text{C}$

7.2.9 SDS-PAGE analysis

Protein samples were mixed in a 3:1 ratio with 4 × loading buffer (typically 15 μl of protein and 5 μl of loading buffer) and heated to $95\text{ }^{\circ}\text{C}$ for 5 minutes. Samples were allowed to cool before loading 10 μL onto the gel. A molecular weight marker was added to one lane of the gel.

Stacking and resolving gels were prepared using the quantities given in Table 7.5. All components were mixed thoroughly by inversion and TEMED was added immediately prior to casting. The resolving gel was poured to fill ~80% of the mould and methanol added to fill the remaining space. After 20 minutes the methanol was removed by blotting and the stacking gel added to the mould on top of the resolving gel and a comb of 10 or 15 lanes was inserted into the mould and left to set for 20 minutes.

Table 7.5 Component quantities needed to make two SDS-PAGE gels.

Component	Stacking gel	Resolving gel
Water (ml)	3.32	4.257
0.5 M Tris (pH 6.8) (ml)	0.945	-
1.5 M Tris (pH 8.8) (ml)	-	2.533
40% acrylamide (ml)	0.624	3
10% SDS (ml)	0.05	0.1
15% APS (ml)	0.1	0.2
TEMED (ml)	0.01	0.01
Total (ml)	5	10

The set gel was incorporated into a running vessel and the inner chamber filled with running buffer (5× SDS-PAGE running buffer diluted 1:4 with water). The gel was

loaded with the required samples and the outer chamber filled to the appropriate level with running buffer. The gel was run at 180 V for 45 minutes.

Gels were stained by immersion in Coomassie stain for 1-2 hours at room temperature with rocking and then destained by immersion in Coomassie destain for 3 hours with rocking or in Coomassie destain for 1 hour followed by immersion in water over night. Gels were washed with water before being photographed.

7.2.10 Crystallography

Instrumentation

Optimisation of crystallisation conditions was set up using an Oryx8 Protein Crystallisation Robot from Douglas Instruments and crystallisation was monitored using a CrystalMation Gallery DT Minstrel DT protein crystal drop imager from Rigaku. Crystallographic data was collected at the Diamond light source, Oxfordshire, UK using either beamline I24 or I04.

Methods

GyrB24 was crystallised at 10 mg/ml in high glycerol TEGD buffer in the presence of 1 mM of inhibitors **69**, **71**, **72** or **86** with or without seed crystals. All crystallisations were carried out at a constant temperature of 20 °C. Conditions previously reported in the literature (20% PEG400, 100 mM Hepes pH 6.5) were optimised using an Oryx8 Protein Crystallisation robot (Douglas Instruments) in 96 well MRC sitting drop plates (Molecular Dimensions) with a reservoir volume of 60 µl and drops consisting of 0.3 µl of protein and 0.3 µl of well solution. In the presence of **72** crystals appeared after a few days from conditions containing 25-30% PEG400 and 100 mM Hepes pH 6.5.

In order to obtain suitable crystals for GyrB 24 with inhibitors **69**, **71** and **86** microseeding was required. A seed stock was prepared by taking a drop containing crystals formed in the presence of compound **72** and crushing them in 60 µl of well solution. Optimisation was then carried out using the same conditions except the drops consisted of 0.3 µl of protein, 0.3 µl of well solution and 0.1 µl of the seed stock. A range of improved crystals were obtained and these were then used to prepare a new seed stock in the same manner. Useable crystals were obtained for GyrB24 in the presence of each of the inhibitors from 25-30% PEG400 and 100 mM Hepes pH 6.5.

Crystals were manipulated using LithoLoops (Molecular Dimensions) and transferred to a cryoprotectant solution containing of 36% PEG400 and 100mM Hepes pH 6.5 with addition of 1 mM of each inhibitor. Crystals were flash-cooled in liquid nitrogen and stored in Unipuck cassettes (MiTeGen) prior to transport to the synchrotron. Crystals were subsequently transferred robotically to the goniostat on the beamline at the Diamond Light Source (Oxfordshire, UK) and maintained at -173 °C with a Cryojet cryocooler (Oxford Instruments). Diffraction data were recorded on beamline I24 or I04. For each crystal a total of 3600 x 0.1° oscillation images were recorded in a single sweep.

All X-ray data were processed using Xia2^{164,165} and the resultant data collection statistics are summarised in **Table 7.6**. The crystals belonged to either space group P3₁21 or P3₂21 with approximate cell parameters of $a = b = 99$, $c = 50$ Å. All subsequent data processing was carried out using programs from the CCP4 suite¹⁴⁴. Estimation of the content of the asymmetric unit (ASU) suggested that 1 copy of the TEV cleaved protein (molecular weight 24,242 Da) was present giving a solvent content of 59.7 %).¹⁶⁶

The compound **72** crystal structure was solved using molecular replacement with PDB entry chain A of 4URO¹⁴¹ with Novobiocin and waters removed using Phaser¹⁶⁷. The top solution was for space group P3₂21. Rigid body refinement following restrained refinement was then carried out giving initial R_{work} and R_{free} values of 0.446 and 0.422 respectively and a figure-of-merit (FOM) of 0.50 at 1.9X Å resolution. Clear density could be seen for the presence of compound **72**. This was drawn using Libcheck¹⁶⁸ and Prodrug¹⁶⁹ was then used to create pdb file and dictionary entry. Compound **72** was successfully built into the density. Several iterations of model building with COOT¹⁷⁰ and restrained refinement with REFMAC5^{168,171} were carried out. For the final stages of refinement TLS refinement was carried out using the suggested 8 TLS domain from the pdb redo server.¹⁷² The final model consisted of 204 residues, 84, water molecules, one inhibitor molecule and one PEG molecule with R_{work} and R_{free} values of 0.201 and 0.223 respectively. This structure was then used as the starting model for refinement of the other 3 structures. Full refinement statistics for all four structures are given in Table 7.6. MolProbity¹⁷³ was used to validate the models.

Table 7.6
X-Ray Data Collection and Refinement Statistics for GyrB24 protein crystal structures.

	69	71	72	86
Data collection				
Crystal	GyrB24_28	GyrB24_12	GyrB24_6	GyrB24_35
Beamline	I04, Diamond Light Source, UK	I24 Diamond Light Source, UK	I24, Diamond Light Source, UK	I04, Diamond Light Source, UK
Wavelength (Å)	0.9795	0.9790	0.9790	0.9795
Detector	Pilatus 6M-F	Pilatus3 6M	Pilatus3 6M	Pilatus 6M-F
Resolution range (Å)	50.27 – 2.50 (2.57 – 2.50)	49.90 – 1.95 (2.00 – 1.95)	49.67 – 1.90 (1.95 – 1.90)	49.68 – 2.35 (2.41 – 2.35)
Space Group	P3 ₂ 21	P3 ₂ 21	P3 ₂ 21	P3 ₂ 21
Cell parameters (Å)	$a = b = 100.20, c = 50.27$	$a = b = 99.79, c = 50.21$	$a = b = 99.34, c = 50.21$	$a = b = 99.36, c = 50.03$
Total no. of measured intensities	101076 (7177)	209856 (14777)	221669 (15948)	117906 (8962)
Unique reflections	10325 (735)	21281 (1561)	22689 (1657)	12122 (878)
Multiplicity	9.8 (9.8)	9.9 (9.5)	9.8 (9.6)	9.7 (10.2)
Mean $I/\sigma(I)$	10.6 (1.4)	7.2 (1.4)	8.0 (1.3)	8.5 (1.5)
Completeness (%)	100.0 (100.0)	99.9 (99.2)	99.7 (99.0)	100.0 (100.0)
R_{merge}^a	0.177 (1.599)	0.188 (1.470)	0.178 (1.426)	0.188 (1.490)
R_{meas}^b	0.197 (1.784)	0.210 (1.646)	0.198 (1.594)	0.210 (1.655)
$CC_{\frac{1}{2}}^c$	0.997 (0.528)	0.993 (0.468)	0.996 (0.506)	0.996 (0.485)
Wilson B value (Å ²)	33.4	28.6	21.5	34.8
Refinement				
Resolution range (Å)	50.27 – 2.50	49.90 – 1.95	49.67 – 1.90	49.68 – 2.35
Reflections: working/free ^d	687: 42	1490: 65	1581: 72	834: 44
$R_{\text{work}}/R_{\text{free}}^e$	0.208/0.249	0.195/0.231	0.201/0.223	0.220/0.252

Ramachandran plot: favoured/allowed/disallowed ^f (%)	98.4/100.0/0.0	98.9/100.0/0.0	98.4/100.0/0.0	98.9/100.0/0.0
R.m.s. bond distance deviation (Å)	0.011	0.013	0.013	0.007
R.m.s. bond angle deviation (°)	1.584	1.651	1.687	1.285
No. of protein residues: chain A	204	204	204	204
No. of water molecules/Compound/PEG	53/1/1	84/1/1	84/1/1	73/1/1
Mean <i>B</i> factors: protein/water/overall (Å ²)	37.7/45.5/36.9		25.9/40.6/26.2	37.7/51.4/37.8

Values in parentheses are for the outer resolution shell.

^a $R_{\text{merge}} = \frac{\sum_{hkl} \sum_i |I_i(hkl) - \langle I(hkl) \rangle|}{\sum_{hkl} \sum_i I_i(hkl)}$.

^b $R_{\text{meas}} = \frac{\sum_{hkl} [N/(N-1)]^{1/2} \times \sum_i |I_i(hkl) - \langle I(hkl) \rangle|}{\sum_{hkl} \sum_i I_i(hkl)}$, where $I_i(hkl)$ is the i th observation of reflection hkl , $\langle I(hkl) \rangle$ is the weighted average intensity for observations i of reflection hkl and N is the number of observations of reflection hkl .

^c $CC_{1/2}$ is the correlation coefficient between symmetry equivalent intensities from random halves of the dataset.

^d The data set was split into "working" and "free" sets consisting of 95 and 5% of the data respectively. The free set was not used for refinement.

^e The R-factors R_{work} and R_{free} are calculated as follows: $R = \frac{\sum (|F_{\text{obs}} - F_{\text{calc}}|)}{\sum |F_{\text{obs}}|} \times 100$, where F_{obs} and F_{calc} are the observed and calculated structure factor amplitudes respectively.

^f As calculated using MolProbity.¹⁷³

References

1. *Antimicrobial Resistance Global Report on Surveillance* World Health Organisation, 2014.
2. O'Neill, J. *Antimicrobial Resistance: Tackling a crisis for the health and wealth of nations*, 2014.
3. Liu, Y.-Y.; Wang, Y.; Walsh, T. R.; Yi, L.-X.; Zhang, R.; Spencer, J.; Doi, Y.; Tian, G.; Dong, B.; Huang, X.; Yu, L.-F.; Gu, D.; Ren, H.; Chen, X.; Lv, L.; He, D.; Zhou, H.; Liang, Z.; Liu, J.-H.; Shen, J. *Lancet Infect. Dis.* **2015**, *16*, 161.
4. Arcilla, M. S.; van Hattem, J. M.; Matamoros, S.; Melles, D. C.; Penders, J.; de Jong, M. D.; Schultsz, C. *Lancet Infect. Dis.* **2015**, *16*, 147.
5. Olaitan, A. O.; Chabou, S.; Okdah, L.; Morand, S.; Rolain, J.-M. *Lancet Infect. Dis.* **2015**, *16*, 147.
6. Webb, H. E.; Granier, S. A.; Marault, M.; Millemann, Y.; den Bakker, H. C.; Nightingale, K. K.; Bugarel, M.; Ison, S. A.; Scott, H. M.; Loneragan, G. H. *Lancet Infect. Dis.* **2015**, *16*, 144.
7. Tse, H.; Yuen, K.-Y. *Lancet Infect. Dis.* **2015**, *16*, 145.
8. Hancock, R. E. W. *Trends Microbiol.* **1997**, *5*, 37.
9. Fernández, L.; Hancock, R. E. W. *Clin. Microbiol. Revs.* **2012**, *25*, 661.
10. Raetz, C. R. H.; Guan, Z.; Ingram, B. O.; Six, D. A.; Song, F.; Wang, X.; Zhao, J. *J. Lipid Res.* **2009**, *50*, S103.
11. Kaconis, Y.; Kowalski, I.; Howe, J.; Brauser, A.; Richter, W.; Razquin-Olazarán, I.; Iñigo-Pestaña, M.; Garidel, P.; Rössle, M.; Martínez de Tejada, G.; Gutschmann, T.; Brandenburg, K. *Biophys. J.* **2011**, *100*, 2652.
12. Greenwood, D. F., Roger; Davey, Peter; Wilcox, Mark *Antimicrobial Chemotherapy*; 5th ed.; Oxford University Press: Oxford, 2007.
13. Jacoby, G. A.; Muñoz-Price, L. S. *N. Engl. J. Med.* **2005**, *352*, 380.
14. Soto, S. M. *Virulence* **2013**, *4*, 223.
15. Taubes, G. *Science* **2008**, *321*, 356.
16. Blair, J. M. A.; Webber, M. A.; Baylay, A. J.; Ogbolu, D. O.; Piddock, L. J. V. *Nat. Rev. Microbiol.* **2015**, *13*, 42.
17. Chopra, I. *Parasitology* **1988**, *96*, S25.
18. Nikaido, H. *Microbiol. Mol. Biol. Rev.* **2003**, *67*, 593.
19. Kefala, G.; Ahn, C.; Krupa, M.; Esquivies, L.; Maslennikov, I.; Kwiatkowski, W.; Choe, S. *Protein Sci.* **2010**, *19*, 1117.
20. Sanbongi, Y.; Shimizu, A.; Suzuki, T.; Nagaso, H.; Ida, T.; Maebashi, K.; Gotoh, N. *Microbiol. Immunol.* **2009**, *53*, 361.
21. De, E.; Basle, A.; Jaquinod, M.; Saint, N.; Mallea, M.; Molle, G.; Pages, J. M. *Mol. Microbiol.* **2001**, *41*, 189.
22. Alvarez-Ortega, C.; Olivares, J.; Martínez, J. L. *Frontiers in Microbiology* **2013**, *4*.
23. Webber, M. A.; Piddock, L. J. V. *J. Antimicrob. Chemother.* **2003**, *51*, 9.
24. Su, C.-C.; Li, M.; Gu, R.; Takatsuka, Y.; McDermott, G.; Nikaido, H.; Yu, E. W. *J. Bacteriol.* **2006**, *188*, 7290.
25. Pradel, E.; Pagès, J.-M. *Antimicrob. Agents Chemother.* **2002**, *46*, 2640.

26. Sulavik, M. C.; Houseweart, C.; Cramer, C.; Jiwani, N.; Murgolo, N.; Greene, J.; DiDomenico, B.; Shaw, K. J.; Miller, G. H.; Hare, R.; Shimer, G. *Antimicrob. Agents Chemother.* **2001**, *45*, 1126.
27. Pérez, A.; Poza, M.; Fernández, A.; del Carmen Fernández, M.; Mallo, S.; Merino, M.; Rumbo-Feal, S.; Cabral, M. P.; Bou, G. *Antimicrob. Agents Chemother.* **2012**, *56*, 2084.
28. Nikaido, H.; Pagès, J.-M. *FEMS Microbiol. Rev.* **2012**, *36*, 340.
29. Murakami, S.; Nakashima, R.; Yamashita, E.; Yamaguchi, A. *Nature* **2002**, *419*, 587.
30. Koronakis, V.; Sharff, A.; Koronakis, E.; Luisi, B.; Hughes, C. *Nature* **2000**, *405*, 914.
31. Hobbs, E. C.; Yin, X.; Paul, B. J.; Astarita, J. L.; Storz, G. *Proc. Natl. Acad. Sci. USA* **2012**, *109*, 16696.
32. Du, D.; Wang, Z.; James, N. R.; Voss, J. E.; Klimont, E.; Ohene-Agyei, T.; Venter, H.; Chiu, W.; Luisi, B. F. *Nature* **2014**, *509*, 512.
33. Okusu, H.; Ma, D.; Nikaido, H. *J. Bacteriol.* **1996**, *178*, 306.
34. O'Shea, R.; Moser, H. E. *J. Med. Chem.* **2008**, *51*, 2871.
35. Brown, D. G.; May-Dracka, T. L.; Gagnon, M. M.; Tommasi, R. *J. Med. Chem.* **2014**, *57*, 10144.
36. Billal, D. S.; Feng, J.; Leprohon, P.; Légaré, D.; Ouellette, M. *BMC Genomics* **2011**, *12*, 1.
37. Zhao, X.; Xu, C.; Domagala, J.; Drlica, K. *Proc. Natl. Acad. Sci. USA* **1997**, *94*, 13991.
38. Nordmann, P.; Nass, T.; Poirel, L. *Emerg. Infect. Dis. J.* **2011**, *17*, 1791.
39. Livermore, D. M. *Clin. Microbiol. Revs.* **1995**, *8*, 557.
40. Silver, L. L. *Clin. Microbiol. Revs.* **2011**, *24*, 71.
41. Payne, D. J.; Gwynn, M. N.; Holmes, D. J.; Pompliano, D. L. *Nat. Rev. Drug Discov.* **2007**, *6*, 29.
42. Chan, P. F.; Holmes, D. J.; Payne, D. J. *Drug Discovery Today* **2004**, *1*, 519.
43. Berg, J. M.; Tymoczko, J. L.; Stryer, L. *Biochemistry*; Fifth ed.; W. H. Freeman and Company, 2002.
44. Cozzarelli, N. R.; Cost, G. J.; Nollmann, M.; Viard, T.; Stray, J. E. *Nat. Rev. Mol. Cell Biol.* **2006**, *7*, 580.
45. Pommier, Y.; Leo, E.; Zhang, H.; Marchand, C. *Chem. Biol.*, *17*, 421.
46. Ullsperger, C.; Cozzarelli, N. R. *J. Biol. Chem.* **1996**, *271*, 31549.
47. Corbett, K. D.; Berger, J. M. *Annu. Rev. Biophys. Biomol. Struct.* **2004**, *33*, 95.
48. Aravind, L.; Leipe, D. D.; Koonin, E. V. *Nucleic Acids Res.* **1998**, *26*, 4205.
49. Laponogov, I.; Veselkov, D. A.; Crevel, I. M.-T.; Pan, X.-S.; Fisher, L. M.; Sanderson, M. R. *Nucleic Acids Res.* **2013**, *41*, 9911.
50. Bellon, S.; Parsons, J. D.; Wei, Y.; Hayakawa, K.; Swenson, L. L.; Charifson, P. S.; Lippke, J. A.; Aldape, R.; Gross, C. H. *Antimicrob. Agents Chemother.* **2004**, *48*, 1856.
51. Laponogov, I.; Pan, X.-S.; Veselkov, D. A.; McAuley, K. E.; Fisher, L. M.; Sanderson, M. R. *PLoS ONE* **2010**, *5*, e11338.
52. Corbett, K. D.; Shultzaberger, R. K.; Berger, J. M. *Proc. Natl. Acad. Sci. USA* **2004**, *101*, 7293.

53. Brino, L.; Urzhumtsev, A.; Mousli, M.; Bronner, C.; Mitschler, A.; Oudet, P.; Moras, D. *J. Biol. Chem.* **2000**, *275*, 9468.
54. Lanz, M. A.; Klostermeier, D. *Nucleic Acids Res.* **2011**, *39*, 9681.
55. Kumar, R.; Riley, J. E.; Parry, D.; Bates, A. D.; Nagaraja, V. *Nucleic Acids Res.* **2012**, *40*, 10904.
56. Hsieh, T. J.; Farh, L.; Huang, W. M.; Chan, N. L. *J. Biol. Chem.* **2004**, *279*, 55587.
57. Hearnshaw, S. J.; Chung, T. T.-H.; Stevenson, C. E. M.; Maxwell, A.; Lawson, D. M. *Acta Crystallogr. Sect. D. Biol. Crystallogr.* **2015**, *71*, 996.
58. Stanger, F. V.; Dehio, C.; Schirmer, T. *PLoS ONE* **2014**, *9*, e107289.
59. Bisacchi, G. S. *J. Med. Chem.* **2015**, *58*, 4874.
60. Mitscher, L. A. *Chem. Rev.* **2005**, *105*, 559.
61. Andersson, M. I.; MacGowan, A. P. *J. Antimicrob. Chemother.* **2003**, *51*, 1.
62. Oliphant, C. M.; Green, G. M. *Am. Fam. Physician* **2002**, *65*, 455.
63. Basarab, G. S.; Doig, P.; Galullo, V.; Kern, G.; Kimzey, A.; Kutschke, A.; Newman, J. P.; Morningstar, M.; Mueller, J.; Otterson, L.; Vishwanathan, K.; Zhou, F.; Gowravaram, M. *J. Med. Chem.* **2015**, *58*, 6264.
64. Jacobsson, S.; Golparian, D.; Alm, R. A.; Huband, M.; Mueller, J.; Jensen, J. S.; Ohnishi, M.; Unemo, M. *Antimicrob. Agents Chemother.* **2014**, *58*, 5585.
65. Biedenbach, D. J.; Bouchillon, S. K.; Hackel, M.; Miller, L. A.; Scangarella-Oman, N. E.; Jakielaszek, C.; Sahm, D. F. *Antimicrob. Agents Chemother.* **2016**.
66. Mizuuchi, K.; O'Dea, M. H.; Gellert, M. *Proc. Natl. Acad. Sci. USA* **1978**, *75*, 5960.
67. Gellert, M.; O'Dea, M. H.; Itoh, T.; Tomizawa, J. *Proc. Natl. Acad. Sci. USA* **1976**, *73*, 4474.
68. Sugino, A.; Peebles, C. L.; Kreuzer, K. N.; Cozzarelli, N. R. *Proc. Natl. Acad. Sci. USA* **1977**, *74*, 4767.
69. Gellert, M.; Mizuuchi, K.; O'Dea, M. H.; Itoh, T.; Tomizawa, J. *Proc. Natl. Acad. Sci. USA* **1977**, *74*, 4772.
70. Brown, P.; Cozzarelli, N. *Science* **1979**, *206*, 1081.
71. Hogberg, T.; Khanna, I.; Drake, S. D.; Mitscher, L. A.; Shen, L. L. *J. Med. Chem.* **1984**, *27*, 306.
72. Goetschi, E.; Angehrn, P.; Gmuender, H.; Hebeisen, P.; Link, H.; Masciadri, R.; Nielsen, J. *Pharmacol. Ther.* **1993**, *60*, 367.
73. Nakada, N.; Shimada, H.; Hirata, T.; Aoki, Y.; Kamiyama, T.; Watanabe, J.; Arisawa, M. *Antimicrob. Agents Chemother.* **1993**, *37*, 2656.
74. Geiwiz, J.; Götschi, E.; Hebeisen, P.; Link, H.; Lübbers, T. EP0675122A3, 1995.
75. Rudolph, J.; Theis, H.; Hanke, R.; Endermann, R.; Johannsen, L.; Geschke, F. *J. Med. Chem.* **2001**, *44*, 619.
76. Angehrn, P.; Goetschi, E.; Gmuender, H.; Hebeisen, P.; Hennig, M.; Kuhn, B.; Luebbers, T.; Reindl, P.; Ricklin, F.; Schmitt-Hoffmann, A. *J. Med. Chem.* **2011**, *54*, 2207.
77. Kato, J.; Nishimura, Y.; Imamura, R.; Niki, H.; Hiraga, S.; Suzuki, H. *Cell* **1990**, *63*, 393.
78. Adams, D. E.; Shekhtman, E. M.; Zechiedrich, E. L.; Schmid, M. B.; Cozzarelli, N. R. *Cell* **1992**, *71*, 277.
79. Kato, J.; Suzuki, H.; Ikeda, H. *J. Biol. Chem.* **1992**, *267*, 25676.
80. Peng, H.; Mariani, K. J. *J Biol Chem* **1993**, *268*, 24481.

81. Hoshino, K.; Kitamura, A.; Morrissey, I.; Sato, K.; Kato, J.; Ikeda, H. *Antimicrob. Agents Chemother.* **1994**, *38*, 2623.
82. Khodursky, A. B.; Zechiedrich, E. L.; Cozzarelli, N. R. *Proc. Natl. Acad. Sci. USA* **1995**, *92*, 11801.
83. Hooper, D. C. *Clin. Infect. Dis.* **2000**, *31 Suppl 2*, S24.
84. Wigley, D. B.; Davies, G. J.; Dodson, E. J.; Maxwell, A.; Dodson, G. *Nature* **1991**, *351*, 624.
85. Lewis, R. J.; Singh, O. M.; Smith, C. V.; Skarzynski, T.; Maxwell, A.; Wonacott, A. J.; Wigley, D. B. *EMBO J.* **1996**, *15*, 1412.
86. Tsai, F. T.; Singh, O. M.; Skarzynski, T.; Wonacott, A. J.; Weston, S.; Tucker, A.; Pauptit, R. A.; Breeze, A. L.; Poyser, J. P.; O'Brien, R.; Ladbury, J. E.; Wigley, D. B. *Proteins* **1997**, *28*, 41.
87. Ronkin, S. M.; Badia, M.; Bellon, S.; Grillot, A. L.; Gross, C. H.; Grossman, T. H.; Mani, N.; Parsons, J. D.; Stamos, D.; Trudeau, M.; Wei, Y.; Charifson, P. S. *Bioorganic and Medicinal Chemistry Letters* **2010**, *20*, 2828.
88. Dale, G. E.; Kostrewa, D.; Gsell, B.; Stieger, M.; D'Arcy, A. *Acta Crystallogr. Sect. D. Biol. Crystallogr.* **1999**, *55*, 1626.
89. Grillot, A.-L.; Tiran, A. L.; Shannon, D.; Krueger, E.; Liao, Y.; O'Dowd, H.; Tang, Q.; Ronkin, S.; Wang, T.; Waal, N.; Li, P.; Lauffer, D.; Sizensky, E.; Tanoury, J.; Perola, E.; Grossman, T. H.; Doyle, T.; Hanzelka, B.; Jones, S.; Dixit, V.; Ewing, N.; Liao, S.; Boucher, B.; Jacobs, M.; Bennani, Y.; Charifson, P. S. *J. Med. Chem.* **2014**, *57*, 8792.
90. Mesleh, M. F.; Cross, J. B.; Zhang, J.; Kahmann, J.; Andersen, O. A.; Barker, J.; Cheng, R. K.; Felicetti, B.; Wood, M.; Hadfield, A. T.; Scheich, C.; Moy, T. I.; Yang, Q.; Shotwell, J.; Nguyen, K.; Lippa, B.; Dolle, R.; Ryan, M. D. *Bioorg. Med. Chem. Lett.* **2016**, *26*, 1314.
91. Zhang, J.; Yang, Q.; Romero, J. A. C.; Cross, J.; Wang, B.; Poutsiaika, K. M.; Epie, F.; Bevan, D.; Wu, Y.; Moy, T.; Daniel, A.; Chamberlain, B.; Carter, N.; Shotwell, J.; Arya, A.; Kumar, V.; Silverman, J.; Nguyen, K.; Metcalf, C. A.; Ryan, D.; Lippa, B.; Dolle, R. E. *ACS Med. Chem. Letts.* **2015**, *6*, 1080.
92. Tari, L. W.; Trzoss, M.; Bensen, D. C.; Li, X.; Chen, Z.; Lam, T.; Zhang, J.; Creighton, C. J.; Cunningham, M. L.; Kwan, B.; Stidham, M.; Shaw, K. J.; Lightstone, F. C.; Wong, S. E.; Nguyen, T. B.; Nix, J.; Finn, J. *Bioorg. Med. Chem. Lett.* **2013**, *23*, 1529.
93. Bisacchi, G. S.; Manchester, J. I. *ACS Infect. Dis.* **2015**, *1*, 4.
94. Basarab, G. S.; Manchester, J. I.; Bist, S.; Boriack-Sjodin, P. A.; Dangel, B.; Illingworth, R.; Sherer, B. A.; Sriram, S.; Uria-Nickelsen, M.; Eakin, A. E. *J. Med. Chem.* **2013**, *56*, 8712.
95. Block, M. H.; Hales, N. J.; Poyser, J. P.; Telford, B.; Timms, D. WO1999001442A1, 1999.
96. Uria-Nickelsen, M.; Neckermann, G.; Sriram, S.; Andrews, B.; Manchester, J. I.; Carcanague, D.; Stokes, S.; Hull, K. G. *Int. J. Antimicrob. Agents* **2013**, *41*, 363.
97. Boehm, H. J.; Boehringer, M.; Bur, D.; Gmuender, H.; Huber, W.; Klaus, W.; Kostrewa, D.; Kuehne, H.; Luebbbers, T.; Meunier-Keller, N.; Mueller, F. *J. Med. Chem.* **2000**, *43*, 2664.

98. Tanitame, A.; Oyamada, Y.; Ofuji, K.; Fujimoto, M.; Suzuki, K.; Ueda, T.; Terauchi, H.; Kawasaki, M.; Nagai, K.; Wachi, M.; Yamagishi, J. *Bioorganic and Medicinal Chemistry* **2004**, *12*, 5515.
99. Appelt, K.; Chu, S.; Li, X.; Yager, K. M. WO2005026162A1, 2005.
100. Zhang, J., Cross, J., Yang, Q., Mesleh, M., Romero, J., Wang, B., Bevan, D., Hall, K., Epie, F., Moy, T., Daniel, A., Shotwell, J., Chamberlain, B., Carter, N., Ryan, D., Metcalf, C., Silverman, J., Nguyen, K., Lippa, B., and Dolle, R. *53rd Interscience Conference on Antimicrobial Agents and Chemotherapy, Denver, CO*, **2013**, abstract F.
101. Sherer, B. A.; Hull, K.; Green, O.; Basarab, G.; Hauck, S.; Hill, P.; Loch lii, J. T.; Mullen, G.; Bist, S.; Bryant, J.; Boriack-Sjodin, A.; Read, J.; DeGrace, N.; Uria-Nickelsen, M.; Illingworth, R. N.; Eakin, A. E. *Bioorg. Med. Chem. Lett.* **2011**, *21*, 7416.
102. Basarab, G. S.; Hill, P. J.; Garner, C. E.; Hull, K.; Green, O.; Sherer, B. A.; Dangel, P. B.; Manchester, J. I.; Bist, S.; Hauck, S.; Zhou, F.; Uria-Nickelsen, M.; Illingworth, R.; Alm, R.; Rooney, M.; Eakin, A. E. *J. Med. Chem.* **2014**, *57*, 6060.
103. Soneda, T.; Takeshita, H.; Kagoshima, Y.; Yamamoto, Y.; Hosokawa, T.; Konosu, T.; Masuda, N.; Uchida, T.; Achiwa, I.; Kuroyanagi, J. WO2009084614A1, 2009.
104. Tomašič, T.; Katsamakos, S.; Hodnik, Ž.; Ilaš, J.; Brvar, M.; Solmajer, T.; Montalvão, S.; Tammela, P.; Banjanac, M.; Ergović, G.; Anderluh, M.; Mašič, L. P.; Kikelj, D. *J. Med. Chem.* **2015**, *58*, 5501.
105. Zidar, N.; Macut, H.; Tomasic, T.; Brvar, M.; Montalvao, S.; Tammela, P.; Solmajer, T.; Peterlin Masic, L.; Ilas, J.; Kikelj, D. *J. Med. Chem.* **2015**, *58*, 6179.
106. Brvar, M.; Perdih, A.; Renko, M.; Anderluh, G.; Turk, D.; Solmajer, T. *J. Med. Chem.* **2012**, *55*, 6413.
107. Charifson, P. S.; Grillot, A.-L.; Grossman, T. H.; Parsons, J. D.; Badia, M.; Bellon, S.; Deininger, D. D.; Drumm, J. E.; Gross, C. H.; LeTiran, A.; Liao, Y.; Mani, N.; Nicolau, D. P.; Perola, E.; Ronkin, S.; Shannon, D.; Swenson, L. L.; Tang, Q.; Tessier, P. R.; Tian, S.-K.; Trudeau, M.; Wang, T.; Wei, Y.; Zhang, H.; Stamos, D. *J. Med. Chem.* **2008**, *51*, 5243.
108. O'Dowd, H.; Shannon, D. E.; Chandupatla, K. R.; Dixit, V.; Engtrakul, J. J.; Ye, Z.; Jones, S. M.; O'Brien, C. F.; Nicolau, D. P.; Tessier, P. R.; Crandon, J. L.; Song, B.; Macikenas, D.; Hanzelka, B. L.; Le Tiran, A.; Bennani, Y. L.; Charifson, P. S.; Grillot, A.-L. *ACS Med. Chem. Letts.* **2015**, *6*, 822.
109. Grossman, T. H.; Bartels, D. J.; Mullin, S.; Gross, C. H.; Parsons, J. D.; Liao, Y.; Grillot, A. L.; Stamos, D.; Olson, E. R.; Charifson, P. S.; Mani, N. *Antimicrob. Agents Chemother.* **2007**, *51*, 657.
110. Haydon, D.; Czaplowski, L. G.; Palmer, N.; Atherall, J.; Steele, C.; Ladduwahetty, T. WO 2007148093, 2007.
111. Stokes, N. R.; Thomaidis-Brears, H. B.; Barker, S.; Bennett, J. M.; Berry, J.; Collins, I.; Czaplowski, L. G.; Gamble, V.; Lancett, P.; Logan, A.; Lunniss, C. J.; Peasley, H.; Pommier, S.; Price, D.; Smee, C.; Haydon, D. *J. Antimicrob. Agents Chemother.* **2013**, *57*, 5977.
112. Axford, L. C.; Agarwal, P. K.; Anderson, K. H.; Andrau, L. N.; Atherall, J.; Barker, S.; Bennett, J. M.; Blair, M.; Collins, I.; Czaplowski, L. G.; Davies, D. T.; Gannon, C. T.; Kumar, D.; Lancett, P.; Logan, A.; Lunniss, C. J.; Mitchell, D. R.; Offermann, D. A.; Palmer, J. T.; Palmer, N.; Pitt, G. R.; Pommier, S.; Price, D.; Narasinga Rao,

- B.; Saxena, R.; Shukla, T.; Singh, A. K.; Singh, M.; Srivastava, A.; Steele, C.; Stokes, N. R.; Thomaidis-Brears, H. B.; Tyndall, E. M.; Watson, D.; Haydon, D. J. *Bioorganic and Medicinal Chemistry Letters* **2013**, *23*, 6598.
113. Butler, D. C. D.; Chen, H.; Hegde, V. R.; Limberakis, C.; Rasne, R. M.; Sciotti, R. J.; Starr, J. T. WO2006038116A3, 2006.
114. East, S. P.; White, C. B.; Barker, O.; Barker, S.; Bennett, J.; Brown, D.; Boyd, E. A.; Brennan, C.; Chowdhury, C.; Collins, I.; Convers-Reignier, E.; Dymock, B. W.; Fletcher, R.; Haydon, D. J.; Gardiner, M.; Hatcher, S.; Ingram, P.; Lancett, P.; Mortenson, P.; Papadopoulos, K.; Smee, C.; Thomaidis-Brears, H. B.; Tye, H.; Workman, J.; Czaplewski, L. G. *Bioorg. Med. Chem. Lett.* **2009**, *19*, 894.
115. Bur, D.; Gude, M.; Hubschwerlen, C.; Panchaud, P. WO2011121555A1, 2011.
116. Zhang, J.; Yang, Q.; Cross, J. B.; Romero, J. A. C.; Poutsiaka, K. M.; Epie, F.; Bevan, D.; Wang, B.; Zhang, Y.; Chavan, A.; Zhang, X.; Moy, T.; Daniel, A.; Nguyen, K.; Chamberlain, B.; Carter, N.; Shotwell, J.; Silverman, J.; Metcalf, C. A.; Ryan, D.; Lippa, B.; Dolle, R. E. *J. Med. Chem.* **2015**, *58*, 8503.
117. Manchester, J. I.; Dussault, D. D.; Rose, J. A.; Boriack-Sjodin, P. A.; Uria-Nickelsen, M.; Ioannidis, G.; Bist, S.; Fleming, P.; Hull, K. G. *Bioorg. Med. Chem. Lett.* **2012**, *22*, 5150.
118. Tari, L. W.; Li, X.; Trzoss, M.; Bensen, D. C.; Chen, Z.; Lam, T.; Zhang, J.; Lee, S. J.; Hough, G.; Phillipson, D. *PLOS One* **2013**, *8*, e84409.
119. Trzoss, M.; Bensen, D. C.; Li, X.; Chen, Z.; Lam, T.; Zhang, J.; Creighton, C. J.; Cunningham, M. L.; Kwan, B.; Stidham, M.; Nelson, K.; Brown-Driver, V.; Castellano, A.; Shaw, K. J.; Lightstone, F. C.; Wong, S. E.; Nguyen, T. B.; Finn, J.; Tari, L. W. *Bioorg. Med. Chem. Lett.* **2013**, *23*, 1537.
120. Sawa, R.; Takahashi, Y.; Hashizume, H.; Sasaki, K.; Ishizaki, Y.; Umekita, M.; Hatano, M.; Abe, H.; Watanabe, T.; Kinoshita, N.; Homma, Y.; Hayashi, C.; Inoue, K.; Ohba, S.; Masuda, T.; Arakawa, M.; Kobayashi, Y.; Hamada, M.; Igarashi, M.; Adachi, H.; Nishimura, Y.; Akamatsu, Y. *Chemistry* **2012**, *18*, 15772.
121. Singh, S. B.; Goetz, M. A.; Smith, S. K.; Zink, D. L.; Polishook, J.; Onishi, R.; Salowe, S.; Wiltsie, J.; Allocco, J.; Sigmund, J.; Dorso, K.; de la Cruz, M.; Martin, J.; Vicente, F.; Genilloud, O.; Donald, R. G.; Phillips, J. W. *Bioorganic and Medicinal Chemistry Letters* **2012**, *22*, 7127.
122. Chiriac, A. I.; Kloss, F.; Kramer, J.; Vuong, C.; Hertweck, C.; Sahl, H. G. *J. Antimicrob. Chemother.* **2015**, *70*, 2576.
123. Yule, I. A.; Czaplewski, L. G.; Pommier, S.; Davies, D. T.; Narramore, S. K.; Fishwick, C. W. G. *Eur. J. Med. Chem.* **2014**, *86*, 31.
124. Czaplewski, L. G.; Fishwick, C. W. G.; Yule, I. A.; Mitchell, J. P.; Anderson, K. H.; Pitt, G. R. WO 2013091011, 2013.
125. Gillet, V.; Johnson, A. P.; Mata, P.; Sike, S.; Williams, P. *J. Comput. Aided Mol. Des.* **1993**, *7*, 127.
126. Morris, G. M.; Huey, R.; Lindstrom, W.; Sanner, M. F.; Belew, R. K.; Goodsell, D. S.; Olson, A. J. *J. Comput. Chem.* **2009**, *30*, 2785.
127. Abad, A.; Agulló, C.; Cuñat, A. C.; Vilanova, C. *Synthesis* **2005**, *2005*, 915.
128. *Calculator Plugins were used for structure property prediction and calculation, Marvin 5.11.1, 2012, ChemAxon (<http://www.chemaxon.com>).*
129. Lovering, F.; Bikker, J.; Humblet, C. *J. Med. Chem.* **2009**, *52*, 6752.

130. Guandalini, L.; Martini, E.; Di Cesare Mannelli, L.; Dei, S.; Manetti, D.; Scapecchi, S.; Teodori, E.; Ghelardini, C.; Romanelli, M. N. *Bioorg. Med. Chem. Lett.* **2012**, *22*, 1936.
131. Yu, H.; Adedoyin, A. *Drug Discovery Today* **2003**, *8*, 852.
132. Sambuy, Y.; Angelis, I.; Ranaldi, G.; Scarino, M. L.; Stamatii, A.; Zucco, F. *Cell Biol. Toxicol.* **2005**, *21*, 1.
133. Gillis, E. P.; Eastman, K. J.; Hill, M. D.; Donnelly, D. J.; Meanwell, N. A. *J. Med. Chem.* **2015**, *58*, 8315.
134. Guengerich, F. P. *Chem. Res. Toxicol.* **2008**, *21*, 70.
135. Lynch, T.; Price, A. *Am. Fam. Physician* **2007**, *76*, 391.
136. Sanguinetti, M. C.; Tristani-Firouzi, M. *Nature* **2006**, *440*, 463.
137. Tari, L. W. In *Structure-Based Drug Discovery*; Tari, W. L., Ed.; Humana Press: Totowa, NJ, 2012, p 1.
138. Cheng, Y.; Patel, D. J. *Biochem. Biophys. Res. Commun.* **2004**, *317*, 401.
139. Phan, J.; Zdanov, A.; Evdokimov, A. G.; Tropea, J. E.; Peters, H. K.; Kapust, R. B.; Li, M.; Wlodawer, A.; Waugh, D. S. *J. Biol. Chem.* **2002**, *277*, 50564.
140. Lafitte, D.; Lamour, V.; Tsvetkov, P. O.; Makarov, A. A.; Klich, M.; Deprez, P.; Moras, D.; Briand, C.; Gilli, R. *Biochemistry* **2002**, *41*, 7217.
141. Lu, J.; Patel, S.; Sharma, N.; Soisson, S. M.; Kishii, R.; Takei, M.; Fukuda, Y.; Lumb, K. J.; Singh, S. B. *ACS Chem. Biol.* **2014**, *9*, 2023.
142. Zidar, N.; Macut, H.; Tomašič, T.; Brvar, M.; Montalvão, S.; Tammela, P.; Solmajer, T.; Peterlin Mašič, L.; Ilaš, J.; Kikelj, D. *J. Med. Chem.* **2015**, *58*, 6179.
143. Eakin, A. E.; Green, O.; Hales, N.; Walkup, G. K.; Bist, S.; Singh, A.; Mullen, G.; Bryant, J.; Embrey, K.; Gao, N.; Breeze, A.; Timms, D.; Andrews, B.; Uria-Nickelsen, M.; Demeritt, J.; Loch, J. T., 3rd; Hull, K.; Blodgett, A.; Illingworth, R. N.; Prince, B.; Boriack-Sjodin, P. A.; Hauck, S.; MacPherson, L. J.; Ni, H.; Sherer, B. *Antimicrob. Agents Chemother.* **2012**, *56*, 1240.
144. Winn, M. D.; Ballard, C. C.; Cowtan, K. D.; Dodson, E. J.; Emsley, P.; Evans, P. R.; Keegan, R. M.; Krissinel, E. B.; Leslie, A. G. W.; McCoy, A.; McNicholas, S. J.; Murshudov, G. N.; Pannu, N. S.; Potterton, E. A.; Powell, H. R.; Read, R. J.; Vagin, A.; Wilson, K. S. *Acta Crystallogr. Sect. D. Biol. Crystallogr.* **2011**, *67*, 235.
145. *Maestro version 10.0*; Schrödinger, LLC, New York, NY, 2014.
146. Hillisch, A.; Heinrich, N.; Wild, H. *ChemMedChem* **2015**, *10*, 1958.
147. Lolli, M.; Narramore, S.; Fishwick, C. W. G.; Pors, K. *Drug Discovery Today* **2015**, *20*, 1018.
148. McPhillie, M. J.; Cain, R. M.; Narramore, S.; Fishwick, C. W. G.; Simmons, K. J. *Chem. Biol. Drug. Des.* **2015**, *85*, 22.
149. <http://accelrys.com/products/collaborative-science/biovia-pipeline-pilot/>; Pipeline pilot, December 2015.
150. Hawkins, P. C. D.; Skillman, A. G.; Nicholls, A. *J. Med. Chem.* **2007**, *50*, 74.
151. O'Boyle, N.; Banck, M.; James, C.; Morley, C.; Vandermeersch, T.; Hutchison, G. *J. Cheminf.* **2011**, *3*, 33.
152. Sun, H.; Tawa, G.; Wallqvist, A. *Drug Discovery Today* **2012**, *17*, 310.
153. Goldsmith, P. J.; Hancox, T. C.; Pegg, N. A.; Shuttleworth, S. J.; Dechaux, E. A.; Price, S.; Large, J. M.; McDonald, E. WO 2008125839, 2008.
154. Coteron, J. M.; Marco, M.; Esquivias, J.; Deng, X.; White, K. L.; White, J.; Koltun, M.; El Mazouni, F.; Kokkonda, S.; Katneni, K.; Bhamidipati, R.; Shackelford, D.

- M.; Angulo-Barturen, I.; Ferrer, S. B.; Jiménez-Díaz, M. B.; Gamo, F.-J.; Goldsmith, E. J.; Charman, W. N.; Bathurst, I.; Floyd, D.; Matthews, D.; Burrows, J. N.; Rathod, P. K.; Charman, S. A.; Phillips, M. A. *J. Med. Chem.* **2011**, *54*, 5540.
155. Zeghida, W.; Debray, J.; Chierici, S.; Dumy, P.; Demeunynck, M. *The Journal of Organic Chemistry* **2008**, *73*, 2473.
156. Huang, X.; Yang, H.; Fu, H.; Qiao, R.; Zhao, Y. *Synthesis* **2009**, *2009*, 2679.
157. Li, Y.; Wilson, J. J.; Do, L. H.; Apfel, U.-P.; Lippard, S. J. *Dalton Trans.* **2012**, *41*, 9272.
158. Gilbert, D. N.; Guidos, R. J.; Boucher, H. W.; Talbot, G. H.; Spellberg, B.; Edwards Jr, J. E.; Scheld, W. M.; Bradley, J. S.; Bartlett, J. G. *Clin. Infect. Dis.* **2010**, *50*, 1081.
159. Zimmer, C.; Hafner, M.; Zender, M.; Ammann, D.; Hartmann, R. W.; Vock, C. A. *Bioorg. Med. Chem. Lett.* **2011**, *21*, 186.
160. Sherman, W. R.; Taylor, E. C. J.; Cairns, T. L.; Acker, D. S. *Org. Synth.* **1957**, *37*, 15.
161. Reiter, J.; Pongo, L.; Dvortsak, P. *J. Het. Chem.* **1987**, *24*, 1685.
162. *Nonlinear fit of log-dose vs response was performed using GraphPad Prism version 6.07 for Windows, GraphPad Software, La Jolla California USA, www.graphpad.com.*
163. *Methods for Dilution Antimicrobial Susceptibility Tests for Bacteria That Grow Aerobically; Approved Standard—Seventh Edition ed.; CLSI: CLSI, Wayne, Pa, 2006.*
164. Winter, G.; Lobley, C. M.; Prince, S. M. *Acta Crystallogr. Sect. D. Biol. Crystallogr.* **2013**, *69*, 1260.
165. Winter, G. *J. Appl. Crystallogr.* **2010**, *43*, 186.
166. Matthews, B. W. *Journal of Molecular Biology* **1968**, *33*, 491.
167. McCoy, A. J.; Grosse-Kunstleve, R. W.; Adams, P. D.; Winn, M. D.; Storoni, L. C.; Read, R. J. *J. Appl. Crystallogr.* **2007**, *40*, 658.
168. Murshudov, G. N.; Vagin, A. A.; Dodson, E. J. *Acta Crystallogr. Sect. D. Biol. Crystallogr.* **1997**, *53*, 240.
169. Schuttelkopf, A. W.; van Aalten, D. M. *Acta Crystallogr. Sect. D. Biol. Crystallogr.* **2004**, *60*, 1355.
170. Emsley, P.; Lohkamp, B.; Scott, W. G.; Cowtan, K. *Acta Crystallogr. Sect. D. Biol. Crystallogr.* **2010**, *66*, 486.
171. Murshudov, G. N.; Skubak, P.; Lebedev, A. A.; Pannu, N. S.; Steiner, R. A.; Nicholls, R. A.; Winn, M. D.; Long, F.; Vagin, A. A. *Acta Crystallogr. Sect. D. Biol. Crystallogr.* **2011**, *67*, 355.
172. Joosten, R. P.; Long, F.; Murshudov, G. N.; Perrakis, A. *IUCrJ* **2014**, *1*, 213.
173. Davis, I. W.; Leaver-Fay, A.; Chen, V. B.; Block, J. N.; Kapral, G. J.; Wang, X.; Murray, L. W.; Arendall, W. B., 3rd; Snoeyink, J.; Richardson, J. S.; Richardson, D. C. *Nucleic Acids Res.* **2007**, *35*, W375.